



UNIVERSITAT DE
BARCELONA

Primary batteries paradigm redefinition within the environmental planetary boundaries

Marina Navarro-Segarra



Aquesta tesi doctoral està subjecta a la llicència **Reconeixement- NoComercial – SenseObraDerivada 4.0. Espanya de Creative Commons.**

Esta tesis doctoral está sujeta a la licencia **Reconocimiento - NoComercial – SinObraDerivada 4.0. España de Creative Commons.**

This doctoral thesis is licensed under the **Creative Commons Attribution-NonCommercial-NoDerivs 4.0. Spain License.**

PRIMARY BATTERIES PARADIGM
REDEFINITION WITHIN THE
ENVIRONMENTAL PLANETARY
BOUNDARIES

Author| Marina Navarro-Segarra

ELECTROCHEMISTRY. SCIENCE AND TECHNOLOGY

Doctoral thesis

July 2022

Supervisors|

Juan Pablo Esquivel Bojórquez

Neus Sabaté Vizcarra

Tutor|

Elvira Gómez Valentín



UNIVERSITAT DE
BARCELONA



CSIC
CONSEJO SUPERIOR DE INVESTIGACIONES CIENTÍFICAS

La presente tesis doctoral titulada 'Primary batteries paradigm redefinition within the environmental planetary boundaries' ha sido realizada por Marina Navarro-Segarra para optar al título de Doctora en Electroquímica. Ciencia y Tecnología por la Universidad de Barcelona bajo la dirección del Dr. Juan Pablo Esquivel y la Dra. Neus Sabaté en el Instituto de Microelectrónica de Barcelona, IMB-CNM (CSIC) y bajo la tutela de Dra. Elvira Gómez Valentín.

Barcelona, Julio 2022

Marina Navarro Segarra

*A la Madre Tierra,
quien tan gentilmente nos acoge
y a quien tan desagradecidamente tratamos.*

Agradecimientos

Antes de dejar plasmado en estas páginas el resumen de lo que ha sido mi desarrollo principalmente científico, pero también personal de los últimos años, me gustaría mostrar mi gratitud a todas las personas que han contribuido a que este trabajo se hiciera realidad.

Primero de todo quiero agradecer al Dr. Juan Pablo Esquivel, por escoger compartir conmigo sus ideas, su entusiasmo y su investigación. Gracias por confiar y por la paciencia, por enseñarme a valorar el proceso y por todo el apoyo demostrado día tras día. También me gustaría agradecer de corazón a la Dra. Neus Sabaté quien, sin intención, se ha convertido en un gran referente. A todas las que han formado parte del SPEED en algún momento estos años, gracias por ser mentoras, compañeras y ejemplo. En especial a Irene, Sole, Lorena y Anna, por ayudarme a dar los primeros pasos en el laboratorio. Gracias también a todos los estudiantes de final de grado y máster, por enseñarme como ser mentora y tener paciencia delante de la falta de experiencia. En especial, gràcies Carles, pels meravellosos renders i per convertir-te en company indispensable de laboratori, despatx, muntanya, rocòdrom i vida. También me gustaría agradecer a todo el personal de IMB-CNM por estos años y por haber creado un entorno de trabajo tan familiar y acogedor. Me gustaría expresar mi gratitud con la Dra. Elvira Gómez, por ser ejemplo y por todo su apoyo incondicional frente a cualquier duda científica o burocrática.

Por otra parte, quiero agradecer al grupo de investigación SAB, a la cooperativa Triunfo Verde y a todos los que nos acompañaron durante el viaje a las comunidades cafetaleras en Chiapas, por compartir conmigo sus conocimientos durante mi estancia en México. También gracias a mis compañeros de casa, que me permitieron revolucionar su vida durante un mes, me acogieron como parte de la familia, me enseñaron a apresurarme despacio e hicieron la experiencia totalmente inolvidable.

Gràcies mare, gracias papa. Por ser mis mayores referentes, alentarme a pesar de la distancia y hacerme saber que siempre estaréis ahí con la tortilla de patata y la moto

preparadas. A Juanjo i a Oso, gràcies per connectar la vostra essència amb la meva, per ser inspiració i per fer-me ser millor cada dia.

Por último, a pesar de poder parecer egocéntrica, me quiero agradecer esta tesis a mí. Por la confianza reafirmada, el sacrificio indispensable, el tiempo dedicado y la toma de decisiones que me han llevado hasta este momento.

Contents

1	Introduction to the development of sustainable portable batteries	1
1.1	Challenges for powering a digital society	2
1.1.1	Portable batteries conventional life cycle	4
1.2	Primary batteries working principle	7
1.3	State of the art of portable batteries with a disruptive end-of-life	9
	Thesis Summary 	14
2	A rationale to ecodesign sustainable batteries based on the doughnut economics model	17
2.1	Batteries inspired by the doughnut economics model	21
2.2	Key tools to ensure portable battery to stay within the sustainable development space	25
2.3	Batteries for a global sustainable development	33
	Conclusions	35
3	A flow-battery driven by evaporation for precision agriculture devices	37
	Overview	38
3.1	Introduction	39
3.2	Battery design and operation principle	44
3.3	Evaporation flow in porous media	46
3.3.1	Influence of the evaporation pad area on the evaporation flow rate	46

3.3.2	Influence of the environmental conditions and evaporation flow modeling	47
3.4	Battery operation and optimization	51
3.4.1	Battery performance characterization	52
3.4.2	Durability of the devices core	54
3.4.3	Redox species stability	55
3.4.4	Optimized prototype continuous operation	58
3.5	Performance estimation under different environmental conditions	60
3.6	Powering a wireless smart monitoring unit for precision horticulture	62
3.7	End-of-life assessment through aerobic biodegradability and phytotoxicity tests	65
3.8	Discussion	70
	Conclusions	71
	Materials & Methods	72
4	A carboard battery for smart packaging applications	79
	Overview	80
4.1	Introduction	81
4.2	Battery design and operation principle	84
4.3	Materials development and battery operation	86
4.3.1	Laser-induced graphene current collectors	86
4.3.2	Bio-based hydrogel as a battery matrix	100
4.3.3	Prototype operation test	103
4.4	Discussion	107
	Conclusions	109
	Materials & Methods	110
5	Exploring local and decentralized biodegradable battery development	115

Overview	117
5.1 Introduction	118
5.2 Project framework and viability	122
5.2.1 Life without electricity	122
5.2.2 Analysing the coffee production process and its residues	126
5.3 Battery design and operation principle	130
5.4 Materials development and battery operation	131
5.4.1 Commercial phenolic compounds as anode materials	131
5.4.2 Hydrogel biopolymer as a battery matrix	133
5.4.3 Current collectors selection	136
5.4.4 Prototype optimization and operation test	138
5.5 Powering a portable lighting system in coffee growing communities in Chiapas	142
5.6 From commercial to extracted: Exploring local material sources for batteries	144
5.6.1 Phenolic compounds extraction at the residue production location	144
5.6.2 Development of an ionic conductive membrane from revalorized biopolymers	152
5.6.3 Battery fabricated from revalorized biopolymers	155
5.7 Discussion	156
5.7.1 Evaluation of project impact through the adaptation of the Social Progress Index (SPI)	157
Conclusions	163
Materials & Methods	164
Conclusions	168
A Materials selection and related experimental methodology	171

A.1	Electrochemical techniques for redox species selection	172
A.2	Paper as capillary structure in microfluidic flow batteries	174
A.2.1	Impedance spectroscopy to asses hydrogels with ionic conductivity	175
B	Standards and regulations	179
B.1	Biodegradability and phytotoxicity standards	179
B.2	Paper and cardboard recyclability standards	181
C	Screening of redox species	183
	References	186
	Scientific contributions related with this thesis	211
	Resumen en español	216

1

Introduction to the development of sustainable portable batteries

1.1 Challenges for powering a digital society

Digital technologies are generating a global transformation with economic, social, and environmental implications. Digitalization has already shown many benefits to society, it has stimulated disruptive innovation, generated new business models providing opportunities for value creation, contributed to transparency, and improved access to information. However, this digital transformation is generating a fierce debate on how to ensure a positive, sustainable, and just social impact. Furthermore, this growing trend arises profound concerns about its environmental impact.^{1;2} Big data analytics, artificial intelligence, and the Internet-of-Things (IoT) are primary enablers of the digital transformation. IoT is constituted by multiple energy-autonomous systems that will be comprehensively capable of sensing, diagnosing, deciding, and actuating in a communicative and collaborative way. Although IoT is still in the early stages of growth, current estimations point to more than 9 billion connected devices around the world. This number is expected to increase exponentially, with estimates ranging from 25 to 50 billion devices in 2025.³ This network of devices will give rise to a new era of information access, well-being, and productivity in many sectors.⁴ However, its manufacture, usage, and waste management will consume a high amount of resources.

As this global trend of society digitalization speeds up, planned obsolescence and linear economy models are consequently generating an unprecedented amount of Waste Electrical and Electronic Equipment (WEEE) or e-waste. WEEE is rapidly becoming the largest waste stream worldwide.⁵⁻⁷ It has not stopped growing since 2014, leaving behind an annual generation of about 50 million metric tons, which are expected to increase up to 75 Mt in 2030, according to the latest Global e-Waste Monitor report.⁸ On the other hand, the World Economic Forum estimates that the material value of our used electronic devices globally amounts to \$ 62.5 billion, three times more than the annual output of the world's silver mines.⁹ Thus this waste stream equally contains hazardous and valuable materials. In 2019, the documented global percentage of collected and properly recycled WEEE was 17.4%, meaning that the large majority of e-waste generated was not formally collected nor managed in a systematic manner. Europe, in particular, ranks first in terms of e-waste generation

per capita with 16.2 kg (12Mt generated in total in 2019).⁸ As depicted in Figure 1.1a, EU member countries show a growing trend since 2014.

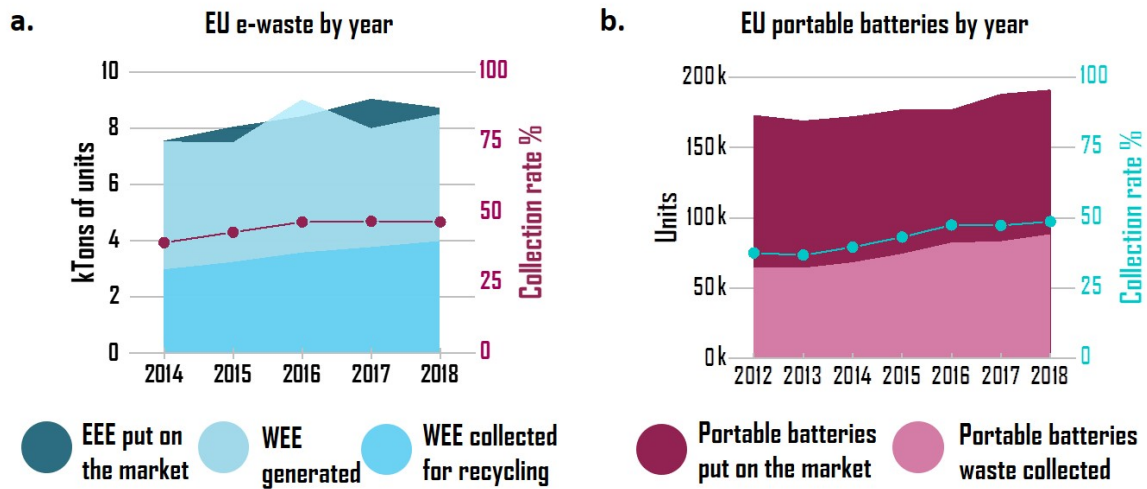


Figure 1.1: a. Electrical and Electronic Equipment (EEE) put on the market compared with Waste Electrical and Electronic Equipment (WEEE) generated and collected by year in EU in kilotons. Represented by dots, the collection rate b. Units of portable batteries put on the EU market in comparison with portable batteries collected for recycling by year. Source: Prepared for this thesis based on the data supplied by Eurostat. Collection rates have been calculated as set out in the WEEE Directive (% of the average weight of EEE put on the market in the three preceding years).

Moreover, the gap of data and statistics on WEEE management has already been exposed, pointing out that the lack of formally documented data implies that e-waste is mainly managed outside the official collection system. This obsolete equipment is, in some cases, shipped to developing countries,ⁱ where there is a complete lack of secure and sanitized facilities for e-waste recycling and material recovery.¹⁰ The problem is even more critical when this waste is not even collected properly. Despite having a developed recycling infrastructure in high-income countries, a high number of small-size electronics are disposed of in general waste bins that usually end up in landfills where, in many cases, are incinerated. One of the most hazardous components in

ⁱAs a part of the official WEEE management, it is usual to incorrectly categorize WEEE under the euphemism Used Electrical and Electronic Equipment (UEEE). As it has been reported by Basel Action Networks in multiple occasions, this illegal practice is used to avoid OECD waste exporting regulations and generates a non-regulated trade of WEEE to developing countries.¹⁰ The interested reader may consult : ban.org/trash-transparency

e-waste are batteries. Due to their chemical composition, encapsulation, and risk of explosion, batteries need special and dedicated recycling processes.¹¹

Due to their suitability in many areas, batteries have become today ubiquitous power sources to feed portable EEE, but also contribute intensively to WEEE generation. Just in 2018, 191 kilotons of portable batteries were sold in the EU (see Figure 1.1 b).ⁱⁱ However, only about 88 kilotons of waste portable batteries and accumulators were collected for recycling, representing ca. 48% of collection rate.¹² Being the highest collection rate archived since records began. Significant efforts are being undertaken at EU level to create a sustainable framework for batteries. Most of these initiatives focus on the recovery of valuable elements, but also include the incorporation of sustainability into batteries value chain^{13;14}, specifically promoting environmental impact assessments.¹⁵

The European Commission (EC) has identified batteries as a strategic value chain where the EU must strengthen investment and innovation through an industrial policy strategy that builds an integrated, sustainable and competitive industrial base.^{16;17} Despite these valuable actions intended to improve sustainability of large-scale batteries (mostly for e-mobility and energy storage sectors), particular considerations should be made to improve portable battery formats as well. Portable batteries have shown to have a high carbon footprint associated, especially during their manufacturing and End of Life (EoL).

1.1.1 Portable batteries conventional life cycle

For portable batteries to stop contributing to environmental degradation, and become an example for sustainable technological development, it is crucial to change the way the batteries value chain is approached. The conventional life cycle of portable batteries follows an obsolete linear economy model. Figure 1.2 gives a schematic view of the main stages of the battery life cycle, pointing out some unsustainable practices currently performed at each of the stages.

ⁱⁱ75% of them non-rechargeable batteries (primary), 25% portable secondary batteries.

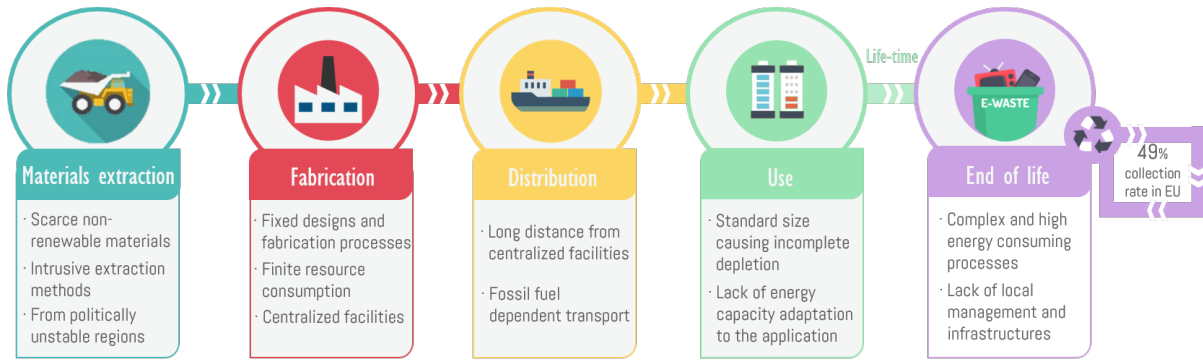


Figure 1.2: Linear life cycle of current portable batteries and practices identified by the authors that contribute to the environmental burden at each of their stages.

Batteries depend on scarce non-renewable materials that are extracted by intrusive methods, contributing to environmental deterioration. Concurrently, there are increasing issues related to raw materials extraction and use of EU critical raw materials (e.g. P, Co, Li), which are not sustainable in the long term.^{18;19} Their fabrication stage takes place in centralized facilities (mostly located in Asia), generating a necessity of a long-distance battery distribution around the world. Furthermore, portable batteries fabrication is usually based on standardized formats. Then, product manufacturers usually decide the battery format for their application on the basis of cost rather than optimal energy requirements. As a result, batteries are often discarded after their use without being completely depleted (sometimes almost fully charged). Finally, during their EoL, if they are collected for recycling, their complex encapsulation together with the hazardous nature of the material they are made of, make the recycling process really energy-consuming.²⁰ Moreover, due to the lack of local management and e-waste recycling infrastructure, battery waste sometimes needs to be exported again.¹⁰ In a large number of cases, as it happens to e-waste, portable batteries are also improperly discarded with general waste streams, ending up in landfills or incinerated, actions that pose risks to human health,²¹ biodiversity, and ecosystems.

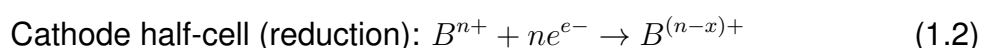
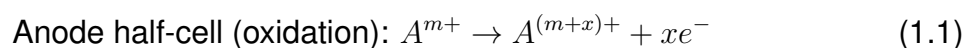
Ongoing strategies related to ecodesign, collection, repurposing, and recycling of batteries for large-scale applications²² cannot be directly applied to portable battery formats – due to the diverse variety of use case scenarios, their ubiquity, and that the success of the strategies depends primarily on the end-user self-responsibility and availability of dedicated collection routes. For these reasons, it is imperative to rethink

the portable battery life cycle in accordance with a holistic sustainable perspective.

This thesis proposes a portable battery development approach that considers social, economic, and environmental implications. The approach, presented in this work, aims to change the current paradigm of portable batteries to a new model in which batteries are designed to follow the life cycle of the device to be powered, as a strategy to minimize their environmental impact along their value chain. Ecodesign is used as the tool to perform a detailed analysis of all the stages involved in their lifecycle, e.g. raw material selection, manufacturing process, demanded energy capacity, operational time, and disposal considerations. In this sense, batteries' life cycle has been entirely reformulated to place sustainability as core priority, by raising for instance alternative end-of-life scenarios; such as being capable of biodegrading, composting with other organic waste or even recycled with paper and cardboard. The following section presents the basics of primary battery working principle, then a review of the state of the art in portable batteries with disruptive end-of-life is presented. And at the end of this chapter, the thesis contents are gathered and summarized.

1.2 Primary batteries working principle

Batteries are energy storage devices based on the electrochemical galvanic cell concept. A galvanic cell spontaneously converts chemical energy from the reactants to electrical energy (i.e. electrons flow) by coupling oxidation-reduction reactions. Hence, as depicted in Figure 1.3a., batteries are composed by a separator (can be an ion exchange membrane, a salt bridge, physical separation or a co-laminar flow interface), the ion conductive media (i.e. electrolyte/s) and two electrodes, an anode in which the oxidation reaction takes place; and a cathode in which the reduction. In particular, primary batteries are non-rechargeable galvanic cells, meaning the electrochemical reactions are irreversible. The electrochemical reaction occurring at the electrodes surface of a primary battery can be generically written as follows:



Primary batteries performance is usually assessed through polarization curves, which provide the cell operational performance as a relation between voltage and current. They are obtained by coupling the battery with an external variable load that forces the battery into different working points (i.e. voltage-current conditions). To obtain a complete assessment, polarization curves are usually run from the voltage value when there is no current flow (i.e. open circuit voltage) to maximum current flow (0V). Figure 1.3b. depicts a generic polarization curve indicating the ranges of overpotential and performance losses.

The cell theoretical potential is set by the battery chemistry, however the actual cell voltage is significantly lower during operation. As it can be seen, there are four sources of voltage loss variate, and each one accumulative appears in a different voltage/current operation conditions:

OCV operpotential: appear due to reactants crossover, side-reactions, and catalyst impurities if catalyst is needed.

Activation losses: are caused because reactions kinetics irreversibility, and become more significant with slow to moderate electrochemical reactions rates.

They are predominant at low current densities and can be minimized increasing operation temperature or through an electrocatalyst.

Ohmic losses: are direct ohmic resistance respond to electrons transport resistance on the electrodes and ions mobility restrictions on the electrolytes. It also include resistance from external connectors or wires. It is minimized through electrolyte concentration optimization, high conductive current collectors and electrodes distance reduction.

Mass transport losses: it occurs when the reaction rate and the reactants transport rate to the active sites are similar. Thus, there appear mass transport limitations at electrodes, causing the depletion of reactant at the electrode surface. They can be minimized by optimization of the cell structure or by increasing the reactants concentration.

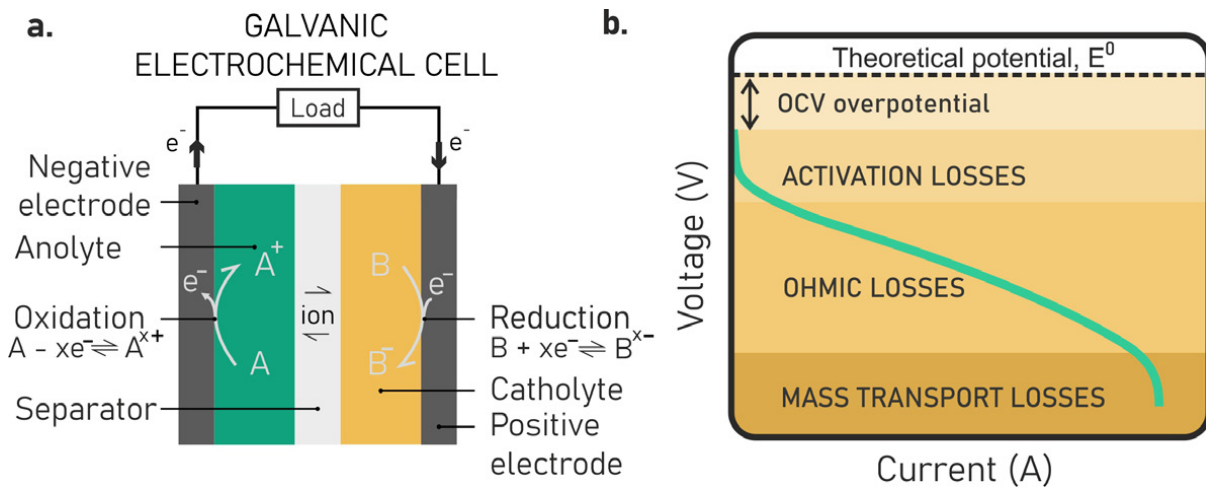


Figure 1.3: a. Schematic representation of a galvanic electrochemical cell, showing its main components, as well as, electrons and ion flows. b. Generic galvanic cell polarization curve indicating the sources of performance loss.

1.3 State of the art of portable batteries with a disruptive end-of-life

In order to mitigate the associated environmental impact of EEE in general, and portable batteries in particular, researchers have focused efforts on seeking alternative end-of-life scenarios that do not require a dedicated collection route with subsequent recycling for materials recovery. In this regards, transient technology is a blooming research area that seeks materials and devices to undergo a controlled degradation process after their operational lifespan. Several recent reviews summarized the application of transiency to materials,^{23;24} electronics^{25;26;27} and battery components.²⁸

The reported degradation mechanisms for transient materials can be classified by the external activator that triggers the material disintegration, such as pH,²⁹ light,³⁰ or temperature³¹. When the degradation process is activated, a series of physical or chemical reactions occur and, after a given time, the material components transform into degradation products. The degradation mechanism depends on the nature of the material and the degrading medium. Some academic approaches have proposed degradable batteries to satisfy the growing need for portable power sources while easing the environmental impact after disposal. In 2014, Rogers and co-workers reported a battery for medical implants made of biocompatible metal foils and polyanhydride packaging and showed its dissolution into its primary components after some hours of operation in physiological conditions (See Figure 1.4a). Later that year, the concept of transient benign batteries for *in-vivo* applications was transferred to *ex-vivo* environments, inaugurating in this way, a new family of so-called '*biodegradable*' batteries.³² As the examples in Figure 1.4 b-c show, magnesium has been used as primary anode material whereas cathode electrodes are implemented with iron,^{33;34} silk-fibroin-polypyrrole³⁵, gold³⁶ or molybdenum trioxide³⁷. In the same way, different biopolymers are used as electrolytes and to confer the batteries with mechanical stability^{38;39}. Alternatives to metal electrodes, such as melanine⁴⁰ or activated carbon^{41;41} have also been presented by Bettinger et al. Both lithium technology and bio-based batteries - using enzymatic or microbial electrodes - have

also been successfully exported to transient configurations.^{30,42–44}^{30;42–44} A remarkable microbial battery onto biodegradable paper-polymer substrates, Figure 1.4 d, was reported by Choi group in 2018, showing a considerable weight loss after 70 days of degradation test.⁴⁵

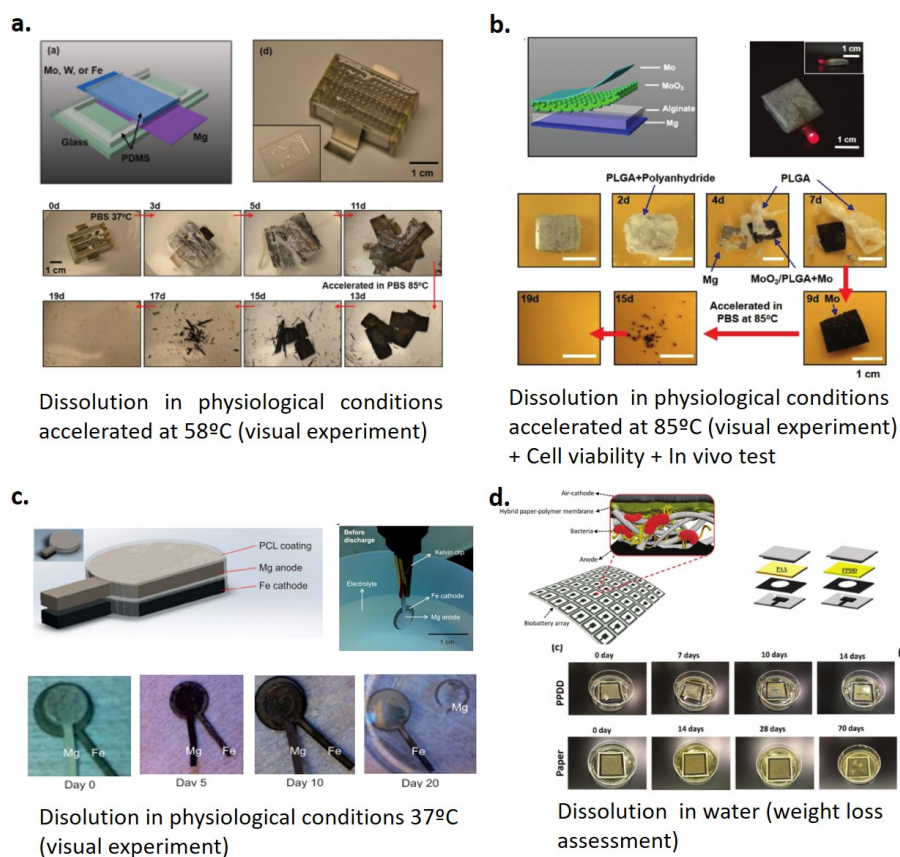


Figure 1.4: Batteries with an alternative end of life: **a.** Dissolvable battery with metal foils and polyanhydride packaging. Adapted from ref.³². **b.** Biocompatible and dissolvable battery with magnesium anode and molybdenum trioxide as cathode. Adapted from ref.³⁷. **c.** Dissolvable battery with Mg as anode and Fe as cathode. Adapted from ref.³³ **d.** Degradable battery with bacteria-based anode and nickel air-cathode. Adapted from ref.⁴⁵.

However, the self-appointed ‘*biodegradability*’ of these approaches relies on their capability to be disintegrated in tiny parts or even dissolved in ions and molecules. In these cases, biocompatibilityⁱⁱⁱ and/or bioabsorbability could be more appropriate

ⁱⁱⁱBiocompatibility is defined by IUPAC as “ability to be in contact with a living system without producing an adverse effect”. Both, organic and inorganic materials can be considered biocompatible, however in vitro culture experiments or in vivo implantation assessments are necessary to demonstrate biocompatibility of a material or device.

properties to claim, since dissolvability tests are reported at physiologic conditions and, in the case of Huang et al., even demonstrated within a Sprague–Dawley (SD) rat model.³⁷ In fact, in literature it is usually assumed that dissolution of biocompatible metals in river waters or soils is a sustainable end-of-life alternative. However, if this EoL was transferred to a battery production scale of billions, it is clear that it would suppose the loss of tons of irretrievable material together with the undesired accumulation of metal in terrestrial and aquatic ecosystems. Therefore, it is important to point out that only when the degradation trigger is the presence of microorganisms present in natural environments, the mechanism are enzymatic reactions executed by bacteria/fungi and the products are CO₂, H₂O, and simple molecules^{iv}, the degradation process can be called biodegradation, according to IUPAC^v⁴⁶ and regulated standards, in particular for EU, the standard EN 13432^{vi}. Figure 1.5 shows a schematic representation of a battery undergoing a biodegradation process. Thus, according to these regulations, only organic compounds can suffer biodegradability. In contrast, inorganic compounds can be considered at most bioabsorbable (if they can be assumed by a living organism), inert (if they do not cause an interaction), or toxic (if it causes a lethal effect at a certain concentration). Appendix B '*Standards and regulations*' of this thesis presents more in deeply the specific conditions and procedures established regarding biodegradability determination assessments.

In 2015, our group reported a metal-free organic redox chemistry-based primary battery, which biodegradability was successfully tested for the first time under a standardized protocol. Showing a biotic degradation measured by the conversion of initial total carbon mass of the material that is transformed into CO₂ and CH₄ (Figure 1.6a). This battery demonstrates that existing regulations to test biodegradability in materials could be adapted to assess complete devices.⁵⁰ Another approach has

^{iv}The above mentioned products of biodegradation are for aerobic conditions (presence of O₂), simple molecules refer to sulfides. In anaerobic conditions (absence of O₂) the products of biodegradation include CH₄.

^vIUPAC definition of biodegradation: "Breakdown of a substance catalyzed by enzymes in vitro or in vivo." <https://doi.org/10.1351/goldbook.B00656>

^{vi}Definition of biodegradation by the European standard EN 13432 "chemical breakdown of at least 90 % material into CO₂, water and minerals in six months by biological actions at 58°C". In this standard, the material conversion to CO₂ (i.e. biodegradation process) must be evaluated accordingly to ISO 17556 or ISO14855.^{47–49}

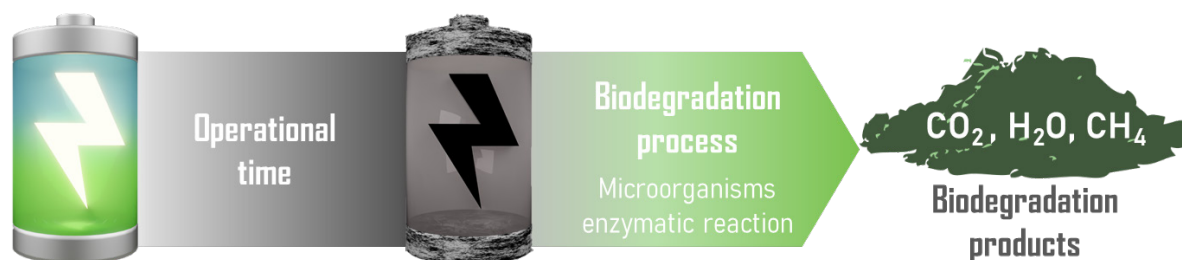
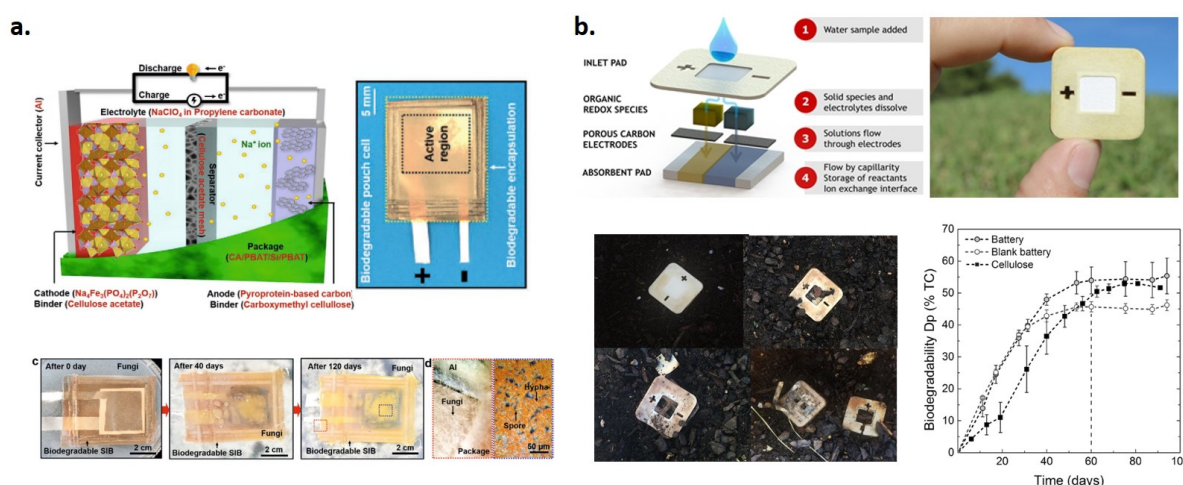


Figure 1.5: Schematic representation of the biodegradation process for a battery as established by regulated standards. Biodegradation assessment parameters, such as temperature, maximum process time and minimum degradation percentage, are specified on the standards and will depend on the type of biodegradation process pursued.

been recently published by M. H. Lee et al. in which a custom-made protocol to test a secondary battery biodegradability and toxicity was used (Figure 1.6b). A cytotoxicity cell assay was used to assess the toxicity of each battery component on biological systems, while at a macroscopic level non-toxicity was also demonstrated by burying the battery and growing a plant in the same soil.⁵¹



Hydrolytic and fungal biodegradation of battery components under self-established guidelines to verify the biodegradability and the non-toxicity of battery compounds via the cytotoxicity test

Biotic degradation test under standardized following the guideline of the OECD Test 31125 that comprises recommendations of other normalized tests (ISO,26 ASTM,27 US-EPA,28)

Figure 1.6: a. Biodegradable battery with redox organic based chemistry. Adapted from ref.⁵⁰ b. Biodegradable secondary battery based in sodium-ion technology. Adapted from ref.⁵¹

Batteries with a disruptive end of life represent a first attempt to minimize batteries' impact on ecosystems. However, as has been demonstrated, the lack of harmonized testing and regulations for batteries biodegradability assessment makes it difficult to

1.3. State of the art of portable batteries with a disruptive end-of-life

ensure battery safety for terrestrial ecosystems. Furthermore, the above reviewed works do not consider the carbon footprint on the rest of the life cycle stages, rising serious doubts on the overall battery sustainability.

Thesis Summary|

This thesis presents a new rationale for the development of sustainable portable batteries, the conceptualized ideas are then materialized with three disruptive primary battery concepts, each one designed on a different framework for an specific application. The work has been organized in 5 chapters: the current introductory chapter, a second chapter in which the disruptive rationale for batteries development is established, and then three experimental chapters each one devoted to a different battery development. Figure 1.7 depicts the contents and distribution of the thesis chapters.

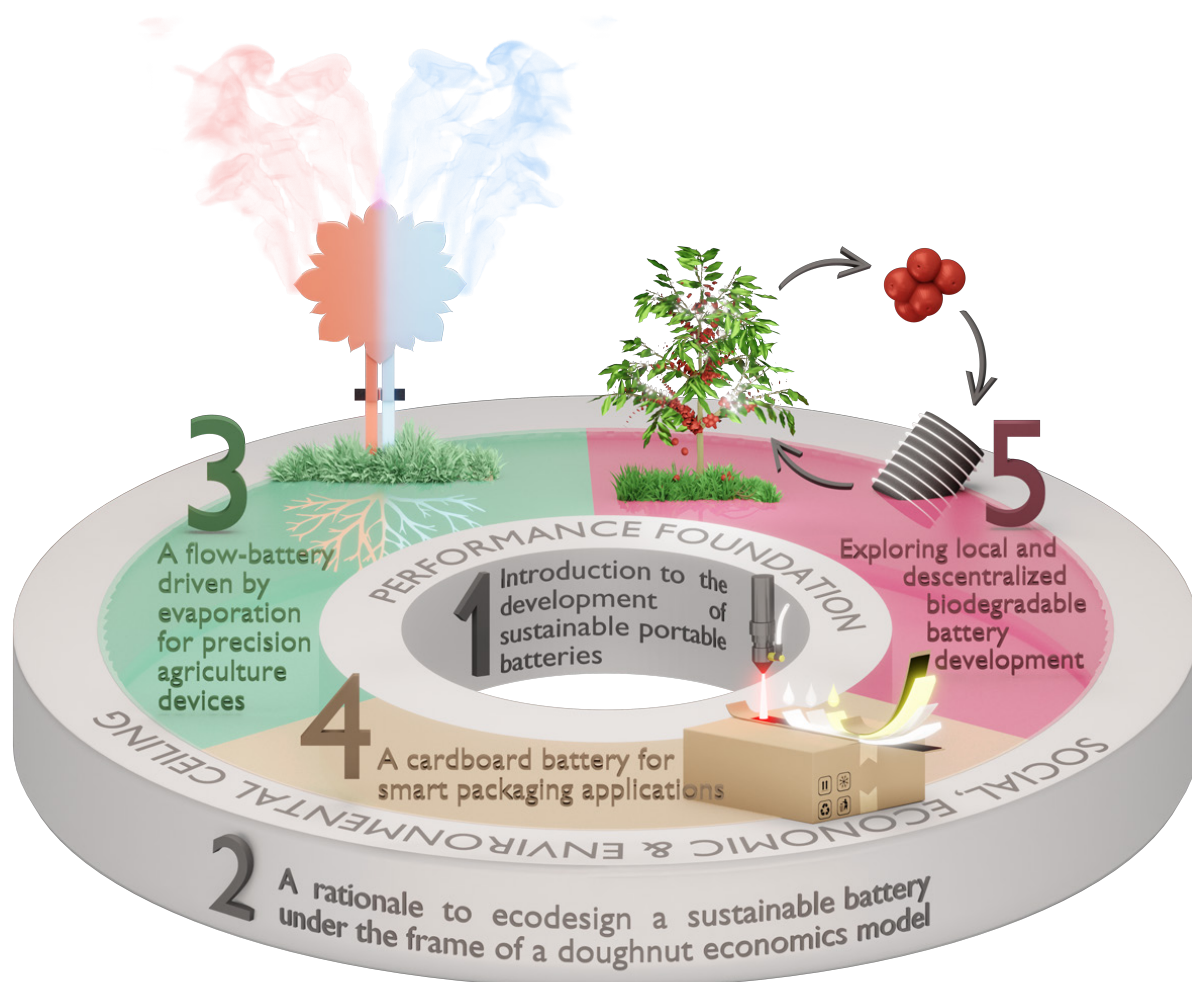


Figure 1.7: Schematic summary of the thesis chapters

After the introduction, the second chapter is devoted to the establishment of a rationale for ecodesign a sustainable battery. The approach is based on the *doughnut economics model* of the economist and professor Kate Raworth published in 2012. The rationale adapts the concepts of planetary and social boundaries to battery research creating a doughnut shape model for battery development that aims to track, minimize and eliminate battery environmental impact while meeting the application requirements. As a strategy, the complete life cycle is analyzed and redefined under ecodesign principles and advocating for a 'tailor-made' approach in such a manner that the battery ends up integrated into the application value chain.

This thesis follows with the materialization of three sustainable battery prototypes conceived under the rationale presented in Chapter 2. All three prototypes invoke a change in the current portable batteries model, pursuing -and implementing at different grades- the proposed battery paradigm, in which power sources are designed to be paired with the life cycle of the intended application. At the beginning of each chapter the conceptualized life cycle for each battery is presented, then each particular work describes the research performed around the battery prototype development and demonstrates the technological feasibility of the concepts proposed by this new rationale.

In particular, the third chapter is devoted to a biodegradable flow-battery driven by evaporation. The battery working principle resembles plant's nurture mechanisms, harvesting its nutrients from the soil and pulling them upwards through the stem, towards the leaves. There, the fluidic system mimics nature by using the transpiration pull to maintain the reactants flow and generate energy. Intended for precision agriculture and fabricated from commercial materials, the prototype has successfully demonstrated to be able of powering a plant monitoring unit. Finally, this chapter presents a dedicated assessment testing the environmental harmlessness of the battery at the end of its operational life.

Chapter 4 introduces a battery intended for smart packaging application. Again, the battery life cycle is aligned with the application value chain, consequently paper and cardboard recycling is proposed as disruptive end-of-life. In order to fulfill the EoL requirements, this chapter revolves around the development of the materials that

compose the battery. In particular, laser induced graphene over cardboard is assessed as current collector and an ionic conductive bio-based hydrogel is presented as battery matrix to contain the active species. Additionally, the selection of fabrication processes has been performed pursuing compatibility with already established cardboard box fabrication, thus bypassing the need of a battery distribution stage. Finally, the electrochemical characterization of prototypes implementing the best performing materials is presented.

The five, and last experimental chapter, presents the more ambitious battery concept of this thesis. In it, the possibility of local and decentralized battery development is explored. The conceptualization of the battery is located in coffee-growing communities in Chiapas, Mexico. In these regions there is a lack of proper battery recycling, thus the development of a biodegradable battery becomes especially appealing. First, the project viability has been assessed through interviewing and sharing it with the local population. This way, the project framework has been created by embracing local people's needs and aspirations, to conceive a sustainable battery for which fabrication processes can be implemented in the communities. As a proof of concept, the battery, able to power portable lighting systems, was fabricated and tested 'in situ'. In parallel, the possibility of directly fabricating the battery from coffee agro-waste has been investigated. Revalorization practices are introduced to recover biopolymers and phenolic compounds that could act as matrix and active species. Finally, the project impact through a custom-made social impact factor is assessed demonstrating from a local perspective the project's potentiality and relevance.

Lastly, general conclusions of the work are presented, highlighting the thesis most meaningful contributions to the scientific community.

2

**A rationale to ecodesign
sustainable batteries based on
the doughnut economics
model**

In 2012, the economist and professor Kate Raworth published an Oxfam discussion paper entitled 'A Safe and Just Space for Humanity'.⁵² In it, Raworth presented a framework for humanity sustainable development by combining the concepts of planetary and social boundaries.

Her theory, known as the doughnut economics model because of its graphical representation by two concentric circles, balances essential human needs (represented as an inner boundary called 'Social Foundation') and environmental degradation (depicted as an outer boundary named 'Environmental Ceiling'). Between these two boundaries lies an area that, according to Raworth, represents the environmentally safe and socially just place for humanity to thrive in balance (see Figure 2.1). The social foundation comprehends those resources needed – such as food, water, health care, or energy - to protect societies from critical deprivation and ensure life is lived with dignity, opportunity, and fulfillment. While the environmental ceiling sets planetary boundaries that sustain the benevolent environmental conditions achieved during the Earth's stable state period known as Holoceneⁱ. In order to define the dimensions of the ecological ceiling, Raworth used the planetary boundaries previously proposed by an international group of Earth-system scientists led by Johan Rockström and Will Steffen; whereas the social foundation comprises 12 social dimensions derived from the priorities specified in the United Nations Conference on Sustainable Development, Rio+20 (see Table 2.1).

ⁱHolocene is the current geological epoch, defined as an interglacial period in which planet Earth enjoys a stable state characterized by proliferation and growth of species worldwide. Researchers from different areas have alerted that current fossil fuel emissions and nature destruction activities are pushing Earth's away from Holocene preservation state. J. Hansen et al. (2013), "Assessing Dangerous Climate Change: Required Reduction of Carbon Emissions to Protect Young People Future Generations and Nature".⁵³

Table 2.1: Dimensions of human deprivation below the social foundation and dimensions of environmental degradation beyond the environmental ceiling according to the doughnut economics model by Kate Raworth.⁵²

SOCIAL FOUNDATION DIMENSIONS	ECOLOGICAL CEILING DIMENSIONS
Water	Climate change
Food	Ocean acidification
Health	Chemical Pollution
Education	Nitrogen &
Income & work	phosphorus loading
Peace & justice	Freshwater withdrawals
Political voice	Land conversion
Social equity	Biodiversity loss
Gender equality	Air pollution
Housing	Ozone layer
Networks	depletion
Energy	Climate change

Among others, Raworth condemns the excessive attention given to the Gross Domestic Product (GDP) as a solo economic indicator to quantify countries' prosperity. Pointing out how such fixation on an ever-growing GDP as a goal has failed to reflect other important societal wealth metrics, such as the continuous degradation of ecosystems or the invaluable but unpaid work of carers. Ultimately, Raworth's theory evidences the necessity of providing a global perspective that takes into account all the dimensions at environmental, social and, economic level when developing a truly sustainable model.

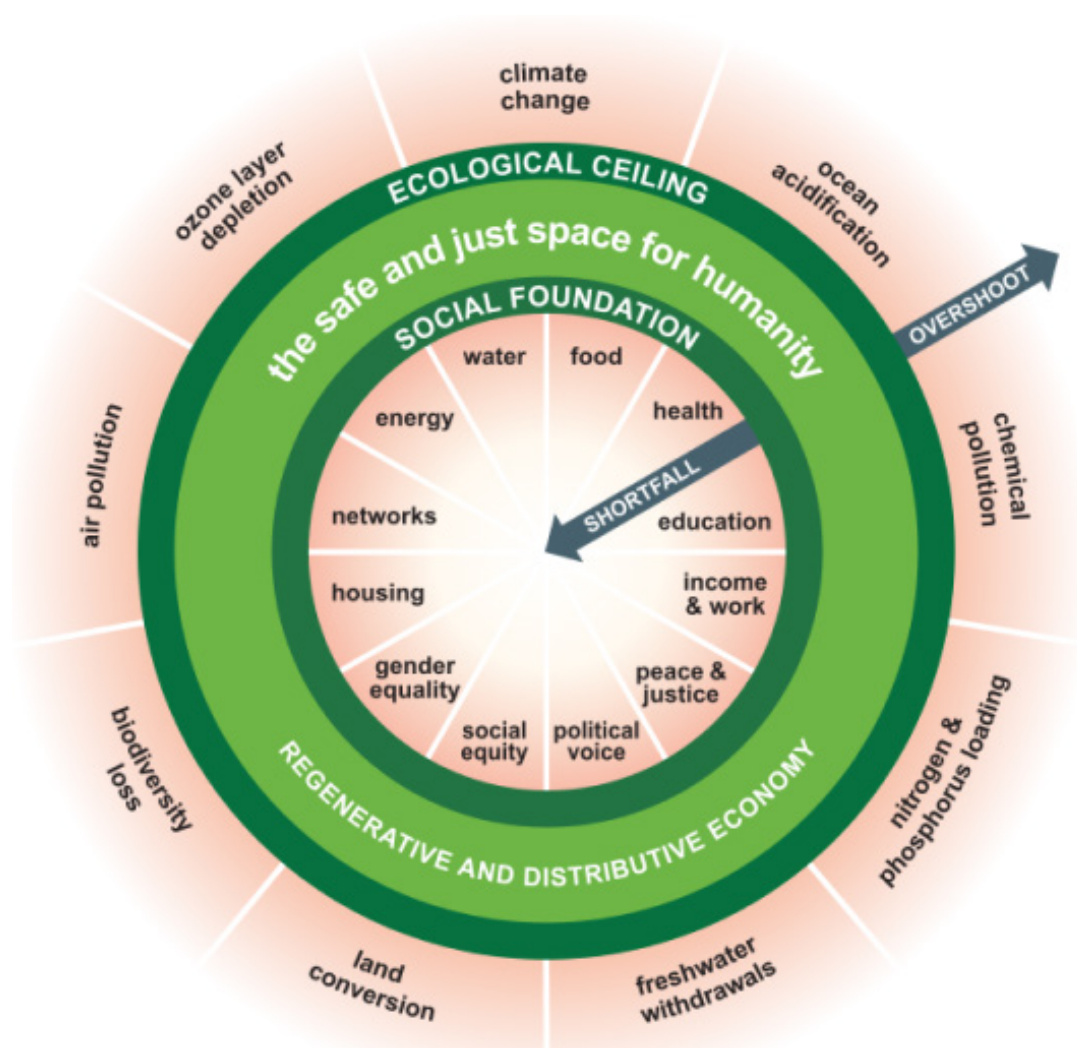


Figure 2.1: The Doughnut of social and planetary boundaries. Source: 'A Safe and Just Space for Humanity' from Kate Raworth.⁵²

2.1 Batteries inspired by the doughnut economics model

As mentioned in the previous chapter, there is a lack of legislation and efficient methods for portable batteries to be recovered and processed, which is leading to an irreversible ecosystem degradation. In view of this perspective, tightened environmental laws and appropriate recycling infrastructure are urgently needed. However, the development of those mechanisms is complex and sluggish, and it is very unlikely that their implementation can keep up with the increasing demand for portable power sources. In this sense, applying the doughnut economy approach to batteries development appears to be a promising way to meet the technological needs of society without compromising future generations.

Looking into Raworth's macroeconomics observations, one can find enormous similarities with the way battery development has been approached up to date. From materials screening to structures and geometries exploration, the main objectives of portable battery research have been to increase battery power, to achieve higher energy densities, and, in the case of secondary batteries, to gain in cyclability. But this excessive attention given to battery performance has overshadowed other relevant indicators. Meaningful metrics such as scarcity of raw materials, energy consumption, and complexity of manufacturing methods, equipment required, hazardousness of secondary materials involved (i.e. solvents), or recyclability of the design, suffer from a pathological lack of attention. In fact, such focus on battery performance, in terms of power and energy density, has completely ignored the indicators of the value chain that set the sustainability of the battery across technical, environmental, economic, and social dimensions. This comprehensive understanding of sustainability suggests that, rather than traditional goal-based approaches, sustainability is a system property that requires a process-based systemic approach to plan and guide it, as defined by F. Ceschin and I. Gaziulusoy.⁵⁴

This thesis proposes to create a systemic approach inspired by Raworth's theory to guide batteries development. Thus, a doughnut shape model applied to battery research and development has been drafted, setting a social, economic and

Table 2.2: Sustainable space for batteries development accordingly to the approach proposed in this thesis. The six dimensions that define the performance foundation are usually used by researchers and companies to measure commercial viability and competitiveness of a portable battery. The six dimensions of the social, economic, and environmental ceiling have been established by the authors to ensure battery sustainability across its three pillars.

PERFORMANCE FOUNDATION DIMENSIONS	SOCIAL, ECONOMIC AND ENVIRONMENTAL CEILING DIMENSIONS
Energy density	Materials toxicity
Power density	Ethical supply chain
Competitive manufacture	Low energy and resources consumption
Portability	Materials abundance
Operation time	Economically affordable
User-friendly	Cost-effective end-of-life

environmental ceiling and a performance foundation (See Figure 2.2). The performance foundation is composed by the six indicators researchers and companies usually use to measure commercial viability and competitiveness of a portable battery. While the ceiling has been established by the authors to ensure batteries sustainability in social, economic, and environmental dimensions (See Table2.2). As depicted in Figure 2.2, by bringing together the two approaches a safe and sustainable space for portable batteries naturally emerges.



Figure 2.2: Defining a sustainable space for batteries development. The six dimensions that define the performance foundation ensure the power supply for the portable battery application. The six dimensions of the social, economic and environmental ceiling prevent the battery to exceed the natural planetary boundaries and ensure a just and accessible technology.

By ensuring the fulfillment of the six environmental ceiling dimensions, this change of paradigm aims to track, minimize and, ideally, eliminate the battery environmental impact through careful device design and development. While at the same time, meeting the application minimum requirements in terms of power and operation time. Advocating for a 'tailor-made' approach, the development of such batteries should be coupled with the device value chain, in such a manner that even the power source end-of-life could follow the device's one. However, to move into the sustainable space for batteries development is complex because the performance and the social, economic and environmental dimensions are interconnected. For instance, a competitive manufacture might require processes that are energy intense. Hence, the production and implementation of portable batteries in a responsible way are only possible if a balance of the whole life cycle is taken into account. This section proposes a research methodology that takes into account the application's energy demand as a cornerstone. This 'tailor-made' approach sets a clear performance foundation from the very beginning of the battery conception. From there, ecodesign is used as linchpin to ensure the fulfillment of the six ceiling dimensions. Applying the doughnut economics model perspective to the batteries' value chain brings forward an opportunity to rethink their entire life cycle, as will be demonstrated in subsequent chapters. Therefore, the framework exposed in this section is the thesis backbone and sets the approach to battery development within this work.

2.2 Key tools to ensure portable battery to stay within the sustainable development space

Ecodesign is a Design for Sustainability (DfS) approach that focuses on lowering the environmental impact of a product throughout the whole life cycle. From raw materials extraction to final disposal, it integrates environmental aspects into the product development process, balancing ecological and economic requirements.⁵⁴ In this sense, ecodesign vision is an essential approach to ensure that portable batteries stay within the social, economic and environmental ceiling and performance foundation. Since, it ensures that the whole battery life cycle (i.e. materials, fabrication, distribution, application and end-of-life) is taken into account from the early battery conception. It is worth to mention that, the implementation of Life Cycle Assessment (LCA) could bring essential and specific metrics to quantify the suitability and effectiveness of the ecodesign process. LCA is a standardized methodology for assessing the potential environmental impact associated with a product or a service over its entire life cycle. This assessment technique provides a holistic view of environmental interactions that will take into account ecological, social, and human health impacts of material consumption and environmental releases to air, water, and land associated with specific manufacturing and distribution processes on local, regional and global scales. The results from LCA would include an estimate of the carbon footprint of developed batteries to benchmark its impact based on standardized and comparable metrics.^{55–57} Ecodesign of batteries would then use this output to make decisions on materials, manufacturing methods, and form factors according to the specific requirements of the application to be powered.

The methodology proposed implements three main aspects to consider during the ecodesign and at each stage of the battery life cycle (conceptualized and adapted from Raworth's theory):

1| An integrated vision: Societies need portable energy, and its demand is expected to significantly increase in the upcoming years. However, while creating wealth, scarce material dependence and costly production methods could lead to inequitable access to battery technology. Sustainability awareness at environmental, social, and

economic dimensions ensures the creation of a fair access to the technology.

2| A refocusing of priorities: Energy demand intensification would increase raw materials and natural resources exhaustion, if not properly managed. Environmental stress must not be seen as a collateral damage, but rather as a decisive assessment to guide battery development.

3| Metrics beyond performance: Batteries should not be ranked exclusively in terms of technical performance. A criteria to provide a holistic evaluation of a battery advantage in all dimensions must be developed by researchers and demanded by consumers. Such criteria should incorporate innovative indicators to assess battery sustainability, as its adequacy for a particular application, ease to be recycled, or efficacy in terms of material utilization.

Gathered hereinafter are exposed the proposed rational pillars, a set of good practices, recommendations, and guidelines to consider at each of the battery life cycle stages to ensure the battery life cycle to stay within the safe space for development as shown in Figure 2.3.

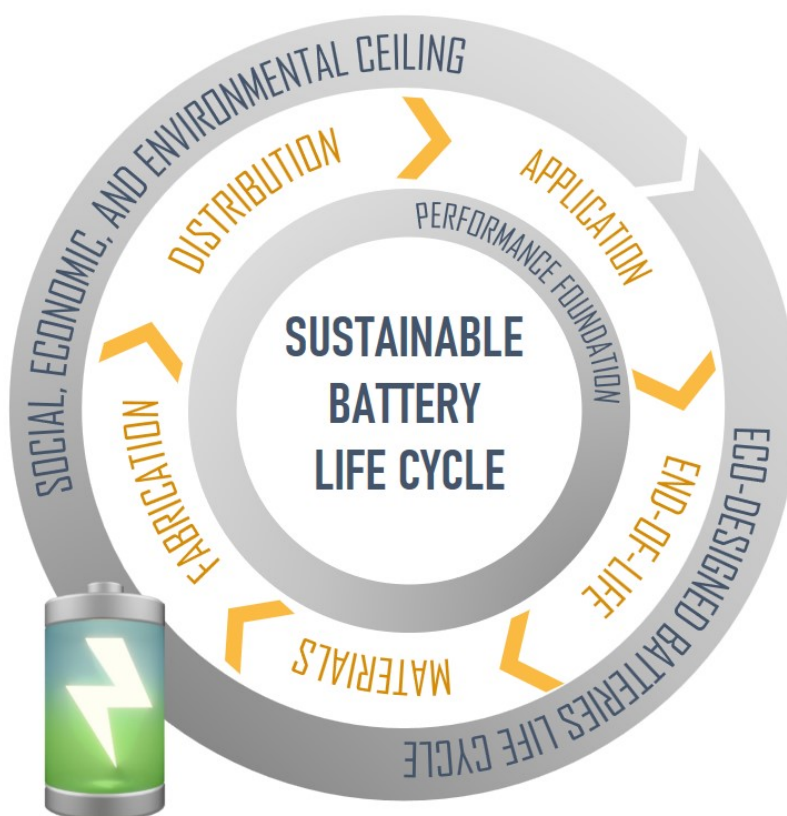


Figure 2.3: Batteries life cycle implementation within a doughnut model of sustainable development.

MATERIALS

Conventional portable batteries have a dependence on materials with supply chain risk. Materials abundance and geographical origin is rarely prioritized against material performance, when analyzing their suitability for an application. Focusing on battery chemistries, current battery technologies rely on toxic and flammable compounds that involve aggressive and hazardous processing that produce toxic by-products and demand stringent safety measures, during their extraction, processing, and end-of-life. Materials selection is the most critical step during a battery conception and design, since it largely determines the battery performance in terms of energy density and operational time. It also affects battery sustainability in terms of toxicity, cost-effectiveness, and affordability. An ethical supply chain is also largely determined by the material selection stage. There are some key points that battery materials research must assess to ensure battery performance while staying within the ceiling:

Screening of chemistries – Selection of suitable chemistries based on metrics such as non-toxicity, availability, and compatibility with proposed end-of-life scenario. More eco-friendly and abundant chemistries already identified for large-scale applications such as Na-ion and Zn-air batteries would provide the starting point for this approach. But also the exploration of organic chemistries (e.g. quinones, vitamins, imides) could provide a feasible alternative that would reduce the current dependence on inorganic chemistries.

Optimal raw materials utilization – According to the features required by the application, the amount of electrochemically active material should be addressed. By adjusting the available energy to avoid material waste while ensuring a sufficient power supply.

Alternative materials sources – Identify and explore battery materials beyond critical raw materials or materials with supply risk currently used in commercial batteries, e.g. Li metal-fluorine (Li/CF_x), manganese (Zn/MnO₂), nickel-metal hydride (NiMH). Alternative sources such as bioderived, recycled or repurposed secondary raw materials would represent great sources.

Subsequently, the exploration of novel extraction and recovery processes based on green chemistry and low energy consuming methods must be implemented.

As mention above, life-cycle assessment could represent a key methodology specially for material selection. The results of a LCA could be used to prioritize the use of one material over another that behaves similarly in terms of performance, providing specifically environmentally conscious metric. The LCA can be used as an iterative tool to assess different materials, while fixing others that are compulsory due to application requirements or performance reasons.

All in all, materials selection must be carried out without neglecting the application power needs but prioritizing sustainability metrics that ensure the optimum selection for each application.

FABRICATION & DISTRIBUTION

Current manufacturing processes of batteries are complex, energy intensive, and usually centralized, mostly in Asia. Transportation of materials to the fabrication sites and then of batteries to the world contributes to a large carbon footprint. Life cycle assessment studies of alkaline batteries account the majority of greenhouse gas emissions to processes related to material extraction and cell manufacturing. Battery design should be carried out leading towards the implementation of cost and energy efficient manufacturing methods. Defining sustainable and affordable fabrication processes will ensure the development of an accessible and inclusive technology, both at economic and social dimensions. Key points that should be address while creating/improving the manufacturing process include:

Energy efficient fabrication – implementation of manufacturing methods based not only on the monetary cost but on the energy efficiency, leading to minimization of the carbon footprint associated.

Clean battery production – prioritize processes with the lowest amount of by-products needed and minimize waste production. Active research on re-use and re-integration methods for produced by-products or reagents is needed. Cost-effective and clean manufacturing can also be tackled from

materials selection and implementation; by prioritizing those materials with lower working temperature or minimizing the use of reagents needed during material processing.

Decentralized manufacturing – efficient processes from Industry 4.0 can be implemented and reproduced locally, leading to a decentralized battery production model. The geographical democratization of battery production would avoid the creation of monopolies since batteries could be produced with available raw materials, distributed, consumed, and repurposed locally, fostering local industrial growth and competitiveness.

Implementation of best practices and policies – foster open innovation to fit with upcoming sustainable regulatory frameworks, and also promote and ensure an ethical fair trade supply chain, that avoids social and political conflicts.

The overall objective of the re-definition of batteries manufacturing routes should be introducing indicators beyond monetary cost. Energy-efficient, waste production, resources consumption metrics should be properly quantified to ensure cost-effectiveness at an environmental, social, and economic level. The implementation of such indicators should lead, ultimately, to the development of an accessible, and inclusive technology.

APPLICATION

Current battery technologies have made progress in their industrialization to reduce production costs. However, this mass production strategy has ended up causing a widespread use of standard-size portable batteries in products, which have based their battery choice on price rather than power requirements. Consequently, sometimes batteries are oversized in terms of power and energy capacity (as in medical single-use tests), implying that they are disposed of before their complete depletion. In other cases, batteries are undersized, provoking excessive need of replacement and structural materials waste (as in hearing aid devices). Moreover, conventional batteries have been optimized for continuous operation and include elements to reduce leakages and overloads over the long periods of time required by

2.2. Key tools to ensure portable battery to stay within the sustainable development space

non-disposable applications. These features are implemented using a wide range of materials from metallic casings, springs, rubber gaskets, paper/polymer separators, spacers, sealants, plastic/metal pouches, etc; which are not always necessary, for instance in short time use applications. Technology integration with a holistic vision is only possible if, during the battery design, the application is taken into account. A tailor-made battery model would aim to ensure the following points:

Tailored design – adapting energy and power to the demands of the application would consume only the required amount of materials, and therefore efficient material utilization would be ensured. The use of additive manufacturing techniques from Industry 4.0 would enable a high level of design customization.

Operating conditions – the faradaic and energy efficiencies quantify the total amount of chemical energy stored in a battery that has been converted to useful electrical energy. These metrics strongly depend on the operating conditions in which a battery is forced to work. Careful examination of application energy demands would allow maximizing active material utilization of the battery during the operation stage.

Operating time – batteries research and development invest great efforts to ensure long and steady operational time. It is often that, while operational, novel battery technologies are discarded in their development phase due to short shelf and operational lifetimes. However, many single-use applications in sectors like portable diagnostics or precision agriculture could benefit from those short-term battery technologies.

Considering the requirements of the application from the beginning of the battery conceptualization would allow adapting battery features such as materials, geometries, operational conditions, and stored energy; which would lead to improving the overall efficiency.

END-OF-LIFE|

Battery recycling requires costly and complex infrastructure. Furthermore, the recycling rates through conventional waste streams are hardly met. Finding

alternative EoL scenarios for batteries could help to ease the load on current recycling facilities while decreasing the environmental impact of improperly discarded batteries. When looking for an appropriate EoL the following points may be useful:

Paired EoL – When considering the target application, the whole life cycle of the product that is being powered can be taken into consideration to match their EoL. On top of that, if the operational time of the product and the battery are very different, the usage scenario can be done considering to adequate the battery EoL to lack or existence of proper recycling facilities.

Reduce, Reuse... and Recycle – Reducing waste materials or products would undeniably reduce their impact. Similarly, reusing them, as long as the quantity of new material and energy resources needed to restore is reasonable. However, recycling implies an energy-consuming process and therefore its benefits depend on the specific product and materials to be recovered. As demonstrated by Linda Gaines, it is important to analyze deeply, and case-by-case, the pros and cons of recycling, to fully understand the involved impact tradeoffs.⁵⁸

Alternative EoL scenarios - As exposed in Section 1.2, batteries can have EoLs as disruptive as biodegradability. Developing different paradigms for battery EoLs, and properly implementing them according to the life cycle of the application, would provide a diversity of viable waste streams that turn used batteries into valuable raw materials or a safe return into nature.

Identifying alternative End-of-Life scenarios in which batteries consider the whole life cycle of the product they are powering can provide a more positive carbon footprint. Biodegradable batteries could eventually be processed as compost (domestic or industrial) or even undergo degradation on soil. The feasibility of this approach must include assessment of biodegradability in laboratory and field conditions, as well as the ecotoxicological impact of discarded batteries in soils for organisms. These characterizations would allow the total computation of environmental impact of the entire battery life cycle.

2.3 Batteries for a global sustainable development

From a global perspective, this battery development approach is in full alignment with the Sustainable Development Goals (SDGs) defined by the United Nations. It specially addresses SDG7 (Affordable and Clean Energy), but also has a relevant impact on SDG9 (Industry, Innovation and Infrastructure), SDG11 (Sustainable Cities and Communities), SDG12 (Responsible Consumption and Production), SDG13 (Climate Action) and SDG17 (Partnerships for the goals).⁵⁹

The technologies created according to this approach would not only produce sustainable power source alternatives for applications in developed regions in the world but would represent a paramount solution for low resource settings in the world. According to the Energy Progress Report, which provides a global dashboard on progress towards Sustainable Development Goal 7 (SDG7), about two billion people – around 1 in 4 people in the world – currently live with no or limited access to electricity. Of those, 860 million people, mostly located in rural areas, live completely without electricity.⁶⁰ The relation between a life with limited access to electric power and the influence that the technology proposed in this thesis could have on living standards is profoundly analyzed in the Chapter 5.

Due to the tailor-made nature of the prototype batteries develop of this thesis, each chapter has its specific relation with the SDGs, Figure 2.4 visually shows these connections.



Figure 2.4: Sustainable development goals in relation with each chapter of this thesis.

Conclusions|

This chapter presented a systematic approach to undertake battery development from a social, economic, and environmental sustainability standpoint. The doughnut economics model principles proposed by Kate Raworth have been used as inspiration and applied, for the first time, to battery technology. A new rationale for battery research and development has been created by setting a social, economic, and environmental ceiling and a performance foundation. Furthermore, ecodesign has been identified as the essential tool to ensure the batteries to stay within the established boundaries, and the key tools, practices and enablers to be applied in each life cycle step have been exposed.

The work presented hereafter constitutes the first steps for the implementation of a sustainable battery development. In order to demonstrate the feasibility of the approach, three novel primary battery concepts have been conceptualized and materialized, tackling two disruptive end-of-life, biodegradability and recycling with paper and cardboard. However, it must be noticed that, the rationale exposed above has been generated from the practices, knowledge and thoughts arisen along the whole path of this thesis. And for this reason, the materialized batteries might not gather all the complexity and fulfillment presented in the rationale. However, its development has been performed under an integrated vision, by refocusing the priorities and giving the proper attention to metrics beyond the performance.

Furthermore, it is worth mentioning that the given recommendations and guidelines can be implemented on any battery but it becomes especially relevant in disruptive technologies that are introducing alternative end-of-life scenarios, such as biodegradability or recyclability with other waste streams. In those cases, all materials used as electrodes, electrolytes, or structural components would be non-toxic and selected to meet the specific end-of-life requirements and safe and scalable manufacturability. This set of prerequisites would lead to choose materials without supply chain risk and move towards materials obtained from a sustainable bioeconomy and recovered from recycling processes. A combination of bioderived organic species, electrolytes, biopolymers, and carbon-based electrodes comprising

the batteries would result in a battery waste that can nurture soil or restore natural systems, radically changing the current battery paradigm. Energy and cost-efficient manufacturing methods from Industry 4.0 would then allow a decentralized local production and consumption model, in which batteries would not have to travel long distances to reach their destination but rather be constructed, distributed, consumed, and repurposed locally, fostering local industrial growth and competitiveness.

This methodology has been created from the point of life of batteries, a critical element in electronic devices and consequently in electronic waste. The same exercise can be carried out in the development of complete devices and systems. The advances in green electronics have already demonstrated the potential to generate devices that could also be biodegradable, and in this way, the whole system could then follow the same waste stream. However, the ambition is that the methodology proposed here becomes the starting point of an open discussion that defies unsustainable practices in battery development. Therefore, this methodology is subject to be continuously improved and updated with contributions from battery developers around the globe and turn into a beacon for the implementation of a new paradigm of portable batteries based on a holistic sustainability approach that satisfies the portable power needs of humanity without compromising our environment.

3

A flow-battery driven by evaporation for precision agriculture devices

Overview

This chapter presents a flow battery profoundly inspired by nature, which mimics fluid transport in plants to generate electric power. Figure 3.1 schematically depicts the battery life cycle, within the frame of the doughnut methodology presented in Chapter 2, i.e. under the sustainability ceiling and over the precision agriculture (PA) required performance foundation.

The battery, made from commercially available materials, represents the first steps towards the materialization of the proposed methodology. Ecodesigned for PA applications, biodegradability has been matched as an alternative end-of-life scenario. Accordingly, the materials selection has been carried out to enable this EoL, while prioritizing low environmental cost and energy-efficient fabrication processes. The prototype practicality has been demonstrated by powering a wireless plant caring commercial device. Furthermore, standardized biodegradability and phytotoxicity assessments show that the battery is harmless to the environment at the end of its operational lifetime. Validating this way its being at the safe space between the projected inner and outer boundaries.

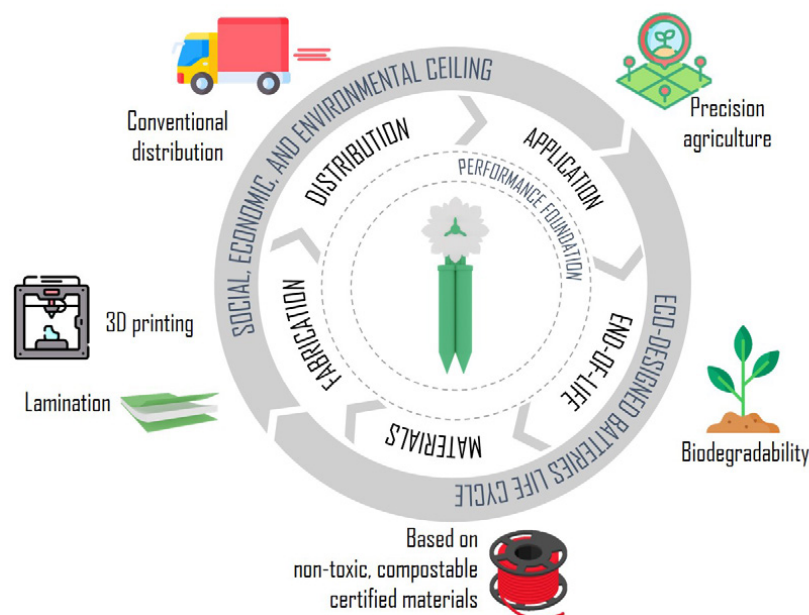


Figure 3.1: Sustainable battery life cycle envisioned for precision agriculture applications.

3.1 Introduction

Agriculture needs a new paradigm. With a worldwide population predicted to reach 9 billion inhabitants by 2050⁶¹, it is likely that the overall food demand will continue to grow. To meet this demand, ever-increasing crop yields are required. Nevertheless, it is today widely recognized that the intensive use of agrochemicals (e.g., fertilizers, pesticides, etc.) that have been utilised so far to boost food production, is not sustainable in the long term. Intensive agriculture based on high inputs of chemicals proves to be one of the major drivers of soil degradation, pollution of natural water resources, and biodiversity loss. In this regard, wireless sensor networks (WSNs) can already help growers to adapt their practices and shift towards precision agriculture (PA). In a nutshell, WSNs for PA are based on a collection of individual nodes deployed across agricultural lands to monitor a variety of local parameters (e.g., air temperature, soil moisture, soil PH, salinity, light, etc.). Measurements are then used to derive microclimate conditions and/or detect variability among different parcels. This way, instead of treating uniformly (and sometimes unnecessarily) a whole field, growers can better apply the right amount of inputs, at the right place and at the right time. To the best of our knowledge, however, WSNs for PA are deployed in a limited number of agricultural settings; mainly those whose configuration stays relatively unchanged from season to season (e.g., vineyards,^{62,63} olive groves⁶⁴ or orchards^{65,66}). Comparatively, there is a scarcity of works reporting the use of WSNs in cereal crops (e.g., wheat, millet, quinoa, etc.). From our personal analysis, a plausible main reason that hampers a wider adoption of WSNs in cereal crops is that nodes may actually constitute obstacles to be avoided during harvesting. Recollecting tens or even hundreds of nodes before harvesting, however, is not a plausible option. In the future, low-cost nodes that could just be left in the soil indefinitely without negatively impacting the environment could bring innovative solutions to such limitations. Nevertheless, there are several technological challenges to be tackled to turn such an ideal case scenario into reality. One of the major hindrances is that current nodes are far from being eco-friendly. In particular, the power source turns out to be a major source of potential pollution. At present, most nodes in PA are battery-powered. Commercially available batteries, however, are

loaded with heavy metals and/or toxic chemicals (e.g., lithium, cadmium, manganese, copper, zinc, etc.) which prove to be highly detrimental to the environment.⁶⁷ The use of solar panels, wind generators, or hydro-generators connected to irrigation pipes was reported for supplying power to nodes in PA.⁶⁸ Nonetheless, such energy harvesting devices cannot be used on their own. Indeed, they solely produce electrical energy sporadically (i.e., if it is windy, if it is not too cloudy, etc.). As a direct consequence, they actually serve exclusively as auxiliary recharging units to prolong the batteries' lifespan. Since conventional batteries are still needed, the situation is actually even worsened from the point-of-view of the environmental impact. For instance, solar panels also include a variety of hazardous materials.^{69:70} Generally speaking, the end-of-life of electrical electronic equipment (i.e., their disposal, dismantling, difficult and limited recycling) has already started to arise alarming societal concerns. The deployment of new digital technologies in PA should not come at the price of an additional uncontrollable electronic waste burden. Because batteries are considered as one of the major sources of e-waste, novel sustainable power sources are needed to enable a more massive deployment of WSNs in PA.⁷¹

In the context of PA, new battery architectures featuring nature-based characteristics appear especially appealing. This is the case for microfluidic galvanic cells (μ GCs). We here refer to μ GCs as miniature fluidic devices that can produce an electric current by means of a redox reaction, such as membraneless microfluidic fuel cells (μ FCs) or microfluidic redox flow cells. One of the great advantages of μ GCs is that they can generate electrical energy using a variety of reactants, including biofuels^{72–76}. For instance, μ FCs exploiting methanol, ethanol, or glucose as fuels were reported^{77–85}. The possibility to drive low-consumption electronic systems, including wireless sensors, was also demonstrated⁸⁶. μ GCs have thereby been envisioned as promising candidates to replace small conventional primary batteries. Unfortunately, even after almost two decades of intense research efforts, μ GCs have not succeeded in leaving the lab bench yet. The problem is that syringe pumps or pressure controllers are required to drive the reactants towards the electrochemical reactive zones inside the μ GCs. Such auxiliary external pieces of equipment are bulky and expensive. Even worse: they may consume more electrical energy than the μ GCs can actually produce. To get rid of the external pumping systems, the scientific

community has come up with μ GCs made of paper materials (See Appendix A, Subsection A.2 *Paper as capillary structure in microfluidic flow batteries*). Paper can indeed serve as a low-cost passive pumping mechanism because it can absorb and drive liquids through capillary action^{87;88}. Paper-based materials are even more appealing for PA because they are nature friendly (e.g., cellulose can be made of fibers coming from corn straw, bamboo, bagasse, grass-plants like reeds, etc.). Nonetheless, if paper offers a very simple and elegant solution to bypass the use of external pumps, many paper-based μ GCs still make use of critical raw materials to produce electricity (e.g., platinum, palladium, platinum-ruthenium alloy, etc.)^{75;89}. The use of such noble metal catalysts does not align well with an ideal circular sustainable approach. Although a paper-based μ GC using enzymes as biocatalysts was reported to be capable of driving a digital clock⁹⁰, the well-recognized restricted stability of enzymes over time appears as a strong limiting factor for targeting real PA applications. Moreover, enzymes are often most active solely for a precise range of temperature^{91;92}. However, unlike in indoor environments, strong variations in ambient conditions over days/nights (e.g., temperature, humidity, etc.) must be expected in an open field. In 2017, our group reported the PowerPAD⁵⁰. Different from the paper μ GCs previously reported, the completely all-organic PowerPAD architecture did not involve the use of any metals or enzymes. As has been discussed in Chapter 1, the authors assessed and validated that the battery could be biotically degraded by microorganisms. This represented a significant step forward, since it means that the battery could be discarded in a field with a minimal environmental impact. A limitation of the PowerPAD, however, was that electricity was produced mainly through a diffusion process which limited the overall battery efficiency. More recently, the same group reported an enhanced design where the battery performance was increased by exploiting quasi-steady capillary flows⁹³. Despite the gain of performance obtained, the operational lifetime remained limited: in both designs, the batteries could generate electric energy only for a few hours. Unfortunately, this is too restrictive for targeting PA applications.

This chapter introduces the FlowER: an Evaporation Flow Redox battery intended to bring new solutions to some of the challenging requirements imposed by PA applications. Environmental sustainability has been placed as the core priority to

create a disruptive technology that can evolve within the environmental boundaries of the planet. In this process, ecodesign was used as a fundamental tool, from materials selection to disposability considerations – including manufacturing processes, operational time, and energy capacity – to create a prototype that meets PA-lifecycle requirements, namely: affordability, extended operational lifespan, and biodegradability. The overall architecture of this new battery is profoundly inspired by nature: both its appearance and the way it operates make it a true “flower-like” battery (see Figure 3.2). The “roots, stem as well as petals/leaves” are all made of low-cost paper-based materials. An absorbent pad, placed on the top of the FlowER, exploits evaporation combined with cohesion and capillary forces in a way analogous to transpiration pull in plants. Liquid reactants contained in reservoirs can thereby flow continuously through porous carbon electrodes where electrochemical reactions take place. Notably, the operation time -which usually ranges from solely tens of minutes to a few hours maximum in conventional paper-based fuel cells- can be significantly extended. Further, the harmless green chemicals selected prove to be powerful enough for real-world applications. As a proof-of-concept, it has been demonstrated that the FlowER can supply power to a commercial wireless monitoring unit dedicated to precision horticulture. Finally, the possibility for the new plant-inspired battery to end its life cycle by returning to nature is assessed by standardized ecotoxicity and biodegradation tests.

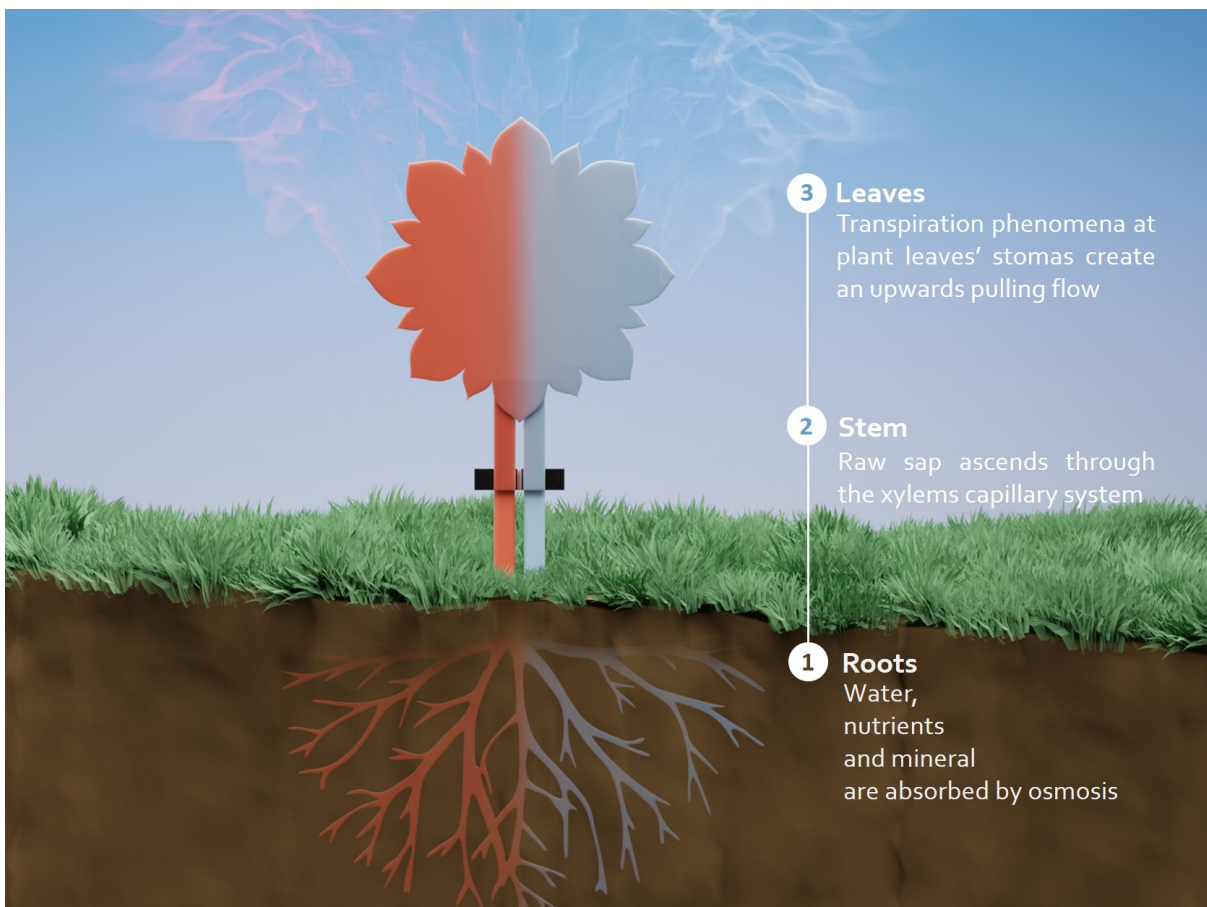


Figure 3.2: FlowER battery concept inspired in the liquid transport in plants.

3.2 Battery design and operation principle

The evaporation-driven flow battery has been designed with a plant-inspired operation principle, meaning it has two inlet channels acting as roots, from which the device nurtures with already dissolved redox species, just like plants take water and nutrients from their surroundings. The main laminated paper core, analogue to a plant stem, includes two porous carbon electrodes connected by a U-shape paper that acts as salt bridge, indispensable components to create a membraneless microfluidic galvanic cell. The core ends with two outlet channels that transport the fluid towards the top of the device. Finally, a rounded leaf-like absorbent pad exposed to atmosphere keeps wicking the solution by transpiration pull through the core (See Figure 3.3).

The prototype has been designed to be able to be planted in the bare ground. In a nutshell, a 110 x 12 mm U-shaped piece of paper, creates the inlet channels for the solutions and it also forms the salt-bridge. Two porous carbon electrodes of 5 x 10 mm create a flow-through electrode configuration and connect to two separate outlet-channels of 40.5 x 12 mm (defining a geometrical electrode area of 0.25 cm²). The fluidic system ends up in the center of a flower-shaped absorbent pad that absorbs liquids omnidirectionally around its 360°, maximizing the evaporation exposed area while keeping a co-laminar flow. Fan-shaped absorbent pads were first proposed by Mendez et al. in 2010, proving that the gradual increase of the unwetted area induces a quasi-steady flow rate in the preceding channel sections.⁹⁴ More recently, our group incorporated this fluid control mechanism in a paper-based redox flow battery.⁹³ The quasi-steady flow translated in a stable power delivery over time. When working in evaporation conditions the absorbent pad will be called evaporation pad. The paper assembly is fed with redox species solutions already dissolved in a 15 ml volumetric capacity reservoir. In order to create the final prototype, the battery paper structure is coupled with a 3D printed compostable casing, which provides verticality, mechanical robustness and compensates the different paper layers.

Using the evaporation action to drive the battery's main flow is, for paper microfluidics, the next natural step towards autonomy and competitiveness. Making use of a transpiration mechanism instead of capillary forces allows the system to

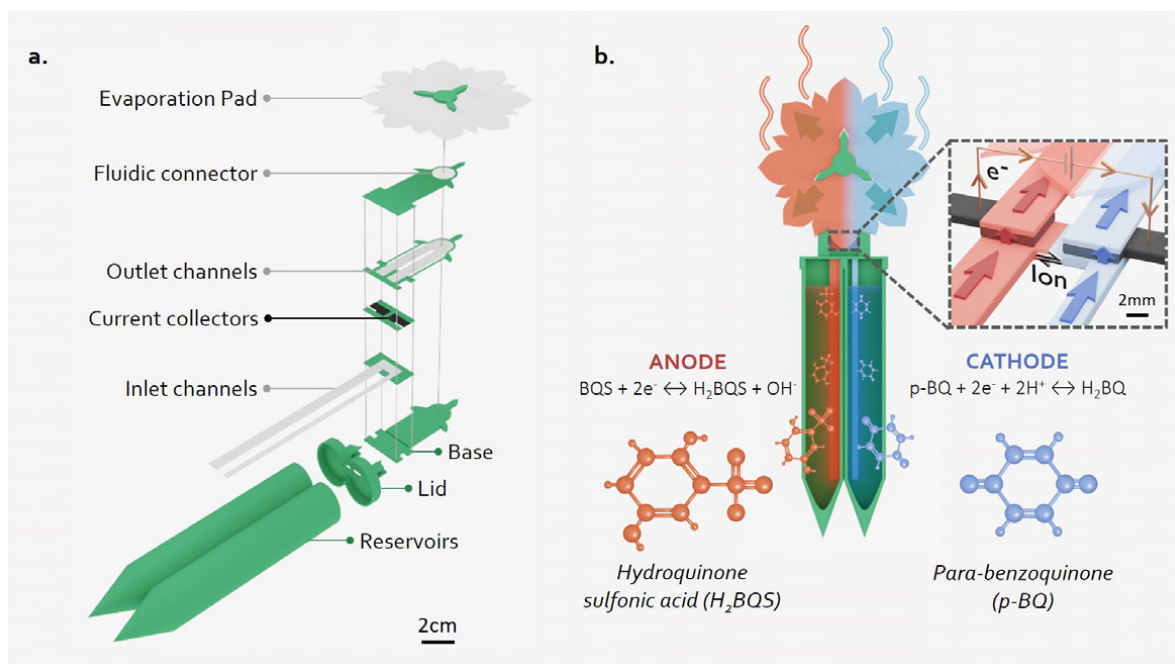


Figure 3.3: The technological adaptation of the FlowER battery concept has been performed through the selection of environmentally harmless materials to produce: two inlet channels acting as roots, from which the device nurtures with dissolved redox species, just like plants take water and nutrients from their surroundings. The main laminated paper core, analogue to a plant stem, includes two porous carbon current collectors and a salt bridge, indispensable components to create a membraneless galvanic cell. The core ends with two outlet channels that transport the fluid towards the top. A rounded leaf-like absorbent pad exposed to the atmosphere keeps wicking the solution by transpiration pull through the battery. Finally, a 3D printed compostable green casing (i.e., reservoirs + lid + base + paper supports) was used to provide mechanical robustness and verticality.

become independent of the absorbent volumetric capacity. Hence, the operation time is also decoupled from the paper's total volumetric capacity (0.137 ml for this system particular shape), but instead depends on the volume of the reactants reservoirs (15 ml in this case). On the other hand, the fluid flow rate changes its dependence from absorbent pad material wicking properties to the evaporation-exposed area, becoming constant (at certain atmospheric conditions) and easily tunable. Combining these two characteristics, the result is a miniaturized low-cost and paper-based autonomous mid-term operational battery (from hours to days), which can start to compete in operational time terms with traditionally commercial ones, thus bringing paper-based microfluidics power suppliers up to the next level.

3.3 Evaporation flow in porous media

Flow rate (Q) is one of the key parameters that determine a flow battery performance, as it defines the reactants' availability for the electrochemical conversion. In the particular case of the device herein presented, evaporation-driving forces govern the flow rate. Even though, the paper structure fills up by capillary forces, once completely full, the FlowER battery takes advantage of the transpiration mechanism naturally occurring on the evaporation pad area to pull fresh redox species through the electrodes and clean the reaction products; keeping an active flow towards the top. Therefore, this section is devoted to the study of the evaporation flow in porous media, in particular, the influence of the total area exposed and the environmental conditions on the evaporation flow rate are presented.

3.3.1 Influence of the evaporation pad area on the evaporation flow rate

Evaporation phenomena has been widely studied in paper microfluidics due to the direct influence it may have on precision and reproducibility of the devices.^{95–98} Here, a study was carried out to investigate how to control and adapt transpiration pull to the battery requirements. The evaporation pad area (A_{pad}) is an easily tunable parameter that determines the total liquid-air interface where evaporation phenomena takes place, and hence the evaporation flow rate (Q_{evap}) generated through the fluidic system. Four different A_{Pad} configurations were tested ($2x A_{Pad}$, $1x A_{Pad}$, $0.5x A_{Pad}$, $0x A_{Pad}$), by covering different percentages of the evaporation pad area, being $1x A_{pad}$ the area of one side of the absorbent pad (19.6 cm^2). A blue dye was used to visualize the total volume of liquid evaporated from the reservoirs through the fluidic system over time. As shown in Figure 3.4, evaporation phenomena at the absorbent pad creates a quasi-steady flow (i.e. constant slope over time) during 8 consecutive hours. Furthermore, the volume of liquid evaporated at a given time, increases proportionally while increasing the A_{Pad} .

Thus, for the same environmental conditions, the ratios between the evaporation flow rates ($467 \mu\text{L/h}$, $231 \mu\text{L/h}$, $98 \mu\text{L/h}$, $8 \mu\text{L/h}$) and the corresponding evaporation exposed

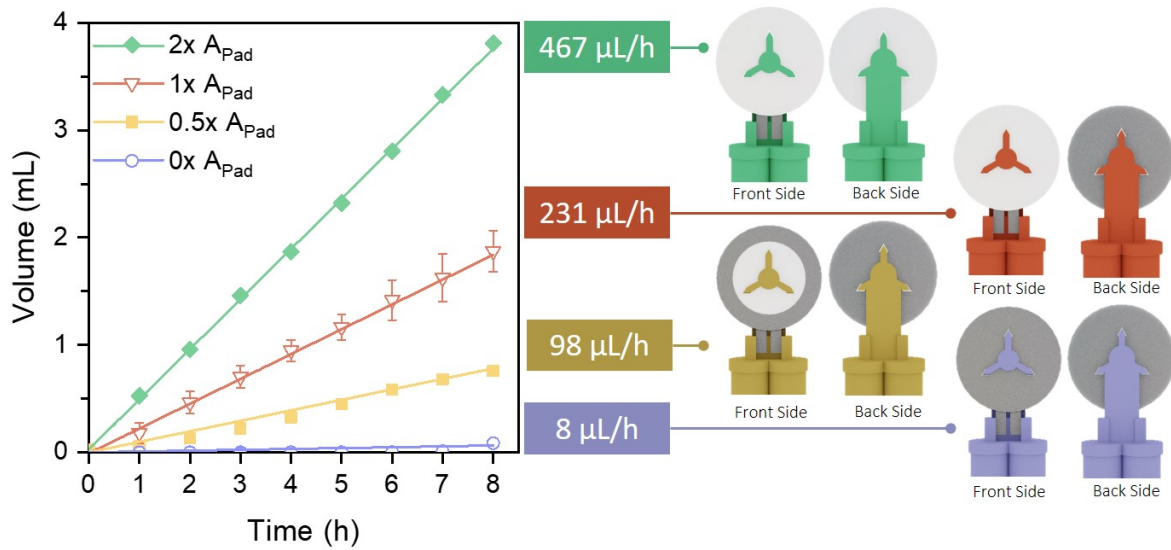


Figure 3.4: Evaporation flow rate control related to the evaporation area exposed to the air: 2x, 1x, 0.5x and 0x times the area of one side of the evaporation pad ($A_{Pad} = 19.6 \text{ cm}^2$). Linear fit adjustment coefficients: $R^2_{2xA} = 0.9997$, $R^2_{1xA} = 0.9996$, $R^2_{0.5xA} = 0.9924$ and $R^2_{0xA} = 0.9427$. Environmental conditions: $HR\% \in [51,56]\%$, $T \in [28,30] \text{ }^\circ\text{C}$ and $P = 1 \text{ atm}$.

areas $2x A_{Pad}$, $1x A_{Pad}$, $0.5x A_{Pad}$, $0x A_{Pad}$ are equal. The flow rates, reported previously by our group, obtained with a capillary-driven fluidic system, were $900 \mu\text{L/h}$, $540 \mu\text{L/h}$ and $288 \mu\text{L/h}$ depending on the outlet channel length.⁹³ With operational times of 7, 13 and 25 minutes, respectively. Comparing both fluidic systems, it can be concluded that using evaporation as a driving force, the flow rates generated are within the same order of magnitude than those generated by capillarity. Finally, it has to be noticed that, by completely covering the absorbed pad area, $0x A_{Pad}$, a negligible evaporation flow was obtained, meaning that no other evaporation sites are created than the ones desired on the evaporation pad.

3.3.2 Influence of the environmental conditions and evaporation flow modeling

As above mentioned, the power delivered by the battery depends on the flow rate. Hence, for the purpose of this work it was necessary to fully understand the influence of environmental conditions on the evaporation flow rate. For this reason, a simplified

evaporation flow rate modeling was derived as follows:

The evaporation rate equation for a liquid in evaporation was derived using the continuity equation at the interface of the two phases, where the process is occurring. For a control volume within the evaporation interface is given by:

$$Q = \oint_S \rho_v \vec{v} \cdot \hat{n} dS \quad (3.1)$$

where Q is the evaporation rate [$g \cdot s^{-1}$], S is the surface of the control volume [m^2], ρ_v is the gaseous phase density [$g \cdot m^{-3}$], \vec{v} is the particles velocity at S [$m \cdot s^{-1}$], and \hat{n} is the normal vector of the surface S [adim].

While evaporating, there's only flow on the top face of the cylinder, of area A , leaving the integral as follows:

$$Q = \rho_v v \oint_S dS = \rho_v v A \quad (3.2)$$

Since mass transport from the interface surface until bulk region is not driven neither by migration nor convection (assuming forced convection from an external air-flow is null, given laboratory conditions), only diffusion is left as the main cause. Thus, diffusion flow J from a substance in dissolution is given by:

$$J = -D \frac{\Delta\phi}{\Delta x} \quad (3.3)$$

where D is the diffusion coefficient of the solute [$m^2 \cdot s$], and $\Delta\phi$ is the concentration gradient of the solute between two points in space ($\frac{\phi_f - \phi_0}{(x_f - x_0)}$) [$mol \cdot m^{-4}$]. Applying the diffusion flow equation to this situation, the concentration gradient between two opposite spots of the control volume will be determined by the humidity of the air at each point: liquid-gas interface is saturated at 100% of humidity (h_{sat}), while at bulk region there will be the room humidity (h_r). This way, the following expression is obtained:

$$J = -D \frac{h_r - h_{sat}}{\Delta x} \quad (3.4)$$

Since the room humidity can be expressed in terms of the relative humidity (in percentage) times the saturation humidity, the previous expression rewrites as follows:

$$J = -D \frac{h_{sat} \cdot HR\% - h_{sat}}{\Delta x} = D \cdot h_{sat} \frac{(1 - HR\%)}{\Delta x} \quad (3.5)$$

where D is the diffusion coefficient of the water vapour [$m^2 \cdot s$] (dependent on T at $P=cnst.$), H_{sat} is the saturation humidity [$g \cdot m^{-3}$] (dependent on T at $P=cnst.$), $HR\%$ is the relative humidity [adim] (in percentage), and Δx is the distance between the two studied points.

Since J is a flow of mass over area and time [$mol \cdot m^{-2} \cdot s^{-1}$], when it's multiplied by a certain area (scalar product $J \cdot \hat{n} \cdot A$) the result is the amount of matter going through that area per unit of time, being equivalent to the situation given at the top part of the control cylinder (in which case the vectors are simplified to a one-dimensional expression, since both the diffusion flow and the surface are parallel).

By the continuity equation, it's known that this amount of matter is the same that is being evaporated. Thus, the following relation is obtained:

$$Q = \rho_v v A = J \cdot A \quad (3.6)$$

Meaning so that the evaporation flow rate [$g \cdot s^{-1}$] will be determined by:

$$Q = ADH_{sat} \frac{1 - HR\%}{\Delta x} \quad (3.7)$$

Eq. 3.7 shows the dependencies and parameters that influence the generated evaporation flow [$g \cdot s^{-1}$]. Where D [$m^2 \cdot s^{-1}$] is the diffusion coefficient of the liquid, Δx [m] represents the distance between 2 points in space, A [m^2] is the exposed area (i.e. total surface of liquid-air interface); H_{sat} [$g \cdot m^{-3}$] is the saturation humidity (i.e., total amount of water that can be dissolved in the dry air at a given temperature); and $HR\%$ is the relative humidity, (i.e., amount of water dissolved in the air in percentage respect to the saturation humidity). Here, D is approximated to $25.6 \cdot 10^{-6} m^2 \cdot s^{-1}$ ($T=20^\circ C$) and Δx is set as $10^{-6} m$ to normalize the orders of magnitude of experimental and theoretical flow rates.

In order to validate the proposed Q_{evap} modeling, the experimental evaporation flow rates presented in the previous section were compared with the theoretical flow rates estimated using Eq. 3.7. The validation was done with $2x A_{Pad}$ configuration, where $A = 35.5 cm^2$. Ambient temperature and relative humidity values were recorded with a sensor during the set-up course. Figure 3.5a shows the comparison between the experimental and theoretical flow rates for nine repeats. As it can be observed, both values significantly differ, however, when computing the percentage difference between theoretical and experimental, a constant $k = 44.3 \pm 2.7 \%$ is obtained.

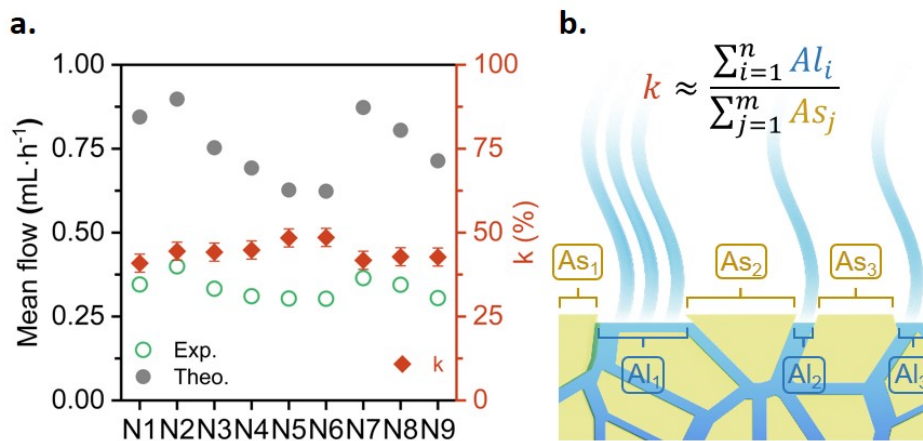


Figure 3.5: Theoretical vs. experimental evaporation flow rates and the corresponding ratio, k (%), between each of them. $N=9$ repeats.

The disagreement between the experimental and theoretical flows, expressed in the k parameter, could be explained due to a discrepancy in the exposed evaporation area.

The parameter A in Eq. 3.7 stands for the total liquid-gas interface; taking into account that in this case a paper-based evaporation pad is being used, the geometrical area does not correspond with the evaporation exposed area (See Figure 3.5b). Due to the physical space occupied by the paper fibers, the actual liquid-gas interface area is lower than the geometric one. The k ratio compensates this disagreement and other collateral effects of using a specific porous material as an evaporation pad (i.e. adhesion forces generated between the liquid and the paper walls). This ratio also allows to calculate the actual flow rate of the paper-based fluidic system directly from the pre-recorded environmental conditions (T , $HR\%$, P). The theoretical modeling of the evaporation flow rate eliminates the need for photographic analysis, deepens the environmental conditions' influence comprehension, and makes it possible to predict the device performance in different climates and environments. Henceforth, all the prototype characterization experiments were conducted while simultaneously measuring ambient parameters with a commercial sensor. The recorded environmental data provides information about the battery working conditions and allows to compute the actual working Q_{evap} , strengthening the prototype control during characterization. Furthermore, as it is further demonstrated in Section 4.6, it allows the prediction of the battery behavior in terms of Q_{evap} , for a wide range of ambient conditions.

3.4 Battery operation and optimization

Once the paper structure was fluidically validated, the configuration creating the highest flow rate ($Q_{evap} = 467 \mu\text{L}$ for $2 \times A_{Pad}$) was selected to further characterize the evaporation flow battery. This section reports the battery electrochemical characterization and the studies regarding the durability of the device's critical components: redox species reactants, paper core (i.e. paper channels and electrodes), and evaporation pad. Isolating and studying each component allows to tightly portray the battery performance and set-up strategies to further expand the operational lifetime.

In this chapter, the battery was characterized using a well-known couple of quinone-based organic species, which have been already used as redox couples in power sources.^{93;99} This particular chemistry has already shown to successfully undergo anaerobic degradation and non-toxicity in previous works reported from our group.⁵⁰ As shown in Figure 3.3, both half-cell redox reactions present a proton-dependence (see Appendix RedoxSpecies), therefore mixed-media conditions are used as a strategy to increase the electrochemical cell voltage.^{100;101} The half-cell reactions characterization in a conventional three-electrodes electrochemical cell are depicted in Figure 3.6.

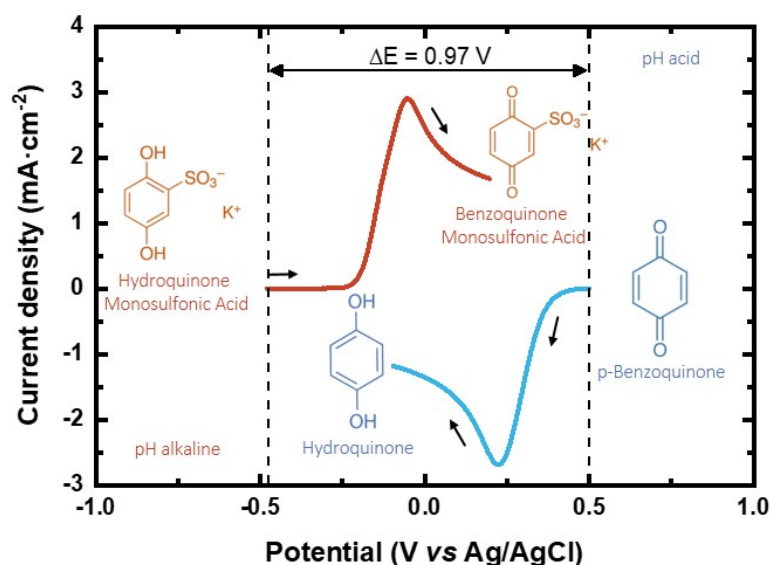


Figure 3.6: Linear sweep voltammograms of the redox chemistry selected to power the FlowER battery. Oxidation of 10mM H₂BQS in 1M KOH as alkaline electrolyte and reduction of 10mM pBQ in 1M C₂H₂O₄ as acidic electrolyte.

3.4.1 Battery performance characterization

In order to set up the prototype, 5 ml of the electroactive species previously dissolved in water-based solutions are placed in the reservoirs. Then, the inlet channels are immersed into the solutions. The paper strips absorb the liquid creating a convective flow driven by capillary forces and filling up the system. Once completely full, the evaporation forces occurring in the liquid-air interface of the absorbent pad become predominant over the capillary effect. This is when the flow battery is mainly evaporation-driven and the prototype is ready to be used. Ultimately, a solution of 0.1M p-BQ in 0.5M of oxalic acid is used as acid catholyte, while a 0.1M H₂BQS in 1M of KOH solution composes the alkaline anolyte.

Discrete characterization of the battery was performed during 8h by consecutively recording polarization curves every hour. The OCV was in all cases between 0.8 and 0.9V. As depicted in Figure 3.7a, the battery yields a maximum power density of 1.42 mW·cm⁻² at time 0h; and then decreases linearly over time until 0.69 mW·cm⁻² at time 8h. It is important to notice that this power density is in the same order of magnitude that the maximum power density reported in our previous work (1.88

$\text{mW}\cdot\text{cm}^{-2}$ at $540\ \mu\text{L}\cdot\text{h}^{-1}$), using the same fluidic system but driven by capillary forces. Despite showing a decrease in output power during the first 8h, these results

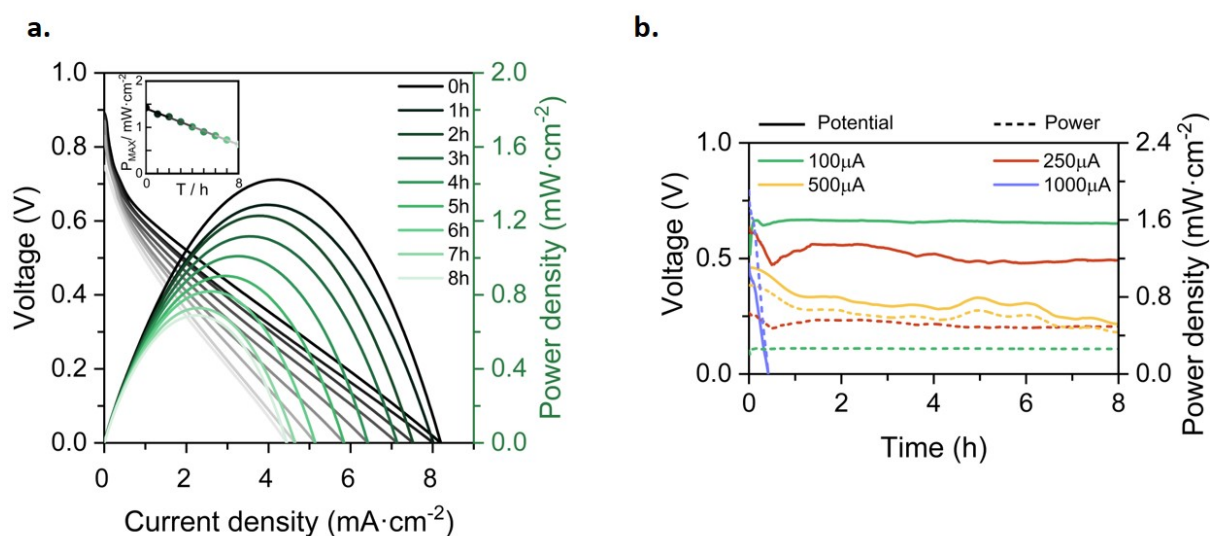


Figure 3.7: Battery characterization for 8h. **a.** Discharge polarization curves of the evaporated driven flow battery, recorded every hour since the start up (black line) until the 8th hour (palest line); **b.** Continuously measured discharge curves at four different discharge currents. Prototype supplied with 0.1M H_2BQS in 1M KOH as anolyte and 0.1M p-BQ in 0.5M $\text{C}_2\text{H}_2\text{O}_4$ as catholyte. Average flow rates calculated from Eq. 1, and environmental conditions recorded with a commercial sensor: a. $Q_{\text{evap}}=239\ \mu\text{L}/\text{h}$, HR% [54,57]%, $T \in [19,21]\ ^\circ\text{C}$. b. $I=100\ \mu\text{A}$; $Q_{\text{evap}} = 276\ \mu\text{L}/\text{h}$, HR% [62,70]%, $T [25,27]\ ^\circ\text{C}$; $I=250\ \mu\text{A}$; $Q_{\text{evap}} = 333\ \mu\text{L}/\text{h}$, HR% [55,59]%, $T[25,26]\ ^\circ\text{C}$; $I=500\ \mu\text{A}$; $Q_{\text{evap}} = 260\ \mu\text{L}/\text{h}$, HR% [58,63]%, $T \in [23,24]\ ^\circ\text{C}$; $I=1000\ \mu\text{A}$; $Q_{\text{evap}} = 351\ \mu\text{L}/\text{h}$, HR% [55,63]%, $T \in [26,28]\ ^\circ\text{C}$ ($P = 1\ \text{atm}$).

demonstrate that evaporation-driving forces are able to maintain the co-laminarity of the two reactants streams, expanding the operational time of the paper-based battery from minutes to hours. The power density loss causes are further studied in the section below when assessing redox species' stability.

Next, continuous operation was characterized by measuring battery voltage evolution over time under four discharge currents. Figure 3.7b shows the discharge curves obtained in terms of battery voltage and power density. This characterization under continuous operation was used to assess the device efficiency. The faradaic efficiency (η_F) allows evaluation of the electroactive species utilization, quantifying the theoretical charge capacity that is actually being converted into current (see Eq. 2 in *Faradaic and*

energy efficiencies subsection of *Materials & Methods*). The energy efficiency (η_E) was also evaluated by comparing the power delivered to the energy that ideally would be delivered (see Eq. 3 *Faradaic and energy efficiencies* subsection of *Materials & Methods*).

The fluidic battery is able to deliver 100 μA during 8h without voltage nor power decrease, delivering a total of 0.8 mAh of capacity and 13.5% η_F and 9% η_E conversion rates. These values are within the average range for reported paper-based microfluidics electrochemical power sources (1-10% η_F and 1-5% η_E).⁹³ As expected, for higher discharging currents the voltage decreases while efficiencies increases, leading to a 15% decrease for 250 μA (with 2 mAh of capacity, 28% η_F and 16% η_E) and a 50% for 500 μA (4 mAh of total capacity, 71% η_F and 24% η_E). The device operating at 500 μA delivered the highest power values (0.2 mW to 0.1 mW) during the whole measurement. In all three cases, the battery was able to maintain a continuous power supply during 8h. However, when the battery was subjected to 1000 μA working current (i.e. 4 mA cm^{-2}), the operational working time decays to 30 minutes, yielding a 0.5 mAh capacity, an increase in faradaic efficiency up to 99% η_F but a decrease in energy efficiency to 12% η_E . Higher current densities provoke a faster depletion of the reactants at the electrodes, thus the galvanic cell evolves from working in ohmic to mass transport losses region in which the performance decays nonlinearly with current density.^{76;102} Hence, a working condition limitation was found above 500 μA , or 2 mA $\cdot\text{cm}^{-2}$ current density.⁹³

3.4.2 Durability of the devices core

To study the durability of the device paper core (paper channels and electrodes), the battery was set up for four days and subjected to continuous current demand of 100 μA . Every 24h the anolyte and catholyte reservoirs were refilled with fresh solutions and the evaporation pad was replaced with a new dry one. Moreover, the battery polarization curve was recorded before and after this daily conditioning. Depicted in Figure 3.8 are the obtained discharge curves together with the polarization curves of the battery over the days. The battery shows a continuous power delivery of around 200 $\mu\text{W}\cdot\text{cm}^2$ for four days. A transition regime appears when changing the species

and the evaporation pad, in which the capillary flow caused by the new evaporation pad replenishment perturbs the battery performance. When analysing the polarization curves, however, it can be observed that the battery performance improves after the daily conditioning during the first three days. This result agrees with the current density peak loss caused by the anodic species degradation, which was obtained from the analysis of the solution in the reservoir every day before replenishment. However, on the fourth day of continuous operation, the battery performance dropped to 0 V. No further improvement was seen from changing the solutions or the evaporation pad, meaning the device's core operational lifetime was reached.

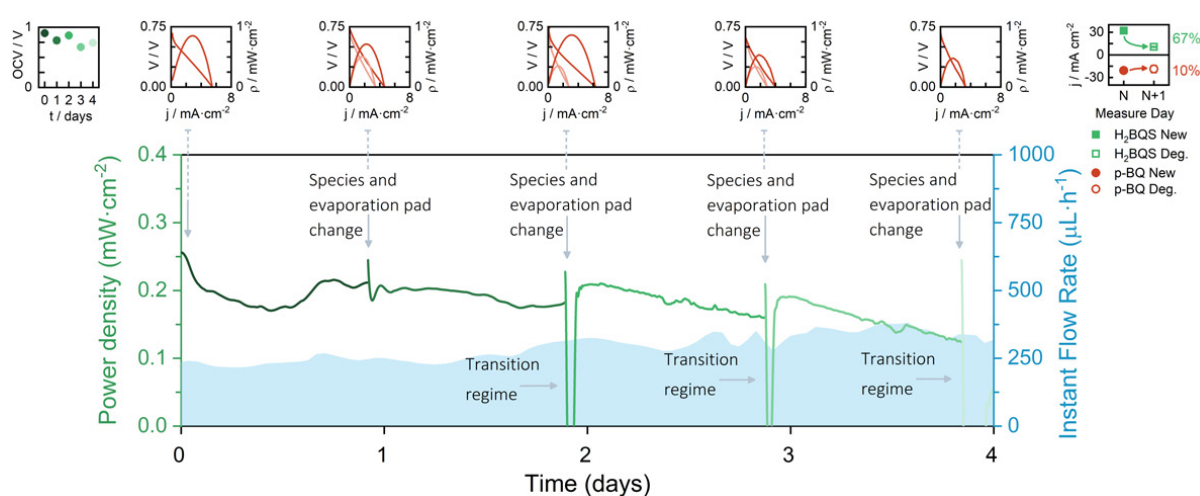


Figure 3.8: Continuous discharge curve of the evaporation-driven flow battery working at $100 \mu\text{A}$ for 4 days with daily renewal of redox species solutions and evaporation pad. Insets: battery open circuit voltages (OCVs) vs time, battery polarization curves before and after evaporation pad and redox species replacement, and anolyte and catholyte degradation study in one day. Average flow rates calculated from Eq. 3.7, and environmental conditions recorded with a commercial sensor: Day 1; $Q_{\text{evap}} = 103 \mu\text{L/h}$, $\text{HR}\% \in [60,81]\%$, $T \in [19,22] \text{ }^\circ\text{C}$; Day 2; $Q_{\text{evap}} = 184 \mu\text{L/h}$, $\text{HR}\% \in [59,64]\%$, $T \in [19,22] \text{ }^\circ\text{C}$; Day 3; $Q_{\text{evap}} = 215 \mu\text{L/h}$, $\text{HR}\% \in [57,66]\%$, $T \in [17,20] \text{ }^\circ\text{C}$; Day 4; $Q_{\text{evap}} = 157 \mu\text{L/h}$, $\text{HR}\% \in [65,73]\%$, $T \in [18,21] \text{ }^\circ\text{C}$ ($P = 1 \text{ atm}$).

3.4.3 Redox species stability

The anolyte and catholyte degradation and its relation with the total loss of performance of the battery were investigated. The redox species were analyzed via cyclic voltammetry (CV) for 9 days. Three different volumes (5, 10, and 15 ml) were

assessed, in order to study the influence of exposed area to oxygen vs. total solution volume stored. Figure 3.9 shows the correlation between the current density peak and storage time for each volume. In the case of the anodic reactant, H₂BQS, the slope decay was palliated when increasing the total solution volume, the signal loss was 100% for 5 ml solution, 47% for 10 ml, and 20% for 15 ml. Showing a direct dependence between oxygen exposure and H₂BQS spontaneous degradation. Since all samples were stored in the same kind of reservoirs, the contact surface area between the reactive and the air was the same, meaning that the amount of H₂BQS oxidized by the air was equal for all three samples. Therefore, the different volumes of reagents led to different concentration changes and thus maximum current peaks. With respect to the cathodic specie, p-BQ, the decay of the current density peak is independent of the storage volume, 94% of the signal loss was measured in all cases.

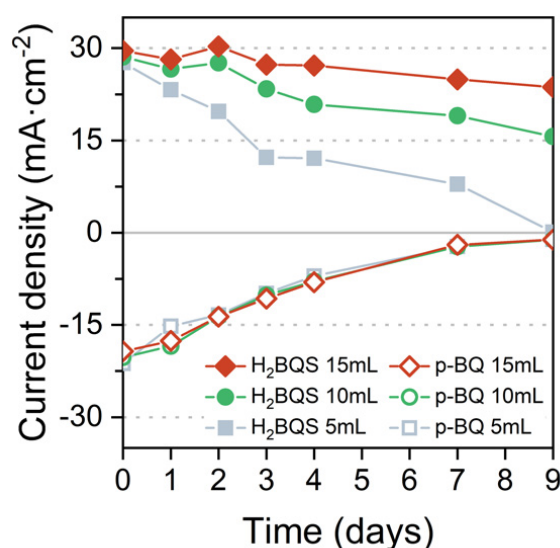


Figure 3.9: Battery reactants degradation through time for different solution volumes.

This result agrees with the naturally occurring reduction of p-BQ in aqueous media. The reduction product, hydroquinone (HQ), spontaneously polymerizes into large poly-hydroquinone chains, losing its electrochemical activity.¹⁰³ As a consequence of these results, the prototype operating volume was increased to 15 ml.

With the aim of preventing the redox species degradation, deoxygenation with N₂(g) and storage of the solutions were assessed with CV during 14 days. Figure 3.10a. shows the current density peaks obtained. This approach demonstrates to

successfully prevents the degradation of the H₂BQS anodic reactant, whereas the p-BQ degradation continues regardless of the deoxygenation. Consequently, as a simple and low-cost method to avoid oxygen molecules from reaching the redox species, we added a 2 mm thick layer of vegetal oil on the top of the reactant solutions. The result of species electrochemical response over 56 days (8 weeks) is depicted in Figure 3.10b., all stored in the same volume (10 ml) and concentration. As it can be seen, H₂BQS current peaks decay less with time when it has the

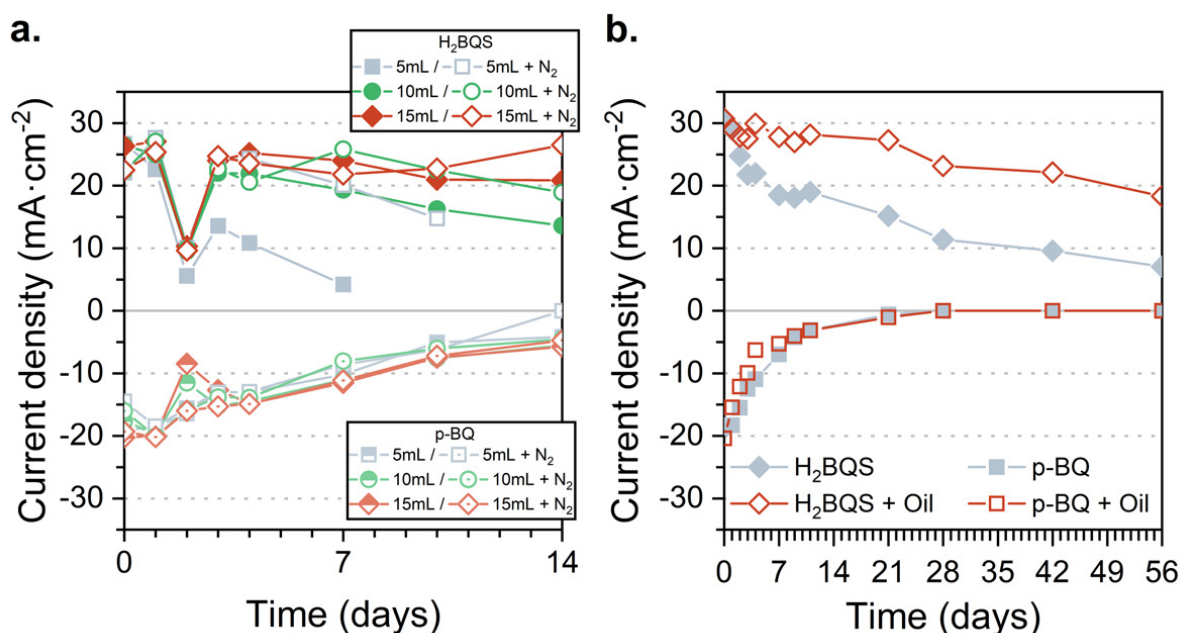


Figure 3.10: Battery reactants degradation through time. **a.** Effect of time storage for different solution volumes **b.** Effect of time storage for 10 ml volume with or without a top protective layer of sunflower oil.

protective oil layer. Quantitatively, only 37% of signal loss was recorded for H₂BQS with the oil protection, while the bare solution presented a 84% decrease. Regarding p-BQ, no stabilization of the redox species was possible, 50% of degradation is reached in 3 days and 100% of degradation in 28 days for both solutions. Confirming that, as previously stated, its degradation comes from the fact of being diluted in a water media and not from being in contact with oxygen from air. The chemical stability of organic redox compounds in aqueous media has been widely studied, due to their interest for redox flow batteries. The quinones containing ketone groups, such as p-BQ, generally show instability because their carbon-oxygen double bonds are susceptible to reacting with nucleophiles, such as water, via Michael addition.^{104;105}

3.4.4 Optimized prototype continuous operation

Finally, an optimized FlowER battery prototype was assembled and tested under a continuous discharge current of $100 \mu\text{A}$. In this case, the $2 \times A_{Pad}$ configuration was selected and a 2 mm of oil protective layer was added on top of the 15 ml solutions at the battery reservoirs. The battery yielded a power density between 0.25 and 0.2 $\text{mW} \cdot \text{cm}^{-1}$ with an average of 13.3% η_F and 7.7% η_E , over 3 days and a half (See Figure 3.11). Perturbations on the power delivered can be attributed to changes in the evaporation conditions (i.e. T_{amb} , P , and HR%) that are reflected in the flow rate. The performance drastically drops during the fourth working day. As stated above, the oil protection layer does not prevent p-BQ species from degradation, the catholyte and anolyte solutions were tested and a 56% signal decrease was obtained for p-BQ. Overall, the flow battery operational time was expanded from hours to days. Achieving an operation time that considerably exceeds those demonstrated in the literature for paper-based energy conversion devices (usually in the range of minutes).⁹³

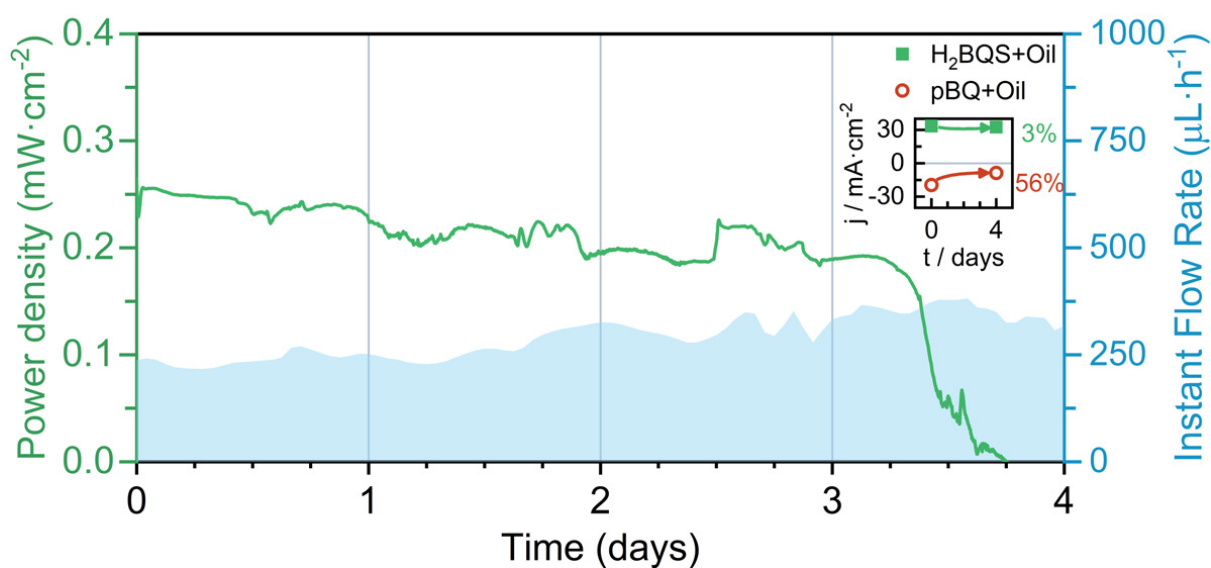


Figure 3.11: Continuous power density delivered by the evaporation-driven flow battery discharged at $100 \mu\text{A}$ for 4 days. Also depicted is the flow rate evolution. Inset: 4 days degradation of the anolyte and catholyte solutions. Average flow rates calculated from Eq. 1, and environmental conditions recorded with a commercial sensor : Day 1; $Q_{evap} = 237 \mu\text{L/h}$, $\text{HR}\% \in [68,72]\%$, $T \in [26,27] \text{ }^\circ\text{C}$; Day 2; $Q_{evap} = 260 \mu\text{L/h}$, $\text{HR}\% \in [61,73]\%$, $T \in [27,27] \text{ }^\circ\text{C}$; Day 3; $Q_{evap} = 308 \mu\text{L/h}$, $\text{HR}\% \in [55,67]\%$, $T \in [23,27] \text{ }^\circ\text{C}$; Day 4; $Q_{evap} = 358 \mu\text{L/h}$, $\text{HR}\% \in [54,58]\%$, $T \in [25,27] \text{ }^\circ\text{C}$ ($P = 1 \text{ atm}$ for all days).

3.5 Performance estimation under different environmental conditions

Since the FlowER battery is driven by evaporation, its performance is directly dependent on the surrounding ambient conditions. For this reason, a hygrometric chart has been constructed as a tool to predict the battery performance under different conditions. The chart, shown in Figure 3.12, represents the effect of the two most influential physical parameters (the temperature and the relative humidity) on our variables of interest (the theoretical flow rate and the output power). The temperature range considered for this study was 5-35 °C, while the relative humidity included the full range from 0% to 100%. Temperatures below 5 °C were discarded since they would compromise the flow of the active solution, due to water solvent freezing. The theoretical flow rate was computed by the model developed in Section 3.4. and the theoretical power density peak can be calculated by adapting Faraday's law as follows:

$$P_{peak,theo} = nc_0QFE \quad (3.8)$$

Where n is the number of electrons per mole of reactive species, c_0 stands for the bulk species concentration, Q is the theoretical flow rate, F is the Faraday constant and E is the theoretical Nernst cell voltage. Finally, a correction factor of 0.251 was applied to take into account all the losses affecting the cell performance. The correction factor is computed as the ratio between the power density peak delivered by the battery at time 0h (shown in Figure 3.7a) and the theoretical power density peak calculated with equation 3.8 for the corresponding working flow rate ($Q_{evap} = 239 \mu\text{L/h}$).

As depicted in Figure 3.12, the FlowER behaviour can be predicted in a wide range of temperature and relative humidity conditions. The highlighted areas stand for laboratory conditions recorded over the course of this work (orange) and greenhouse optimal conditions (green).¹⁰⁶ Recalling that the FlowER battery has been conceived to power precision agriculture applications it is interesting to analyse the battery performance within a greenhouse environment. For instance, the theoretical power output for the worst-case scenario (HR% = 80% and $T = 18 \text{ }^\circ\text{C}$) would be $2.2 \text{ mW}\cdot\text{cm}^{-2}$, which translates to $0.6 \text{ mW}\cdot\text{cm}^{-2}$ after applying the efficiency factor.

3.5. Performance estimation under different environmental conditions

Conversely, in the warmest ($T = 25^{\circ}\text{C}$) and less humid ($\text{HR}\% = 70\%$) greenhouse environment, the battery would yield a corrected power density of $1.25 \text{ mW} \cdot \text{cm}^{-2}$.

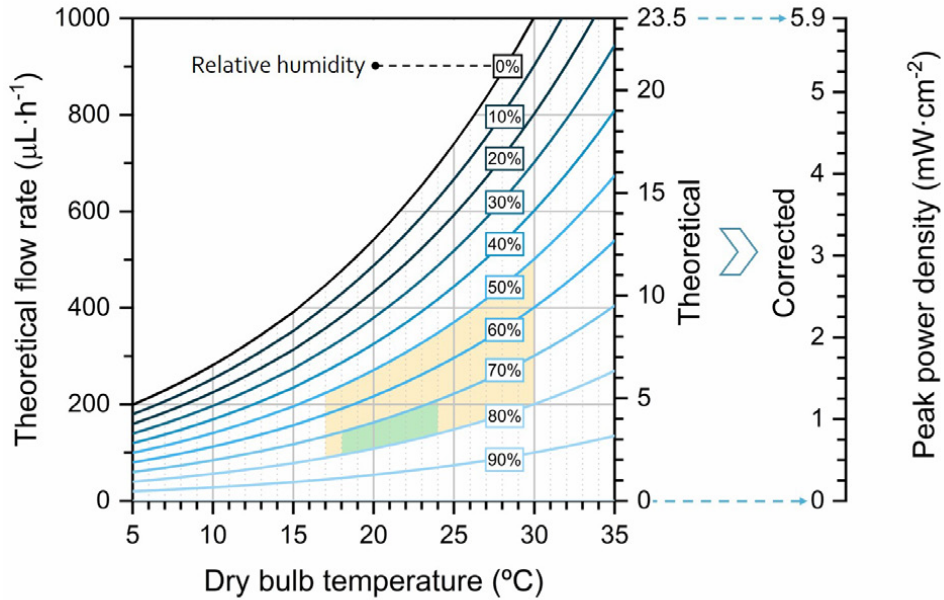


Figure 3.12: Hygrometric chart to predict the FlowER battery performance under different ambient conditions. A correction factor has been applied to take into account battery efficiency. Highlighted areas represent the windows of different ambient conditions: orange area stands for laboratory conditions recorded over the course of this work; green area covers optimal greenhouses conditions.

3.6 Powering a wireless smart monitoring unit for precision horticulture

With the aim to test a realistic PA application scenario, a Flower Care™ smart monitoring unit was purchased. Flower Care™ is a low-cost device commercialized for horticulture or indoor gardening. The unit encompasses four sensors for measuring essential PA parameters. In particular, the unit can concurrently monitor the soil conductivity, soil humidity, air temperature, and light exposure of a nearby plant. Flower Care™ runs the Bluetooth Low Power (BLE) protocol for transferring the data measured on a smartphone. Normally, a primary 3V cell coin battery (i.e., lithium battery model CR2032) powers the device. As a first prerequisite to drive the sensor's internal circuitry using the FlowER battery, we need to amplify the voltage generated (initially inferior to 1 V, see for instance Figure 3.7). A common strategy used in the literature to increase the output voltage of paper power sources is cell stacking, different works have reported stacking designs and their effects on the cell output.^{102;107–110} In this work, however, a voltage boost converter (VBC) integrated circuit was used to amplify the operating voltage up to 3.1V. We favoured this option because the commercial Flower Care™ sensing unit is not an eco-friendly sensing unit; namely it is made of conventional electronic components (e.g., printed circuit board, integrated circuits, etc.). Consequently, the additional use of the VBC did not appear critical for demonstration purposes at this stage of development. In addition, it turns out that the communication modes of the BLE protocol frequently imposed current peaks up to 5-6 mA (e.g., see Figure 3.13 insets). This means net power consumption peaks up to 18 mW. Comparatively, the maximum net power generated by the FlowER battery did not exceed 0.4 mW (see maximum power points in Figure 3.7). To overcome this difficulty, a 6.8 mF super-capacitor was selected as a refillable energy reservoir capable of absorbing any punctual current/power peaks that could not come directly from our evaporation-driven battery.

First, it was verified the capability of the FlowER battery to fully charge the super-capacitor fully discharged. As soon as the FlowER battery with the VBC were connected, the voltage generated abruptly dropped from its initial OCV value to 0.5 V

(see ① in Figure 3.13). The battery output dropped further down to ≈ 0.3 V when the VBC started to charge the super-capacitor (see ②). The full charging process took about 15 min, with two distinct phases. Indeed, the VBC needed to overcome a cold-start phase before it could normally charge the capacitor. During the first slower charging rate phase (see ②-③), the current demand was higher. Comparatively, the charging rate became much higher during the last 3 minutes of the process (see ③-④). In the course of this second phase, the VBC's internal circuitry could exploit its advanced non-linear switch-based technique to optimize the voltage across the storage element. As a direct consequence, the current demand decreased and the battery voltage re-increased to 0.5 V. At the end of the charging process (i.e., when the super-capacitor voltage reached 3.1 V), the current consumption dropped to the nano-microamps range and the FlowER battery voltage returned swiftly to 0.7 V (see ④). After the full charge of the super-capacitor, the Flower CareTM sensor was turned on. At this moment, the capacitor voltage suddenly dropped from 3.1 to 2.3 V (see ⑤). This was due to the start-up sequence Flower CareTM. Once activated, the sensor entered in sleep mode and ran advertising events every 1 s (see Figure 3.13 inset). These events also include three current peaks reaching 6 mA, but their duration was very short (< 1 ms). Despite their presence, the battery proved to be powerful enough to recharge the capacitor back to the 3.1 V in less than 2 min. The sensor can thereby stay activated and run the advertising mode as long as needed. To transfer data, the Flower CareTM was connected to the smartphone. A second sudden drop in the capacitor voltage occurred (see ⑥). Using this scenario, Figure 3.13 shows that the FlowER feasibility battery could successfully recharge the capacitor and maintain wireless data transmission to a smartphone. Despite the fact that this first proof-of-concept is based on the use of additional external electronic components (i.e., the VBC and a super capacitor), it clearly demonstrates that the FlowER battery is already capable of generating enough electrical power to drive off-the-shelf electronic components useful for PA applications.

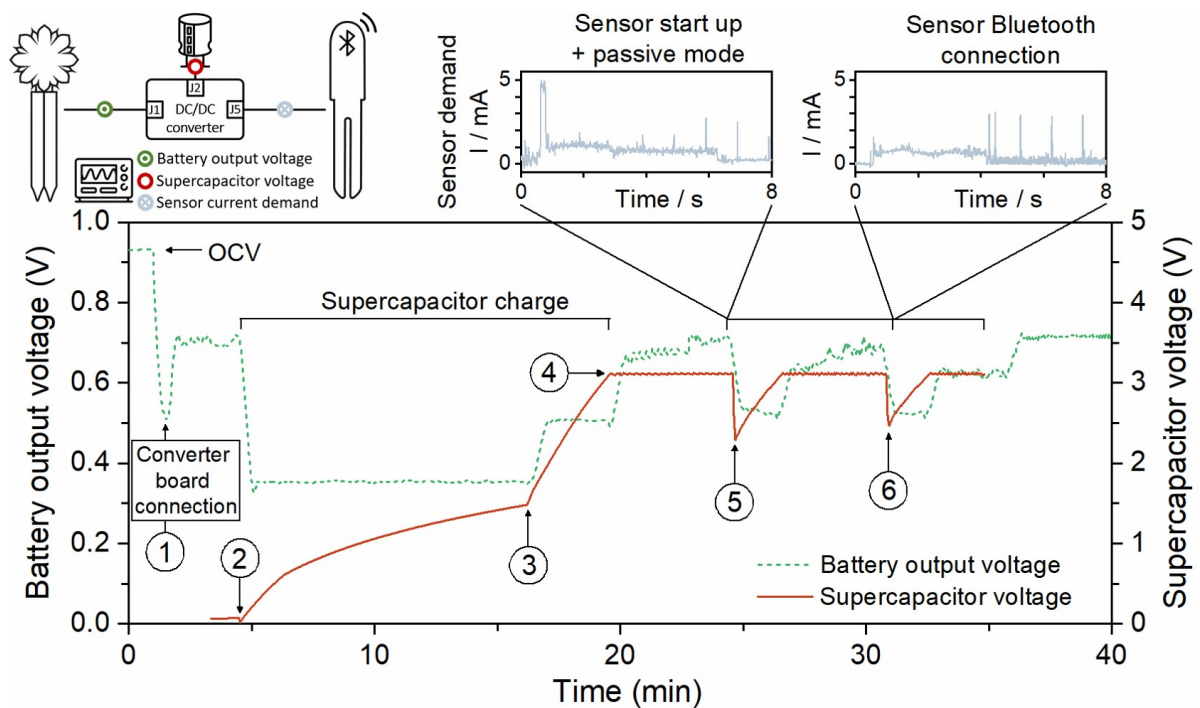


Figure 3.13: Proof of concept of the evaporation driven flow battery demonstrating the capability of powering the start-up, sensing and Bluetooth data transmission stages of a horticulture caring device.

3.7 End-of-life assessment through aerobic biodegradability and phytotoxicity tests

The FlowER battery is intended as a sustainable power supply for PA applications. For this reason, it is compelling to demonstrate that the prototype end-of-life is completely aligned with this purpose. Thus, emulating the way a plant comes back to nature, the biodegradation capability of the battery was assessed. This EoL also enables the possibility of battery composting with agroindustrial waste streams. The harmlessness of the prototype during its EoL was studied through a collaboration established with the Composting Research Group (GICOM) from the Autonomous University of Barcelona (UAB).

The FlowER battery green casing structure is made of COMPOST3D, a commercially available material certified as biodegradable under OK Compost standard (OK Compost HOME, TUV Austria). Hence, the tests reported in this section analyse the evaporation pad as a representative portion of the paper structure which, furthermore, ends up having the highest accumulation of redox species and electrolyte salts. Biodegradation pathways for standard organic molecules as cellulose or simple aromatic compounds, like the battery components, are well established in general literature related to composting and bioremediation.^{111–115} Both natural environment soil and composting matrices are complex ecosystems with a rich microbiome (including meso and thermophilic bacteria and fungi). Therein, molecules are first hydrolyzed by extracellular enzymes to simpler molecules and later fully mineralized to CO₂ and H₂O by the involved microorganisms.

First, biodegradability was assessed under controlled aerobic conditions and following a procedure adapted from the standard EN 13432.⁴⁷ Three different types of samples were analysed: i) compost alone (used as control); ii) compost with un-used evaporation pads (i.e., cellulose without reactants); iii) compost with used evaporation pads (i.e., cellulose with reaction products accumulated during 3 days). The dynamic respiration index (DRI) was computed as an indicator of the microbial activity evolution through the degradation process using Eq. 4.^{116;117} The high initial DRI values (Figure 3.14a) indicate a rapid microbial growth derived from the presence of

easily biodegradable carbon. This behaviour is even sharper in the case of the evaporation pad with reaction products. Moreover, the dynamics up to the 12th day support this trend, confirming that the samples are acting as a substrate, and being consumed by the consortium of microorganisms present at the compost. From day 15th onwards, the DRI curves flatten and there are no remarkable differences in the microorganisms' activity for the different samples.

Figure 3.14b depicts the accumulated oxygen uptake (see Eq. 3.12 in Materials & Methods section) by the three samples over 18 consecutive days. The total oxygen consumed was 2.75 ± 0.54 g by the compost, 3.30 ± 0.38 g by the evaporation pads without products, and 4.02 ± 0.60 g for the evaporation pads with accumulated products. Total oxygen consumed by the microorganisms during the biodegradation process allows for the calculation of the percentage of biodegradation as compared to the theoretical oxygen demand (see Eq. 3.13 in Materials & Methods section). Standard EN 13432 requires 90% of biodegradation in less than 6 months to consider a material is biodegradable. The levels of biodegradation reached in only 18 days were 66 ± 16 % and 90 ± 6 % for the evaporation pads without and with reactants, respectively. It is noteworthy that the oxygen uptake rate of the used evaporation pads was considerably higher than the unused. This may be due to physico-chemical changes in the cellulose structure during the battery lifespan or to the presence of the reaction products, both factors favouring microbial degradation of the evaporation pads. This effect was confirmed when the reactors were opened at day 18 and non-recognizable parts of the sorbents were found in evaporation pads with reactants while small fragments from un-used pads were observed in the final compost.

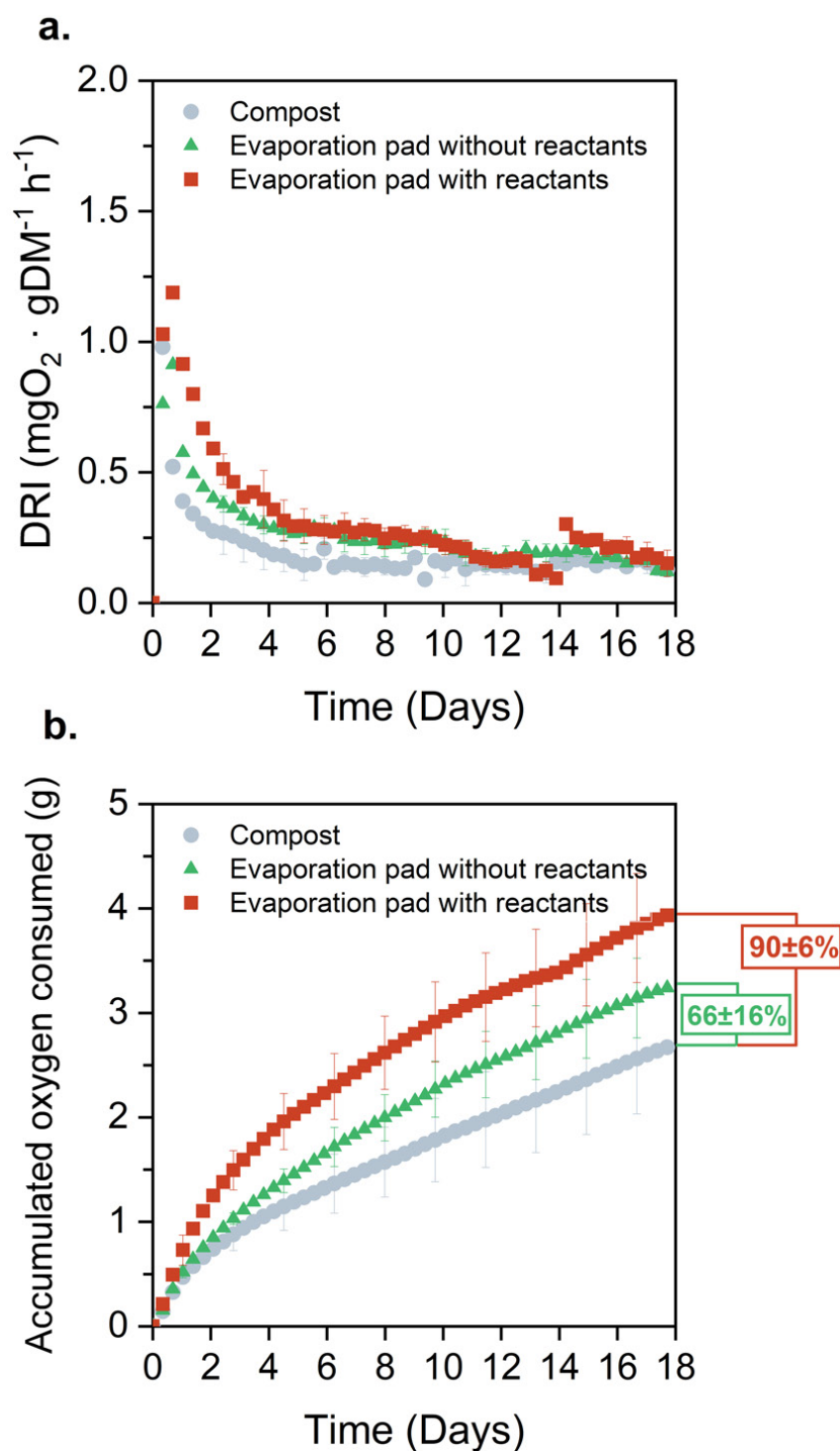


Figure 3.14: Aerobic biodegradability assessment of the FlowER battery, (N=3). a. Dynamic respiration index (DRI) of evaporation pads with and without reaction products accumulated over 3 days and compost used as a blank; b. Total oxygen consumed by the three samples and level of biodegradation achieved at day 18.

After the aerobic biodegradation assay, seed germination tests were carried out in order to assess the toxicity of the three generated composts. Germination Index (GI), Relative Root Elongation (RRE), and germination percentage of all composts are shown in Table 3.1. GI values over 100% are considered to have a positive effect on germination and root elongation whereas compost with GI values higher than 80% assure the absence of phytotoxic substances.¹¹⁸ As observed, compost control has a positive effect both in IG and RRE. Regarding compost from aerobic biodegradation of evaporation pads with reaction products, RRE does not show significant differences with reference to compost control whereas, the percentage of germination is slightly lower. In any case, the GI is higher than 100% ensuring its beneficial use. However, when the same chemical species used in the battery were added directly to a compost control but not subjected to a biodegradation process, a significant negative effect is observed. This effect is especially harmful in RRE, inhibiting radicle growth, which is a more sensitive indicator of toxicity than the percentage of germination¹¹⁹. The evaporation pad without species (cellulose) used as a control affected more than expected the germination indices. We assume this may be due to the uncompleted degradation of cellulose during the test. Instead, as above mentioned, the alterations of the cellulose structure during the battery operation and the presence of the reaction products seem to speed up evaporation pads degradation and lead to a more stable, harmless final material.

Altogether, the results above reported confirm the FlowER battery capability of being aerobically biodegraded according to standardized tests. Furthermore, a nutritious non-toxic compost was obtained from the biodegradation test, ensuring the harmlessness of the biotic degradation products.

3.7. End-of-life assessment through aerobic biodegradability and phytotoxicity tests

Table 3.1: Germination test for compost generated from biodegradation assessments of evaporation pads of the FlowER battery: with and without products in comparison with a compost control and compost with pure reactants added directly. The results have been statistically analysed using Holm-Sidack pairwise multiple comparison procedure, hence the compost samples have been paired under different letters. Those samples paired under the same letter showed non-significant differences ($p < 0.05$) (Holm-Sidack Test, Sigmaplot 11).

COMPOST GENERATED FROM THE BIODEGRADABILITY ASSESSMENT OF:	GERMINATION INDEX (%)	PERCENTAGE OF GERMITATION (%)	RELATIVE ROOT ELONGATION (%)
Control compost	195±75 a	100±20 a	195±83 a
Evaporation pads without products	77±44 c	81±12 b	95±61 b
Evaporation pads with reaction products	147±46 b	86±15 ^b b	171±65 a
Control compost with pure reactants	7±5 d	52±4 c	13±6 c

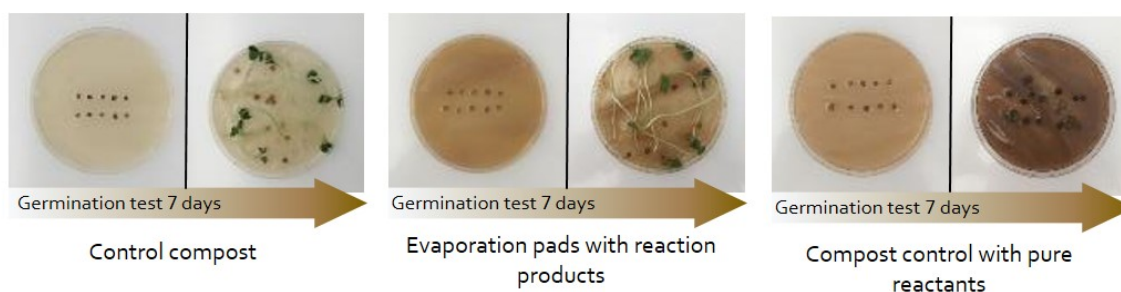


Figure 3.15: Pictures on day 0 and day 7 of experiment showing the evolution of the representative samples analyzed through germination tests.

3.8 Discussion

This chapter presented a flow battery based on transpiration pull to maintain an reactants flow through the electrodes. The implementation of this creative strategy has allowed extending the operational time of portable capillary-based power sources from hours to days. Decoupling the battery operational lifespan from the absorbent pad capacity remarkably widens paper-based batteries' technological application plausible niches. However, after the conducted studies, a few situations that could produce a decrease in the device performance were identified.

Depending on the cause, these failure modes can be categorized as effects related to the intrinsic assembly of the battery or to external events due to the environmental conditions. For example, the evaporation process results in an accumulation of solid compounds in two regions, the evaporation pad and the electrodes edges. This effect of saturation of the evaporation area could be mitigated by introducing a washing buffer, whereas the electrode zone sealing could be improved to avoid parasitic evaporation. Regarding working conditions, the prototype has demonstrated good performance in typical greenhouse conditions, however, high working temperatures and/or low relative humidity would increase the flow rate, thus causing early exhaustion of the active materials. In this case, the design should be appropriately scaled to the targeted ambient conditions. Thus providing an adequate volume of active solutions according to the estimated flow rate in the hydrometric chart (Figure 3.12). Furthermore, extreme ambient conditions, such as heavy rain or flooding, would cause a malfunction. To mitigate the detrimental effect that excess water would have in the paper-based prototype, a breathable impermeable and biodegradable coating (such as natural wax) could be applied onto the paper structure. It is foreseen that these failure modes could be tackled with design optimization and through a tailoring process addressing specific working conditions or requirements. Furthermore, thanks to the modular design, the FlowER battery could be easily modified to enable evaporation pad and/or electrode replacement or accessible refilling of the active solutions, which would also result in an extension of its operational lifespan.

Conclusions|

The FlowER battery presented in this chapter has been conceived and ecodesigned to follow the lifecycle of agriculture procedures, the FlowER battery mimics plant mechanisms of fluid transport to passively move reactants through a paper-based fluidic structure. This plant-inspired operation principle enables the creation of a flow-through configuration cell for energy harvesting. Due to transpiration phenomena, co-laminar flow is maintained and reactants are refreshed on the electrode surface. Thus, the need for external pumps is bypassed, while overcoming the operation time limitations of capillary-based flow cells. Parameters affecting the evaporation flow rate and battery performance have been studied, leading to an energy autonomy of up to four days with the present configuration. Operational time was found to be constrained to the particular selected quinone redox couple degradation, thus it could be expanded by using more stable redox chemistries. The prototype practicality has been tested by powering a wireless plant monitoring system; providing enough energy for the start-up, passive monitoring, and Bluetooth communication sequences. Ultimately, the results obtained in aerobic biodegradation and germination tests show that the depleted FlowER battery could be safely disposed of or composted as agricultural waste, resembling the way a plant comes back to nature at the end of its lifecycle.

Materials & Methods

Chemicals

The redox species used for setting up the battery were pBenzoquinone (pBQ) and hydroquinone sulfonic acid potassium salt (H₂BQS), with oxalic acid and potassium hydroxide (KOH) as electrolytes. All of them were purchased from Sigma Aldrich (Sigma Aldrich, St Louis, Missouri, USA) and used as received, as well as the blue colorant used for the evaporation flow rate characterization, erioglaucline disodium salt. All solutions were prepared in deionized water; 0.1M pBQ in 0.5M C₂H₂O₄ and 0.1M H₂BQS in 1M KOH were used as catholyte and anolyte, respectively.

Device fabrication

The device's paper-based fluidic system was designed using a CAD program (CorelDRAW, Corel, Ottawa, ON, Canada). The paper structure was fabricated as follows: due to its low fluidic resistance glass fiber (Standard 14, 355 μm thick) is chosen as inlet channels; whereas cellulose (Whatman 1, 180 μm thick) is used to fabricate the outlet channels, fluidic connector and absorbent/evaporation pad. Whatman 1 material is a well-known cellulosic filter paper, typically used in microfluidics as an absorbent pad, since it creates a homogeneous capillary pressure. This material seemed also adequate as evaporation pad because it is one of the thinnest commercially available cellulosic filters, a property that allows the reduction of the absorbent volume versus its superficial area, resulting in an enhancement of the total liquid-air interface. Both materials were purchased from GE Healthcare, Pittsburgh, PA, USA. These paper-like materials were cut using a CO₂ laser cutter (Mini 24, Epilog Laser, Golden, CO, USA). Porous carbon electrodes were cut to size (10x5 mm) from sheets of Toray carbon paper (TGPH-090 E-TEK, 280 μm). For the purpose of this work, the porous carbon electrodes were thermally pre-treated to confer them hydrophilic behaviour. A compostable and 3D printable filament, COMPOST3D, was used for building the mechanical structure (B4Plastics, IQ Parklaan 2A, 3650 Dilsen-Stokkem, Belgium), by 3D-printing a custom-made model, designed using an open-source software, Blender (Blender Foundation,

Stichting Blender Foundation, Buikslotermeerplein 161, 1025 ET Amsterdam, the Netherlands). The different parts of the prototype were manually assembled with a waterbased bioadhesive, BioTAK S100, a double-sided PSA formulated to include a high content of renewable materials (BioTAK, Sustainable Adhesive Products B.V., Venkelbaan 82, NL-2908 KE Capelle aan den IJssel, The Netherlands).

A compostable and 3D printable filament, COMPOST3D, was used for building the mechanical structure (B4Plastics, IQ Parklaan 2A, 3650 Dilsen-Stokkem, Belgium), by 3D-printing a custom-made model, designed using an open-source software, Blender (Blender Foundation, Stichting Blender Foundation, Buikslotermeerplein 161, 1025 ET Amsterdam, the Netherlands). The different parts of the prototype were manually assembled with a waterbased bioadhesive, BioTAK S100, a double-sided PSA formulated to include a high content of renewable materials (BioTAK, Sustainable Adhesive Products B.V., Venkelbaan 82, NL-2908 KE Capelle aan den IJssel, The Netherlands).

Flow rate characterization

The experimental evaporation flow rate over time was characterized by measuring the decrease of the liquid height in the device trays. To enhance image contrast, in these experiments, 100 mM solution of euroglaucine disodium salt dye was used to simulate and visualize anolyte and catholyte flow. The images were recorded with a camera (C920, Logitech, Fremont, CA, USA) controlled by time-lapse software (Sky Studio Pro, free licensed), which saved images at a rate of 1 frame every 20 min. The flow rates were calculated from the captured images by measuring the height decrease in the trays over time. The images were analysed by using ImageJ software (US National Institutes of Health, Bethesda, Maryland, USA).

The theoretical evaporation flow rate over time was characterized through the environmental conditions of humidity and temperature, recorded with a sensor (ALPS Sensor IoT Network Smart Module, Alps Electric Co., Ltd., Osaki, 04, JP).

Electrochemical studies

The effect of the storage time in redox species degradation was characterized via cyclic voltammetry. In the case of different storage volumes and deoxygenation studies, the measurements were performed in a three-electrode electrochemical cell. Glassy carbon electrode (0.071 cm²), platinum electrode, and Ag/AgCl electrode (CH Instruments Inc., TX, USA) were used as working, counter and reference electrodes, respectively. The effect of the sunflower oil protection layer was assessed on carbon SPEs (Screen-Printed Electrodes), which use Ag/AgCl as reference electrode (fabricated by the authors).

The polarization and power curves for battery characterization were generated using linear sweep voltammetry technique, from premeasured OCV to 0V at a scan rate of 20 mV·s⁻¹. The discharging curves were generated with chronopotentiometry technique by holding the battery at different discharging currents. All electrochemical measurements were recorded with a DropSens μ Stat400 bipotentiostat/galvanostat and DropView 8400 Software (DropSens S.L., Asturias, Spain), at a scan rate of 20 mV·s⁻¹.

Faradaic and energy efficiencies

The faradaic efficiency allows evaluation of the redox species utilization, by comparing the total theoretical charge capacity with the one experimentally harvested. It can be computed with the following expression:

$$\eta_F = \frac{\int_0^t I(t) dt}{n c_0 V F} \quad (3.9)$$

where $I(t)$ is the current recorded or demanded during the measure, t is the measurement time [s], n is the number of electrons per mole of reactive specie, c_0 stands for the bulk species concentration, V is the total volume that has gone through the electrodes and F is the Faraday constant.

On the other hand, the energy efficiency compares the energy that the battery could theoretically deliver with the power actually delivered under a continuous operation. It

can be expressed as follows:

$$\eta_E = \frac{\int_0^t I(t) \cdot E(t) dt}{nc_0 V F E} \quad (3.10)$$

where $E(t)$ is the operating voltage and E is the theoretical Nernst cell voltage [V].

Flower Care™ sensor and voltage boost converter

A Flower Care™ (HHCC-Xiaomi, Beijing, China) wireless plant monitoring unit was purchased from an ecommerce platform. The accompanying app was installed on a smartphone running Android 11. The sensor was preliminary linked to the app before running experiments.

To monitor the voltage variations of the FlowER battery under load, a portable potentiostat/galvanostat was used (Dropsens μ Stat400, DropSens S.L., Oviedo, Spain) coupled to the Dropview 8400 software installed on a laptop.

To amplify the initial voltage generated by the FlowER battery, the evaluation module of an ultra-low-power DC-DC boost converter (BQ25504-EVM, Texas Instruments, Dallas, USA) was used in association with a 6.8 mF super-capacitor (BZ05FB682ZSB, AVX). The BQ25504-EVM is equipped with three terminal blocks: the input source (J1), the charger output (J5), and the battery connection (J2). The FlowER battery was connected to J1 after the establishment and stabilization of the evaporation phase (i.e., the evaporation effect became dominant over the capillary effect so that the battery was predominantly evaporation-driven). The Flower Care™ sensor and the super-capacitor were connected to J5 and J2, respectively. The functions available on the evaluation board (e.g., maximum power tracking point, under-voltage settings, etc.) were used as provided by the manufacturer.

Electrical signals with a duration ranging from a few milliseconds to several tens of seconds were measured using digital oscilloscopes (DSOX2002A, Agilent Technologies, Santa Clara, USA and Waverunner 44Xi, LeCroy, Chestnut Ridge, USA) coupled to a standard probes (P2200, Tektronix). Built-in high-resolution and/or fine modes were used to filter background noise and facilitate the visualization of the overall signal shapes.

Other electrical signals lasting longer than a few tens of seconds were recorded using

a digital multimeter 6.5 digit resolution (34401A, Hewlett Packard, Palo Alto, USA). The multimeter was connected to a computer using a GPIB-USB-HS Card (National Instruments, Austin, USA). A block diagram-based interface in LabVIEW (National Instruments) was developed to automate the acquisition of the data.

Aerobic biodegradability and phytotoxicity assessment

Aerobic biodegradability tests were performed in 0.5 L self-made PVC cylindrical reactors (13 cm high x 7 cm diameter) with forced air inlet (at 20.9% O₂) and outlet. Constant flow rate was controlled with a mass flow meter (Mass-Stream D-6311, Bronkhorst, NL) at 15 ml/min.⁷⁴ Incubator (Memmert IF 160, Schwabach, Germany) temperature was set at 58.9 °C to favour the growth of thermophilic microorganisms. Compost moisture content was initially adjusted to 54% and maintained by constant water vapour-saturation of inlet air. Three samples were analysed: 60 g of compost from industrial plant (Consorti per a la Gestió dels Residus del Vallès Oriental, Barcelona, Spain) were used as a control, 60 g of compost plus three un-used evaporation pads (0.49 g of cellulose) and 60 g of compost plus three used evaporation pads (1.30 ± 0.05 g of cellulose and reaction products accumulated for 3 days). The quantities were set based on proportions proposed by Ruggero et al. (2019), slightly reduced due to sample quantity limitations.¹²⁰ Oxygen content at the outlet air flow was monitored using electrochemical O₂-A2 oxygen sensors (Alphasense, UK). The Dynamic Respiration Index (DRI) was determined following UNI 11184:2016,

$$DRI = \frac{F(O_{2,in} - O_{2,out})}{M100} \cdot \frac{P \cdot 32 \cdot 60}{T \cdot R \cdot \%DM} \quad (3.11)$$

where DRI [mg O₂ · h⁻¹ · g⁻¹ DM]; F, air flow rate into the reactor [L·min⁻¹]; O_{2, in}, percentage of oxygen at inlet air flow [%; mol O₂ · mol⁻¹ · O₂], in this experiment was set at 20.9; O_{2,out}, oxygen concentration at outlet air flow [%; mol O₂ · mol⁻¹ · O₂]; M, total mass inside the reactor [g]; P, atmospheric pressure [atm]; 32 oxygen molecular weight [%; mol O₂ · mol⁻¹ · O₂]; 60, conversion factor from minutes to hours; T, ambient temperature [K]; R, ideal gas constant (i.e. 0.08206 L · atm · mol⁻¹ · K⁻¹); %DM, fraction of dry matter [g DM · g⁻¹].¹²¹

The accumulated oxygen consumed [g·O₂] depicted in Figure 3.14b is obtained by

integration of DRI and then multiplying by the sample dry mass [g];

$$\int_0^t DRI dt = gO_2 \cdot g^{-1} DM \quad (3.12)$$

Finally, the biodegradation level [%] was obtained as follows;

$$\%Biodegradability = \frac{TotalOxygenConsumend}{ThOD} \quad (3.13)$$

The total oxygen consumed [g O₂] was calculated by the accumulated oxygen uptake of the sample in 18 days while ThOD is the theoretical oxygen demand [g O₂].⁴⁸ The calculated samples' ThOD are: 0.576 g for the evaporation pads without reaction products and 1.408 g for the used evaporation pads. A germination test using radish seeds (*Raphanus sativus*) was performed to evaluate compost phytotoxicity¹²². A compost extract (10 ml) in a ratio of 10:1 (water volume, in ml, to dry weight, in g) was used to evaluate the germination of 10 radish seeds plated in a Petri dish in triplicate. Germinated seeds and root length were measured after five days in a lighted area at room temperature. Seed germination percentage and relative root elongation (RRE) were calculated and expressed as a percentage about the results of the control using distilled water. Germination Index (GI) was calculated considering both germination percentage and RRE as described by Komilis and Tziouvaras (2009).¹¹⁸

4

A carboard battery for smart packaging applications

Overview

The this chapter explores the viability of a battery ecodeign for smart packaging applications and with paper and cardboard recycling process as inherent end-of-life. Figure 4.1 depicts the circular battery life-cycle convinced within sustainable planetary boundaries and over the projected performance foundation.

In order to enable the devised EoL the research presented in this chapter goes one step further by developing the materials that conform the battery. Furthermore, the fabrication processes have been selected and implemented taking into account their compatibility with a cardboard box established fabrication process. In a way that the complete suppression of the battery distribution EoL step could be achievable. In this sense, this chapter constitutes the first attempt of a comprehensive redefinition of a battery life cycle by completely paring it with the application value chain.

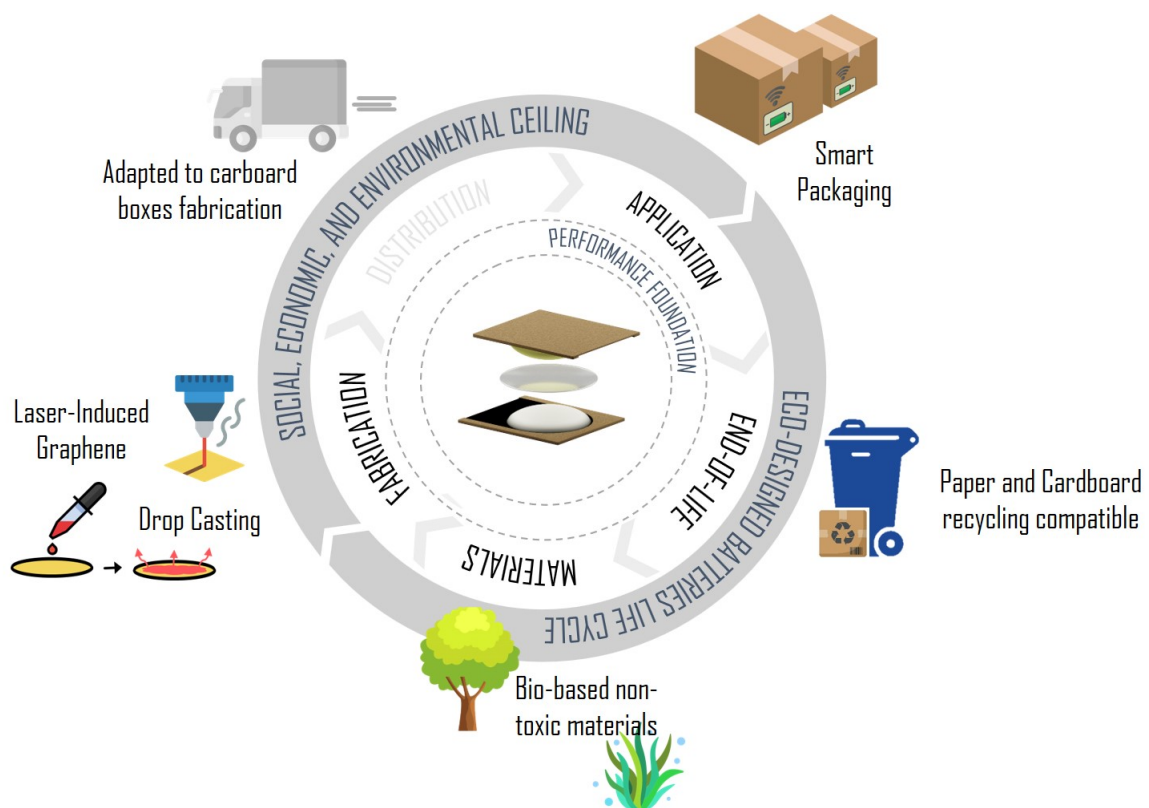


Figure 4.1: Sustainable battery life cycle envisioned for smart packaging sector.

4.1 Introduction

Digitalization has also permeated until the packaging sector, in which to ensure efficient logistics, and an improved client experience, different electronic systems such as trackers, sensors, displays, or communication modules are progressively being incorporated into supply chains. These IoT systems are englobed under the so-called smart packaging solutions, and they are intended to add many advantages to the packaging industry, both at an economic and a sustainability level.^{123;124} However, currently innovative smart-packaging technologies, are being designed around traditional existing primary batteries. Due to their exceptional performance, compactness and significant operational time, systems such as coin cell or alkaline cells have monopolized the market over years. These cells, however, suffer from a lack of format-adaptability and, despite being recyclable, need dedicated collection routes, as they are metal-based cells containing hazardous chemicals. These drawbacks become a limitation to the spread of an efficient and environmentally conscious smart packaging industry.

During the past years some alternative battery technologies have emerge, mostly focused on the enhancement of battery versatility formats and implementing new functionalities such lightness and flexibility. However, despite the efforts this alternatives still do not represent a truly sustainable solution thus, they rely on a metal based chemistry and synthetic polymers derived from petroleum hydrocarbons.^{125;126} The use of these conventional materials is especially unsuitable for the packaging sector, thus it might critically affect the cardboard and paper recycling process.

Cardboard and paper waste steam has the highest recycling rate among all materials, reaching almost 74% recycling rate in 2020 for EU.^{127;128} Furthermore, cardboard packaging materials have a highly circular life cycle, as their fibers may be recycled up to 25 times.¹²⁹ Therefore, the proliferation of battery-powered devices in smart packaging applications could lead to a significant disturbance in the recycling system (due to the compelled rejection of cardboard boxes including conventional batteries) causing a reduction of cardboard circularity and recycling rates.

This chapter is devoted to the development of a primary battery particularly

ecodesigned targeting smart packaging applications. As in Chapter 3, the main objective has been to combine the battery EoL with cardboard and paper recycling route to ensure the power source correct management, while overcoming the need for separate collection and treatment routes. However, in this chapter, the battery conception process has been more ambitious, and besides paring the end-of-life with the application, the redefinition of other steps of the battery life cycle have been tackled. The selection of materials has been done with under the guidelines of *EN 643:2001 Paper and board - European list of standard grades of paper and board for recycling*. This standard clearly defines the tolerances for unwanted, and prohibited, materials during recycling. On the other hand, fabrication techniques have been carried out to make the battery fabrication implementable to the packaging system; for instance, paired with a cardboard boxes fabrication process. As presented in Chapter 2, the deconstruction and redefinition of batteries materials and fabrication processes allow to avoid the distribution step and simplify the battery life cycle, resulting in a direct reduction of the environmental impact associated. Figure 4.2 conceptually shows process that has been implemented for the battery development. After the currently introductory chapter, Section 4.2 presents the prototype design. Then, Section 4.3 gathers the materials development. Identification, optimization, and application of new materials have represented a pivotal step in this work, to ensure that the battery can be directly coupled to the established packaging cardboard value chain, specially its EoL. In consequence, the primary materials selection, development and implementation has been carried out under an integrated sustainability vision. As mentioned in Chapter 2, energy demand intensification is hugely contributing to raw materials and natural resources exhaustion. For this reason, while developing this battery, conventional metal-based energy storage materials have been deliberately avoided. Naturally abundant, plastic-free, non-toxic materials have been selected from the substrate to the active redox species for all battery parts. In particular, two main contributions are described hereafter, Subsection 4.3.1 explains in detail how carbon-based current collectors have been generated via Laser-Induced Graphene (LIG) over pre-treated cardboard surfaces. While, in Subsection 4.3.2 bio-polymer matrices, synthesized from naturally occurring polymers, such as cellulose and alginate, are presented as hydrogels to retain the

electrochemically active species acting as electrolytes and as ion exchange membrane. Finally, to validate the viability of the theorized concepts the developed materials are implemented on the previously designed battery testing units in Subsection 5.3.3, creating the first demonstrators of an ecodesign battery for smart-packaging applications. The chapter ends up gathering in the discussion section an insight on the future improvements for the battery; and finally some conclusions are presented.

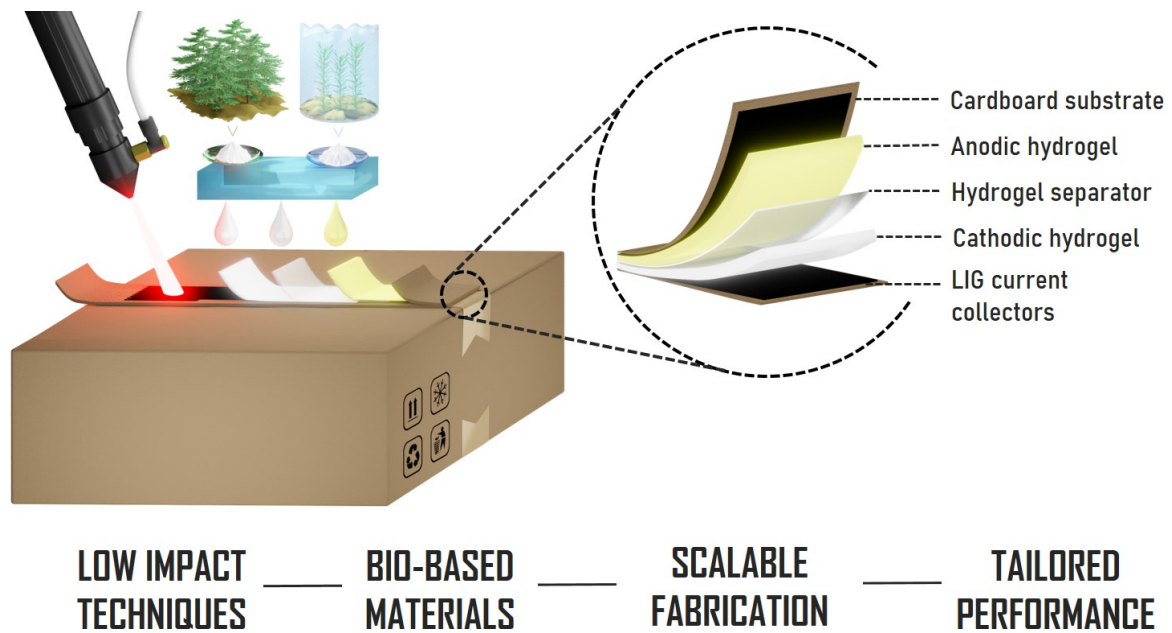


Figure 4.2: Cardboard battery tailored smart packaging application. Fabricated from bio-based materials with low impact techniques.

4.2 Battery design and operation principle

In this chapter a battery has been designed with a sticker like structure, meaning it is a planar prototype composed by a set of layers with different purposes. As depicted in Figure 4.3, Two layers of cardboard act both as structural material, and substrate over which the carbon-based current collectors are defined by laser-induced graphene technique. The electroactive compounds are contained in a hydrogel matrix, which is synthesized from naturally occurring polymer and directly dropcasted on top of the current collectors. Finally, a biopolymeric membrane is sandwiched between anode and cathode, to perform the ionic exchange. The preparation of each layer is done separately and then the battery is assembled through a lamination process. This approach facilitates the battery fabrication implementation in a cardboard box production line.

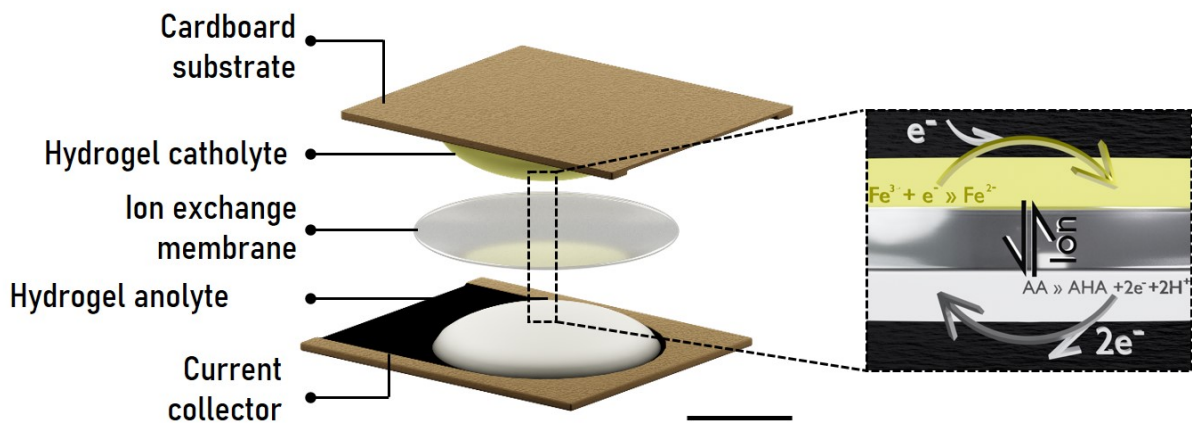


Figure 4.3: The battery is based on a layered design. A cardboard substrate is selected to engrave the current collectors using laser induced graphene technique (LIG). Then, a hydrogel matrix is used to create the ion exchange membrane and to retain the active species. Scale bar: 0.6cm

The battery fabrication process starts by generating LIG current collectors on top of the substrate of interest, then the electrode area is defined by an adhesive rounded pool of 1.6 cm diameter. The anode and cathode are created by incorporating the redox species (and its respective salts to tune the pH) to the hydrogel matrix and stirring at room temperature. Then, 260 μ L of anodic and cathodic hydrogels matrix are drop-cast on the top of the LIG current collectors and incubated at 25°C for 48h. The ion-

exchanged membrane is synthesized separately by dropcasting 15ml of the selected matrix ratio (see Section 4.3.2) in a petri dish (\varnothing : 8.6 cm) and incubating it at 25°C for 72h to obtain a hydrogel film. Finally, the individual cells are manually laminated. The membranes are cut with a 1.6cm diameter punch and sandwiched between the negative and positive electrodes; three layers of pressure sensitive adhesive are used to compensate the membrane width and keep the battery glued. Figure 4.3 depicts an exploded view of the testing cell design and its working principle. The materials development, testing and selection is discussed in detail on next section.

The simple testing battery design described in this section integrates all the essential elements to build a functional hydrogel based galvanic cell. It is worth to mention that the use of a hydrogel to contain the redox species creates a ionic conductive medium, that allows the battery to work without the need of an external liquid addition. For some application, this represent a clear advantage in front of microfluidic galvanic cells.

4.3 Materials development and battery operation

This section is devoted to battery materials exploration, selection and implementation in a testing cell, which was a key step while ecodesigning the battery.

To ensure the battery to meet the projected end-of-life it was compulsory to use non-metallic current collectors. Thus, as deeply explain above, laser-induced graphene technique was use to engrave the current collectors over a cardboard substrate. LIG technique was selected for its versatility which allows an easy implementation on cardboard boxes fabrication processes. Futhermore, in order to potentiate a maximum cellulose content within the battery, a nanocellulose and alginate hydrogel matrix was developed to contain the active species and to act as ion-exchange membrane.

4.3.1 Laser-induced graphene current collectors

Current collectors have a crucial influence on the performance of batteries. Characteristics such as electrical conductivity, contact resistance, density, or corrosion resistance, directly affect the battery capacity and efficacy. More commonly used current collectors in batteries are metals (Al, Cu, Ni, Ti, or stainless steel) due to their high electrical conductivity, electrochemical stability, and mechanical strength. However, metallic current collectors' suitability arises concerns due to their non-renewable nature, increasing costs, and sustainability implications.

In this sense, carbonaceous current collectors (e.g. carbon papers, carbon felts, CNF or graphene) overcome metal-based drawbacks while maintaining the essential properties. It is well-known that of all carbon-based material with energy storage applications, graphene has demonstrated outstanding properties, thus attracting intensive research interest.¹³⁰ However, despite its extraordinary properties, graphene wide application in commercial products has been sluggish, mainly because its limiting traditional preparation methods. Based in either chemical vapor deposition or hydrothermal processing, graphene preparation usually implies high-temperature steps, complex synthesis routes and expensive economic costs.¹³¹ Regarding conventional graphene patterning, despite it is possible using

hydrated graphene oxide, it usually involves acidic and oxidizing waste. In this scenario, laser-induced graphene (LIG) appeared as an easy to synthesize 3D porous graphene-like material, that furthermore exhibits many of graphene excellent properties.¹³²

LIG methodology is based on photochemical and photothermal processes occurring when lasing a selected substrate at specific conditions. The laser energy is absorbed by the precursor substrate material, breaking carbon bonds (i.e. C-C, C-O, C=O and N-C) and allowing the carbon atoms rearrangement to 3D porous graphene.^{131;133–135} In 2014, LIG technique was reported for the first time over a commercial polyamide tape (Kapton polyamide, PI) by J. Lin et al; and it meant a huge breakthrough promoting graphene implementation.¹³⁶ In essence, LIG technique arises as a simpler, low-energy, zero waste and accessible technique to create 3D graphene, that, additionally, merges graphene generation and patterning in 1 step. The resulting graphene qualityⁱ will depend on the material selected as substrate. Despite the most commonly used substrate is PI, later investigations have demonstrated the possibility of using organic substrates as LIG precursors. Some of the successfully tested bio-based precursors include wood¹³⁷, cellulose nanofiber¹³⁸, lignin^{137;139–141}, potato skin, bread, cotton, cardboard and cloth¹³³. However, it is usually implemented over plastic-based substrates.¹³⁴ Regardless the selected substrate, LIG material has been reported to preserve graphene upstanding attributes, such as a high surface area, stable chemical and physical properties and remarkable electrical conductivity. For these reasons, many LIG applications have been reported so far: supercapacitors^{136;142}, sensors¹⁴¹, photodetector¹⁴³, heaters¹⁴⁴ or flexible electrodes¹⁴⁵. It has also been use as current collector in batteries, always combined with a metallic catalyzer and with polyamide as precursor substrate.^{146–150}

In this subsection, the possibility of using laser-induced graphene (LIG) as a current collector when an electrochemical reaction is involved is explore to determine its suitability to be implemented in a biopolymer based battery. It is worth to emphasize that, the successful incorporation of this technique into battery development

ⁱGraphene is commonly characterized with Raman Spectrum. Raman spectroscopy is a technique usually used to determine the material chemical structure. Hence, it provides information of the structural defect, allowing to determine the material 'quality' or 'perfection'.

generates great outcomes. Specially, it needs to be notice the remarkable substrate versatility that the technique has demonstrated. Which, in the particular scenario of this thesis, has allowed to develop electrically conductive material on top of a cardboard substrate, representing a key step towards the reinvention of the battery end-of-life. Furthermore, LIG technique allows to easily redesign and fabricate 2D current collectors geometries, thus allowing the exploration of further batteries configurations and enabling easy energy capacity tailoring.

LIG generation on pre-treatread cardboard surfaces

First, the conditions to generate LIG over different substrates of interest were sought. As it has been widely reported, polyimide (PI, DuPont™ Kapton®) was chosen as reference precursor material. On the other hand, taking into account that the battery is conceived for smart packaging application, cardboard was selected as organic substrate as it is the most used and recycled packaging material in EU. Several cardboard samples were considered for this study, and their suitability was analyzed in terms of structural stability, mechanical properties and surface roughness. Corrugated type was discarded as its surface is heterogeneous because of slight ripples. In contrast, Manilla type typically employed in file folder, present flat homogeneous surfaces. Mechanically, Manilla cardboard is a relatively rigid and resilient solid paper, with 2650 m breaking length and 140 kPa bursting strength. It presents high dimensional stability allowing surface treatments without compromising the substrate integrity. As for structure, it is 370 μm thick and weights 250 $\text{g}\cdot\text{m}^{-2}$, with high fiber density.¹⁵¹

Cardboard has already been reported as a substrate for LIG generation.¹³³ by using a flame retardant surface treatment before the definition of LIG structures. In this section, three pretreatments are evaluated for LIG generation on the selected cardboard surface. Two fire retardants already used for LIG generation in published reports were tested as commercial available options: phosphate ammonium based ForceField® FireGuard (FG) and boric acid based FireChief® Flame Retardant Spray (FRS). Then, a lignin-based biopolymer coating was also synthesized with two main purposes. First, to act as a flame retardant with a more sustainable chemical

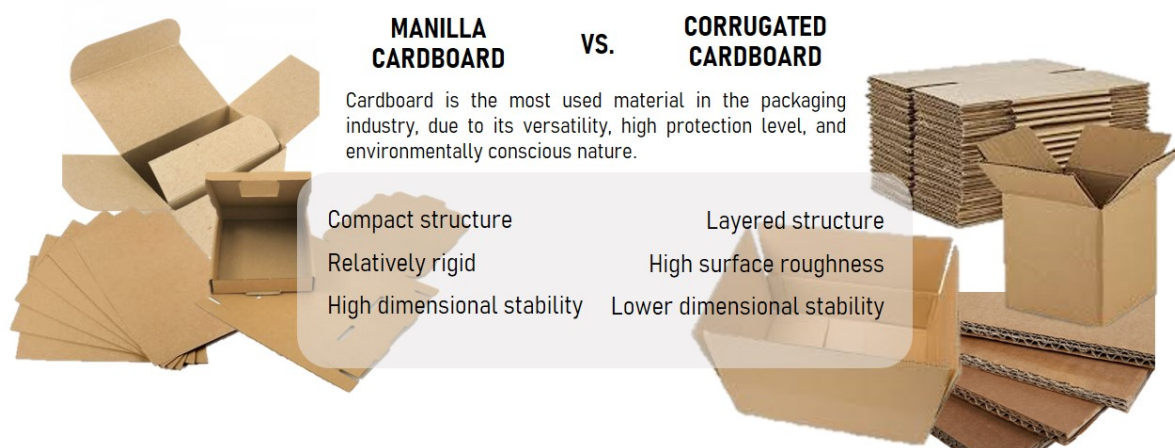


Figure 4.4: Properties of the to most used cardboard types in the packaging sector together with some photographically examples of application.

composition. And second, as a strategy to increase the lignin content on the substrate. This second reason is based on previous results by Ye et al. where concluded that in lignocellulosic biomaterials a higher lignin content over cellulose and hemicellulose generates a higher quality graphene (details about this self-made lignin coating can be found in Materials & Methods Section *Coatings preparation and application*).¹³¹

As mentioned before, LIG technique requires specific and optimized laser conditions. The quality of the graphene generated using LIG technique is subjected to the precursor substrates, the laser features (i.e. light wavelength and atmosphere composition) and the lasing process characteristic (i.e. power and speed, number of lasing steps and defocusing).^{133;152;153} The influence of these parameters has already been studied in the literature. Power and speed will determine exposition time and, consequently the energy radiated over the substrate atoms. Then, higher powers and lower speeds will result in a larger photon flow rate, which translates in more energy absorbed per area. Y. Chyan et al. demonstrated that higher powers generate LIG structures with higher porosity and pore size, with an upper limit beyond which structural failure is reached. Simultaneous lasing steps has also been explored as strategy to generate LIG using milder speed and power conditions (i.e. less irradiance per step). The first raster creates amorphous carbon that turns into graphene after consecutive scans. Finally, defocusing the laser beam can be achieved by systematically varying the relative laser-substrate z-axis relation. The effect is similar

to consecutive lasing steps strategy but reducing the LIG generation process to one step. Figure 4.5 shows the CO₂ Epilog Laser Mini used during this study.

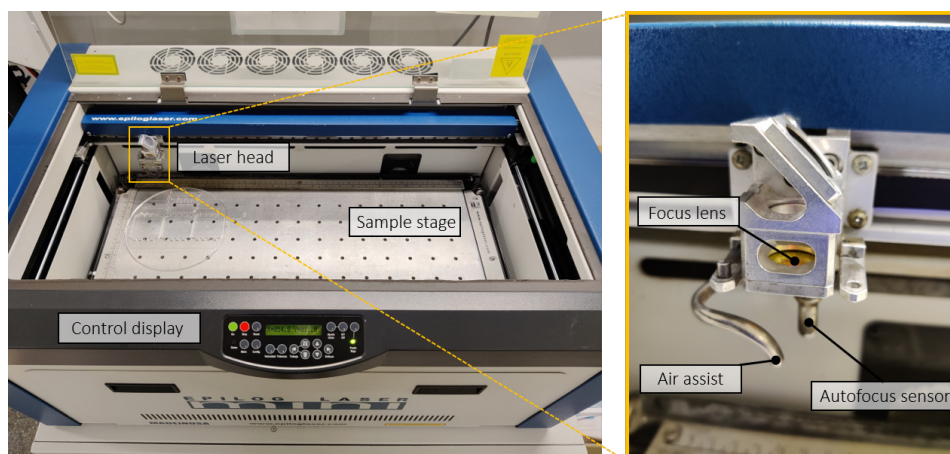


Figure 4.5: Image of the CO₂ laser used for laser induced graphene generation (Epilog Legend Mini 24) and its main parts.

To export the technique onto the substrates of interest an study involving adjustment of lasing power (P) and speed (S), number of lasing steps and defocusing was performed (See Figure 4.6b.). It is important to emphasize that a small percentile units of laser speed and power make the difference between obtain LIG and perforating the substrate or not modifying it at all. Thus, to agile the process of seeking for the adequate LIG generating conditions a matrix based procedure was used. Using CorelDRAW software, 7x7 squares matrices where defined. Each row was assigned to a P value, while each column was designed to a S value. The pre-established condition matrix can be then sent to the laser for engraving. The P - S conditions range and unit steps of the matrices were iteratively adapted and narrowed until LIG yielding conditions were find. An example of a matrix used in this work is shown in Figure 4.6 b., as it can be appreciated the matrix contains a total of 49 squares, with 4x4mm size and covers S and P from 14 to 2 % conditions explored with a 2x step.

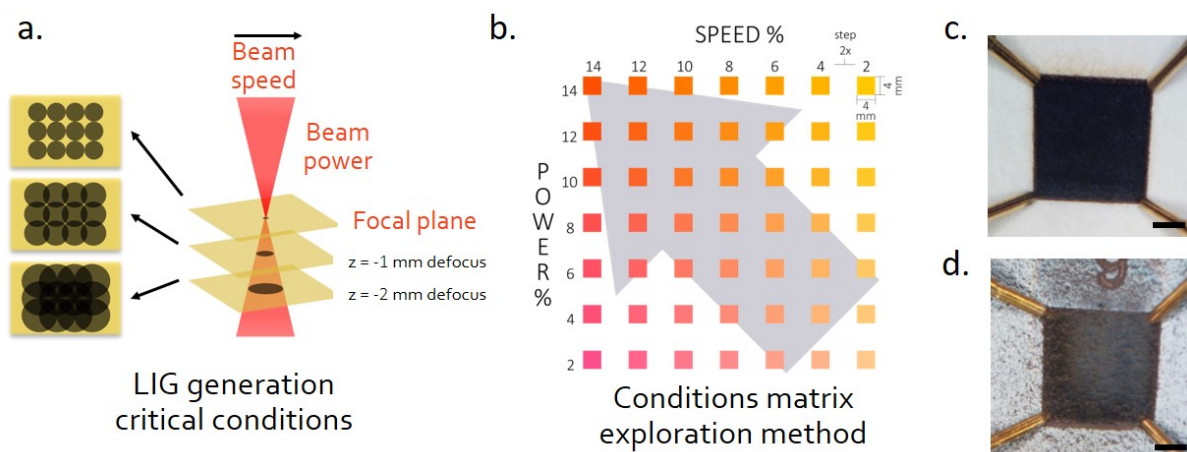


Figure 4.6: **a.** Diagram of a laser beam impacting on a LIG precursor and the effect of the generated pattern accordingly to the defocus applied (i.e. $z = 0, -1$ or -2 mm). **b.** Example of a matrix used for LIG generation conditions screening. The matrix covers from 2 to 14 % speed and power conditions combinations, with 2 unit steps. **c.** and **d.** respectively show LIG squares successfully and unsuccessfully generated.

After lasing, a visual inspection is enough to determine which range of conditions is closer to generate LIG, thus the substrate turn deeply black if success. Figure 4.6 shows two examples of a successful LIG generated square with well-define boundaries and a continuous deep-black surface; and d. an unseccessful LIG square. To recap and summarise, Kapton substrate easily yields to LIG in a single lasing step with out any need of defocusing. Regarding pretreated cardboard further applying either multiple lasing steps or a single step with defocusing (1, 1.5 or 3mm), was required.

LIG characterization | Electrical

The Van der Pauw method¹⁵⁴ was used to determine sheet resistance (R_S), and applied as screening methodology. The conditions generating the most conductive LIG where then characterized electrochically and morphologically. Figure 4.7 schematically describes the basis of this technique. Briefly, the fourth vertices of a sample were electrically contacted with four metallic needles, then a current scan was forced between two vertices while the voltage drop between the opposite two was

recorded (Figure 4.7b.). Current values from 0 to 2mA with 4 μ A steps were employed. An average of the resistivity of the sample was calculated applying eq. 4.1. Due to the orientated raster nature of LIG methodology, LIG material has intrinsic anisotropy. To cover this LIG property, the resistivity analysis was performed forcing the current parallel to the raster direction and perpendicular to it, thus obtaining two R_s values, $R_{s,\parallel}$ and $R_{s,\perp}$ (Figure 4.7c.).

$$I = V \frac{\pi}{\ln 2} R_s \quad (4.1)$$

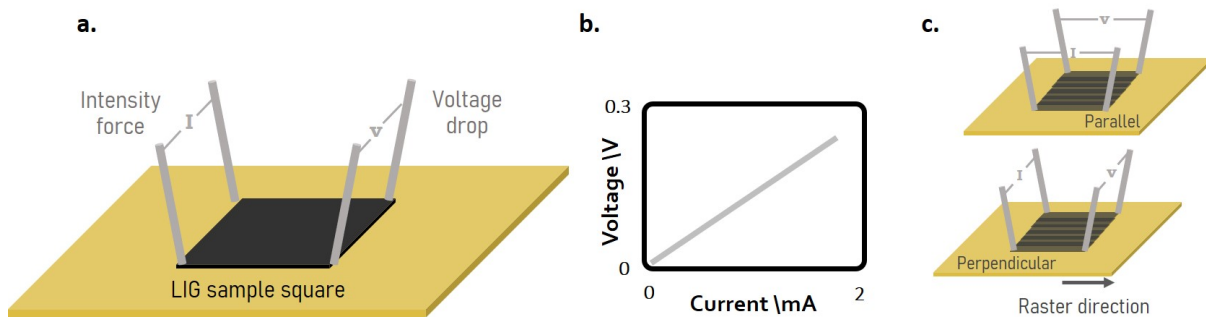


Figure 4.7: a. Schematic representation of Van der Pauw technique in a fourth vertices station used to determine sheet resistance. b. Resistivity analysis configuration to obtain LIG sheet resistance in both directions, i.e. parallel and perpendicular to the raster direction. c. I-V diagram obtained from applying a current screening from 0 to 2mA with 4 μ A steps onto LIG square.

A different matrix was optimized, engraved and tested for each cardboard treatment. It is worthily to notice that the conditions were optimized to produce LIG in just one lasing step. By using 3mm defocusing as alternative, time and energy are greatly optimized specially if scaling the process. The R_s values for the selected conditions are depicted in Figure 4.8.

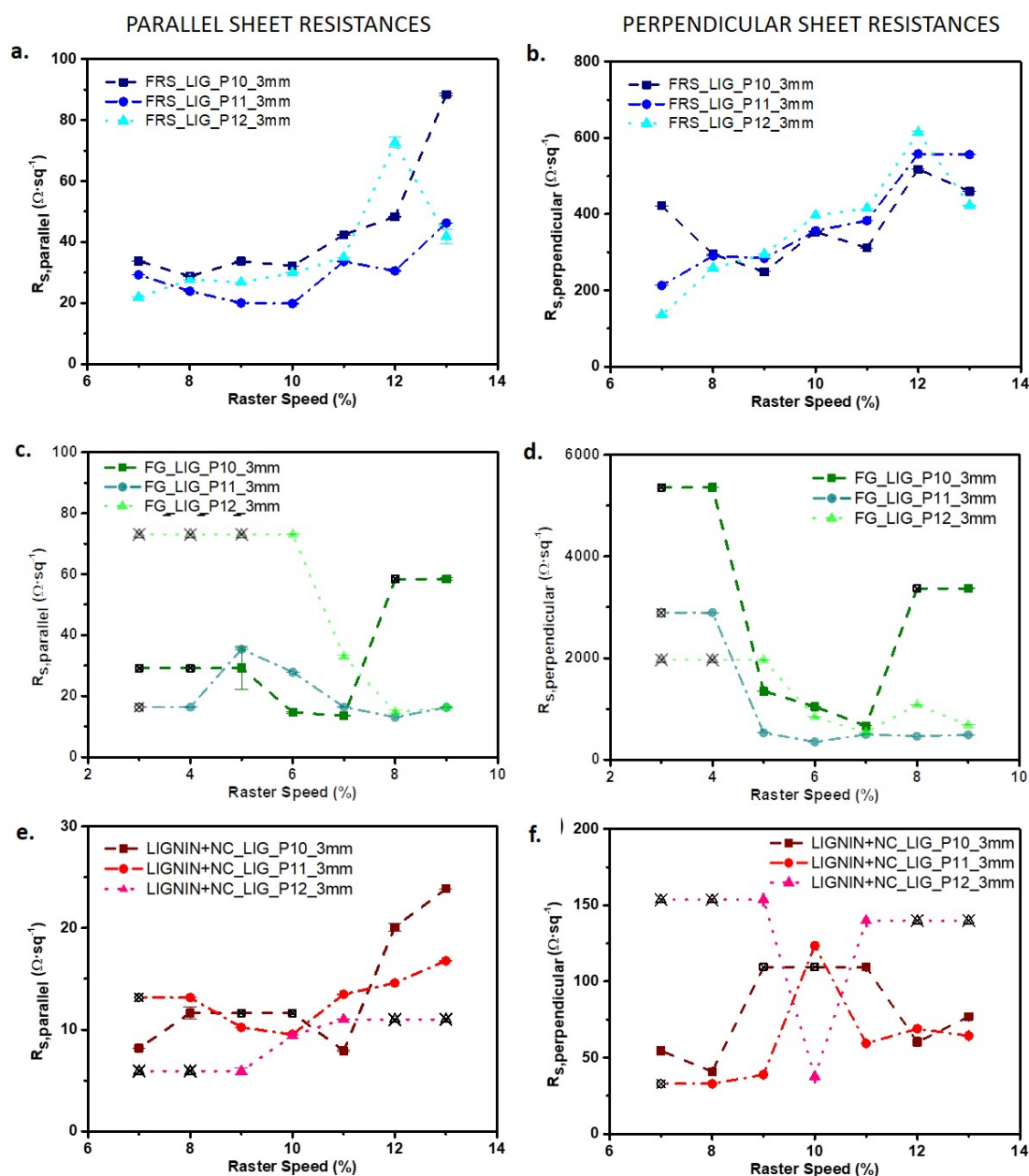


Figure 4.8: Sheet resistance for the three tested cardboard pre-treatments. **a.** $R_{s,||}$ and **b.** $R_{s,\perp}$ values for FRS pre-treatment with 3mm defocus substrate; **c.** $R_{s,||}$ and **d.** $R_{s,\perp}$ values for FG pre-treatment with 3mm defocus substrate; and, **e.** $R_{s,||}$ and **f.** $R_{s,\perp}$ values for lignin pre-treatment, focused. Selected powers from 10 to 12 %, selected speeds from 7 to 13 % for FRS and lignin pre-treatments, and from 3 to 9 % for FG.

First, it can be observed that effectively LIG shows conductivity anisotropy, meaning that for the same lasing conditions $R_{s,\perp}$ is one order of magnitude bigger than $R_{s,\parallel}$. In addition, it can be concluded that LIG sheet resistance does not follow a clear tendency with P and S values; which evidences there is a critical correlation between P-S LIG generating conditions. However, in general terms, lower resistance values were obtained for the lignin based-coating than for the commercial fire retardants. Power values at 11% result the most optimum for the three substrate pre-treatments. Ultimately, the best conditions found via matrix condition method were reproduced in triplets to perform a repeatability study. Figure 4.9 depicts the final LIG generating conditions and their respective R_s values, the results are also numerically gathered in Table 4.1.

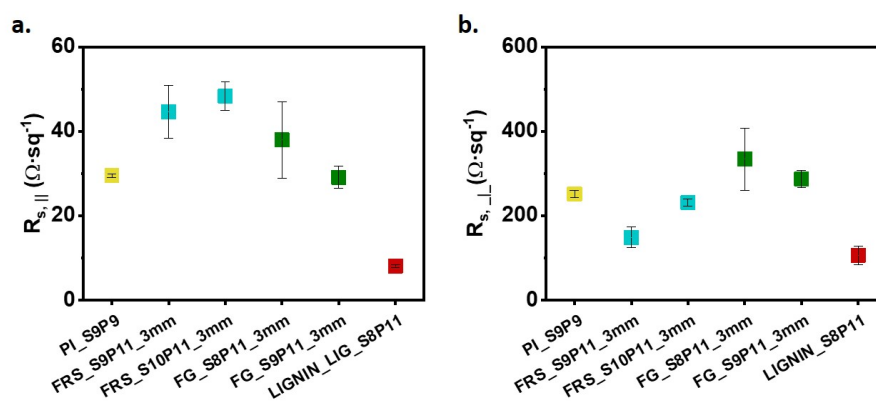


Figure 4.9: Sheet resistance values for laser induced graphene over cardboard precursor with FRS and FG fire retardants (3mm defocus) or lignin-based as pre-treatments. Polyamide (PI) as reference value.(N=3) **a.** R_s values obtained parallel to the laser raster direction. **b.** R_s values obtained perpendicular to the laser raster direction.

Table 4.1: LIG generating conditions leading to the lowest sheet resistances. Cardboard selected as precursor with different pre-treatment, polyamide substrate as reference control.

Precursor substrate	Pre-treatment	Generation conditions (%)	$R_{s,\parallel}$ ($\Omega \cdot sq^{-1}$)	$R_{s,\perp}$ ($\Omega \cdot sq^{-1}$)
Polyamide	-	S9 P9	29.5 ± 0.4	251.2 ± 8.8
Cardboard	FRS	S9 P11_3mm	44.6 ± 6.2	148.9 ± 25.1
	FRS	S10P11_3mm	48.4 ± 3.4	231.3 ± 8.3
	FG	S8 P11_3mm	38.0 ± 9.0	334.3 ± 73.9
	FG	S9 P11_3mm	29.1 ± 2.6	287.0 ± 20.7
	LIGNIN	S8 P11	8.11 ± 0.37	106.7 ± 22.0

The lowest $R_{s,\parallel}$ was $8.11 \pm 0.37 \Omega \cdot sq^{-1}$, for the lignin-based coating with P 11% S 8% conditions. This value outranks reported R_s , being in the same order of magnitude than the lowest value found in literature for a bio-based substrate derived LIG, $3.8 \Omega \cdot sq^{-1}$.

LIG characterization | Morphological

The produced LIG was morphologically characterized via SEM. The obtained images are shown in Figure 4.10. Low magnification pictures visually demonstrate LIG anisotropy, as there can be seen patterned lines in the direction of laser rastering, which confirm the difference measured in $R_{s,\parallel}$ and $R_{s,\perp}$ (see Figure 4.10a,c) This pattern was recently reported by Mikheev et al.¹⁵⁵ However, resistivity anisotropy has not been reported before, nor related with the observed morphological anisotropy.

In high magnification images, LIG morphology varies depending on the substrate and its pre-treatment. Cardboard with fire retardant treatments present a highly porous structure, which has also been reported for other LIG precursors. While LIG on PI surface is completely rough. On the other hand, as can be observed in Figure 4.10 c and d, lignin pre-treatment leads to the presence of long filaments nanostructures, which may be responsible for the low R_s values found.

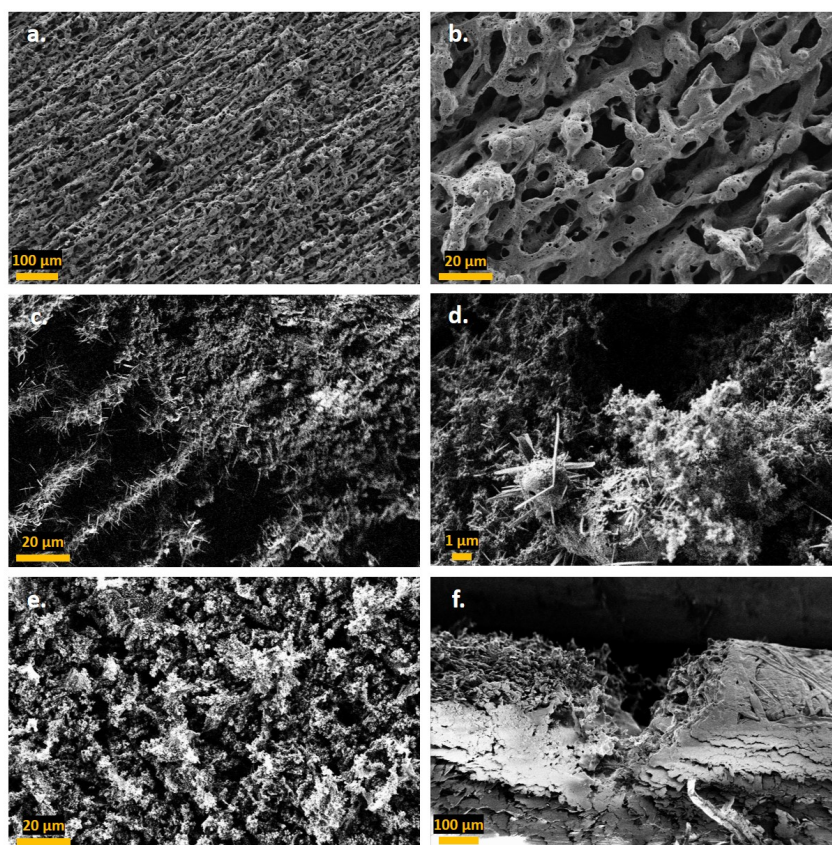


Figure 4.10: SEM images of sample surfaces: **a.** and **b.** FG_S9P11_3mm.**c.** LIGNIN_S10P12.**d.** LIGNIN_S8P11. **e.** PI_S9P9. Cross section: **f.** FG_S8P11_3mm.

Finally, the thickness of produced LIG from different precursors and lasing conditions can be estimated from the cross-section of the SEM images, as in Figure 4.10f. The values are gathered in Table 4.2. As expected, porous LIG thickness (cardboard derived) is larger compared with non-porous LIG (obtained from PI) with around 170 μm and 38 μm thickness, respectively. The generated LIG architectures and its thickness will be directly correlated with the electrochemical active area ratio reported in next section.

Table 4.2: Laser induced graphene thickness values for cardboard as organic precursor material with FRS or FG fire retardants or lignin pre-treatments. Polyamide precursor as reference control.

Precursor	Pre-treatment	LIG Thickness (μm)
Polyamide	-	38 ± 1
Cardboard	FRS	182 ± 11
	FG	164 ± 9
	LIGNIN	171 ± 3

LIG characterization | Electrochemical

LIG suitability as electrodic surface when an electrochemical reaction is involved was assessed studying its cyclic voltammogram (CV) response. Electrodes, with an area of πcm^2 , were engraved over the pre-treated cardboard surfaces and appropriately sealed as shown in Figure 4.11. A pre-activated carbon screen printed electrode (SPE) was employed as control. An electrochemical cell was assembled inside a beaker with LIG-electrodes as working electrode, a commercial Ag/AgCl (3M KCl) reference electrode and a Pt counter electrode. 10mM ferricyanide was used as well-known redox specie, with 1M KCl electrolyte to prevent migration effects. CVs comparison at

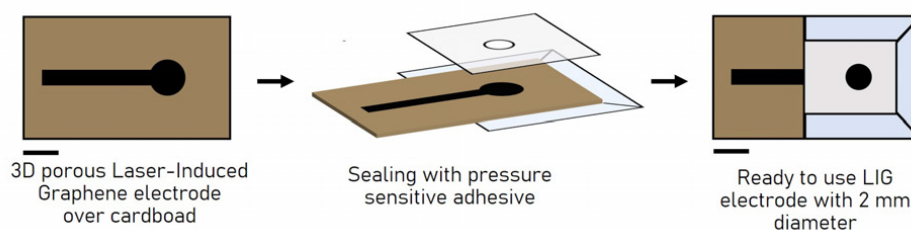


Figure 4.11: Schematic representation of LIG electrodes over cardboard preparation steps: sealing and working area definition process via pressure sensitive adhesive. Scale bars: 3mm.

$20\text{mV}\cdot\text{s}^{-1}$ for LIG electrodes response as working electrode is depicted in Figure 4.12. As first remark, LIG surfaces show good capability for electrons exchange in a redox reaction. By analysing each CV more in deeply, it can be seen as LIG over PI has similar electrochemical behavior as the SPE, with slightly higher reduction peak, at 0.2V. Cardboard electrodes, on the other hand, deliver between two and fourth times

the SPE' density current and have bigger capacitive currents; as expected from the tridimensional-porous nature they shown in the SEM images.

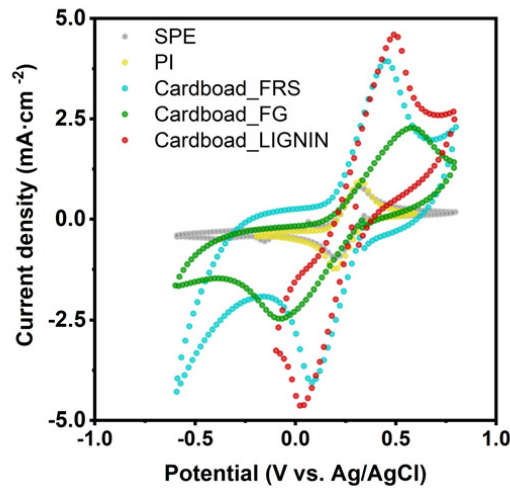


Figure 4.12: Comparison of LIG suitability as electrodic surface via cyclic voltamperometries. Experiment performed in beaker with 10mM ferricyanide, 1M KCl, at 20mV·

To further study LIG behavior, CV experiments were performed at increasing scan rates (5, 10, 20, 50, 75 and 100 $\text{mV}\cdot\text{s}^{-1}$). For LIG electrodes over PI and cardboard with FR treatments, active electrode surface area (ECSA) was calculated from current peaks using Randles–Ševčík equation (eq. 4.2) for reversible systems, and (4.3) for quasi-reversibles.^{156;157}

$$i_p = 0.446nFAc^0\left(\frac{nF\nu D}{RT}\right)^{\frac{1}{2}} \quad (4.2)$$

$$i_p^{qr} = \pm(2.6510^5)n^{\frac{3}{2}}ACD^{\frac{1}{2}}\nu^{\frac{1}{2}} \quad (4.3)$$

where, n is the number of electrons transferred, F is the Faraday constant, A is the area of the electrode, c^0 is the analyte bulk concentration, ν is the scan rate, D is the diffusion coefficient, R the gas constant and T the temperature. Furthermore, using eq. 4.4, electron transfer rate constant (k^0) was calculated via Nicholson method¹⁵⁸, i.e. obtaining the kinetic parameter ψ from eq. 4.5

$$\psi = k^0\left[\frac{\pi Dn\nu F}{RT}\right]^{-\frac{1}{2}} \quad (4.4)$$

$$\psi = \frac{-0.6288 + 0.0021\Delta E_p}{1 - 0.017\Delta E_p} \quad (4.5)$$

where ΔE_p is the oxidation and reduction peaks potential difference. In those cases in which the system showed a quasi-reversible behavior, above equations were replaced by:

$$k^0 = 2.18 \left[\frac{D\alpha n \nu F}{RT} \right]^{\frac{1}{2}} \exp \left[-\frac{\alpha n F \Delta E_p}{RT} \right] \quad (4.6)$$

where α is the transfer coefficient.

Values obtained are shown in Table 4.3. Concerning lignin coating, problems of mechanical instability in water were found, so it was discarded for further electrochemical studies.

Table 4.3: Active electrode surface area vs. geometrical area and electron transfer rate constant for LIG electrodes in comparison with a screen printed electrode.

Electrode type	Precursor	ECSA/GS ratio	k^0 (cm · s ⁻¹)
Screen Printed	-	0.90 ± 0.02	(1.8 ± 0.1) · 10 ⁻³
Laser-Induced-Graphene	PI	1.29 ± 0.08	(2.3 ± 0.3) · 10 ⁻³
	Cardboard FRS	2.11 ± 0.06	(4.6 ± 0.8) · 10 ⁻⁴
	Cardboard FG	2.20 ± 0.70	(1.6 ± 0.7) · 10 ⁻⁴

ECSA has been compared with the geometrical area (GA) obtaining a ratio that reflects the surface structure of the electrode. Looking at these ratios it can be deduced that LIG_FRS and LIG_FG electrodes present a 3D surface structure (since, ECSA/GA > 1). This property is maintained for the LIG_PI, albeit lessened. It is worth to be highlighted that three dimensionality is a really advantageous property when using a material as electrode. 3D architecture increments the total available surface for the redox reaction to take place and improve the transport of redox species to the electrode surface. So when assembling the electrodes in a galvanic cell, these two effects result in an increase in the energy density and a reduction of the system's internal resistance, providing a more efficient electrochemical system. Regarding the k^0 , all results are between 10⁻³ and 10⁻⁴ which is within the same order of magnitude of the literature gold standard glassy carbon.

The values obtained in this section cannot be compared with figures from the literature as no electrochemical characterization of LIG has been reported so far. For this reason, this study is expected to serve as means for comparison in future

research on this aspect. All in all, these results validate the successful creation of a useful electrode over cardboard substrate with a 3D surface able to oxidate and reduce redox species in solution.

4.3.2 Bio-based hydrogel as a battery matrix

In this subsection, a hydrogel matrix is presented to be implemented as a ion exchange membrane and solid polymer electrolyte in the battery.

As part of the battery ecodesign process, natural abundant bio-polymers sodium alginate and micro-nanocelulose were choose to fabricate this hydrogel network. Sodium alginate (AL) is a well-known edible polysaccharide used as gelling agent in food industry. It is present in brown algae cell walls, from which it can be refined. Its gelation property is based on the substitution of sodium ions by cations present in aqueous media.^{159–161} On the other hand, micro-nanocelulose (nCel) is a relatively novel material. Cellulose attracted researches attention years ago, because of being most abundant and renewable polymer on earth. However, its application on electronics and/or energy sector was partially held due some intrinsic cellulose properties, such high surface roughness or structural porousness. To overcome this drawbacks, researches have synthesized micro and nanocelulose papers by applying a pre-treatment step to cellulose fibers. Processes such as mechanical grinding or chemical oxidation are used to remove the defects and fibrillate cellulose fibers into micro-nano fibers. From there micro-nano cellulose paste and paper has arise as an 'green' raw material candidate with excellent mechanical and chemical properties.^{162–164}

In the particular context of this work, commercial microfibrillated cellulose was selected to create the hydrogel matrix with two purposes, we aim to increment the total cellulose content of the battery to enhance its compatibility with paper and cardboard recycling processes; while exploring its suitability to act as solid polymer electrolyte. The syntetized hydrogel matrix should meet certain properties to be suitable as polymeric electrolyte, such as, high ionic conductivity (preferably higher than 10^5), good chemical and mechanical stability and high range pH tolerance.

To create the polymer electrolyte matrix, the selected biopolymers affinity was tested

by combining different ratios and testing its ionic conductivity. Because of the bio-polymers selected, hydrogel membrane synthesis could be performed with non-toxic reactants using mild gelation conditions by a simple solvent casting (SC) method. The synthesis protocol developed is schematically described in Figure 4.13. Five X nCel:Y AL ratios were synthesized (0:100, 25:75, 50:50, 75:25 and 100:0) as follows: 2% wv AL solution is prepared with deionized water and stirred between 2 and 3 hours applying mild heat. While 1% wv nCel solution is dispersed with a dispersing instrument by 5 minutes at 10000rpm (specifications from the manufacturer). Then the mixtures are combined following the ratios of interest, doped with 5% wv of glycerol and stirred again at room temperature over 2h. Finally, 40ml of each polymeric mixture is cast into a Petri dish (8.6 cm diameter) and dry at 25 °C in an incubator for 5 days. After the drying process flexible self-standing membranes were achieved for all ratios except for 100:0, in which case it was not possible to unmold it (see Figure 4.14).

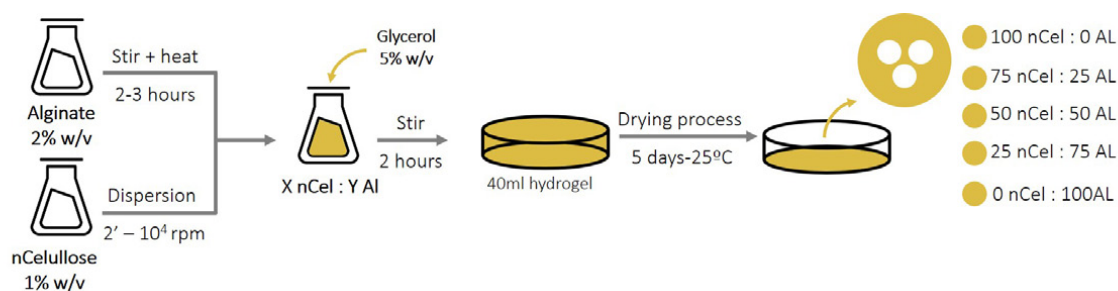


Figure 4.13: Schematic representation of hydrogel membranes synthesis protocol.

The matrices suitability as ion conductive media was assessed by characterizing its ionic conductivity via electrochemical impedance spectroscopy (EIS) method. From each synthesized membrane three circular sections were cut with a circular punch to perform the EIS analysis. The average conductivity for each ratio depicted in Figure 4.14 a. was calculated by eq. A.2 after analyzing the Nyquist plot (Figure 4.14 inset) and obtaining the resistance solution (R_s) as explained in Appendix B. All the obtained values are in the range of 10^{-4} which based on literature is adequate for their use as polymeric electrolyte.¹⁶⁵ The conductivity study also reveals that a synergistic effect is created when combining the two biopolymers, resulting in an enhancement of ion transport through the membrane. The highest ionic conductivity of $7.83 \cdot 10^{-4} \pm 2.49 \cdot 10^{-5} \text{ S cm}^{-1}$ was obtained for 25nCel:75AL ratio, which

moreover presents a adequate mechanical characteristic for the purpose of this work. Thus, this membrane was established as ionic conductive membrane for the battery development in next section.

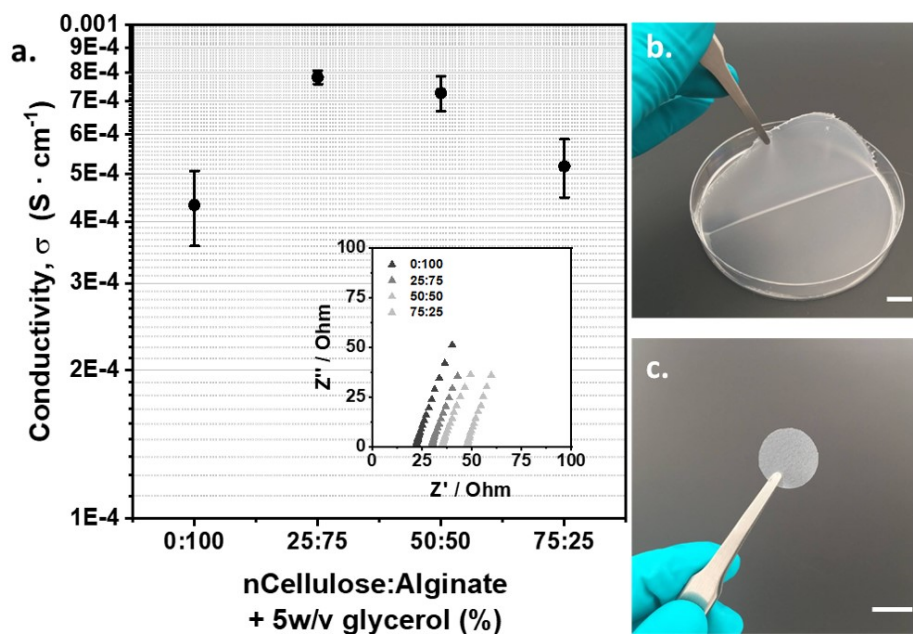


Figure 4.14: a. Ionic conductivity variation as a function of nanocellulose and alginate biopolymers ratios.(N=3) Inset: Nyquist plot obtained from impedance spectroscopy analysis. b. Example of the synthesized biopolymeric membranes appearance. c. Punch cut for the electrochemical analysis. Scale bars: 1cm

4.3.3 Prototype operation test

Once the polymeric matrix was synthesized, the next step was to combine it with the LIG generated current collectors to evaluate the different materials performance within an electrochemical galvanic cell.

Ascorbic acid (AA) and iron nitrate ($\text{Fe}(\text{NO}_3)_3$) were selected as anodic and cathodic redox species respectively. From the redox species screening performed (see Appendix C) AA and $\text{Fe}(\text{NO}_3)_3$ show an open-circuit voltage difference of 1.15V. As shown in Figure 4.15, to achieve this voltage output mixed media conditions are require.

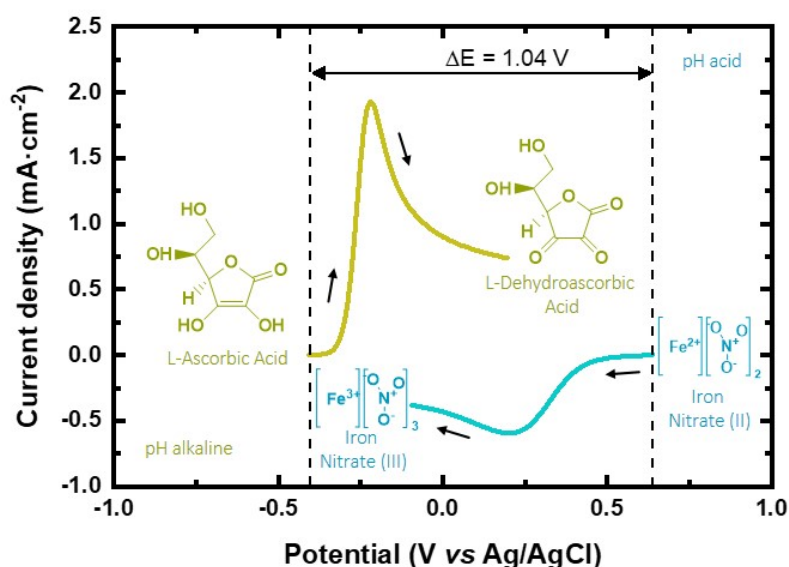


Figure 4.15: Linear sweep voltammograms of the redox chemistry selected to power the battery. Oxidation of 10mM AA in 1M KOH as alkaline electrolyte and reduction of 10mM $\text{Fe}(\text{NO}_3)_3$ in 1M $\text{C}_2\text{H}_2\text{O}_4$.

To adapt this chemistry to the hydrogel based battery, the polymeric matrix tolerance to pH was tested. Alkaline media was created by simply adding KOH (0.1M) to the hydrogel matrix during the doping with glycerol step. After the 2 hours of stir process an homogenized matrix with pH 14 has been created. The same process was follow to generate an acidic medium, by the addition of oxalic acid (0.25M). However, in this case, the change in pH produced a drastic change in viscosity, creating unbreakable clumps. This behavior has been already reported in the literature, concluding that for

pH lower than 3-3.5 the carboxylate groups in the alginate chain become protonated, forming hydrogen bonds that increase exponentially the alginate solution viscosity. As the selected matrix is 75% composed by an alginate solution this behavior heavily affected the acidic hydrogel stability. For these reason, we substituted the 25:75 ratio matrix by the 75:25 as cathode electrolyte. Finally, the anode and cathode are created by incorporating 0.1 M AA or 0.2 M $\text{Fe}(\text{NO}_3)_3$ to the respective hydrogel matrix and stirring at room temperature, with light protection in the case of AA-hydrogel.ⁱⁱ. Figure 4.16 recaps the final prototype materials.

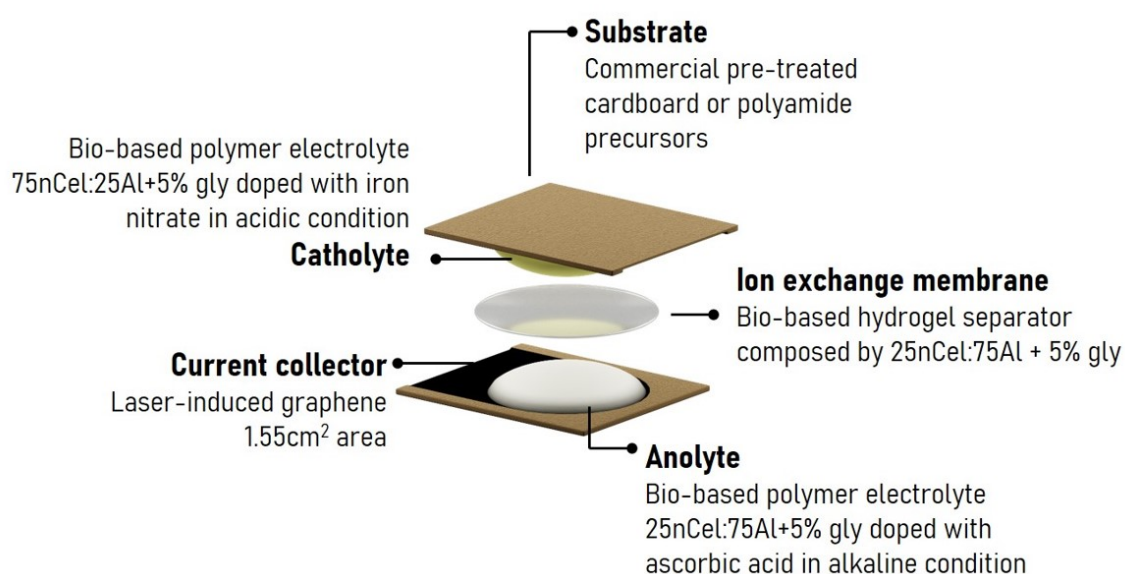


Figure 4.16: Schematic representation of a LIG testing unit battery core materials.

The cell performance was first tested with Kapton substrate as LIG current collectors precursor. The electrochemical characterization was assessed through polarization curves, sweeping from pre-measured open circuit voltage to 0V at 20mV/s scan rate; and continuous discharge recorded under a external load, $R=3.3\text{k}\Omega$. The plots are depicted in Figure 4.17. The battery showed an 1V OCV and a maximum power output of 0.4-0.5 mW. Moreover, stable discharge was recorded over 10 minutes. This demonstrates a good synergy between the selected materials and the feasibility of using LIG as current collector in a hydrogel based battery.

ⁱⁱThis particular concentration of actives species is selected to perform the prototype test. They are mild concentrated values that do not compromise the hydrogel stability, allowing a rapid materials testing. In particular, the $\text{Fe}(\text{NO}_3)_3$ concentration doubles the AA, to compensate charge transfer, i.e. one electron transfer from Fe^{+3} ion reduction reaction over the two electron AA oxidation reaction.

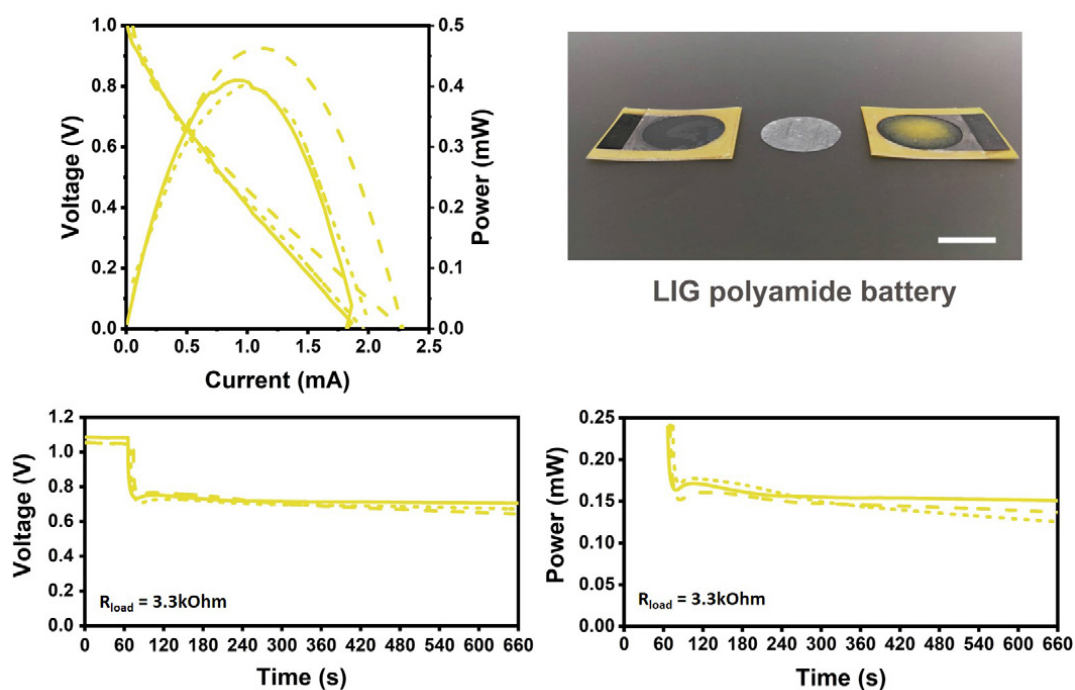


Figure 4.17: Bio-polymer based battery electrochemical characterization with LIG current collectors over polyamide substrate. Scale bar: 1cm.

Once the unit testing battery was proved to be functional, the polyamide LIG electrodes were substituted by cardboard electrodes, FRS fire retardant and lignin coating pre-treatments were chosen as precursors substrates. The results are depicted in Figure 4.18 and 4.19 respectively. In the two cases functional batteries were recorded, with an OCP around 0.9-1V. However, a dramatic decrease of one order of magnitude in the current output was found for the FRS battery, directly related with the higher R_S value found (see Table 4.1). Regarding the lignin coating cardboard battery, a maximum power output of 0.3mW was achieved, but the continuous discharge showed instability. When using cardboard as a LIG precursor, certain incompatibility was observed during the process of casting the water-based hydrogels on top of the electrodes. Due to the cardboard's hydrophilic nature, the substrate integrity was partially compromised, which can explain the difference in performance between the plastic-based polyamide battery and the cardboard batteries.

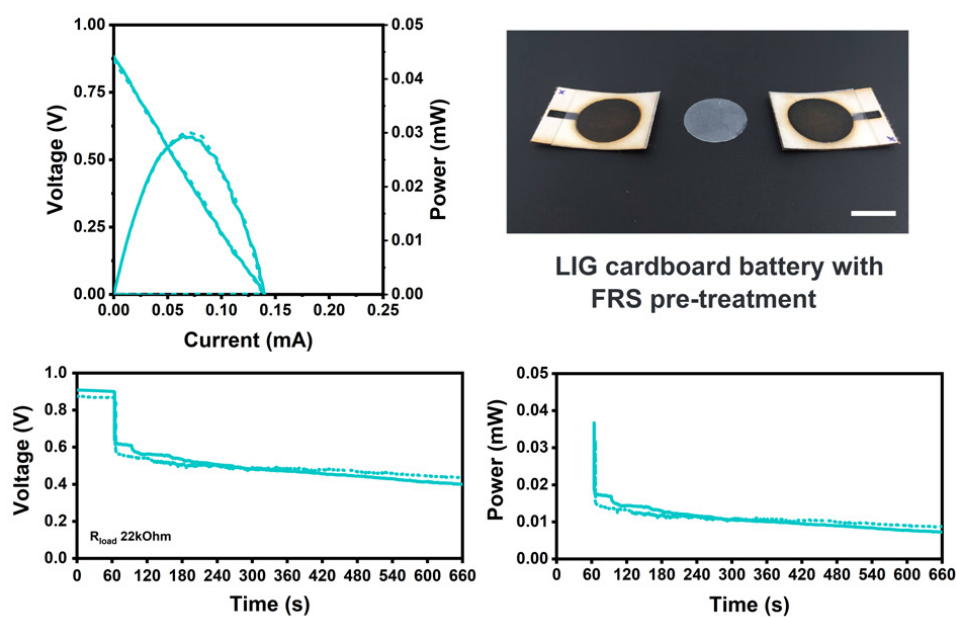


Figure 4.18: Bio-polymer based battery electrochemical characterization with LIG current collectors over cardboard substrate with fire-retardant FRS pre-treatment. LIG generating conditions: S9P11_3mm defocusing. Scale bar: 1cm

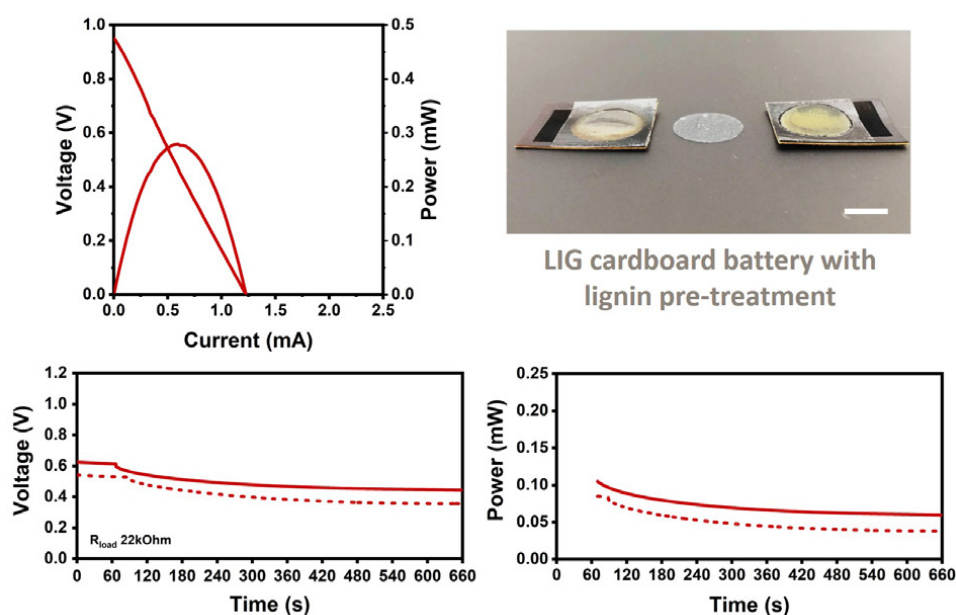


Figure 4.19: Bio-polymer based battery electrochemical characterization with LIG current collectors over cardboard substrate with lignin coating pre-treatment. LIG generating conditions: S8P11. Scale bar: 1cm

4.4 Discussion

The work herein presented sets the guidelines, and first steps, towards the development of a primary battery tailor-made for the smart packaging sector; and is expected to be a cornerstone on the definition of batteries paradigm in this sector. Nevertheless, further work is needed to achieve a completely functional prototype. In this sense, future work will tackle three main objectives: the enhancement of the power output, increasing the battery fabrication compatibility with cardboard boxes production and standardized tests of battery recyclability.

In order to meet the power requirements of small sensing devices, a straightforward strategy to be implemented is increasing the concentration of redox species. The prototypes presented herein were fabricated with test concentrations of 100mM AA and 200mM $\text{Fe}(\text{NO}_3)_3$, however these concentrations could be raised up to the maximum solubility values (i.e. 1.85M AA and 3.70M $\text{Fe}(\text{NO}_3)_3$). The hydrogel matrix conductivity could also be enhanced, for instance, by incrementing the glycerol content, so that the overall battery internal resistance is decreased. On the other side, due to the versatility of LIG fabrication technique, all conceivable electrodes design, area sizes, and stacks can be easily implemented thus allowing to adapt the power output to each specific energy intake.

Furthermore, some design improvements could be implemented to enhance battery fabrication compatibility with cardboard box production lines. Two strategies can be tackled in this sense, one possibility is to fabricate the battery with a sticker like concept, thus the battery could be easily glued to the package. On the other hand, the battery can be directly fabricated during the box fabrication, implementing LIG technique together with lamination processes directly to the package manufacture process.

The prototype presented in this chapter has been developed by performing a conscious selection of materials. In this sense, it does not contain any unwanted or prohibited material that could compromise the paper recycling process (accordingly to EN 643:2001). It is worth mentioning that, PSA and PET compensation layers, used because of its practicality, must be substituted by waterproofed cardboard layers

and a compatible glue. Furthermore, in order to ensure that the final implementation of the battery in the smart packaging system does not compromise cardboard's high recyclability rates, the battery unit test should be evaluated under European standard *EN 134030-Packaging – Requirements for packaging recoverable by material recycling*. This standard assesses a product's suitability for recycling by validating two criteria: 50% of the product must consist of paper-cardboard weight and a study of the pulp quality after product defibering (see Appendix B *Standards and regulations*). Currently, the battery testing unit approximately contains 47.5 % w/w of cellulose based materials, almost fulfilling EN 134030 first requirement to be considered recycling as a solo element. However, the battery final prototype should be adapted to a particular package in terms of dimensions and materials weight content. In this sense, the battery final dimension would be tailored for instance to a box or an envelope; and its recyclability tested accordingly as a joint design.

Conclusions|

This chapter has introduced a primary battery specially design for smart-packaging applications. The implementation of a holistic vision since the beginning of the battery development has enabled an entire redefinition of the battery concept.

Four interrelated aspects of the battery life cycle have been integrally tackled to lower the battery environmental impact. The battery application has been placed as the linchpin to guide the materials selection, the fabrication process implementation, and the targeted end-of-life. First, the material selection has been carried out advocating for a functional battery but without ignoring the environmental impact along its life cycle. Cardboard has been selected as substrate precursor to generate graphene electrodes via a low energy consuming lasing method. LIG technique has been sucesfully implemented over Manilla cardboard, by using two pre-treatments: commercially available fire retardants and, a self-synthesized lignin coating. The electrical characterization showed an intrinsic anisotropy property of LIG material, never reported before. Moreover, LIG generation conditions have been optimized reaching R_s values in the same order of magnitude of those reported in the literature ($8.1 \pm 0.4 \Omega \cdot \text{sq}^{-1}$). More significantly, LIG suitability as electrode in a redox reaction processes has been proven founding appropriate electron transfer constants. And, its conductive properties have been strongly correlated with the electro-active area measured and the morphology found via SEM images.

Once the LIG technique was implemented, the next step was to develop a bio-polymeric matrix that could act both, as a ion-exchange membrane and solid polymer electrolyte. The hydrogel created by combining commercial alginate and micro-fibrillated cellulose showed adequate mechanical properties and an optimum ionic conductivity to be implemented in a battery. Synergetic effect appears when combining the two bio-polymers, favoring the ion conductivity. Specially a 25nCel:75Al ratio presented the higher conductivity of $7.38 \cdot 10^{-4} \pm 2.49 \cdot 10^{-5} \text{ S cm}^{-1}$. Finally, the development of LIG over a cardboard substrate in conjunction with the bio-polymer hydrogel has allow to create a battery testing unit. Selecting acid ascorbic and iron nitrate as anodic and cathodic active species respectively. Three different batteries haven been successfully characterized demonstrating the approach feasibility.

Materials & Methods

This section details the processes and methodologies followed during the research presented in this chapter. Despite some of the protocols that have been briefly described in the main text, this section aims to bring together all the followed procedures in order to consistently presented them to the interested reader.

Coatings preparation and application

Phosphate ammonium based ForcedField FireGuard for Fabrics (Shield Industries, Inc., Woodstock, Georgia, USA) and boric acid based Flame Retardant Spray (FireChief) were purchase online and use as received from they spray bottles. Each product is separately apply to a 10x10cm² cardboard square by spraying 6 time and dried overnight.

On the other hand, for the preparation of the lignin coating a nanocellulose 1% w/v dispersion is use as supporting matrix. As during the hydrogel matrix preparation, 5g of 10% w/v nCel (nCel, Exilva P 01-V from Borregaard) are dispersed in 45 ml of DI water by using an T 25 digital ULTRA-TURRAX (IKA-Werke) dispersion instrument, at 10000 rpm for 5 minutes. Then, 1.5g of pure lignin alkali (Lignin alkali 471003 from Sigma-Aldrich). Finally, to create the coating, 20 ml of dispersion are poured over the cardboard using a 8.6cm diameter petri dish and dry during 72 hours in an incubator at 25 °C (Hach Lange S.L.U. L2-01).

Prototype materials

Manilla cardboard from recycled office folders is used as substrate and modified by the coating methods described above for LIG generation.

The hydrogel matrix is synthetized as follows, 1 g of sodium alginate (Al, W201502 from Sigma-Aldrich) is stirred in 50 ml (2w/v % concentration) deionized (DI) water at 80°C until dissolution is complete. 1 w/v % nanocellulose (nCel, Exilva P 01-V from Borregaard) dispersion is prepare accordingly to the manufacturer recommendations. Meaning, 5g of 10% w/v nCell are dispersed in 45 ml DI water at 10000 for 5 minutes

with T 25 digital ULTRA-TURRAX (IKA-Werke). Then, the ionic conductive membrane hydrogel is created by mixing both dispersions in 75Al:25nCel proportion and doped with 5%w/v glycerol. The mixture is homogenized during 2h using a magnetic stirrer. Finally, as described above 15mL of the obtained hydrogel is poured in a 8.6 cm diameter petri dish and dried at 25°C over 48h in an incubator (Hach Lange S.L.U. L2-01).

Similarly, the anodic and cathodic matrices are synthesized by mixing 75Al:25nCel and 25Al:75nCel bio-polymer proportions respectively. Then, incorporating 0.1 M ascorbic acid (AA) with (KOH) to create the anodic hydrogel and 0.2 M iron nitrate ($\text{Fe}(\text{NO}_3)_3$) with oxalic acid ($\text{H}_2\text{C}_2\text{O}_4$) for the cathodic. This addition takes place during the glycerol addition. After, 2h of magnetically All chemicals purchased from Sigma Aldrich (Sigma Aldrich, St Louis, Missouri, USA) and use has received.

The different prototype structural layers are designed using CorelDRAW CAD program (Corel, Ottawa, ON, Canada) and cut using the same CO_2 laser cutter. To fabricate the testing prototype, hydrogel cathodic and anodic pools are composed by a combination of 125 μm polyethylene terephthalate (PET) plastic (Melinex ST504 PET, DuPont Teijin Films, USA) and 48 μm 92712 pressure sensitive adhesives (PSA) from Adhesive Research. While the membrane is compensate using 3 layer of 92712 adhesives.

Lasing process

The laser induced material study presented in this chapter has been performed with an Epilog Legend Mini 24 instrument. A flat glass panel is used to label the lased materials and ensure an uniform surface platform. The laser has two modes, engrave or cut. In this work engrave mode is used to scribe on samples and generate LIG samples. Different parameters can be custom set to control the laser beam. 1200 DPI resolution and autofocus modes are selected for all the generated samples. While speed of the moving lens (S) and power are chosen from 1% to 100% to the designed value accordingly to the designed condition matrix. Being 30W the maximum power density (i.e. 100%) in the case of this particular laser. Additionally, Air Assist is used to blow compressed air on the material surface helping to reduce heat and removing

combustible gases, while a gas extractor (BOFA AD Base2) takes away the expelled gases.

Membranes ionic conductivity studies

The hydrogels were prepared as described above, then mixed at the different ratios (100:0, 75:25, 50:50, 25:75 and 0:100) and doped with 5% w/v of glycerol as plasticizer. For the ionic conductivity study presented, 40 mL volume of hydrogel is used to create the membranes, and the incubation process is extended to 4 days. The increment in the volume yields to thicker membranes facilitating the ionic conductivity measures.

After the drying process the membranes are manually cut with a 1.55 cm² diameter punch and its thickness is measured with a dial indicator (RS PRO, Amidata S.A.U., Alcobendas, Madrid, Spain).

LIG electrical characterization

The LIG material was electrically characterized in a four-point station (EP6, Suss MicroTec)

Electrochemical studies

All electrochemical measurements were performed using a PalmSens4 potentiostat / galvanostat / impedance analyzer (PalmSens BV, Houten, The Netherlands). All tests were performed at room temperature.

LIG electrodes electrochemical characterization is performed by cyclic voltammetry analysis adapting the voltage window and with a constant 20 mV·s⁻¹ scan rate for all the samples. A conventional electrochemical cell is assembled using commercial Ag/AgCl (KCl 3M) reference and platinum counter electrodes. 100 mM ferricyanide is selected as well-known electroactive species and phosphate-buffered saline (1M KCl) is used as aqueous electrolyte.

Hydrogel membranes' ionic conductivity is done by performing an Electrochemical Impedance Spectroscopy (EIS) analysis from 1 kHz to 1 MHz. The value of the matrix conductivity is obtained, as explained in Appendix A subsection '*Impedance*

spectroscopy to asses hydrogels with ionic conductivity', from the resistance value extracted from the total impedance when the imaginary component is zero.

Battery polarization and power curves are generated using linear sweep voltammetry technique, sweeping from pre-recorded OCV to 0 V at a scan rate of $20\text{mV}\cdot\text{s}^{-1}$. While the discharge curves are recorded under different external loads to force the battery to work at 0.5V aprox.

LIG morphological assessment

1 kV electron acceleration is selected for sample surface and cross-section imaging. The sample, connected via

5

Exploring local and decentralized biodegradable battery development

Special acknowledgment

Antes de continuar con los últimos resultados experimentales de esta tesis, me gustaría expresar mi gratitud hacia todas las personas que han hecho posible este capítulo.

Las siguientes páginas se han utilizado como canal para compartir y difundir un conocimiento generado tras las visitas e interacciones con los habitantes de Jaltenango, Chiapas (México). En este sentido, cabe mencionar que no hubiera sido posible sin la colaboración de la cooperativa de productores de café Triunfo Verde. En particular, me gustaría mostrar mi agradecimiento a Hugo Lares, Lenin Ruiz, Calixto Guillen y Moises Mazariegos, por haber estado siempre predispuesto a colaborar con nosotros y compartir sus conocimientos y experiencia dentro del mundo del café. También me gustaría mostrar mi gratitud a la familia de Pérez, Ema, Corazon y Erik, por compartir con nosotros su hogar, su tiempo y sus experiencias como productores de café y habitantes de las comunidades cafetaleras.

Mi gracias de corazón por vuestra paciencia enseñándonos a valorar, respetar y cuidar el café.

Overview

This chapter has been created on the basis of the *'thinking globally, acting locally'* concept. The battery development process for this chapter is located at a conceptual level in coffee growing communities of southern Chiapas, Mexico. The communities energetic needs and resources have been deeply analyzed in order to develop a battery grounded on the local reality. In this sense, the battery presented herein represents the most ambitious goal of this thesis. The hollistic vision claimed in Chapter 2 has been integrally applied in this chapter to developed a battery for which: coffee waste is proposed as a source of battery materials, the fabrication processes have been restricted to a feasible decentralized production, the application tackles coffee communities real necessities, such as lighting systems and UV water disinfection devices, and finally, biodegradability has been chosen as the most appropriate end-of-life (see in Figure 5.1 the proposed battery life cycle). Furthermore, the project impact has been assessed through the adaptation of the Social Progress Impact.

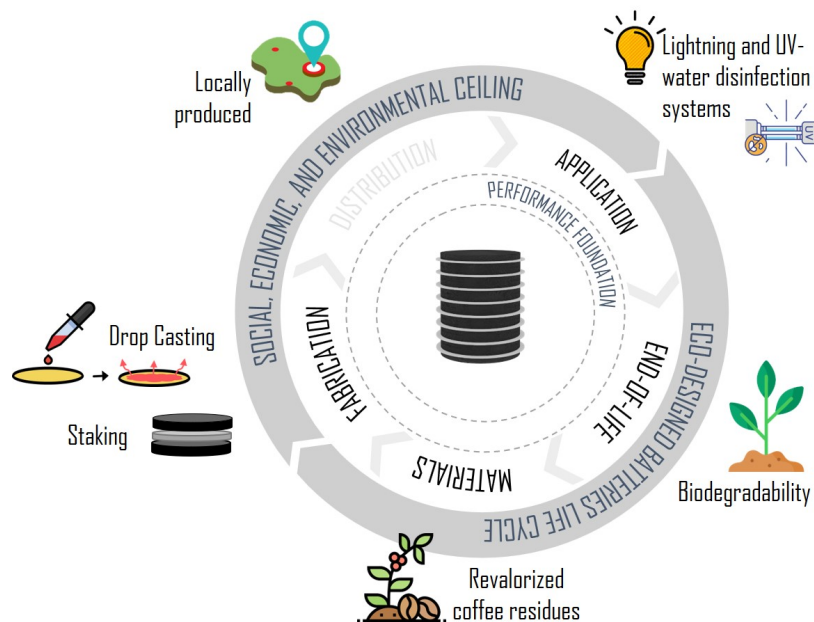


Figure 5.1: Sustainable battery life cycle envisioned for powering lighting systems and UV water disinfection devices in coffee growing communities.

5.1 Introduction

As exposed in the rationale at the beginning of this thesis, the whole battery life cycle must be taken into account from early battery conception; in order to ensure the batteries to stay within the safe space for a sustainable development. In this sense, when conceptualizing the battery one must think *what* it is going to power, but also *where*. The answers to these two questions will contribute to define the battery design and purpose. Thus, this chapter explores the creation of a decentralized and sustainable power source. In a way that, batteries are ecodesigned and materialized under the local framework, through the revalorization of the available resources and tackling specific needs. Therefore, in order to fully understand the research purpose of current chapter our thinking process needs to be placed in Chiapas, Mexico. More precisely in the coffee growing communities of the nature reserve of 'El Triunfo'.

Chiapas, or Chyapas, is one of the thirty two federal entities that conform Mexico. It is located at the south of the country and it is the entity with the highest social gap according to CONEVAL ('Consejo Nacional de Evaluación de la Política de Desarrollo Social' or National Council for the Evaluation of Social Development Policies).^{166;167} In 2015 a multidimensional social well-being indicator at a national level was launched by the *Mexico, ¿Cómo vamos?* researchers association, based on the international Social Progress Index (SPI) proposed by nonprofit Social Progress Imperatives. The SPI arises from the need of transcending and measure societies' wellness in terms beyond economics. It is not the only attempt to address these alternative metrics of social progress towards happiness and well-being. Governments and institutions worldwide have proposed alternative metrics to measure societies' progress beyond economic performance, such the European Union '*Beyond GDP*' program or the Human Development Index (HDI) and the Gross National Happiness Index (NHI) proposed by the World Bank. These indicators aim to create metrics that complement Gross National Product (GNP). In this sense, they represent the quantification of holistic development philosophies such as the doughnut economic model presented in Chapter 2. Displacing GNP as a solo indicator of a country's well-being allows to evaluate prosperity through a holistic vision.¹⁶⁸ In this context, the SPI was selected by Mexican researchers to be adapted and computed for each one of the 32 federal

entities that compose Mexico state. Their objective by implementing this metric was to create a benchmark to better assessed the needs of each particular country entity; and to enable social, environmental, and economic policies creation to become grounded on living realities.^{169;170}

The indicator is constituted by three dimensions, named Basic Human Needs, Foundations of Wellbeing and Opportunity. As shown in Figure 5.2 each dimension is defined by four main components encompassing from good Nutrition & Basic Medical Care access to Environmental Quality or Society Inclusiveness.¹⁶⁸

Figure 1 / Structure of the Social Progress Index

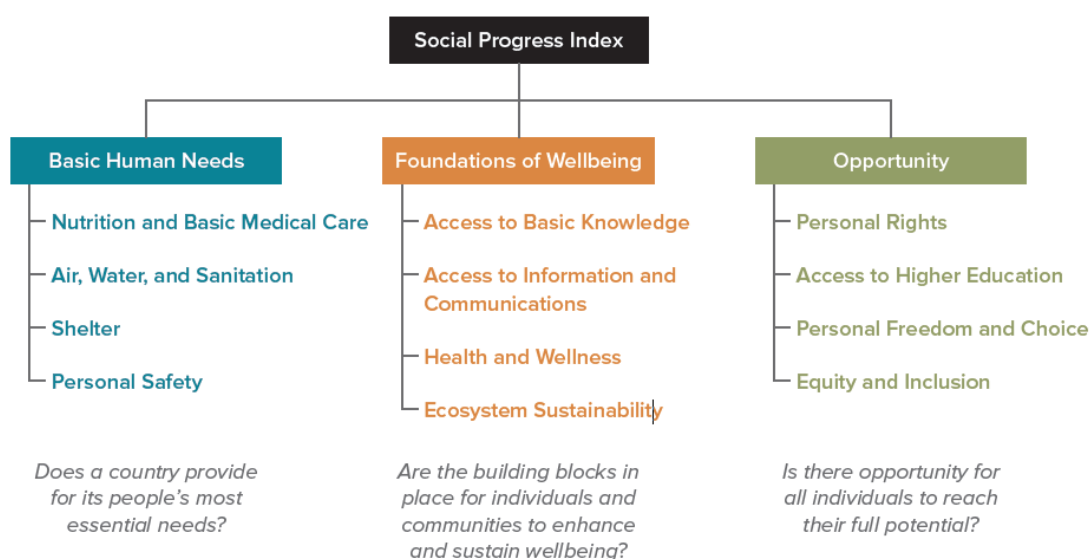


Figure 5.2: Social Progress Index (SPI) takes into account three dimensions, i.e. Basic Human Needs, Foundations of Wellbeing and Opportunity, and their related four components, each one composed by a set of indicators. Source: Social Progress Imperatives¹⁶⁸.

Mexico, ¿Como vamos? has been computing this indicator for each country entity since 2015. According to those results, Chiapas is one of the three entities presenting lowest SPI. In 2020 Chiapas ranked 49.9, far from the average national value of 63.2. In contrast to this social reality, Chiapas owns an enormous environmental richness and a huge agricultural capability. Mexico is the 9th coffee producer country in the world and producers in Chiapas are responsible of most of the coffee generation in the country, creating richness and employing more than 180 thousand producers among the territory.¹⁷¹ Specifically, 41% of national coffee production is grown in chiapan

territory, followed by Veracruz and Puebla entities, with a 24 and 15 % respectively. Furthermore, with an annual production around 370kT of coffee cherries, Chiapas is believed to be one of world leading producers of organic coffee, meaning that the use of agrochemicals is very restricted to protect the land quality and respect the natural environment.¹⁷²

Coffee production has associated a considerable organic waste throughput. Investigations estimate that for each kilogram of harvested coffee, 452 grams of associated by-products are obtained. In this context, agro-industrial waste revalorization seems to be specially appealing. Biomass residues associated to agricultural practices have been identified as rich source of valuable biocompounds. Adding value to those wastes by reformulating them as raw materials do not only generates an additional income, but also fosters their correct management, reducing their environmental impact. In particular, coffee production by-products have been already identified in the literature as valuable feedstock to recover.^{173;174} Some of the proposed applications are biodiesel production, bioethanol production,^{37;175} recovery of sugars, or source of phenolic compounds.^{176–178} However, currently the main application of coffee residues is compost production.^{179;180}

The research presented in this chapter was carried out within the framework of the iLINK project *"Biodegradable batteries for underprivileged coffee-growing communities"* financed by CSIC and Tecnológico de Monterrey. The project main goal is to use revalorized materials from local resources, coffee residues in particular, to fabricate biodegradable batteries. The batteries are intended to power lighting systems and water UV-disinfection devices in coffee growing communities in Mexico. The work was performed in collaboration with Sustainable and Applied Biotechnology research group from Tecnológico de Monterrey university. Figure 5.3 schematically represents a conceptualization of the battery and the first steps towards the goal of the chapter.

First, the project framework is presented, to validate the project viability coffee local producers were interviewed about their day-life experiences. The interviews provided a unique and realistic approach to the development process of the batteries, enhancing its implementation viability to those locations since the beginning of the

battery conception. Their daily-life realities, together with an 'in situ' study of coffee production processes and main by-products analysis are presented in Section 5.2. Then, the battery prototype is designed to power a portable lighting system is presented in Section 5.3. The battery is fabricated from commercial materials but aligned with the project vision, and the viability to be fabricated in Chiapas mountains is assessed (Sections 5.4 and 5.5). Finally, the viability of using revalorized materials from coffee waste, and integrate them as battery components was explored as explained in Section 5.6, ending up with a proof of concept test, fabricated with bio-polymers extracted from residues. Finally, in the Discussion section the project social impact is presented through an adaptation of the Social Progress Index.

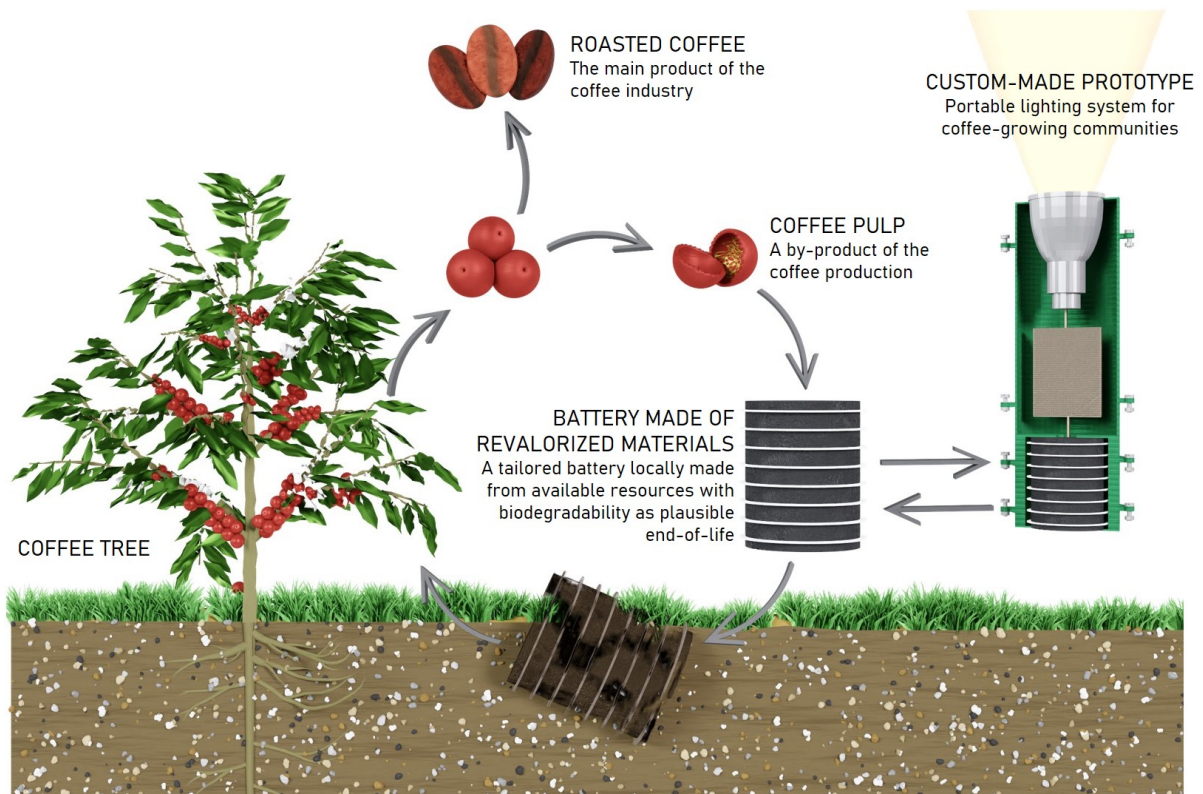


Figure 5.3: Schematic conceptualization of a potentially biodegradable battery fabricated from coffee residues to power lighting systems in coffee growing communities.

5.2 Project framework and viability

Think global, act local is one of the most claimed sustainability chants over the years. It has been repetitively proposed as strategy to address transboundary environmental problems from a well-defined actions at a local level. However, despite being a basal idea among sustainability defenders, examples of its implementation at a technological or research levels are rare. In this sense, sustainable solutions must generated from a holistic vision, taking into account local needs and resources, to be grounded in the socio-economical context of the communities they are addressed for. In this particular case, with the objective of validating the research and nurture it with the local agronomic knowledge, we traveled to Chiapas, to a small village called Jaltenango de la Paz. In Jaltenango, a collaboration was established with the small and organic coffee producers cooperative Triunfo Verde. The association is constituted by 497 organic coffee producers living in different municipalities around Jaltenango.

This sections aims to humbly summarize the knowledge from the local coffee growing communities gathered during our stay in Chiapas, and implemented it to battery research to generate viable solutions.

5.2.1 Life without electricity

Societies living in so called developed economies usually take for granted privileges associated with electrification. However, that reality can not be globalized. As reflected by last Energy Progress Report tracking SDG 7, global rates of access to electricity show an increasing, although slow, trend. Since 2010 to 2020, access rose from 96 percent to 97 percent in urban areas, while it only reached at 83 percent for rural communities. Despite this, today, about 733 million people live with limited or no access to electricity, mostly of those located in rural areas. Furthermore, invisible to the statistics, those who live with electricity on developing economiesⁱ often suffer

ⁱThe terminology 'developed economies' and 'developing economies' used in this chapter has been adopted as conventionality to enhance clarity. It goes beyond the scope of this work evaluate the appropriateness of those terms. However, the author would like to express her no-intentionality of

from an unreliable or inadequate grid connection.⁶⁰

Socioeconomic electrification indicators show a direct relation between electrification and straight improvement of sanitation, access to clean water, nutrition, and security. However, albeit electrification impact transcends primary life-changers, such access to light, the importance of first kWh must not be underestimate. Those areas deprived of electrical light, usually rely in candles, kerosene lamps or diesel generators, which emit toxic volatile pollutants and increase fire risk at households. Futhermore, acording to G. Desarnaud analysis, reported on Sustainable Electrification for Asia and Africa, a direct correlation has been found between electricity consumption and the improvement in Human Development Index (HDI). Above 2500kWh per year and person, the electrical lighting initial impact diminished its effect on HDI. Therefore, first kWh have the most significant impact on living standards, which supports the need for decentralized energy systems.¹⁸¹

According to SPACE 10 report¹⁸² barriers to universal electrification vary upon territories, but two main constrains can be globally identify: communities isolation and systems unaffordability. Sparse population located on difficult terrain access is not cost-effective to reach, meaning that even when the grid reaches the communities, families are not able to afford the high costs associated with installation, complimentary equipment, and maintenance.

Mexican coffee growing communities| *A particular insight*

In order to understand coffee producers' day-to-day life, local needs and resources, we visited three different municipalities. A selection of photographs taken during the visit is shown in Figure 5.4 to provide context about the region.

Location|

The coffee-growing communities were located in the mountains of natural reserve El Triunfo, 980-1600 meters altitude, where conditions are perfect for growing high-quality coffee. Coffee fields extend vertically on mountainsides, and coffee is manually harvested, pulped, and sundried by producers and their co-workers. Access to those locations takes between 3 and 5 hours

establishing a hierarchy or ranking of countries/regions when using those terms.



Figure 5.4: Mexican coffee growing communities contextualization. Photographs taken in a typical household during the interview of a organic coffee female producer.

through unpaved roads. Household clusters create communities on the mountains. However, isolated edifications placed in the middle of coffee crops are also a common reality.

Daily life|

Activity is frenetic during the harvesting period, preparations start in December to be ready for a continuous working period from January to April. During harvest, the producers, their families, and workers cohabit at cultivation plots. Trips to Jaltenango are costly and time consuming. Thus, they are not frequent, and are mainly focused on transporting parchment coffee for its sale.

Dwellings|

Households usually are composed by different isolated structures at different grades of development. The main structure functionality is at the same time producers home and coffee storage, complemented with a semi-open fire based kitchen. A secondary structure is devoted for workers hosting.

Electrification status and energy needs|

Electrical grid has penetrated only to lowest altitude communities. However,

in some cases, power transformers have to be bought by users (with a cost around 1500 euros), and can be shared among 10-15 houses to get access to the grid. Thus, some houses are equipped with a few bulbs for light and a fridge. Still, this is very costly for most isolated producers. Furthermore, the main concern among the locals is the unreliability of grid. For instance, months without power are usual when floods causes damages on the electrical cable structures, and transformers get usually damaged and need to be replaced.

Decentralized solutions have gained popularity over past years, examples of small solar panels, mainly dedicated to powering light bulbs, can be found in the communities. However, in some of these cases the coupled energy storage systems are not enough. For instance, the particular experience shared by the female coffee producer showed on Figure 5.4, battery capacity was 10000 mAh battery capacity, to power 3 bulbs (3W each), meaning light last no longer than 5 hours. Thus, she had to choose between having three bulbs turned on all night for security or cooking in the morning with light. Furthermore, the system has no portability, restricting light location to 3 fixed spots.

All in all, above mentioned reasons lead to a high dependence on kerosene lamps, candles and firewoods.

Residues management

In the communities, generated waste is usually incinerated as a common practice, whereas organic daily waste is mostly composted or directly thrown on the ground. When it becomes about hazardous waste (such as batteries used for radios), unsafe accumulation on households is produced, as a consequence of the above mentioned scarce trips to Jaltenango prevents.

Regarding coffee pulp residue, it is usually piled at the same ground where coffee is grown. Composting process naturally occurs on the pile, leading to acid leaks in the surrounding land. Which in the long term can lead to an unwanted soil acidification.



Figure 5.5: Pulp residue pile and wasted batteries. Photographs taken in a typical household during the interview of a organic coffee female producer.

The importance of affordable and clean energy|

Conducted interviews in Chiapas validated and supported the realities, aspirations and barriers reported previously by SPACE10 and SDG studies in other regions of the world. Access to light does not just brings comfort, but opportunities.

5.2.2 Analysing the coffee production process and its residues

Coffee plant is a small sized perinnial woody plant arround 2 and 3 meters tall that generates small fleshy fruits. Native from Etiopia or Yemen, now a days coffee plantations can be found in many other countries, being Brasil Vietnam and Colombia the three main producers worldwide. There are a total of 124 species of coffee plants, however Coffea arabica and Coffea canephora (know as 'Robusta') are the more common ones. Coffee growing conditions and seasons vary from place to place, being cultivated in altitudes that range from 0 to 2100 meters above sea level. Despite this, coffee crops are commonly shade plantations situated at tropical climate regions on high altitude remote locations.

Figure 5.6 summarizes the states and processes that a coffee bean goes trough from harvesting to roasting, together with the main residues generated at the producers locationsⁱⁱ. Coffee cherries are a red or yellow fruits manually harvested. They

ⁱⁱAs a clarification, coffee by-products obtained at the consumers locations are out of the scope of thesis. Hence the diagram above presented do not take into account silver-skin residue which is produced during roasting in the roasters facilities. Neither the most known coffee residue, spent coffee grounds, produced after beverage preparation.

comprise different 'layers' or skins, that are gradually removed during post-processing. First, the outer layer, the pulp, is removed during the pulping process, then the pulped cherries are sun dried becoming parchment coffee. After, coffee is usually transported from the growing locations to cooperatives at the village, where the husk covering the 'green' coffee beans is removed and, finally, the coffee is roasted. Coffee is exported by growers countries both in 'oro verde' and roasted coffee states. To be accurate, the process described herein is know as wet coffee processing and is was the predominately used by Triunfo Verde producers ⁱⁱⁱ.



Figure 5.6: Timeline describing coffee evolution from coffee cherry state to roasted coffee and the associated processes and residues. Described the wet processing methodology. All photographs were taken during the visits to coffee growing communities in Chiapas, Mexico.

ⁱⁱⁱThere is an alternative way to process coffee beans known as dry processing. The interested reader may consult M. Echevarria et al. from 2017¹⁸⁰

As clearly reflected on the diagram, there are two main by-products produced at coffee growers locations. The wet residue or coffee pulp and the dry residue or coffee parchment husk ^{iv}. Another important parameter to take into account during this studio was the location where the by-products are produced. The pulping process often takes place at the grower cultivation plots, meaning that it is a delocalized by-product, while parchment husk removal takes place in centralized facilities in Jaltenango village.

An analysis on the Triunfo Verde production showed that in 2019 aproximatly 1 052 307.5kg \approx 1T of parchment coffee was produced by a total of 497 producers. For each 1kg harvested berries approximately 0.210 kg of parchment coffee is obtained accordingly to the cooperative. Hence, \approx 4T of wet residue is produced during pulping process (see calculation 5.1).

$$1\ 052\ 307.5\ \text{kg of parchment coffee} \cdot \frac{0.790\ \text{kg wet residue}}{0.210\ \text{kg parchment coffee}} = 3\ 958\ 680.6\ \text{kg} \quad (5.1)$$

On the other hand, every 1 kg of parchment coffee transforms to 820 gr of 'oro verde' after husk removal. Meaning that same year 189 415.4 kg of dry residue were generated (see calculation 5.2)

$$1\ 052\ 307.5\ \text{kg of parchment coffee} \cdot \frac{0.180\ \text{kg dry residue}}{1\ \text{kg parchement coffee}} = 189\ 415.4\ \text{kg} \quad (5.2)$$

Coffee pulp and parchment husk composition has been widely studied in the literature. Both coffee skins have reported to contain a wide variety of components such as lipids, ashes, proteins and carbohydrates. In particular, all studies have found a high content of polysacharides, which are specially interesting for the research herein presented. Polysacharides are the main constituent of bioplastics or biofilms, and as reported in Chapter 4 they could be used to form the battery hydrogel matrix. Futhermore, they are intrinsically biodegradable. Parchment coffee husk has reported a polysacharides content of: 15-46 % cellulose, hemicellulose 10-30% hemicellulose, 10-34% lignin

^{iv}It is worth mentioning that there are two more by-products associated to coffee value chain. The silver skin, is a paper-like thin husk that usually felts off during coffee roasting; and coffee grounds produce during the beverage preparation. Despite this by-products are also interesting as raw materials revalorization their are usually produced at the consumer's countries not the producers, thus their analysis is out of the scope of this thesis.

and 4-7% pectins. While coffee pulp has reported a content of: 26-26% of cellulose, 4-20% of hemicellulose, 9-20% of lignin and 4-7% of pectins.¹⁷⁵ Table 5.1 gathers the potential quantities for biopolymers recovery taking into account worst case scenario (i.e. lowest reported % contents).

Table 5.1: Potential quantities for biopolymers recovery from the annual organic coffee production of Triunfo Verde cooperative.

Bio-Polymer	Potential quantity from coffee-husk (kg)	Potential quantity from coffee-pulp (kg)
Cellulose	27 844	633 389
Hemicellulose	18 942	142 513
Lignin	18 942	356 281
Pectin	7 577	174 182

Regarding bioactive compounds content, polyphenols group has arisen special interest. Due to their intrinsic antioxidant properties, their retrieval has been recurrently proposed, to be used as food industry additive. In particular, coffee pulp has reported to contain higher contents of phenolic compounds than coffee parchment husk, and they could serve as battery anodic redox species.

As it can be seen, the reported results on the physicochemical characteristics of coffee by-products can vary depending on the extraction method and coffee geographical origin. For the particular scenario of this project and taking into account the methodologies employed by SAB group with the residues of Triunfo Verde producers, 5% of pectins content was recovered from coffee pulp. Thus, ≈ 0.2 T of pectins could be potentially recovered from one year production.

After the analysis perform on the coffee residues, there was not found any potentially retrievable compound that could be used as electrochemically active species for the battery cathode. Thus, iron nitrate was selected to act as cathodic redox species.

The quantities herein reported greatly validate the project viability, ensuring enough raw material is available during the harvesting period to carry on the project.

5.3 Battery design and operation principle

The battery presented in this chapter has been conceived with an easy-stack design. Intended to power lighting systems and UV-disinfection devices, power and energy enhancement becomes a must. Thus, the prototype is easily scalable to relatively high power demands. Meaning that electrical contact areas have been favored to facilitate unit connections while maintaining compactness. As can be observed in Figure 5.7, each individual cell has a sandwich like structure, composed by two current collectors, two hydrogel matrices containing cathodic and anodic redox species and an ionically conductive separator to charge-close the circuit. The different battery cells are separately fabricated and then assembled in a stack as shown in Figure 5.7. Each stack is composed by eight unitary battery cells: two semi-stacks in parallel composed by four unitary cells connected in series, theoretically yielding to $2 \times I_{UnitaryCell}$ and $4 \times V_{UnitaryCell}$. For simplicity, this first prototype is designed to power lighting systems has shown in deep in next sections.

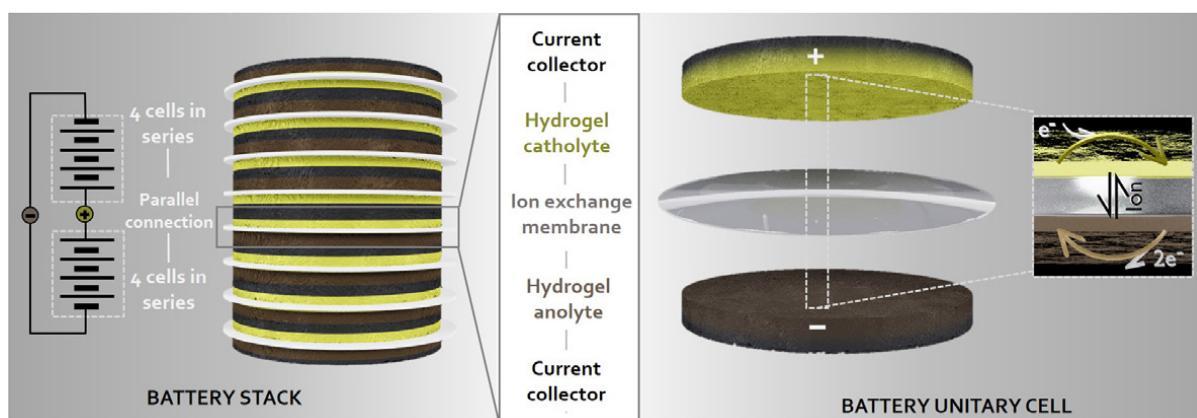


Figure 5.7: The first battery prototype to power portable lighting systems in coffee growing communities in Mexico has been designed with an easily stackable configuration. The battery stack contains eight unitary battery cells, two stacks in parallel of four unitary cells connected in series. Each unitary cell has a coin cell design of 5.5 cm diameter, a hydrogel matrix synthesized from biopolymers is used as ion exchange membrane and solid polymer electrolyte, and two carbon-based materials are used as current collectors.

Battery fabrication process begins with the preparation of the ion exchange membrane. 10 mL of the selected matrix ratio (see Subsection 5.4.2) are dropcasted

in a petri dish (8.6 cm diameter) and incubated at 25 °C, for 4 days to obtain a completely dry hydrogel film. Finally the individual membranes are cut with a 5.5 cm diameter punch and stored. Anode and cathode are synthesized by incorporating the redox species (and its respective salt to extreme pH conditions) to the hydrogel matrix. The mix is magnetically stirred until complete homogenization. Meanwhile, carbon felt current collectors are manually cut and thermally treated to enhance cathodic and anodic hydrogel matrices penetration, and hence, increment the total electroactive area. 3.5mL of the hydrogel are dropcasted on top of the current collectors and spread with a plastic scraper. Finally, the individual cells are manually laminated and the stack is assembled, electrical connection between individual cells take place electrode-electrode, avoiding the need of external metallic connectors or cables between cells.

The detail about, materials selection, synthesis and testing are provided in the next section.

5.4 Materials development and battery operation

This section is devoted to the battery materials exploration and presents the battery first prototypes development workflow. The commercial materials selection was carried out according to the literature by prioritizing those materials that have been reported to be present in coffee residues. In this sense, phenolic compounds with high antioxidant capacities were explored as anode active species. While potentially extractable bio-polymers were assessed as hydrogel matrices, in terms of ionic conductivity, chemical suitability, and mechanical stability. Furthermore, different commercial carbonaceous materials were tested as current collectors. Finally, a battery stack was successfully fabricated to power a commercial LED.

5.4.1 Commercial phenolic compounds as anode materials

Extensive bibliographic research revealed that terpenoids, alkaloids, and phenolic compounds are present in the different parts of the coffee plant (beans, leaves, pulp, etc.). From that variety, phenolic compounds were selected because of their water

solubility and accessibility, despite no exhaustive electrochemical study that could be found. Commercial chlorogenic acid (CloA), epigallocatechin gallate (EP), and gallic acid (GA) were then assessed in terms of water solubility and extreme pH stability. Further, 1mM species oxidation behavior was studied at alkaline (1M KOH) and neutral (Phosphate Buffered Saline, 1M KCl) pHs via cyclic voltammetry technique on SPE (see Figure 5.8)). Caffeic acid was discarded because its maximum solubility was low, $\approx 3\text{mM}$. Ascorbic acid (AA) is incorporated to this study as a reference phenolic compound already used in the battery presented in Chapter 4.

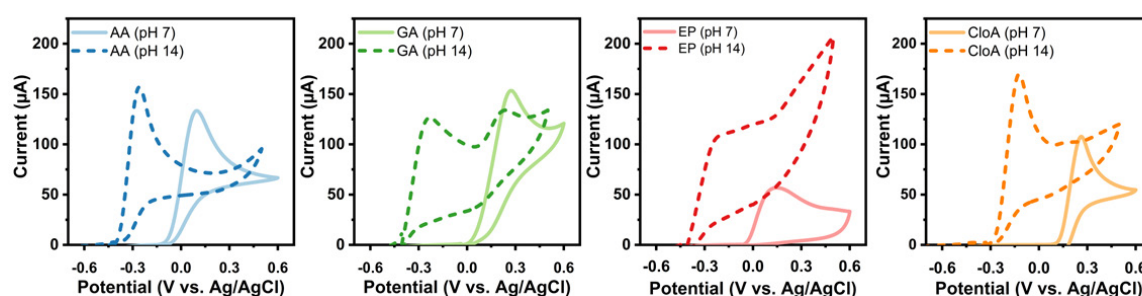


Figure 5.8: Characterization of commercial phenolic compounds electrochemical response via cyclic voltammetry. 1mM concentration of ascorbic acid (AA), gallic acid (GA), epigallocatechin gallate (EP) and chlorogenic acid (CloA), tested in neutral 7 pH (1M KCl as electrolyte) and alkaline 14 pH (1M KOH as electrolyte). Experiments performed in a $50\mu\text{L}$ drop over a screen printed carbon electrode at a 20mV/s scan rate.

As expected, alkaline pHs displace open circuit cell potentials towards more negative values. Measured OCP for pH14 was $-0.4\text{ V vs. Ag/AgCl}$ (SPE) for AA, GA and EP, while in the case of CloA was $-0.32\text{ V vs. Ag/AgCl}$ (SPE). All organic compounds demonstrated similar oxidative behavior, meaning their electron transfer is irreversible, delivering between $100\ \mu\text{A}$ and $150\ \mu\text{A}$ peak currents in alkaline medium, being the lowest value $108\ \mu\text{A}$ for EP. Thus, from the electrochemical study it was concluded that all species could potentially be implemented as anodic compound in the battery.

Solubility was assessed based on the literature and visual inspection of solid precipitation absence. GA, EP and CloA maximum concentration were found to be $\approx 80\text{ mM}$, $\approx 70\text{ mM}$ and $\approx 100\text{ mM}$ respectively. EP was therefore discarded. Finally, because economical cost^v reasons GA in alkaline medium was selected over CloA as anodic

^vGA commercial cost is around $172\ \text{€}$ for 250 g ($\approx 688\ \text{€/kg}$), while CloA commercial cost is around $74.5\ \text{€}$ for 250 mg ($\approx 2980\ \text{€/kg}$)

battery redox species.

Over the course of this investigation no plausible cathodic redox species extracted from coffee plant were found in the literature, thus GA 80mM was combined with iron nitrate 160mM in acidic medium to complement the battery chemistry. Figure 5.9 shows that combination of this chemistry results in a open-cell voltage of 1.04V.

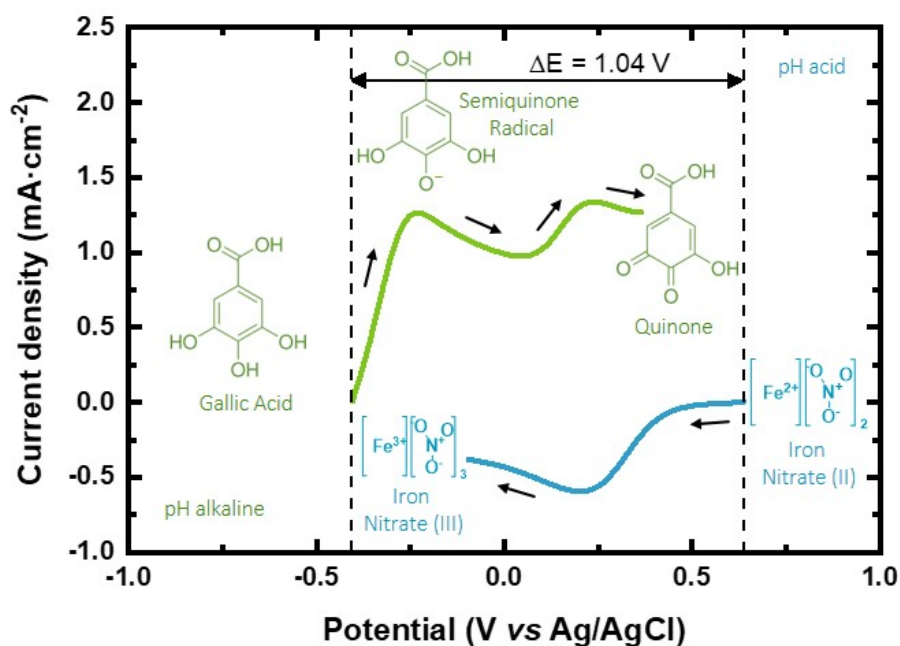


Figure 5.9: Linear sweep voltammograms of the redox chemistry selected to power the battery. Oxidation of 10mM GA in 1M KOH as alkaline electrolyte and reduction of 10mM Fe(NO₃)₃ in 1M C₂H₂O₄.

5.4.2 Hydrogel biopolymer as a battery matrix

Carboxymethyl cellulose derivative (CMC) and pectins (PEC) were chosen as preferred biopolymers to fabricate the battery hydrogel network, due to the fact that they can be potentially recovered from coffee residues. CMC is a cellulose derivative with carboxymethyl groups (-CH₂COOH) added to the polymer chain. CMC has been widely applied in the literature to synthesized bio-based ion-exchange membranes or electrolyte. When dissolved in water it becomes negative ionized, being able to create physical crosslinking and enhancing the mechanical properties of the hydrogel.^{165;183} On the other hand, pectins (PEC) are usually recovered from citrus peels and used

as additive in food industry and pharmaceuticals due to its gelation capacity. However, it has not been yet widely explored in the polymer electrolyte field.^{184;185} As in the chapter before, sodium alginate (AL) was incorporated to the blend with the aim of creating a synergistic effect and enhance membranes' mechanical properties and ionic conductivity. Furthermore, SAB research group had experience on the recovery of this polysaccharide from Mexico beaches brown algae, thus it became an appealing biopolymer for the project.

In this context, AL was combined with CMC or PEC, to synthesize two different blends. Both matrices were created following the protocol depicted in Figure 5.10). Briefly, 2% w/v SA, 1.5% w/v CMC and 2% PEC solution is prepared in DI water and magnetically stirred between 2 and 3 hours applying mild heat until complete solid solution. Then, the biopolymers are combined in different ratios, and doped with 5% of glycerol, the blends are stirred again at room temperature over 2h. Finally, 40 mL of each mixture is poured into a Petri dish (8.6 cm diameter) using a syringe and dried in an incubator for 4 days at (T=25°C). Five X CMC: Y AL and five X PEC : Y AL membrane ratios were synthesized (100:0, 75:25, 50:50, 25:75 and 0:100) and in all cases flexible self-standing membranes were obtained. It worth mentioning, that the selected bio polymers allow to developed an easily exportable synthesis protocol, meaning it is based in drop casting method and uses non-toxic reactants with mild gelation conditions.

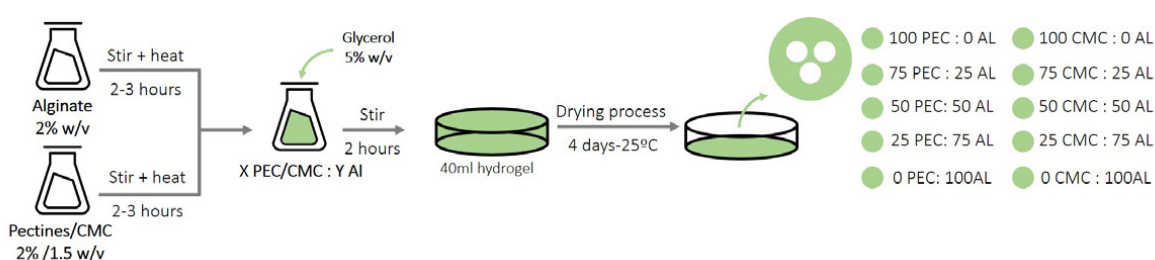


Figure 5.10: Schematic representation of hydrogel membranes synthesis protocol.

As mentioned in Chapter 4, in order to be suitable as polymeric electrolyte, the synthesized hydrogel matrix should meet certain requirements, meaning high ionic conductivity, good mechanical stability and high pH range tolerance. Thus, once synthesized, matrices' ionic conductivity was characterized via electrochemical impedance spectroscopy (EIS) method. Three circular sections were cut with a

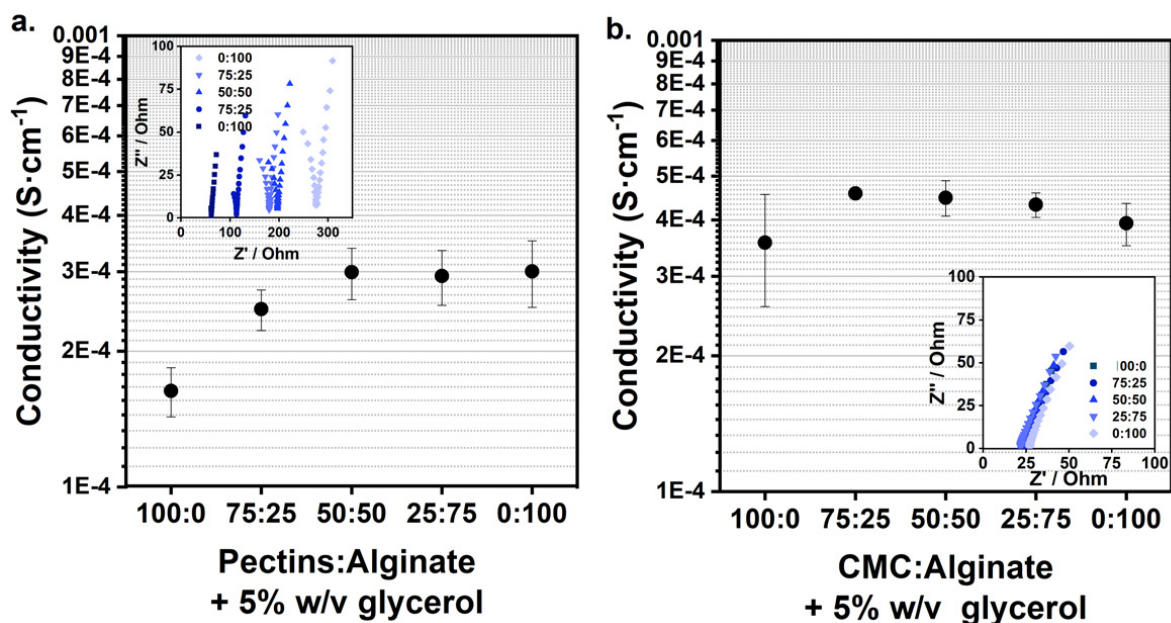


Figure 5.11: **a.** Ionic conductivity as a function of pectins and alginate biopolymers ratios. (N=3) Inset: Representative Nyquist plots obtained from impedance spectroscopy analysis in a 10^6 to 1000 Hz range. **b.** Ionic conductivity as a function of carboxymethyl-cellulose and alginate biopolymers ratios. (N=3) Inset: Representative Nyquist plots obtained from impedance spectroscopy analysis in a 10^6 to 1000 Hz range.

circular punch to perform the analysis. The average conductivities gathered in Figure 5.11, were calculated with eq. A.2 after obtaining the resistance solution from the Nyquist plot (Figure 5.11 inset), consult Appendix B.

All obtained conductivities are in the range of 10^{-4} S·cm⁻¹. All CMC:AL values are above PEC:AL values, partially because of a small difference in the batches preparation as it is observed in 0:100 values (i.e. $3.0 \pm 0.5 \cdot 10^{-4}$ for PEC:AL, and $3.9 \pm 0.42 \cdot 10^{-4}$ for CMC:AL batch). In the case of PEC:AL blend, despite 50:50, 25:75 and 0:100 present similar conductivities values, the ion mobility decreases when incrementing the PEC concentration. In the context of this project, higher PEC concentration is preferable, 50:50 ratio was selected as the best option to incorporate it as battery separator. Regarding CMC, highest conductivity is reached with 75:25 ratio, revealing a synergetic effect when combining both biopolymers. This translated in a noticeable improvement of the 100% CMC membrane mechanical properties. Thus, this membrane was established as the most appealing option for CMC:AL combination.

When testing the selected matrices to extreme pH conditions, the addition of KOH and oxalic acid salt did not change 75CMC:25Al blend viscosity, meaning they have a suitable pH stability. However, in the case of 50PEC:50Al the addition of oxalic acid produced a drastic change in viscosity, creating unbreakable clumps (as explained in Chapter 4, this behavior can be associated to the carboxylate groups in the alginate chain). Thus, 75PEC:25AL blend was selected to contain the redox species acting as solid polymer electrolyte. In next sections, the implementation of both bio polymeric hydrogels as ionic conductivity membrane and battery electrolyte is presented.

5.4.3 Current collectors selection

In order to select the most suitable current collectors, three different commercially available carbonaceous materials were tested. These materials are typically used as Gas Diffusion Layers in fuel cells. Specifically, one carbon paper, two carbon cloths, and two carbon felts were tested. Table 5.2 gathers the main materials properties, together with their electrical conductivity and sheet resistance characterized by our group at CNM facilities. Carbon papers are rigid and fibrous materials, while carbon felts are usually thicker materials with sponge-like structure; and carbon cloths are thread-based flexible films with high porosity.

Table 5.2: Commercially available carbonaceous materials electrical properties and description.

Material reference	Material type	Thickness (um)	Electrical conductivity (S/cm)	Sheet resistance (Ω/\square)
MGL 370	Carbon paper	440	279 ± 9	0.081
C100	Carbon felt	3240	4.82 ± 0.02	0.640
GF020	Carbon felt	1890	10.46 ± 0.08	0.506
B1B	Carbon cloth	600	14.8 ± 0.3	1.128
B1A	Carbon cloth	390	33.1 ± 1	0.777

Collectors material selection was performed with a coin cell like battery unit test containing all essential elements (two current collectors, anodic and cathodic matrices and a separator). Figure 5.12 summarizes the materials used.

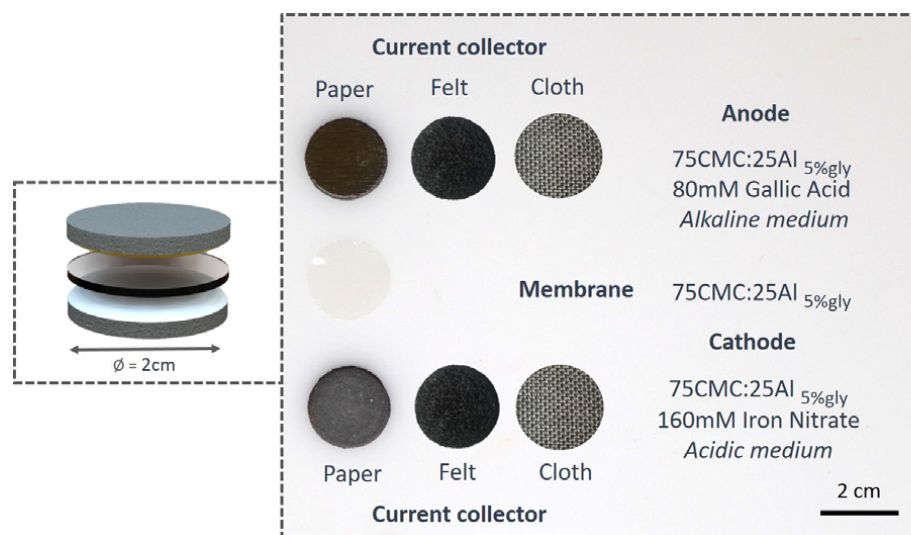


Figure 5.12: Batteries composition summary for the carbon-based material selection as current collector assessment.

Gallic acid and iron nitrate were selected as redox anodic and cathodic species respectively; in mixed media condition. 75CMC:25Al + 5% glycerol hydrogel was used as matrix to synthesize the membrane and contain the redox species. The methodology to fabricate the battery unit test is similar to above described processes. Briefly, first the membrane is separately synthesized by dropcasting 15 mL of the hydrogel matrix in a 8.6 cm diameter petri dish and dried at 25 °C in an incubator over 2 days. Subsequently commercial carbonaceous materials are manually cut with a 2 cm diameter punch and, in the case of carbon paper and carbon felt, terminally treated. Carbon cloths were used as received.

The material performance as a current collector was assessed through polarization curves, sweeping from pre-measured open circuit voltage (OCV) to 0V at 20mV/s scan rate. The coin cells characterization and its repeats are shown in Figure 5.13. In all cases, recorded OCV was $\approx 0.9V$, except for some carbon cloths repeats. However, a drop in voltage rapidly occurs during the first moments of current deliver, related with slow reaction kinetics between current collectors and redox species. Carbon paper batteries delivered the highest power output, 2.2mW. This could be related with higher electrical conductivity, hence lower Ohmic losses; or a greater affinity between carbon paper and redox species. Carbon cloth was found to have low reproducibility and difficult workability, as a consequence it was discarded as current collector for

future experimentation. Finally, carbon felt C020, presented a mild 0.97 ± 0.03 mW maximum power output and good reproducibility. Furthermore, flexibility property of felt material facilitates battery stacking and direct electrical connection between cells, thus carbon felt C020 was selected as current collector for the battery stack prototype presented in this chapter.

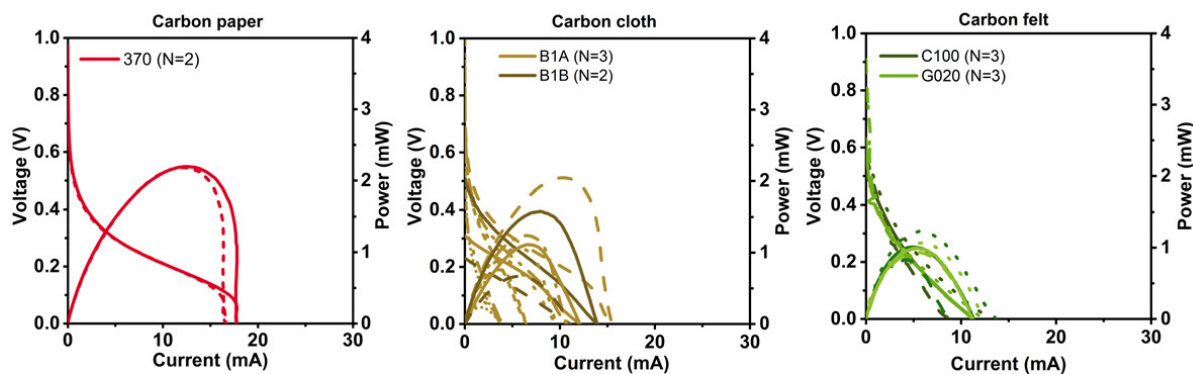


Figure 5.13: Polarization curves of a 2 cm diameter hydrogel coin cells with three different carbon-based materials: carbon paper, carbon cloth (B1A and B1B types) and carbon felt (C100 and G020 types). Characterization performed at 20mV/s scan rate.

5.4.4 Prototype optimization and operation test

In order to run the final battery optimization, the two synthesized hydrogel matrices, 75CMC:25Al and 50PEC:50AL + 5% w/v glycerol in Subsection 6.4.2., were tested as battery ion conductive membrane and solid electrolyte to contain the redox species. Figure 5.14 shows electrochemical characterization of the battery unitary cells fabricated with the matrices of interest. These experiments took place in parallel with the current collectors selection, thus the batteries were fabricated using the same protocol and carbon paper was used as current collector.

As it can be seen in Figure 5.14a., CMC:AL matrix showed a higher power output and reproducibility than PEC:AL. On the other hand, when continuous working under a 96Ω load, PEC:AL matrix delivered a more stable output, reaching 0.4C of accumulated charge in ten minutes. In comparison, CMC:AL matrix discharge delivered 0.72C.

In conjunction with the results presented above, when selecting the final matrix for the battery cell prototype, other factors must be taken into account in order to be

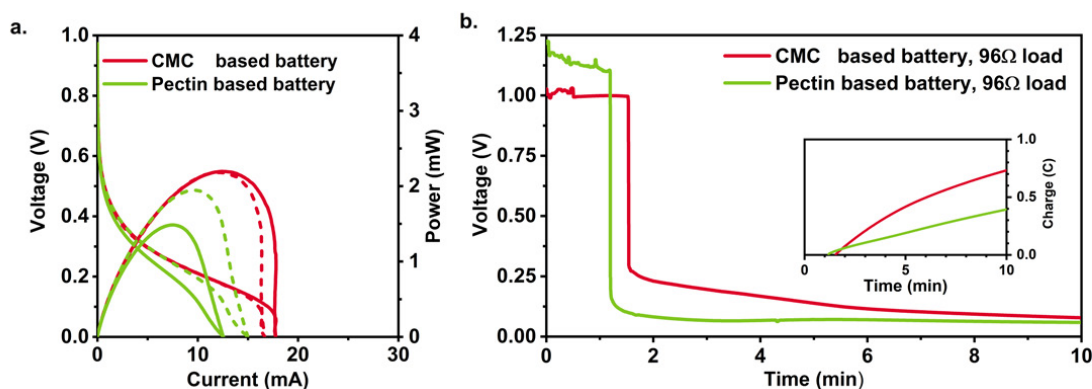


Figure 5.14: Comparison between coin cell 2cm diameter performance in relation with the bio polymer matrix used. 2cm diameter carbon paper MGL 370 used as current collectors. Batteries fabricated from carboxy methyl cellulose (CMC), alginate (AL) and/or pectins (PEC) commercial polymers with 75CMC:25AL or 50PEC:50AL ratios. **a.** Polarization curves at 20mv/s scan rate (N=2). **b.** Discharge curves under 96 Ω external load. Inset: Accumulated charge during 10 minutes.

consistent to the ecodesign process. CMC is not a directly refinable material, so to obtain revalued CMC from coffee residues, pure cellulose must first be used, and then add a second step required to add the carboxyl and methyl groups to the cellulose chain. In this sense, PEC:AL biopolymer hydrogel was prioritized against CMC:AL combination, as final battery matrix, thus, PEC can be directly refined from coffee pulp residue, as further explained in Section 6.6 *From commercial to extracted: Exploring local material sources for batteries*.

Figure 5.15 recaps the final battery materials composition, together with an electrochemical characterization of a unitary battery cell with 5.5 cm diameter. As a strategy to enhance the battery power output, the anodic and cathodic hydrogels were spread on top of the current collectors and used without drying process. The high humidity content, improved ionic conductivity facilitating ions transport within the electrolyte. As it can be seen in Figure 5.15 b., the final unitary battery cell presented OCV \approx 0.8 V and delivered 12.5 mW maximum power output, being able to deliver 12.5C after 5 hours of continuous operation.

Finally, the battery stack was built and a commercial LED bulb was powered as a proof of concept. A voltage boost converter (VBC) integrated circuit was used to increase the operating voltage up to 3.1V. The VBC was coupled with a 0.1F supercapacitor, that

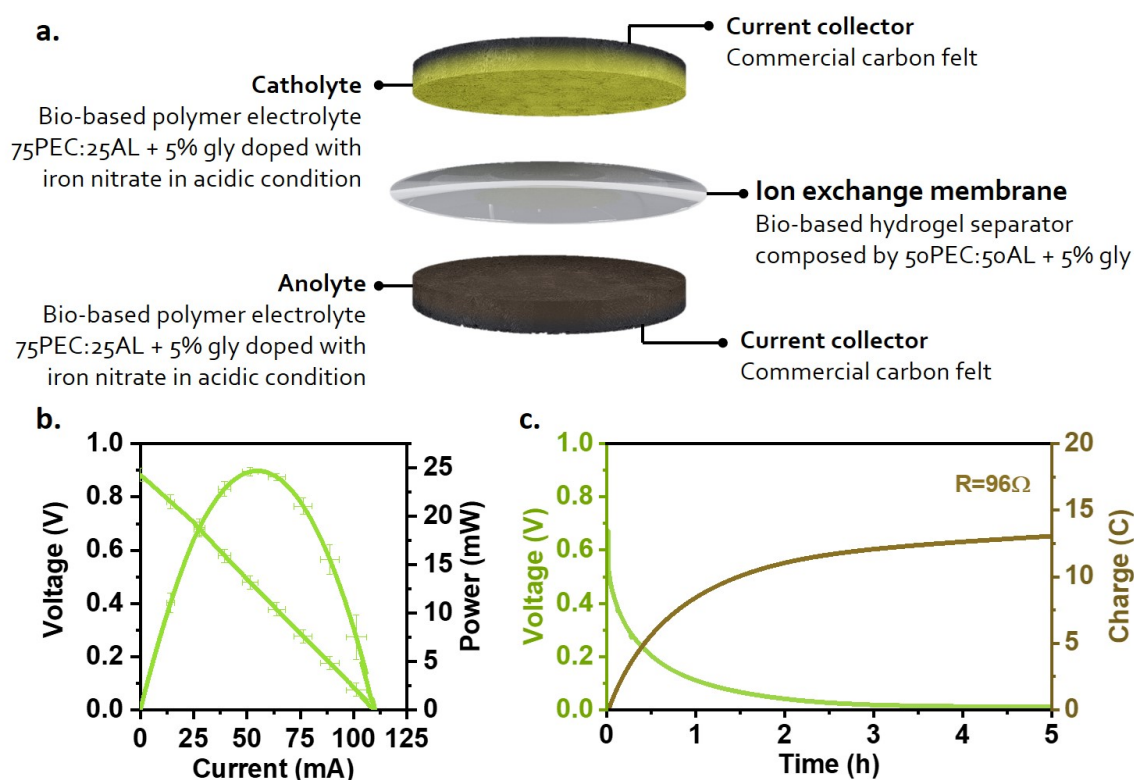


Figure 5.15: a. Schematic representation of a testing unit battery final selected materials. b. Battery 5.5 cm diameter discharge polarization curve sweeping potential from prerecorded OCV to 0V at 20mV/s scan rate. c. Continuous discharge voltage curve under a 96 Ω external load and accumulated charge over 5 hours.

served as an energy reservoir, that also smooths the punctual current/power peaks demand. As it can be seen in Figure 5.16, the battery prototype stack delivers 3.25V OCV, thus validating the connections design (i.e. two stacks in parallel of four cells in series). After 1 minute, the integrated circuit together with the supercapacitor and the bulb are connected, and the battery potential suffers a drastic drop. The LED light was successfully powered during 10 minutes and the supercapacitor potential was maintained at 2.5V. After 10 minutes the LED was disconnected, and the battery voltage was rapidly recovered up to 1V.

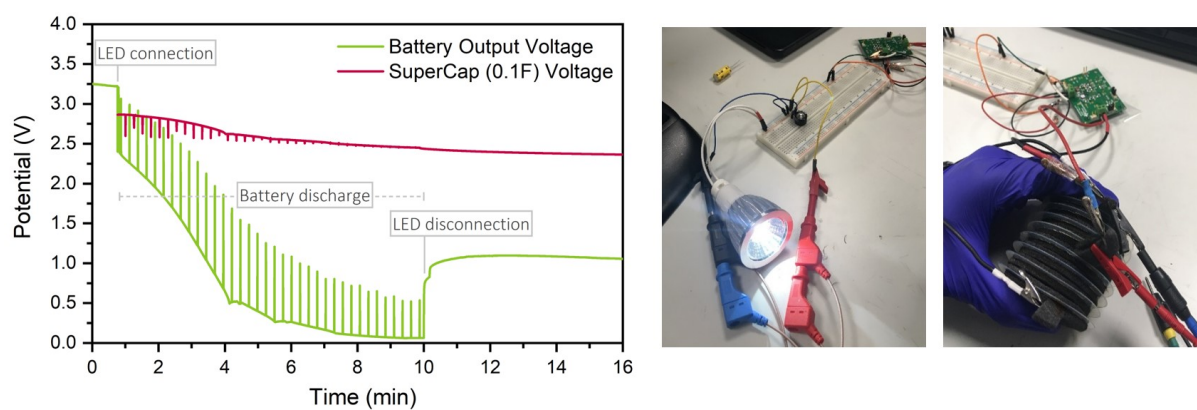


Figure 5.16: Battery stack proof of concept demonstrating the capability of powering a visible light LED.

5.5 Powering a portable lighting system in coffee growing communities in Chiapas

With the aim to test the battery in a realistic scenario a portable lighting system was brought to coffee growing communities in Chiapas. Figure 5.17 shows a photographic collage of the lantern prototype main components during the first validation performed at Triunfo Verde facilities in Jaltenengo village. The lantern prototype is a 3D printed cylinder (6.85 cm diameter x 22.2 cm length) composed by three main parts, each one devoted to contain the bulb, the electronics or the battery. The battery compartment, that also acts as battery casing, can be easily detached to facilitate the power source substitution. Three 5 cm diameter copper plates are used as connectors to couple the battery to the VBC integrated circuit, the capacitor and the bulb. The battery fabrication

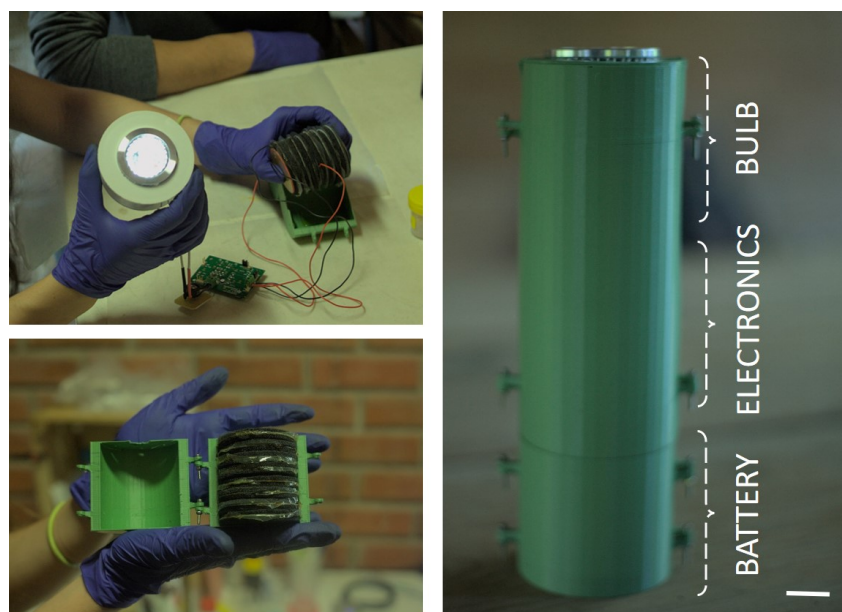


Figure 5.17: Photographic composition depicting the battery prototype implementation in a portable lighting system. Proof of concept conducted at the facilities of coffee producers Triunfo Verde cooperative in Chiapas, México. Scale bar: 2cm.

process was slightly modified due to the fact that no incubator was available. Hence, the used membranes were previously synthesized at CNM research center and stored over a week. Anodic and cathodic hydrogels were synthesized 'in situ' manually stirring until complete dissolution of chemical species.

5.5. Powering a portable lighting system in coffee growing communities in Chiapas

Finally, to prove that the battery fabrication process is easily exportable not only to a non-scientific environment but directly to coffee growing emplacements, the portable lighting system was tested in a local household on a coffee plantation. Figure 5.18 portrays the successful implementation of the first lantern prototype in an isolated coffee producer home in Chiapas, powered by a battery made from materials potentially recoverable from coffee residues.



Figure 5.18: Photographic composition depicting the battery prototype fabrication and implementation in a portable lighting system at a coffee producer household in high altitude cultivation plots, chiapan natural reserve of El Triunfo, Mexico.

5.6 From commercial to extracted: Exploring local material sources for batteries

Finally, the possibility of using revalorised materials to implement them as battery components was explored. In this sense, two investigations were carried out. First, phenolic compounds were extracted from coffee pulp residue just after coffee harvesting. The effect of storage conditions was studied over the first days. With the main objective of finding the best storing technique to keep the highest phenolic compounds' concentration before extraction. On the other hand, ionic conductive membranes were synthesized from revalorized pectins and alginate bio-polymers.

5.6.1 Phenolic compounds extraction at the residue production location

After coffee harvesting and pulping, coffee wet residue rapidly starts to rot, due to the oxidation reaction naturally occurring. Due to the high water content, sugars and temperature, this process takes place really fast, and its effect directly affects coffee pulp compounds and causing a noticeable change in coloration and smell. In particular, phenolic compounds are highly antioxidant chemicals, which means they can be easily oxidated by ambient condition exposition, such as light and oxygen. For this reason, in order to study phenolic compounds recovery capability for its implementation as battery anode active species, it was compelling to perform an assessment of how time and storage conditions affect phenolic compounds recovery from coffee pulp.

The proposed study presented various challenges. It was a very time sensitive study, meaning that it had to be taken place at the residue production location (cultivation plots), which is a non-scientific environment. Therefore, extraction and measurement protocols, including characterization techniques, needed to meet certain requirements, such as easy portability, short analysis time and low residues production.

The study took place at Triunfo Verde coffee cooperative facilities, where a field-laboratory was prepared. The final protocol, shown in Figure 5.19, was prepared

5.6. From commercial to extracted: Exploring local material sources for batteries

in collaboration with SAB research group. Phenolic compound extraction was performed by infusing 50g of pulp in 150mL of preheated ($T=90^{\circ}\text{C}$) mineral water during 30 minutes, followed by 10 minutes of precipitation and cool down process. 1 mL of infusion was then recovered with a syringe and 1M KCl was added as electrolyte. A drop of solution was then analyzed via differential pulse voltametry (DPV), a well-known electrochemical technique used for compound detection due to its high sensitive capacity (see Appendix A). It must not be disregarded that electrochemical techniques are non-selective techniques. Meaning that, two different compounds could have the same electrochemical signal when displaying similar conditions, in contrast with HPLC compound detection gold-standard. Therefore, the current recorded in DPVs portrays the oxidation process of the wide variety of electroactive compounds that may be present in the infused pulp broth. However, electrochemical techniques evolution over the years have led to very compact analytical systems, which endow the field with practicality, portability and effectiveness, essential attributes in these specific study.

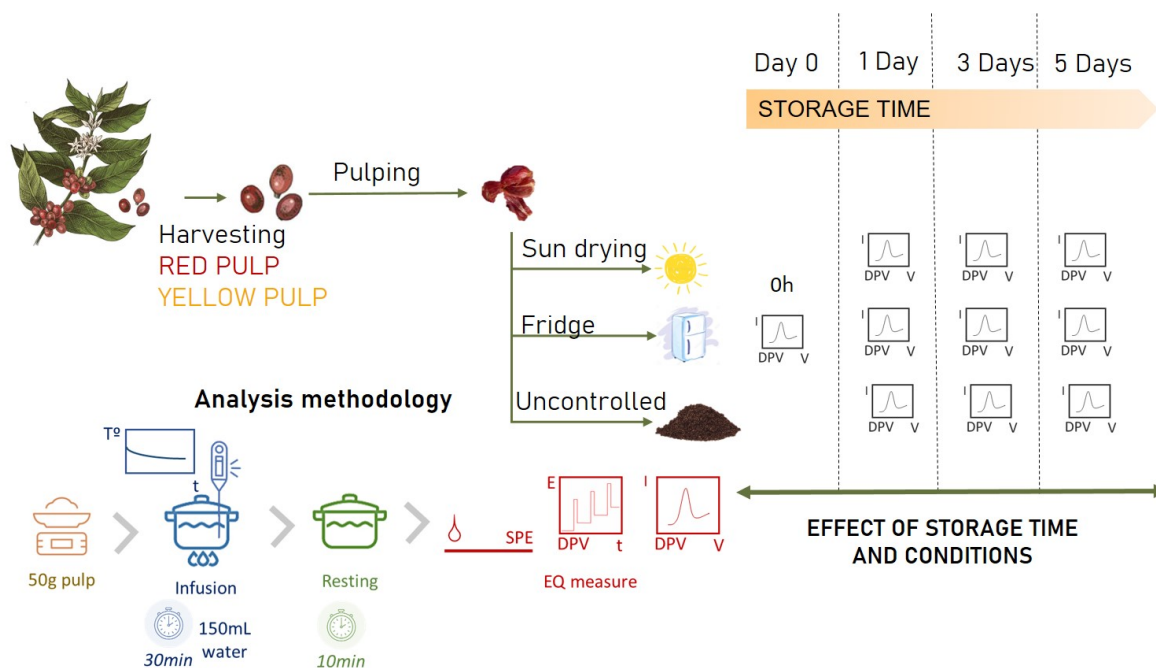


Figure 5.19: Methodology for phenolic compounds extraction from coffee pulp and characterization of the oxidation signal effects of storage time and conditions.

After manually harvesting the coffee and pulping it *in situ* two coffee types (i.e. red and yellow varieties), three storage methods were considered for the study. Coffee

pulp storage in the fridge was selected as 'ideal storage condition', but with low implementation success potential. Sun drying the pulp was proposed as a more viable alternative, because it is an already established practice for coffee parchment. Finally, piling the pulp on the ground was also considered, as it is the current residue treatment practice (uncontrolled soil conditions). The effect of these three storage conditions on the oxidation signal of the pulp infusion was assessed during five days.

Figure 5.20 shows the different responses obtained by DPV measurement for all the extractions, each one regarding a storage technique for each type of pulp. In all cases the pH was measured and values between 4-5 were found.

The results show how each storage condition affects the pulp degradation differently. Under uncontrolled soil conditions, the oxidation current peak disappears after the first day of storage, for both types of coffee pulp, meaning the complete degradation of electrochemically active species. Regarding fridge storage condition, the signal experienced a decay the first day, but later the signal stabilized over the course of the experiment. This effect was more significant on red pulp. Finally, sun drying conditions, showed a slow progressive degradation of the compounds over the days.

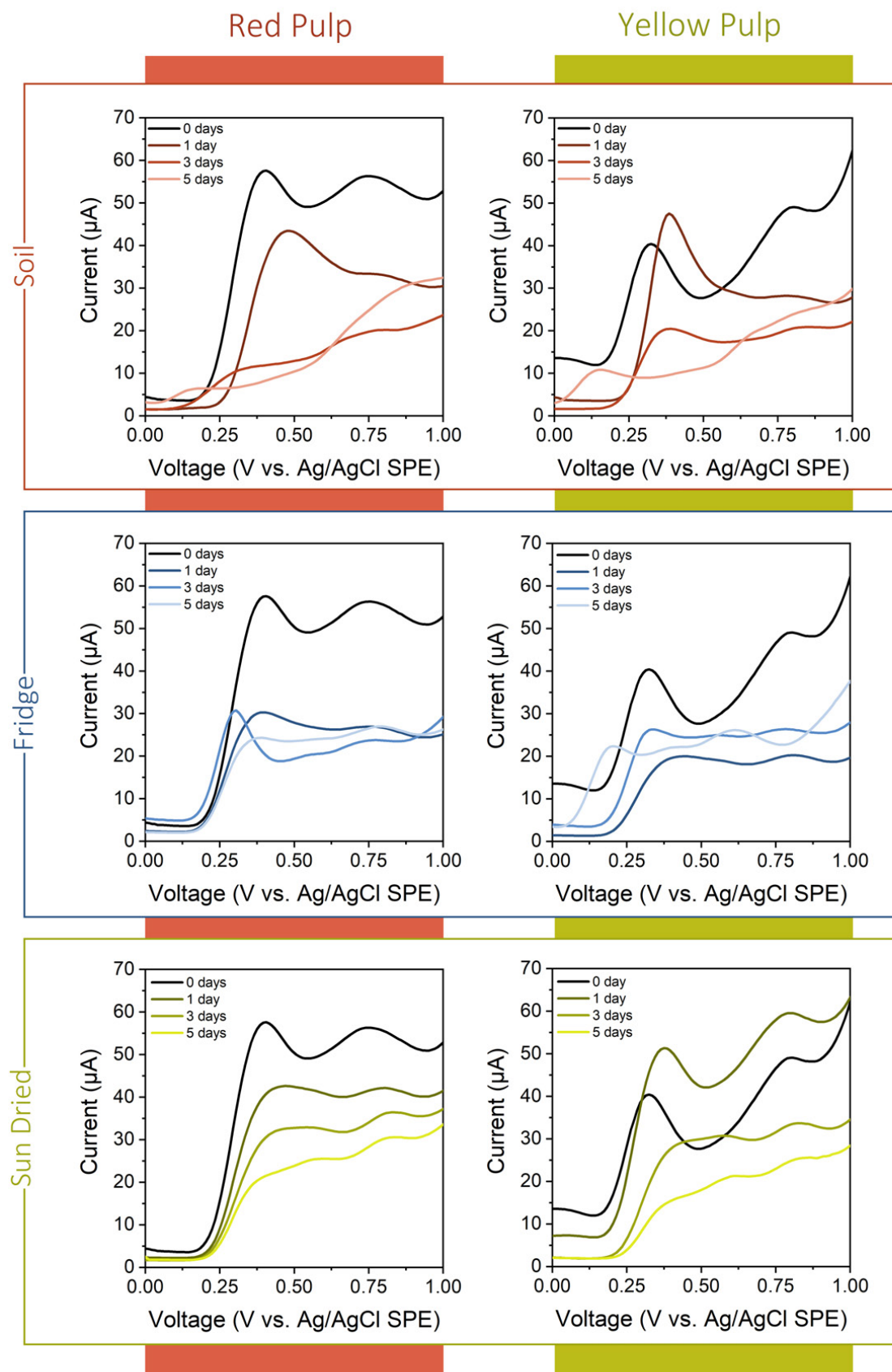


Figure 5.20: Analysis of the oxidation currents of red and yellow coffee pulp infusions. Assessing the effect of storage conditions and time via differential pulse voltammetry technique.

In order to further estimate the concentration of the active redox species present in the coffee pulp infusion and to quantify the antioxidant capacity loss, the surface area (Q) under the first oxidation peak was analyzed. Q measures the total quantity of exchange charged in coulombs. Higher Q are directly related with higher concentration of antioxidant compounds on the samples, i.e. larger antioxidant natures. The estimation of active redox species the concentration was assessed in terms of equivalent gallic and caffeic acid concentration. These two representative commercial phenolic compounds were found to have comparable electrochemical behavior in terms of oxidation potentials and currents when analyzed at 50 μM to 1 mM concentration, pH adjusted to 5 and 1M KCl as electrolyte (see Figure 5.21). DPV responses show similar starting oxidation potentials for all three samples ($\approx 0.2\text{-}0.25$ V vs. Ag/AgCl SPE). Red pulp infusion presented two oxidation peaks 0.4 V and 0.75 V; agreeing with GA response, first one around 0.25-0.35V and second one between 0.65-0.7 V. CA only shows the first peak, around 0.3 V. Finally, it can be seen that CA delivers higher current levels than GA at each same concentration value. This could be due to greater affinity between CA molecules and electrode's surface.

To calculate the equivalent concentration, two calibration curves were compute using the integrated charge values for GA and CA DPV curves. The resulting regression lines are depicted in Figure 5.21 b.^{vi}

^{vi}Limit of detection (LOD) and limit of quantification (LOQ) have been calculated at levels of confidence $k=3$ and $k=10$, respectively, for both calibration curves. Obtained values for Gallic acid are $\text{LOD}=1.4\mu\text{M}$ and $\text{LOQ}=4.6\mu\text{M}$; while for Caffeic acid are $\text{LOD}=2.9\mu\text{M}$ and $\text{LOQ} 9.7\mu\text{M}$. Thus, validating the precision of the calibration curves.

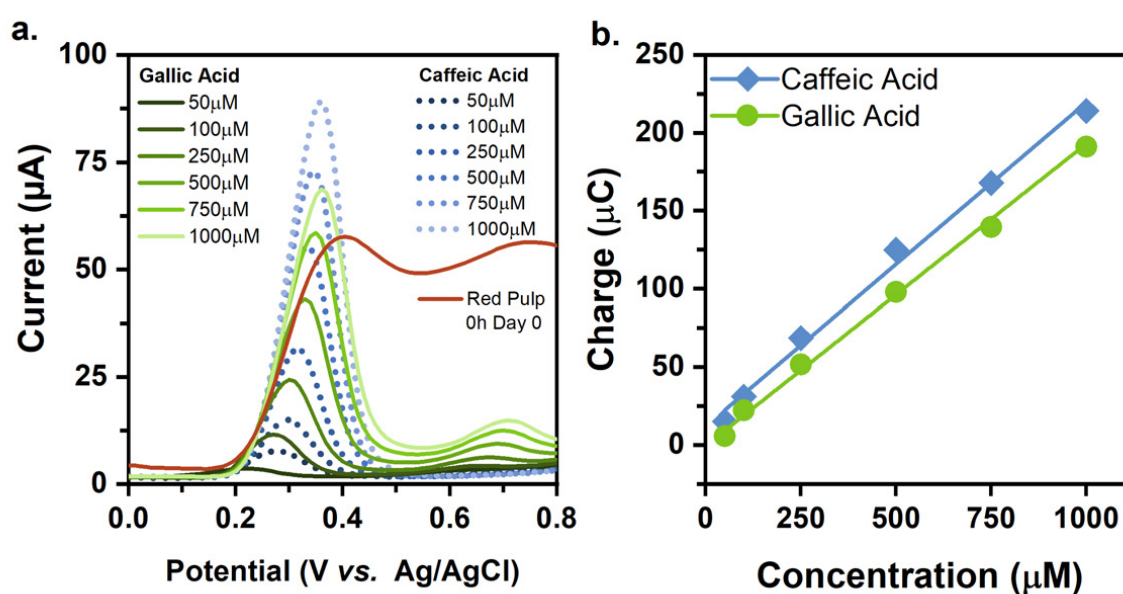


Figure 5.21: The differential pulse voltammetry (DPV) responses obtained from commercial phenolic acids (Gallic and Caffeic) at 50 to 1000 μM concentration range in KCl 1M at pH=5 (Oxalic acid 10 μM). In comparison with infused red coffee pulp oxidation signal. b. Calibration curves computed with the integrated charged from graphic a.

Finally, Figure 5.22 shows the experimental integrated charges obtained for all infused samples under DPV measurements from Figure 5.20 and their corresponding concentration equivalence through Gallic acid model.

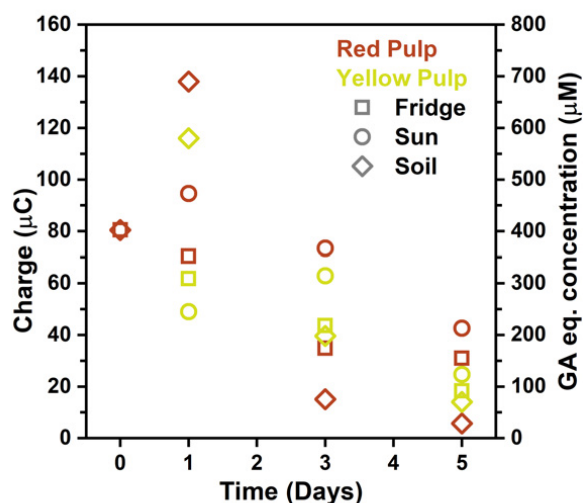


Figure 5.22: Integrated charges and equivalent gallic acid concentration for the different coffee pulp samples comparing the storing techniques over 5 days.

First measurement (Day 0), which is equal for all the samples, is set as reference. After 24h (Day 1 after pulping process), soil conditions' samples deliver the highest amount of charge, for red and yellow pulp, in this order; followed by sun-red pulp sample. Those three samples exchange higher amounts of charge than the day 0 reference. Increasing percentages of charge's values: Soil-red pulp 71.4%, Soil-yellow pulp 44.1%, and Sun-red pulp 17.5%. Below those values are fridge conditions' samples, for red and yellow pulp, respectively. Sun-yellow pulp is the one with least charge exchange, decreasing a 39.1% at day 1. The relation between the drying process and the infusion method can explain this distribution: the samples dried from day 0 to day 1, decreasing the berries' density, so the 50g of weighted pulp resulted in a higher number of coffee berries. Thus, the end infusions were more concentrated than the day before.

However, after day 3 phenolic compounds suffered from a severe degradation, reflected in a loose on transferred charged and mitigating concentration boost caused by drying effect. Fridge conditions' samples actuate as control for visualizing this

phenomenon, since coffee berries' drying process is estimated to be negligible in that storage condition. In this sense, it can be seen how integrated charge's values decrease regularly the first 3 days, remaining quite stable for the last 2 days. This way, a certain proportion of the decay can be assigned to lightless degradation for each time gap. For red pulp is 12.6% for day 1, 56.8% for day 3 and 61.5% for day 5; all with respect to day 0 reference value.

Despite soil storage conditions' showed the highest charge's values for day 1, it also delivered the lowest values for days 3 and 5, for both types of pulp. This could be due to the bio-chemical processes occurring to coffee berries while heaped on the soil, which contains living matter in the form of bacteria, fungi and little forms of life (both micro and macro), which accelerate the pulp degradation. Finally, regarding sun conditions batch, it can be seen that red pulp samples kept the higher eq. concentrations on day 5.

Overall, the best storing technique will depend on the intended time of storage (which in turn depends on the desired application of the extracted compounds), however from the study it can be concluded that phenol compounds extraction should be ideally performed immediately after pulping process, to enhance the maximum electroactive compounds recovery. Furthermore, it is worth mentioning that from the three studied storage methods, sun dried was concluded to be the most appealing one.

Beyond quantifiable results, this study evidences the strength and potential of delocalized scientific research. Residues revalorization research usually focuses on the last residues of the main product value chain (i.e. coffee grounds in this particular case). Thus, dismissing the great potentiality of other by-products, especially those which transportation becomes difficult as a cause of their rapid degradation. This is a by-side effect of excessively centralized research facilities. Due to the intrinsic nature of the residues, the analysis of potential refinable compounds becomes inaccessible. This subsection evidences that the use of electrochemical simple and low-cost analytical techniques endows the extrapolation of the research methodologies to the residue production location, bypassing the need for complex characterization systems and enabling the assessment of the most produced coffee residue, usually dismissed because of the aforementioned reasons.

5.6.2 Development of an ionic conductive membrane from revalorized biopolymers

Through the collaboration established with SAB reserach group, alginate, pectins and cellulose were refined from, brown algae, coffee pulp and coffee husk, respectively. In order to incorporate the extracted biopolymers as hydrogel battery matrix the necessary degree of purification was tested. In this sense, cyclic voltammetry were perform, to the three matrices. As it can be seen in Figure 5.23, none of them presented representative peaks on the potentials working window, indicating that no additional refining processes was necessary to test the biopolymers as ionic conductive membranes. Cellulose was discarded because SAB research group extraction protocols were better optimized in the case of pectins recovery.

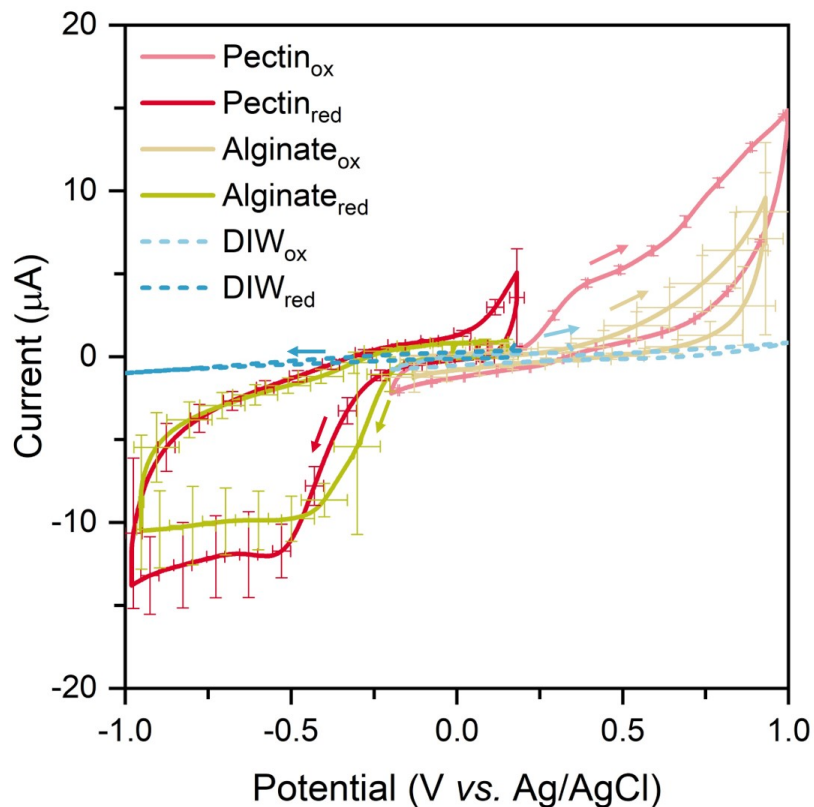


Figure 5.23: Cyclic voltammetry of valorized 2% w/v biopolymers. Analysis performed in screen printed electrodes, at 20mV/s with 1M KCl as electrolyte. Arrows show the scan direction towards oxidative or reduction potentials.

Subsequently, hydrogel membranes were synthesized with the recovered biopolymers,

5.6. From commercial to extracted: Exploring local material sources for batteries

in five different ratios of XPEC:YAL combination. To synthesized the matrices, the same protocol as the one explain for commercial biopolymers was followed (consult Subsection 6.4.2.), with the difference that, instead of 4 drying days, 6 days were necessary to obtain self-standing manageable membranes. Figure 5.24 gathers the measured ionic conductivity for each membrane ratio in comparison with the ones obtained for commercial biopolymers. Also depicted are the synthesized biofilms.

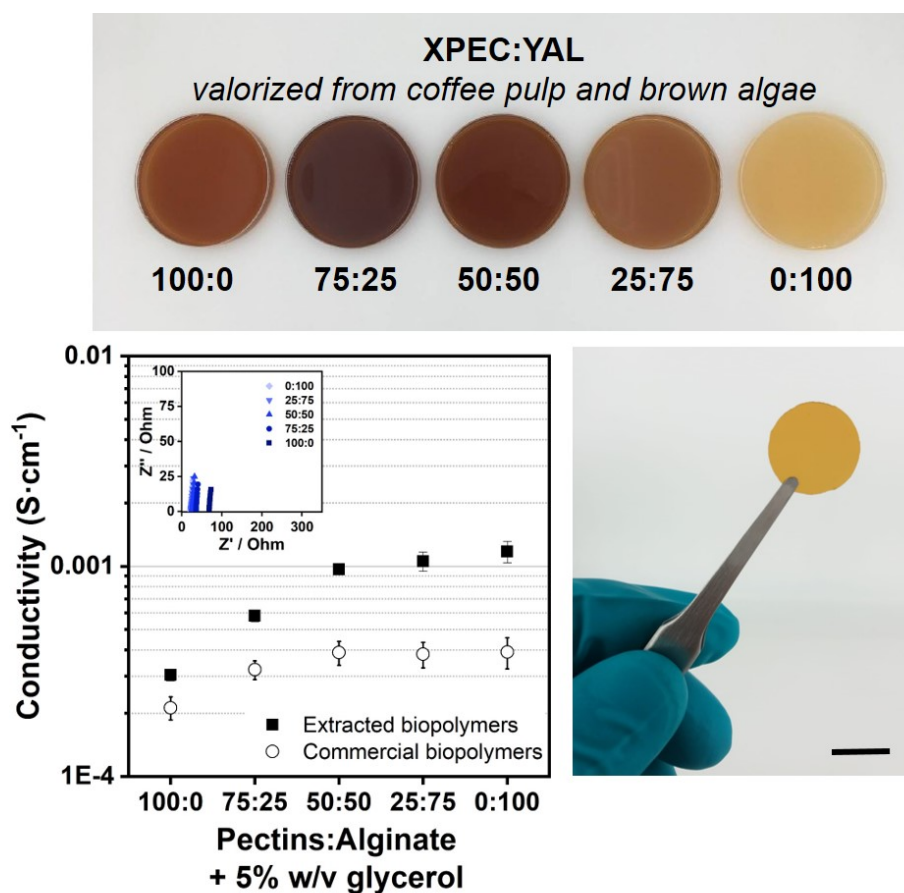


Figure 5.24: Ionic conductive self-standing membranes synthesized from valorized pectins from coffee pulp and alginate from brown algae. Ionic conductivity variation as a function of pectins and alginate biopolymers ratios. (N=3) Inset: Nyquist plot obtained from impedance spectroscopy analysis. Scale bar: 1cm.

Conductivities computed from EIS analysis of the ion exchange membranes from extracted biopolymers were higher than the ones obtained for commercial biopolymers, in all cases. This could be explained due to the lower purity of the biopolymers, which possibly translates in a higher concentration of free ions, that facilitate charge movement. Furthermore, XPEC:YAL ratios show an increasing

conductivity pattern when increasing alginate concentration, reaching a maximum of $1.18 \pm 0.14 \cdot 10^{-4} \text{ S} \cdot \text{cm}^{-2}$ for 0PEC:100AL concentration.

Overall, these results validate the feasibility of using pectins directly extracted from coffee residues in conjunction with alginate, refined from brown algae recovered in mexican beaches, as hydrogel matrix in a battery.

5.6.3 Battery fabricated from revalorized biopolymers

Finally, a coin cell battery (1.4 cm diameter) was fabricated with a hydrogel matrix synthesized with extracted biopolymers as a proof of concept. The battery composition emulates the described in one Figure 5.15a. for commercially available biopolymers. In order to adapt the previously described protocol to the battery fabrication with extracted materials, it was necessary to increase the total hydrogel volume poured in the Petri dish from 10 mL to 40 mL, thus membranes from extracted biopolymers prepared with volumes under 40 mL can not be unmold.

Figure 5.25 shows the battery performance in comparison with a coin cell fabricated with commercial materials. As it can be seen, both batteries are comparable in terms of power, reaching values of 4.5 and 5.4 mW/cm^2 power peak for extracted and commercial matrices respectively.

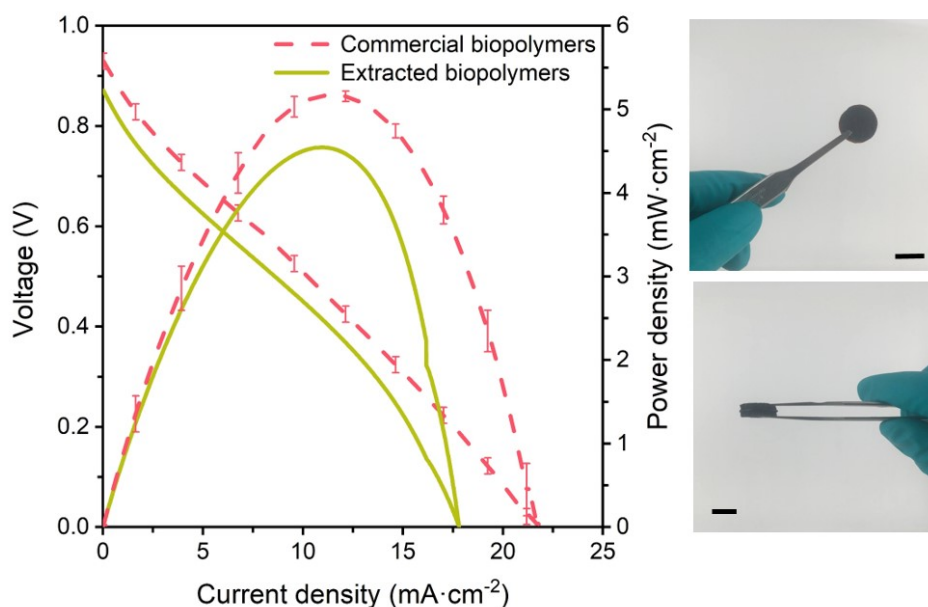


Figure 5.25: Polarization curves comparing the performance in terms of current and power density of hydrogel based primary batteries, fabricated from commercial and extracted pectins and alginate biopolymers. Real photographs of the extracted biopolymers coin cell battery. Scale bars: 1 cm

5.7 Discussion

The work presented in this chapter lays the foundations for the development of a locally fabricated primary battery, specially conceived to power portable lighting systems in coffee growing communities in Mexico. The feasibility of the concept has been proven by developing a battery stack with commercially available materials to power a portable lantern system. A first battery cell prototype has been presented using materials revalorized from coffee waste was presented. However, there are some challenges to be assessed in order to achieve the ambitious goal of building a battery completely fabricated from materials recovered from agrowaste.

First, as presented in subsection 6.6.1 the phenolic compounds concentration recovered from coffee pulp infusion is in the range of μM . Thus, a methodology to further concentrate the redox species present in the coffee pulp is needed. Furthermore, it has been shown that the residue generation occurs at coffee growing plots; and the antioxidant compounds recovered are rapidly degraded in ambient conditions. Thus, a delocalized protocol needs to be developed and implemented to facilitate the pulp residue management for phenolic compound recovery and preservation.

Regarding current collector material, non-toxic carbon felt has been selected thanks to its versatility and appropriate electrochemical performance. This material could be substituted by pyrolyzed coffee ground or husk, a novel material recently reported by Kang et al.¹⁸⁶

Moreover, the second proposed application in this project is still ongoing. A UV-water disinfection self-made device is currently been developed. The efficient integration with the battery would represent a great challenge due to the high amount of power demanded by UVC range LEDs.

Finally, the final battery prototype projected end-of-life needs to be assessed under EN 13432 standard. This assessment in conjunction with a fitotoxicity test are compulsory to test the compostability of the battery materials, and ensure the harmfulness of the battery prototype when returning to the nature after its operational lifespan.

5.7.1 Evaluation of project impact through the adaptation of the Social Progress Index (SPI)

When applied, the project is expected to have real and positive impact in the progress coffee growing communities. In order to quantify the project impact, a first adaptation of the SPI was proposed and computed.

As explained in the introduction, the Social Progress Index (SPI) is a holistic indicator of social wellness and progress. Every year the association *México, ¿cómo vamos?*, in collaboration with the initiative Social Progress Imperative, computes the SPI at a country level, i.e. they calculate one index for each federal entity and compare it with the national one. These assessments allow to portray the particularities of the different territory realities. Figure 5.26 gathers the Social Progress Index different layers and components.



Figure 5.26: Social progress index dimensions, components and indicators. Source: Social Progress Imperative

The index, usually reported at a country level, takes into account three dimensions named Basic Human Needs, Foundations of Wellbeing and Opportunity; and is mathematically expressed as:

$$IPS = \frac{1}{3} \sum_d Dimension_d \quad (5.3)$$

As depicted in Figure 5.26, each dimension is composed by four components, meaning it is compute as follows:

$$Dimension_d = \frac{1}{4} \sum_c Component_c \quad (5.4)$$

and each component gathers from three to five indicators that equally compute to the metric.

$$Component_c = \sum_i (w_i \cdot Indicator_i) \quad (5.5)$$

where w_i stands for the indicator weight and will depend on the total quantity of indicators in each component.

Figure 5.27 gathers the metrics by year computed by *México, ¿cómo vamos?* for each one of the 32 federal entities of Mexico state.

Año	Nacional	AGS	BC	BCS	CAMP	COAH	COL	CHPS	CHIH	CDMX	DGO	GTO	GRO	HGO	JAL	MEX	MICH	MOR	NAY	NL	OAX	PUE	ORO	QROO	SLP	SIN	SON	TAB	TAM	TLAX	VER	YUC	ZAC
2015	61.5	68	67	63.4	62.6	61.2	61.6	47.7	61.4	70.1	62.7	56.2	45.2	59.1	66.4	61.2	56.5	58.3	62	70.8	51.7	55.7	68.5	66	60.7	65.1	67.2	56.3	63.6	61.8	56.6	65.5	58.3
2016	62.2	68.4	68.5	64	62.6	66.2	65.5	50.2	64.9	71.6	65	62.4	46.3	60.7	66.8	62	58.8	59.3	63.4	69.8	50.8	57.3	68.3	66.6	61.2	65.8	67.6	57.4	63.8	61.6	55.4	66.6	59.5
2017	62.5	68.1	67.7	61.8	62.8	66.4	65	51.1	64.8	71	64.5	62.5	47.3	60.5	66.9	63.9	59.1	58.9	61.7	69.6	51.7	58	68.5	66.6	60.7	68	68.3	57.7	63.9	61.7	55.6	67.9	58.7
2018	63.6	70.1	67.8	64.3	62.9	67.2	66.7	51.3	65.8	73.6	65.5	63.1	48.5	61.7	68.5	64.5	60.3	60.6	63.1	71.6	53	59.9	68.9	67	62	68.2	69.3	56.8	66.5	63.2	56.9	67.9	60.4
2019	63.4	70.5	68	64.5	61.8	67.5	64.2	51.3	65.5	72.9	65.5	62.5	47.5	62.1	68.6	64	59.8	60.1	63.6	71.8	53.5	59.5	69	66.6	61.9	68.3	68.7	57.8	67.3	63.2	56.2	69.1	60.2
2020	63.2	70.3	68.3	64.6	62.3	67	65.6	49.9	63.7	69.7	66.6	60.9	48.4	62.9	68.1	62	58.3	58.9	63.3	72.5	51	58	70.5	65.9	59.8	68.4	67.4	56.8	67.2	61.9	56.2	68.8	58.3

Figure 5.27: Social progres index evolution at national level and by state from 2015 to 2020. Elaborated by: México, ¿cómo vamos? from public information. AGS: Aguas Calientes, BC: Baja California, BCS: Baja California Sur, CAMP: Campeche, COAH: Coahuila de Zaragoza, COL: Colima, CHPS: Chiapas, CHIH: Chihuahua, CDMX: Ciudad de México, DGO: Durango, GTO:Guanajuato, GRO: Guerrero, HGO: Hidalgo, JAL: Jalisco, MEX: México, MCH: Michoacán, MOR: Morelos, NAY:Nayarit, NL:Nueva Leon , OAX:Oaxaca, PUE:Puebla, QRO:Querétaro, QROO:Quintana Roo, SLP:San Luis Potosí, SIN:Sinaloa, SON:Sonora, TAB:Tabasco, TAM:Tamaulipas, TLAX:Tlaxcala, VER:Veracruz, YUC:Yucatán and ZAC:Zacatecas.

According to the Social Progress Index México 2015-2020 report, Chiapas (CHPS) population severest deprivations (i.e. SPI < 40) are related to Water and Sanitation (SPI: 27.4), Access to Knowledge (SPI: 36.8), Personal Freedom & Choice (SPI: 26.8) and Access to Advance Education (SPI: 39.3). Shelter dimension it is also specially appealing for this project thus it takes into account access to electricity, ranked in 66.1 Chiapas value is the lowest along the country.

In order to compute the potential impact of the battery conceptualized in this chapter, two different levels of project implementations were projected: Chiapas entity level and coffee growing communities, called local level. To construct the second scenario there were taken into account the locations of the producers from Triunfo Verde cooperative, which are 3 specific municipalities, named Ángel Albino Corzo, La Concordia and Siltepec.

Hence, a data collection was performed from the public databases from mexican government, each one of the 53 indicators was gathered from the different available databases ^{vii}. It has to be noticed that some of the indicators for the calculation of SPI at mexican national level vary with the ones showed in Figure 5.2. The adaptation was performed by performed by *México, ¿Cómo vamos?* to mach the available statistical data, and in this thesis it was also applied in order to compute the project impact.

Once all the indicators values were gathered, we identified the four indicators that will be affected by the implementation of the technology in the coffee growing communities at Chiapas and Municipalities:

Water availability in households: this metric is a component of Water and Sanitation indicator. Currently 88.75% of the Chiapas population has water availability in households, while the value is 75% for municipalities population.

^{vii}The data basis used to compute the project impact were: Medición de la pobreza from CONEVAL, INEGI, Encuesta Nacional de los Hogares, Mexico Peace Index, Sistema Nacional de la Información de Escuelas publicas, Encuesta Nacional sobre Disponibilidad y Uso de Tecnologías de la Información en los Hogares, Sistema de Indicadores para Monitorear los Avances de la Estrategia Nacional para la Prevención y el control del Sobrepeso, la Obesidad y la Diabetes, World Resources Institute, Global Forest Watch, Doing Business en Mexico, Censo Nacional de Gobierno, Seguridad Pública y Sistema Penitenciario Estatales and CONACYT.

Lot of households obtain their water from a nearby river stream. However, they do not have a proper water treatment system. In this sense, it was considered that when implemented the UV- water sanitation device powered by the developed batteries will provide safe water suitable for drinking.

Continuous water service: this metric is a component of Water and Sanitation indicator and at present its value for Chiapas population is 79.03%, this value was not available at municipalities level. Similarly to the above component, it was considered that the UV- disinfection device will provide a continuous safe water service.

Access to electricity: this metric is a component of Shelter indicator and its value at a Chiapas level is 99.28 %, while its reduced to 82% when computed at local level. The implementation of biodegradable batteries will give access to a lighting system and thus a first access to electricity.

Energy saving light bulbs: this metric is a component of Environmental Quality. The lighting system will completely rely on LED technology, thus this metric value would be maximized. At present, 77% of the population uses energy saving light bulbs at Chiapas level, while the indicator decreases to 56.46% at local level.

To calculate the project impact, these four indicators values were transformed to 100%, and the IPS was recomputed at Chiapas and local levels. Figure 5.28 shows the percentage improvement for each dimension and in the IPS that the project would cause. As it can be seen, the project impact is noticeable in Basic Human Needs and Foundations of Well Being dimensions, while no impact at Opportunities dimension can be expected. In particular, the project could be expected to increment the Chiapas SPI in a 1.2%, while the local SPI would benefit from a 6.34% of improvement. Of course, the computation of the project impact assuming that all the affected indicators will rank 100% is rough and simplistic. However, the approach herein presented to assess the project impact based on the adaptation of the SPI is a first attempt to create a metric that evaluates the social impact of scientific research. Beyond the metrics, it can be clearly concluded that the project implementation in the municipalities it was conceived for, generates a greater impact than at Chiapas level. Thus validating the project basis of thinking globally, acting locally.

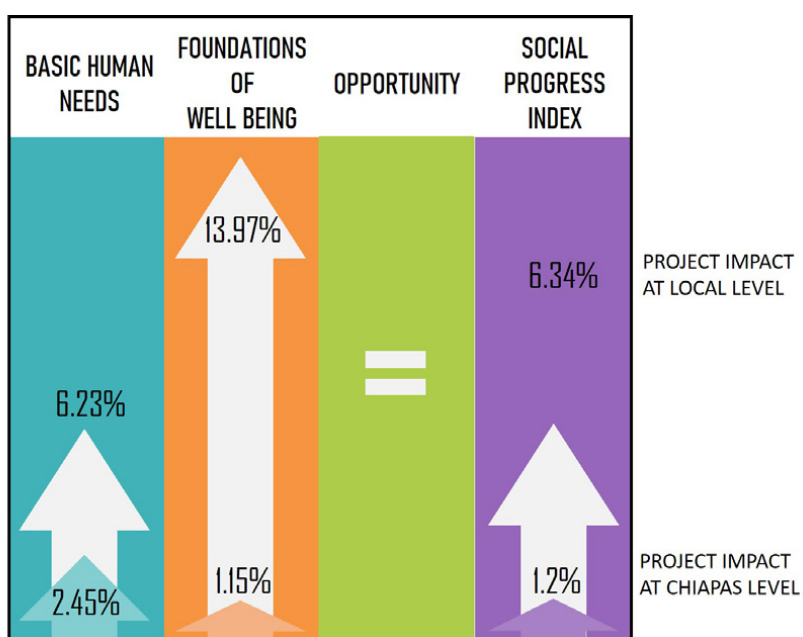


Figure 5.28: Potential impact on the Social Progress Index of the implementation of locally fabricated biodegradable batteries for powering portable lighting systems and UV water disinfection devices.

Conclusions|

The battery presented in this chapter was ecodesigned to address coffee growing communities life and needs. The global application of a holistic vision has enabled the project to assess lighting needs from a local perspective; while tackling environmental concerns. In this sense, an incisive analysis of coffee producers daily life has been performed to better understand socioeconomic impacts of electrification. By placing the project foundations in the local context of the communities it is devoted to, we ensured the generation of truly sustainable and tailor-made solutions.

The development of the first battery prototype was carried out through a conscious material selection, that will allow to partially substitute them for compounds directly recovered from residues. After battery optimization and as a proof of concept, the battery stack was tested in a realistic scenario. A portable lighting system was powered in coffee growing communities in Chiapas, Mexico and the battery fabrication process was satisfactory exported to a non-scientific environment in a local household at a coffee plantation.

Furthermore, this chapter has laid the first steps towards the revalorization of pulp coffee residue, a remotely localized abundant waste, for its implementation as a battery compound. In this respect, phenolic compounds extraction was carried out at the production location, and the effect of storage conditions and time was studied. Moreover, ion conductive membranes were synthesized and analyzed via impedance spectroscopy. The ionic conductivity obtained values greatly overcome the ones found for commercial bio-polymers membranes, thus it can be concluded that revalorized polymers are suitable for its implementation as hydrogel battery matrix.

Despite there is plenty of room for improvement, this chapter has proven the feasible and huge potentiality of developing decentralized and sustainable technology, which could locally address societal deprivations without compromising the environment.

Materials & Methods

This section brings together and further elaborates the methodologies and processes used along Chapter 5. Some of the protocols have already been described in the main text; however, here the reader can find more details about the procedures and materials used.

Chemicals

All following chemicals were purchased from Sigma Aldrich (Sigma Aldrich, St Louis, Missouri, USA) and used as received: sodium alginate (W201502), pectins (P9135), glycerol (G7757), gallic acid (G7384), caffeic acid (C0625), iron (III) nitrate nonhydrate (254223), potassium chloride (P3911), oxalic acid (O0376) and potassium hydroxide (221473). Carboxymethylcellulose sodium salt was purchased from Glentham Life Sciences (GC7698, Glentham Life Sciences Ltd, Corsham, United Kingdom). All solutions have been prepared in deionized water.

Bio-polymer membranes synthesis

The hydrogels synthesis proceeds as follows: 1 g of sodium alginate is stirred in 50 mL deionized water (2% w/v concentration) at 80 °C until its complete dissolution. Similarly, 1.5% w/v concentration carboxy-methyl cellulose (CMC) and 2% w/v pectins solutions are prepared. Then, the hydrogel is created by mixing both gels in the desired ratios (100:0, 75:25, 50:50, 25:75, 0:100) and doping the blend with 5% w/v of glycerol as plasticizer. Finally, 40 mL of blend are poured into an 8.6 cm petri dish and dried at T 25 °C in an incubator (Hach Lange S.L.U. L2-01).

After the drying process the membranes are manually cut with a punch into three circles of 1.55 cm diameter. The bio-films thickness is measured with a dial indicator (RS PRO, Amidata S.A.U., Alcobendas, Madrid, Spain).

In the case of extracted bio-polymers the same protocol was followed, but extending the drying process to 5 days.

Battery materials and fabrication methods

Two proportions of the hydrogel matrix were selected for its implementation on the batteries, 50PEC:50AL and 75CMC:25AL. Its synthesis is performed as described above; then, 15 mL of the hydrogel is dried over 2 days in a 8.6 cm diameter petri dish and manually cut with a punch to obtain the battery membrane.

On the other hand, the anodic and cathodic matrices are synthesized by simply adding gallic acid 80 mM with potassium hydroxide 1 M, and iron nitrate 160 mM with oxalic acid 0.25 M; respectively. The anodic hydrogel must be protected from light to prevent gallic acid degradation.

The anodic and cathodic solutions are poured on top of the current collectors with the use of a syringe. The volume was adapted to the current collector area, being 3.5 mL in the case of the 5.5 cm diameter final unitary battery cell, and 400 μ L in the case of the 2 cm diameter testing batteries. For the test batteries, the electrodes go through a drying process of 24 hours at 25 °C. While, for the case of the final battery, a plastic spatula is used to evenly distribute the hydrogel on the current collector's surface, and the system is used without removing the humidity.

All carbonaceous materials tested as current collectors were purchased from Fuel Cell Store (Fuel Cell Store, Texas, USA), being their name the provider's reference.

Electrochemical studies

All electrochemical measurements were performed using a PalmSens4 potentiostat/galvanostat/impedance analyzer (Palmsens BCm Houten, the Netherlands) at room temperature, except for the final characterization of a single cell battery (depicted in Figure 5.15) where a EmStat4S USB powered potentiostat/galvanostat was used to avoid current limitations. In the case of the studies performed in Chiapas, the EmStat4S potentiostat was also prioritized for portability reasons.

Redox species characterization

The commercial phenolic compounds were characterized by cyclic voltammetry in self-fabricated screen printed carbon electrodes (SPE), SPEs fabrication was performed as

described in¹⁸⁷. The redox species analysis was performed from pre-recorded OCP to 0.6V in the case of neutral pH or 0.5V in the case of alkaline pH, 20mV/s in all cases.

Regarding coffee pulp infusion characterization, differential pulse voltammetry was used. The voltammograms were performed at the following conditions: $s_{rate} = 50\text{mV/s}$, $E_{step} = 0.01\text{V}$, $E_{pulse} = 0.1\text{V}$, $t_{pulse} = 0.035\text{V}$, $E_{begin} = -0.2\text{V}$, $E_{end} = 0.8\text{V}$.

In both cases, the SPEs were pre-activated with a 1M KCl aqueous medium at 1.5V over 5 minutes, to eliminate any surface pollutants or remaining solvents from the screen-printing process.

Membranes ionic conductivity studies

Hydrogel membranes's ionic conductivity assesment was performed by Electrochemical Impedance Spectroscopy (EIS) analysis, ranging from 1kHz to 1MHz. The conductivity value is obtained from the total impedance value when the imaginary component is zero (See Appendix B).

Batteries characterization

Batteries polarization and power curves are generated by sweeping the potential value from OCV pre-recorded value to 0V, using linear sweep voltammetry (LSV) electrochemical technique at a controlled scan rate of 20 mV/s. Discharge curves were recorded using open circuit potentiometry (OCP) technique and connecting an external load in series to the battery.

Portable lighting system prototype materials

The lighting system was 3D-printed with a compostable filament, COMPOST3D (B4Plastics, IQ Parklaan 2A, 3650 Dilsen-Stokkem, Belgium). The design was custom-made by using an open-source software, Blender (Blender Foundation, Stichting Blender Foundation, Buikslotermeerplein 161, 1025 ET Amsterdam, the Netherlands). Then, steel screws were use to manually assemble the different parts.

A generic LED bulb was purchased from Farnell (2536217, Farnell, Leeds, UK) and connected to the DC-DC boost converter (BQ25504-EVM, Texas Instruments, Dallas, USA) in association with a 0.1 μF supercapacitor (RS PRO, Amidata S.A.U., Alcobendas, Madrid, Spain) through a lamp holder (3376478, Farnell, Leeds, UK).

The battery stack was connected to the J1 input source of the voltage boost converter. Three copper circles (5.5 cm diameter) were used as battery terminals. The LED bulb and the supercapacitor were connected to J5 charger output of the converter.

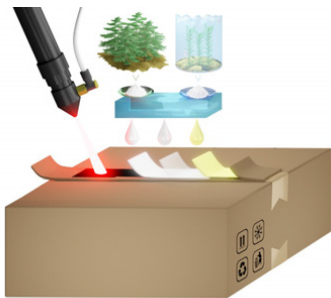
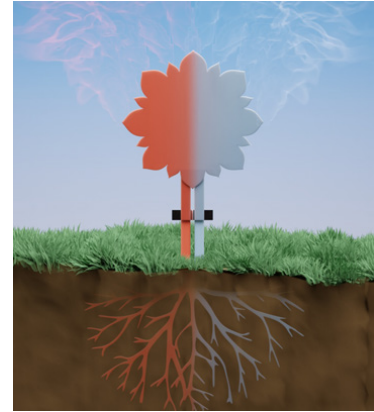
Conclusions|

This thesis presents a new rationale for sustainable portable batteries development in which the complete life cycle is analyzed and redefined under ecodesign principles and advocates for a 'tailor-made' approach, where the battery ends up integrated into the application value chain. The rationale sets an environmental ceiling and a performance foundation for portable batteries, defining a safe space for sustainable and environmentally conscious battery development. The approach is then materialized with three novel primary battery concepts, tackling two disruptive end-of-life, biodegradability and recycling with paper and cardboard.



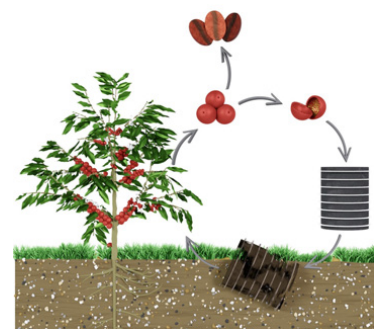
The boundaries for portable batteries development have been established, defining a safe and sustainable space for batteries conceptualization and creation. Inspired in the doughnut economics model created by Kate Raworth, this thesis defines six dimensions comprising the social, economic and environmental ceiling, i.e. materials toxicity, ethical supply chain, low energy and resources consumption, materials abundance, economically affordable and cost-effective end-of-life. Concurrently, energy density, power density, competitive manufacture, portability, operation time and user-friendliness define the performance foundation dimensions. Then, ecodesign has been identified as a key enabler to keep batteries within the safe-space and a set of recommendations, tools and good practices have been gathered to be considered at each stage of the battery life cycle. Thus, a systematic methodology has been created for portable batteries development, which is specially appealing for batteries with a disruptive end of life.

A flow battery profoundly inspired by nature, which mimics fluid transport in plants to generate electric power has been made from commercially available materials. The FlowER battery represents the first steps in the materialization of the proposed methodology. Specifically ecodesigned for precision agriculture applications, biodegradability has been matched as an alternative end-of-life scenario. Accordingly, the materials selection was carried out to enable the selected EoL. The prototype practicality was demonstrated by powering a wireless plant caring commercial device during sensing and Bluetooth connection stages. Furthermore, standardized biodegradability and phytotoxicity assessments were carried out, showing that similarly to a plant the battery is harmless to the environment at the end of its operational lifetime.



A novel battery ecodesign for smart packaging applications and with paper and cardboard recycling process as inherent end-of-life was demonstrated. In order to enable the devised EoL the research presented in this chapter has gone one step further by developing the materials that conform the battery. Furthermore, the fabrication processes were selected and implemented by prioritizing compatibility with a cardboard box established fabrication process. In this sense, this battery constitutes the first attempt of a comprehensive redefinition of a battery life cycle by completely paring it with the application value chain.

The battery development process for this chapter has been located in coffee growing communities at southern Chiapas, Mexico. An analysis of the communities energetic needs and ambitions has been carried out. Coffee waste was proposed as a source of battery materials, the fabrication processes were restricted to a feasible decentralized production, and the proposed application tackles coffee communities real necessities,



i.e. lighting systems and UV water disinfection devices. Finally, the possibility of implementing valorized biopolymers to synthesize the battery hydrogel matrix was demonstrated.

As an ultimate conclusion, this thesis' final goal is to raise awareness and understanding on how our individual choices and actions, even at a research-level, collectively affect our natural resources. It demonstrates that feasible and efficient solutions can be created by placing sustainability as a core priority. In essence, the batteries presented in this thesis are the evidence that it is imperative but also possible to redefine society's technological priorities to consciously reduce humanity's environmental impact.

A

Materials selection and related experimental methodology

This appendix is devoted to explain the theoretical principles and experimental basics particularly applied to the electrochemically active species and battery matrices selection. The content of this appendix regarding the applied electrochemical analytical techniques has been gathered from the well-known literature,^{188–190} with the aim that the unfamiliarized reader can easily follow the development of batteries conducted in this thesis.

The evaluation methodology of potentially anodic and cathodic redox species through electroanalytical techniques is elaborate on *Redox species selection* subsection. On the other hand, two types of containing matrices were used on the batteries taking place in this thesis. A paper-based capillary structure was implemented for the battery development in Chapter 4, while ion conductive hydrogels are synthesized and utilized in Chapters 5 and 6. Thus, the practices related to the assessment of these matrices are introduced in *Paper as capillary structure* and *Hydrogels with ionic conductivity* subsections.

A.1 Electrochemical techniques for redox species selection

In order to identify the most suitable candidates to be implemented as anodes and cathodes in the batteries developed during this thesis, the electrochemical (EQ) behavior of several organic and inorganic species was evaluated via cyclic voltammetry (CV) and linear sweep voltammetry (LSV). The evaluations were performed in a three electrodes electrochemical cell, composed by a working electrode (WE), a counter or auxiliary electrode (CE) and a reference electrode (RE). Within this thesis two types of three electrodes electrochemical cells have been used, the choice was made based on the redox species quantity available. Screen printed cells with carbon based WE and CE have been used to characterize redox species in small volumes of samples ($\approx 50\mu\text{L}$). To clean the WE surface and remove any pollutant left from the screen printing process, 1.5V over five minutes pre-treatment in an ion conductive neutral media was applied to all screen printed cells. When bigger volumes of samples were available, a conventional cell composed by a glassy carbon WE (0.07 cm^2) and a platinum wire CE in a beaker was utilized. In this case, WE was prepared by manual polish with a water-alumina slurry. In both cases silver-silver chloride electrode (Ag/AgCl) is used as reference electrode.

Figure A.1 summarizes the main features of CV and LSV electroanalytical methods.

CV is a potentiodynamic measurement by which a potential (E) sweep (from E_1 to E_2 and back) is applied to the WE as a function of the RE potential (input signal), forcing the reaction of interest to take place at the WE interface. The electrons flow between the WE and CE is recorded (output signal). The relation between voltage variation and time is called scan rate (V/s). If the sweep only goes from E_1 to E_2 the measurement is called LSV. As a IUPAC convention, when the potential scan is applied from lower to higher potentials oxidation reaction is forced, given as a result positive currents, in contrast if the sweep takes place from higher to lower potential a reduction reaction is forced, given as a result negative currents.

The voltammogram pattern indicates many attributes about the EQ system and the species nature. For the particular interest of this thesis, the redox species oxidation or

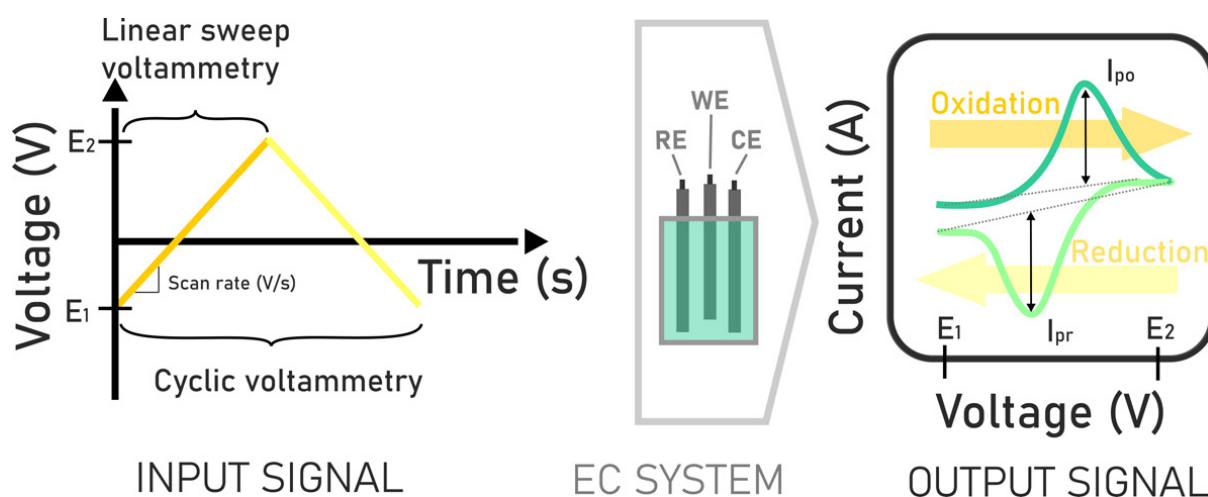


Figure A.1: Schematic representation of cyclic voltammetry and linear sweep voltammetry electroanalytical methods to study the oxidation and reduction behavior of a redox species in a three electrode electrochemical system, represented as a screen printed cell (working electrode: WE, counter electrode: CE and reference electrode: RE)

reduction kinetics was studied by comparing current and potential peak values (I_p , E_p), which is related with the battery maximum power output. And potential value at zero current conditions, which will determine the battery voltage at open circuit.

Furthermore, the redox species maximum solubility was also taken into account when selecting the final redox couples, since the concentration of the active materials greatly determines the battery performance in terms of power. The final redox couple selected for each battery can be found in the related chapter. While, Appendix C gathers the complete catalogue of the evaluated redox species in alkaline, neutral and acidic medias. Although some inorganic species were also considered, the screening of electroactive species was focused on organic compound, due to its potentially capability of biodegradation.

In the particular case of electroactive compound characterization of coffee pulp infusion carried out in Chapter 5, differential pulse voltammetry (DPV) was used. DPV is also an electroanalytical technique, analogue to CV, that instead of applied the voltage scan as a linear ramps, applies short voltage pulses. The output signal (current) is measured before and at the end of the application of each pulse. This procedure enables the drastic reduction of capacitive currents, which leads to a high sensitivity technique. Furthermore, the short voltage steps lead to narrower current

peaks than CV. All in all, contributing to a better discrimination of analytes with similar electroactive potentials. Figure A.2 schematizes the fundamentals of this technique.

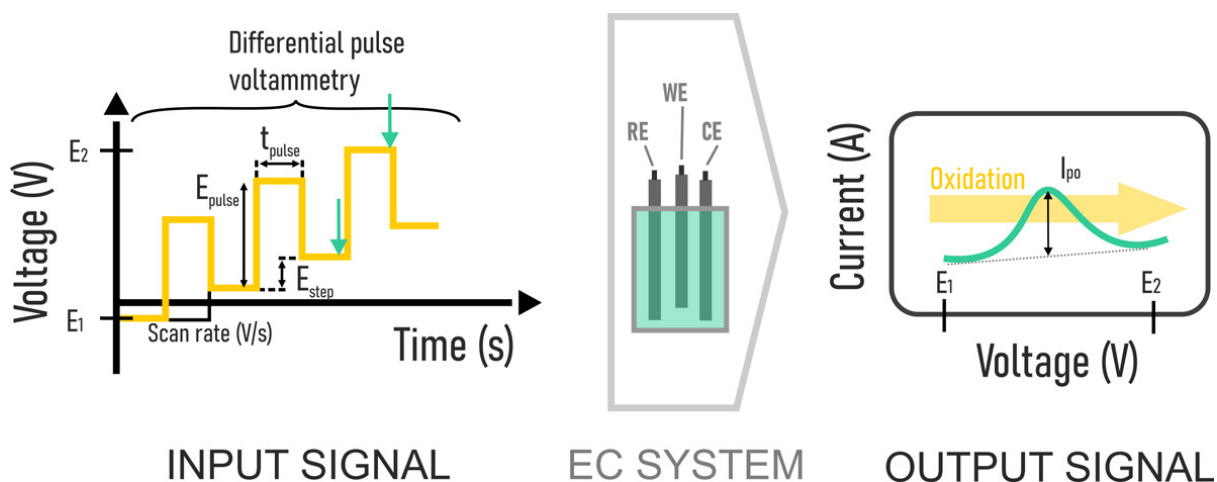


Figure A.2: Schematic representation of differential pulse voltammetry electroanalytical method to study the oxidation behavior of an electroactive species in a three electrode electrochemical system, represented as a screen printed cell (working electrode: WE, counter electrode: CE and reference electrode: RE)

A.2 Paper as capillary structure in microfluidic flow batteries

Microfluidics has been employed for electrochemical conversion since 2002 when the first microfluidic galvanic cells (μ GC) were invented. μ FG use flow at low Reynolds numbers to keep the two reactants streams flowing in colaminar equilibrium without mixing, enabling the removal of the physical separator (i.e. ion-exchange membrane). μ FG field is a wide research field that has provided a great variety of energy conversion devices designs and functions.

One of the most acclaimed breakthrough in μ FG design was the use of paper-based materials as capillary structure that passively pumps the reactants, erasing the need of external pumps. Figure A.3 depicts a generic structure for a paper-based μ GC and the phenomenas related to its working principle.

Paper-based microfluidic flow cells are μ FG that use the capillary forces to drive the catholyte and anolyte through the paper microporous. Capillary forces result from the

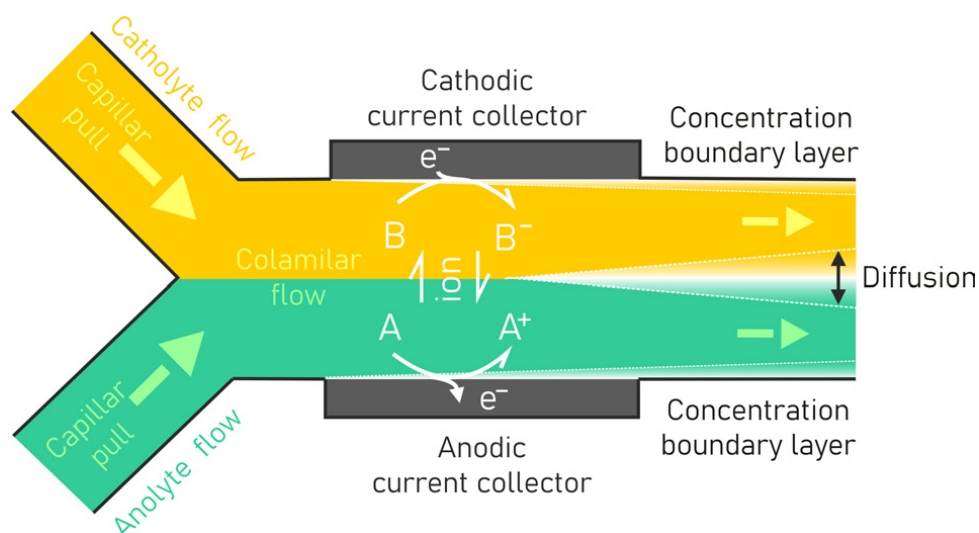


Figure A.3: Schematic representation of a paper-based microfluidics galvanic cell and its working principle.

pressure difference at an immiscible fluids interface, in this particular case, cell reactants -air inside the porous; wicking the liquids through the capillary system. Furthermore, as the paper porous are on the order of μm Reynolds numbers values are maintained lower than 1, allowing the creation of a colamilar flow within the electrochemical system. The absence of a physical separator to separate the anolyte and catholyte streams, results in a fluid-fluid interface, in which ions flow through the electrolytes to compensate charge and the slowing mixing is governed by diffusion.

Chapter 4 brings paper-based μFG to the next level, investigating the use of evaporation pull to drive the reactants flow through the paper structure.

A.2.1 Impedance spectroscopy to asses hydrogels with ionic conductivity

The second battery structural material proposed in this thesis are ion conductive hydrogels, chemically or physically bonded polymer networks able to retain water. In this work, hydrogels have been deliberately synthesized from naturally occurring polymers such as cellulose derivatives, alginates or pectins, which are abundant, low-cost and environmentally conscious materials.^{165;191} These bio-based hydrogels have been implemented as battery separator and solid polymer electrolytes. As it will be further discussed in Chapter 5 and 6, in order to act as battery separator the

hydrogels must be able to form thin (100-250 μm) self-standing membranes to ensure the separation of the two half-cells reactants and avoid undesired crossover. While, to be implemented as solid polymer electrolyte chemical stability at extreme pH was imperative. But overall, to ensure the hydrogels are appropriate to be battery matrices it is an essential requirement they have high ionic conductivity¹.

Electrochemical Impedance Spectroscopy (EIS) analytical method was used to assess the suitability of the hydrogels as ion conducting material. As shown in Figure A.4 in EIS technique a sinusoidal signal of potential ($E(t)$) -or current ($I(t)$)- is applied to the electrochemical system. As every sinusoid, the input signal is characterized by a wave amplitude (E_0) and a phase i.e. angular frequency per time (ωt). The ω also determines the wave frequency (f), both related by the expression $\omega = 2\pi f$. As a consequence of going through the EQ system the sinusoidal signal is slightly perturbed, and the phase shifts, that difference amount is called phase angle, Φ .

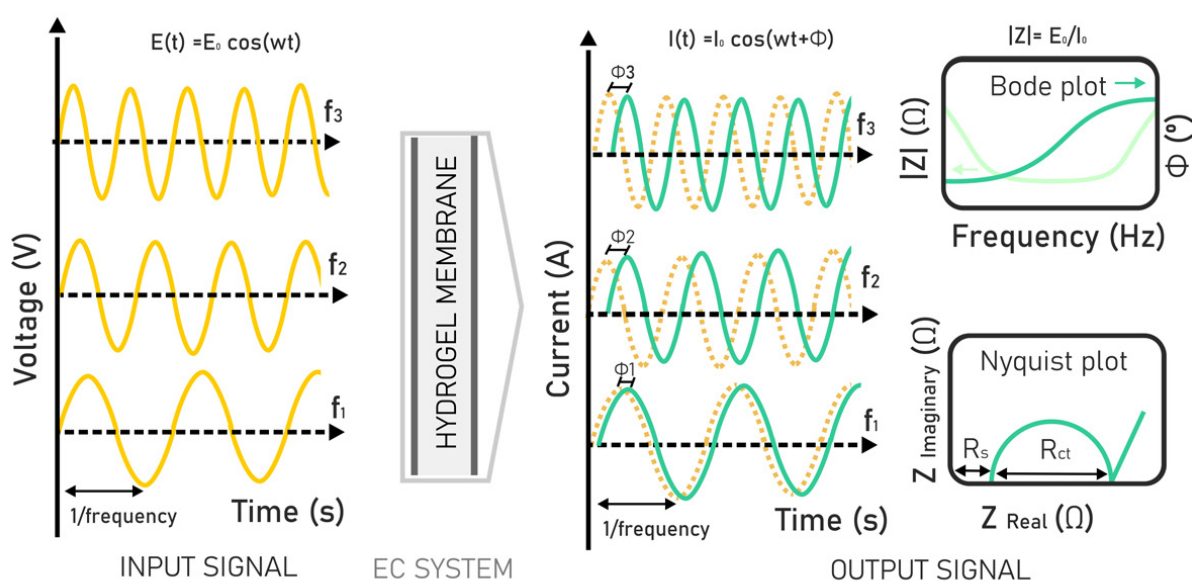


Figure A.4: Schematic representation of the basics regarding Electrochemical Impedance Spectroscopy (EIS) method applied to the study of hydrogel membranes conductivity.

¹The properties aforementioned may not cover all the desirable features established in the literature for proton-exchange membranes technologies. In this sense, it is worth to kindly remember that the technology herein proposed aims to reinvent the battery paradigm, thus properties such as long lifetimes or mechanical stability at high temperatures were relegated to a secondary level, as a consequence of prioritizing battery sustainability in front of performance.

A complete EIS analysis consist in the sequentially application of sinusoidal signals to the EQ system, maintaining constant the signal amplitude but varying the signal frequencies. Each f perturbs a different phenomena on the EQ system, obtaining a complete set of ϕ values. Thus, the EQ system portrait is obtained as a collection of $E(t)$ and $I(t)$ values. The impedance of the system at each perturbation can be therefore obtained though Eq. A.1, and Bode and Nyquist plots can be plotted.

$$\begin{aligned} |Z| &= \frac{E_0}{I_0} \\ Z_{Real} &= |Z|\cos\Phi \\ Z_{Imaginary} &= |Z|\sin\Phi \end{aligned} \tag{A.1}$$

EIS is a complex and powerful electroanalytical tool, tha in this tesis have been particularly applied to the study of membranes conductivity. The hydrogel membranes were placed between two ion-blocking electrodes and subjected to EIS analysis with a potential sinusoidal input signal, at typical frequencies between 1kHz to 1MHz. Its ionic conductivity (σ) has been determined according to the following equation:

$$\sigma = \frac{d}{R_s A} \tag{A.2}$$

where, d is the distance between electrodes (membrane thickness in this case), A is the electrode contact area and R_s is the ion mobility resistance of the sample. R_s is obtained from $|Z|$ values when the imaginary part contribution equals 0, as it can be visualized in Nyquist plot.

B

Standards and regulations

Two battery disruptive end-of-life are suggested in this thesis, biodegradability is proposed in Chapter 4 and 6, for batteries respectively devoted to power precision agriculture devices, and lightning systems in remote locations. Whereas recyclability with paper and cardboard waste stream is proposed for batteries created for smart packaging applications in Chapter 5. Therefore, in order to ensure that the batteries do not pose a risk to the value chain they have been designed for, the end-of-life must be taken into account from the early beginning of the battery conception. In addition to that, the proposed battery EoL must be assessed under standardized regulations to ensure a safe battery disposability after its operational life span.

In this context, an introduction to the European Standards (EN) from the European Committee for Standardization (CEN) regarding biodegradability and cardboard recyclability is presented in this section. Given that there does not exist a standardized regulation about batteries requisites to be considered biodegradability or recyclable, in this thesis those standards and assays proposed for packaging products have been embraced for batteries.

B.1 Biodegradability and phytotoxicity standards

According to ISO 13432 in order to certify a product as biodegradable there are four requisites that must be assessed: physical-chemical characteristics, inherent biodegradability, desintegration capability, and generated compost quality. If the product is composed by diverse materials each one must be separately assessed.

- **Physical-chemical characterization:** tests the volatile solids percentage present in the product (which must be higher than 50%) and establishes a harmful materials that can not be present in the product or that can not overcome a weight percentage limit.
- **Inherent biodegradability:** asses the biodegradable nature of the product in a controle conditions assay known as dinamic respirometry, by which the product introduced in a composting reactor. This analytical method determines the biodegradation level of a sample (%) as the relation between the total oxygen consumed, as a consequence of the microbial degradation activity, and the theoretical oxygen demand.
- **Desintegration capability:** ensures that over 90% of the sample fragments are smaller than 2mm after the compostability test.
- **Compost quality:** test the final compost quality after the biodegradation test. This step is based on OEDC Guideline for testing of chemical 208 "Terrestrial plants. Growth test", and in basically consist in a germination test of seeds by which the compost toxicity is checked.

Furthermore, in Europe the company TUV Austria has established specialized product certifications. The certifications, called OK Compost, are even more specific differentiating between Industrial, Home and Soil compost, among others. Pioneer on this field, these certifications have become the basis to the developed of some of the latest European standards (as for example *prEN 17427 (2020) - Packaging - Requirements and test scheme for carrier bags suitable for treatment in well managed household composting plants*). Figure B.1 summarized the main characteristics of the OK Compost Industrial, Home and Soil assessments.

During the research in Chapter 4, the battery biodegradability is assessed through a dynamic respirometry compostability test and a compost quality test, under the conditions established in EN 13432.




			
GUARANTEES	Complete biodegradation at industrial compost conditions under requisites of European directive 94/62/CEE	Complete biodegradation at home compost conditions with low temperatures and more instable conditions	Complete biodegradation at soil with complete innocuity to the environment
	REFERENCE STANDARD		
	EN13432-EN14855	EN17427-EN1855	EN17556
METHODOLOGY	Dynamic respirometry at 58°C, measuring CO ₂ of >50g of sample in 2-3kg of compost.	Dynamic respirometry at 25°C, measuring CO ₂ of >50g of sample in 2-3kg of compost.	Dynamic respirometry at 58°C, measuring CO ₂ of 100-300mg of sample in 100-300g of soil.
OK compost	90% in 6 months The sample must reach 90% of biodegradability in a maximum of 6 months	90% in 12 months The sample must reach 90% of biodegradability in a maximum of 12 months	70% in 2 years The sample must reach 70% of biodegradability in a maximum of 2 years

Figure B.1: TUV Austria criteria and methodologies summary regarding OK Compost certifications in Industrial, Home and Soil conditions.

B.2 Paper and cardboard recyclability standards

Paper and cardboard is the main packaging material in the EU, and thus the main materials produced in packaging waste. The Directive 825 in packaging and packaging waste was launched by the European Parliament on 2018. It was established that no later than 2030, a minimum 85% of paper and cardboard weight present in packaging should be recycled. Being the highest target above contemplate materials (overcoming for instance, glass (75%), o aluminum (60%) targets). This evidences the importance of not corrupting paper and cardboard waste stream, which moreover is already the most efficient recycled material regarding current reclining rates (73.9 % in 2020 according to the Paper recycling European council). In this sense, Directive 2018/825 sets a framework to determine if packaging residues can be recovered through recycling. While, the tolerances for the unwanted materials

during the recycling processes are define in *EN643-European list of standard grades of paper and board for recycling*, and the assessment to verify a product recyclability are specify in *EN 13430:2005- Packaging-Requirements for packaging recoverable by material recycling european standard*.

During the research gathered in Chapter 5 the *European list of standard grades of paper and board for recycling*, was used as a guideline. In this sense the material selection for the battery fabrication was carried out avoiding forbidden and unwanted materials specify on sections 5.2 and 5.3 of this standard.

On the other hand, EN 13430 standard sets two criteria to validate a product recyclability with paper and cardboard stream. First, it dictates that al least 50% of the mass composition of the product should be a paper-cardboard based material. Second, it established a procedure to assess the product suitability for recycling. The procedure includes debriefing the product and verify it disintegrates and disperses in fibers. Then a filtered out step is applied followed by the determination of the percentage of recyclable fraction of the extraction. Finally, the quality of the pulps and manufactured papers produced from the recovered material. As a conclusion of this procedure it can be established if the product is recyclable or not.

C

Screening of redox species

In this appendix a catalog of different redox species is presented, evaluating each one in three different media (attaining pH: acid, neutral and alkaline).

All species concentrations were 10mM, while electrolyte concentrations were 1M potassium hydroxide (KOH) for the alkaline media of pH 14, 1M potassium chloride (KCl) in a phosphate-buffered saline (PBS) to create a neutral media of pH7 and 0.25M sulfuric acid (H_2SO_4) to create an acidic media of pH 1.

The assessment was performed by Open Circuit Potentiometry (OCP) and Cyclic Voltammetry (CV) techniques, using a conventional three-electrode electrochemical cell in beaker: a glassy carbon electrode ($A=0.07cm^2$) as working electrode, a platinum wire electrode as counter electrode and a Ag/AgCl (3M KCl) electrode as reference electrode all purchased from CH Instruments (CH Instruments Inc., TX, USA).

All voltammograms were performed at a scan rate of $s_{rate}=20mV/s$, starting from the pre-recorded OCP value. Each species was evaluated N=3 repeats.

Figure C.1 presents four plausible cathode redox species: given the amount of current delivered by each one, it can be stated that p-BQ is the most suitable to be chosen as cathode for a battery, at least in terms of electrochemical performance.

Figure C.2 presents four plausible anode redox species: regarding the electrochemical behavior tryptophan should be discarded as anode for a battery due to the high potentials at which oxidation starts.

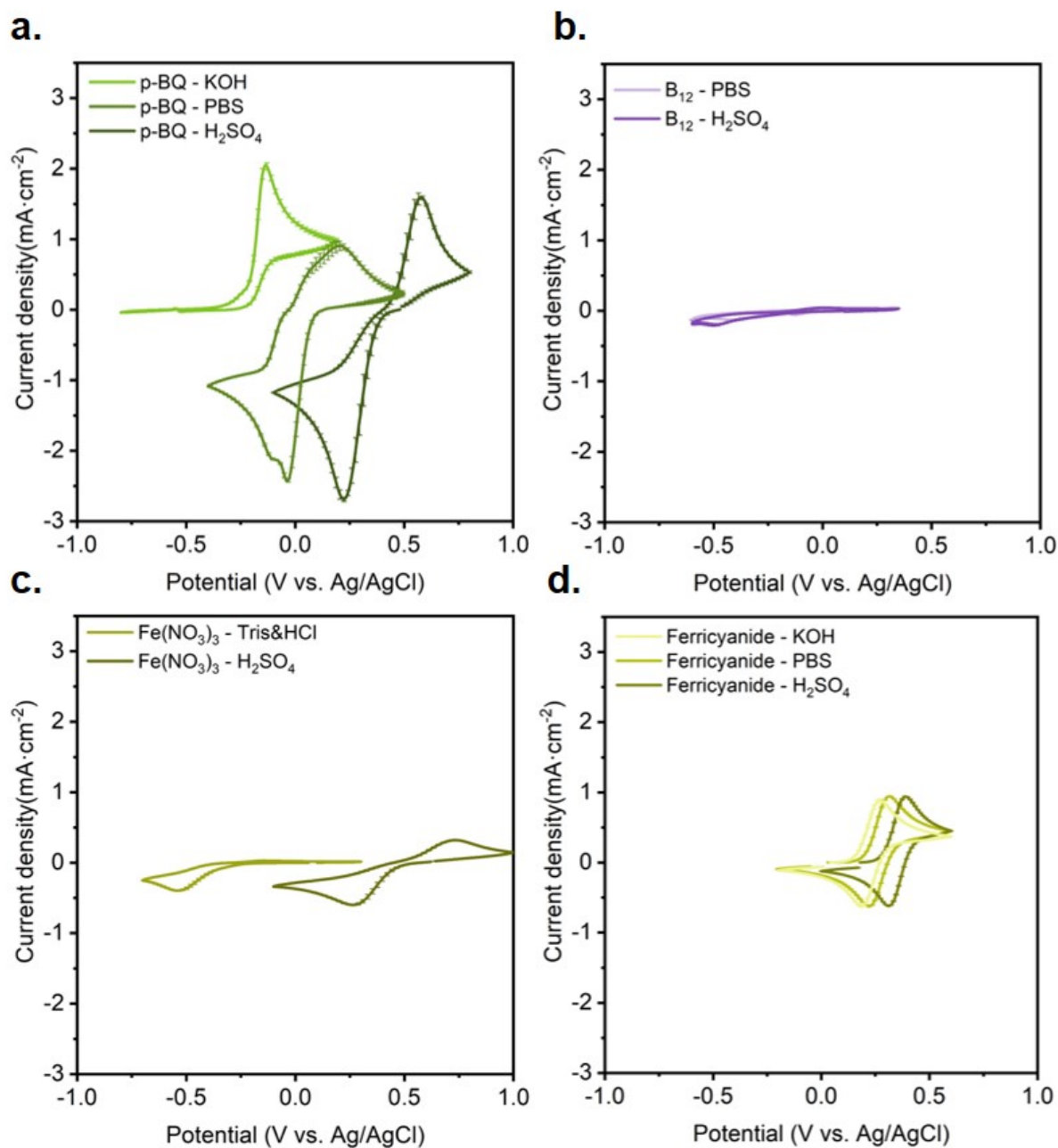


Figure C.1: Screening of four plausible cathode redox species in three different media (acid, neutral and alkaline). **a.** p-Benzoquinone (p-BQ). **b.** Vitamin B₁₂ (B₁₂). **c.** Iron Nitrate (III) (Fe(NO₃)₃). **d.** Ferricyanide. $s_{rate} = 20\text{mV/s}$.

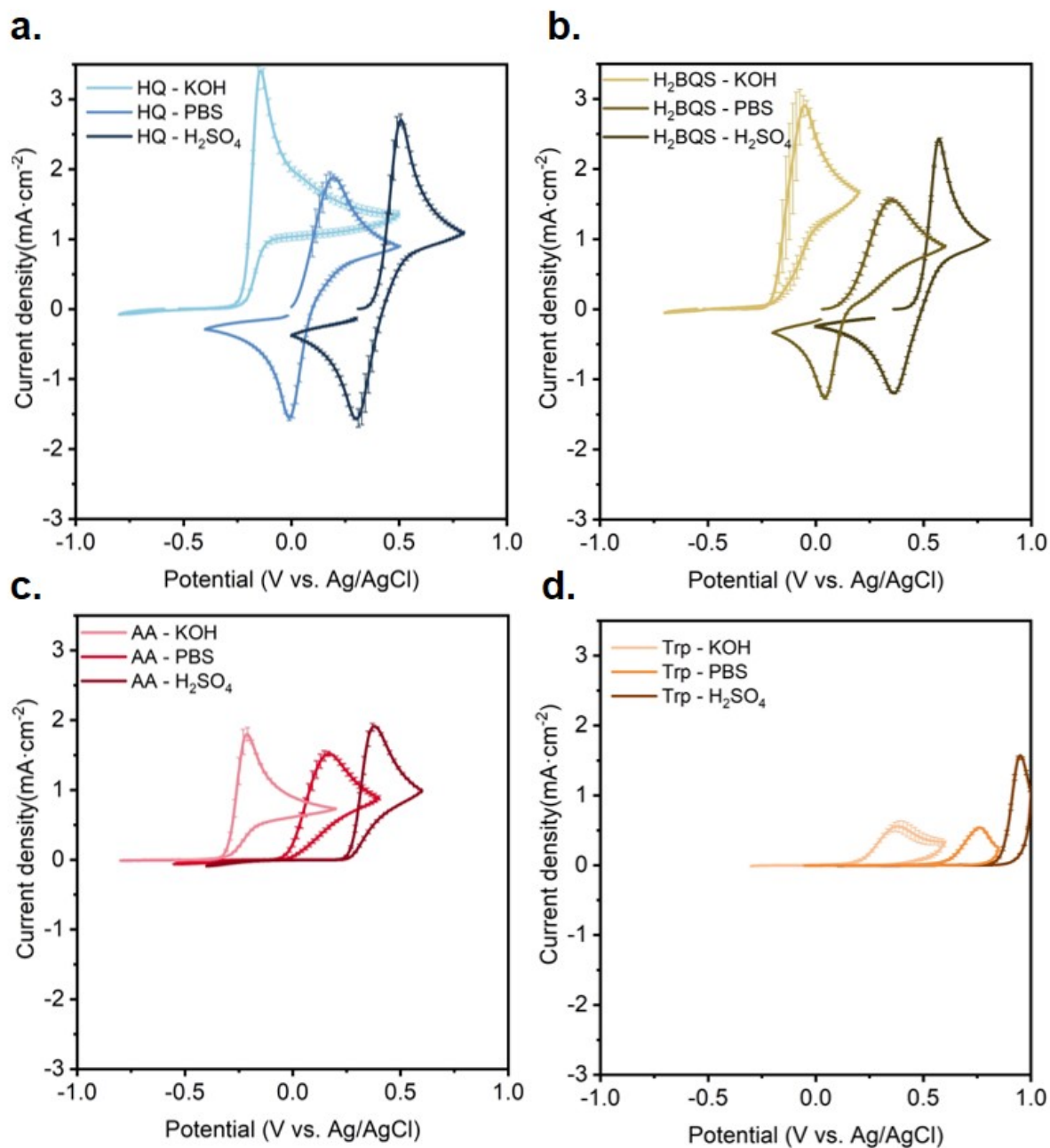


Figure C.2: Screening of four plausible anode redox species in three different media (acid, neutral and alkaline). **a.** Hydroquinone (HQ). **b.** Hydroquinonesulfonic acid (H₂BQS). **c.** Ascorbic acid (AA). **d.** Tryptophan (Trp). $s_{rate} = 20mV/s$.

The species current density peak and open circuit potential summarized in Figure C.3. As it can be seen alkaline pH is selected for the anodic species and at acidic pHs for the cathodic species. This mixt-media conditions is used along the thesis as strategy to enhance the batteries performance. The final redox species selection contemplates different factors, like solubility, stability, availability, matrix compatibility, etc. The particular selection of each battery chemistry is presented at each chapter. While the acid phenolic compounds assessment as anode materials can be found in Chapter 5.

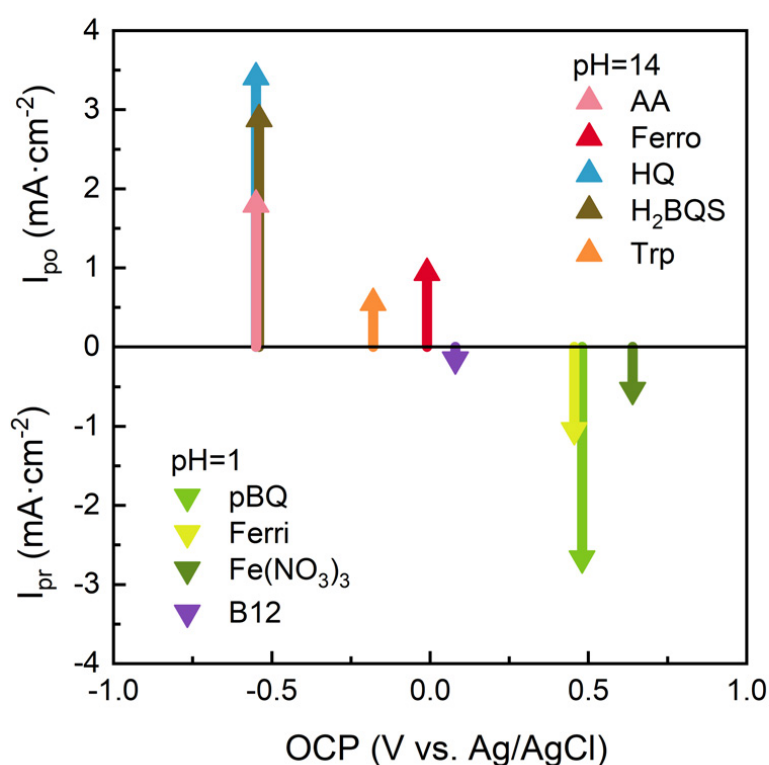


Figure C.3: Catalog of plausible redox species to be implemented on primary batteries. Summary in terms of open circuit potential (OCP) and oxidation (I_{po}) and reduction I_{pr} currents peaks for anodic and cathodic redox species, respectively. Current peak are compared at $s_{rate} = 20\text{mV}/s$.

Table C.1: Summary of all different reactions occurring on each assessment.

Cathodic reactions	Structure	Reduction
p-benzoquinone(p-BQ)		$p\text{-BQ} + 2 e^{-} + 2 H^{+} \longrightarrow \text{HQ}$
Oxygen		$O_2 + 2 H_2O + 4 e^{-} \longrightarrow 4 OH^{-}$
Potassium ferricyanide		$Fe^{3+} + e^{-} \longrightarrow Fe^{2+}$
Vitamin B12 (B ₁₂)		$Co^{3+} + e^{-} \longrightarrow Co^{2+}$
		$Co^{2+} + e^{-} \longrightarrow Co^{+}$
Iron nitrate (III) (Fe(NO ₃) ₃)		$Fe^{3+} + e^{-} \longrightarrow Fe^{2+}$
Anodic reactions	Structure	Oxidation
Potassium ferrocyanide		$Fe^{2+} \longrightarrow Fe^{3+} + e^{-}$
Ascorbic acid (AA)		$AA \longrightarrow AHA + 2 e^{-} + 2 H^{+}$
Hydroquinone (HQ)		$HQ \longrightarrow p\text{-BQ} + 2 e^{-} + 2 H^{+}$
Tryptophan (TrpH)		$TrpH \longrightarrow Trp + e^{-} + H^{+}$
Hydroquinonesulfonic acic (H ₂ BQS)		$H_2BQS \longrightarrow BQS + 2 e^{-} + 2 H^{+}$

References

- [1] Abdul Karim Feroz, Hangjung Zo, and Ananth Chiravuri. Digital transformation and environmental sustainability: A review and research agenda. *Sustainability (Switzerland)*, 13(3):1–20, feb 2021.
- [2] World Economic Forum. Digital Transformation of Industries: Societal Implications. *World Economic Forum White Paper*, (January):1–34, 2016.
- [3] McKinsey Global Institute. The Internet of Things: Mapping the Value beyond the Hype EXECUTIVE SUMMARY. *McKinsey & Company*, (June):1–18, 2015.
- [4] EPoSS. Strategic Research Agenda. (June), 2013.
- [5] I.M.S.K. Ilankoon, Yousef Ghorbani, Meng Nan Chong, Gamini Herath, Thandazile Moyo, and Jochen Petersen. E-waste in the international context – A review of trade flows, regulations, hazards, waste management strategies and technologies for value recovery. *Waste Management*, 82:258–275, dec 2018.
- [6] V Pérez-Belis, M. D. Bovea, and V Ibáñez-Forés. An in-depth literature review of the waste electrical and electronic equipment context: Trends and evolution, nov 2015.
- [7] Michelle Heacock, Carol Bain Kelly, Kwadwo Ansong Asante, Linda S. Birnbaum, Åke Lennart Bergman, Marie Noel Bruné, Irena Buka, David O. Carpenter, Aimin Chen, Xia Huo, Mostafa Kamel, Philip J. Landrigan, Federico Magalini, Fernando Diaz-Barriga, Maria Neira, Magdy Omar, Antonio Pascale, Mathuros Ruchirawat, Leith Sly, Peter D. Sly, Martin van den Berg, and William A. Suk. E-waste and harm to vulnerable populations: A growing global problem. *Environmental Health Perspectives*, 124(5):550–555, 2016.

- [8] Vanessa Forti, Cornelis Peter Baldé, Ruediger Kuehr, and Garam Bel. *The Global E-waste Monitor 2020*. Number July. 2020.
- [9] World Economic Forum. The world's e-waste is a huge problem. It's also a golden opportunity.
- [10] Jim Puckett, Chris Brandt, and Hayley Palmer. Holes in the Circular Economy: WEEE Leakage from Europe. A Report of the e-Trash Transparency Project. *A Report of the e-Trash Transparency Project*, page 120, 2018.
- [11] A New Circular Vision for Electronics Time for a Global Reboot. 2019.
- [12] Waste statistics - recycling of batteries and accumulators - Statistics Explained.
- [13] ReCell Center.
- [14] ReLiB – Sustainable Management of Lithium-ion Batteries.
- [15] Chunwei Liu, Jiao Lin, Hongbin Cao, Yi Zhang, and Zhi Sun. Recycling of spent lithium-ion batteries in view of lithium recovery: A critical review. *Journal of Cleaner Production*, 228:801–813, aug 2019.
- [16] European Commission. European Battery Alliance | Internal Market, Industry, Entrepreneurship and SMEs, 2020.
- [17] State aid: €3.2 billion public support battery value chain.
- [18] European Portable Battery Association | What is a battery?, 2020.
- [19] ECa. European Commission, Critical Raw Materials for Strategic Technologies and Sectors in the EU. *A Foresight Study*, 2020.
- [20] Final Report. IMPACT ASSESSMENT ON SELECTED POLICY OPTIONS FOR REVISION OF THE BATTERY DIRECTIVE. Technical report, European Commission, Directorate General for Environment, 2003.
- [21] WHO. Soaring e-waste affects the health of millions of children, WHO warns. *World Health Organization*, pages 1–2, 2021.

- [22] Maximilian Fichtner, Kristina Edström, Elixabete Ayerbe, Maitane Berecibar, Arghya Bhowmik, Ivano E. Castelli, Simon Clark, Robert Dominko, Merve Erakca, Alejandro A. Franco, Alexis Grimaud, Birger Horstmann, Arnulf Latz, Henning Lorrmann, Marcel Meeus, Rekha Narayan, Frank Pammer, Janna Ruhland, Helge Stein, Tejs Vegge, and Marcel Weil. Rechargeable Batteries of the Future—The State of the Art from a BATTERY 2030+ Perspective, 2022.
- [23] Yue Cao and Kathryn E Uhrich. Biodegradable and biocompatible polymers for electronic applications: A review. *Journal of Bioactive and Compatible Polymers*, 34(1):3–15, dec 2019.
- [24] Eduardo Di Mauro, Denis Rho, and Clara Santato. Biodegradation of bio-sourced and synthetic organic electronic materials towards green organic electronics. *Nature Communications*, 12(1):1–10, may 2021.
- [25] Won Bae Han, Joong Hoon Lee, Jeong Woong Shin, and Suk Won Hwang. Advanced Materials and Systems for Biodegradable, Transient Electronics. *Advanced Materials*, 32(51):2002211, dec 2020.
- [26] Alexandra Zvezdin, Eduardo Di Mauro, Denis Rho, Clara Santato, and Mohamed Khalil. En route toward sustainable organic electronics. *MRS Energy & Sustainability*, 7(1), jul 2020.
- [27] Rongfeng Li, Liu Wang, Deying Kong, and Lan Yin. Recent progress on biodegradable materials and transient electronics, sep 2018.
- [28] Neeru Mittal, Alazne Ojanguren, Markus Niederberger, and Erlantz Lizundia. Degradation Behavior, Biocompatibility, Electrochemical Performance, and Circularity Potential of Transient Batteries, jun 2021.
- [29] Kun Fu, Zhengyang Wang, Chaoyi Yan, Zhen Liu, Yonggang Yao, Jiaqi Dai, Emily Hitz, Yibo Wang, Wei Luo, Yanan Chen, Myeongseob Kim, and Liangbing Hu. All-component transient lithium-ion batteries. *Advanced Energy Materials*, 6(10):1502496, may 2016.
- [30] Kun Fu, Zhen Liu, Yonggang Yao, Zhengyang Wang, Bin Zhao, Wei Luo, Jiaqi Dai, Steven D Lacey, Lihui Zhou, Fei Shen, Myeongseob Kim, Laura

- Swafford, Louise Sengupta, and Liangbing Hu. Transient Rechargeable Batteries Triggered by Cascade Reactions. *Nano Letters*, 15(7):4664–4671, 2015.
- [31] Chan Woo Park, Seung Kyun Kang, Hector Lopez Hernandez, Joshua A. Kaitz, Dae Seung Wie, Jiho Shin, Olivia P. Lee, Nancy R. Sottos, Jeffrey S. Moore, John A. Rogers, and Scott R. White. Thermally Triggered Degradation of Transient Electronic Devices. *Advanced Materials*, 27(25):3783–3788, jul 2015.
- [32] Lan Yin, Xian Huang, Hangxun Xu, Yanfeng Zhang, Jasper Lam, Jianjun Cheng, and John A. Rogers. Materials, designs, and operational characteristics for fully biodegradable primary batteries. *Advanced Materials*, 26(23):3879–3884, 2014.
- [33] Melissa Tsang, Andac Armutlulu, Adam W. Martinez, Sue Ann Bidstrup Allen, and Mark G. Allen. Biodegradable magnesium/iron batteries with polycaprolactone encapsulation: A microfabricated power source for transient implantable devices. *Microsystems and Nanoengineering*, 1, 2015.
- [34] Didi She, Melissa Tsang, and Mark Allen. Biodegradable batteries with immobilized electrolyte for transient MEMS. *Biomedical Microdevices*, 21(1), mar 2019.
- [35] Xiaoteng Jia, Caiyun Wang, Chen Zhao, Yu Ge, and Gordon G. Wallace. Toward Biodegradable Mg-Air Bioelectric Batteries Composed of Silk Fibroin-Polypyrrole Film. *Advanced Functional Materials*, 26(9):1454–1462, 2016.
- [36] Xiaoteng Jia, Caiyun Wang, Vijayaraghavan Ranganathan, Bradley Napier, Changchun Yu, Yunfeng Chao, Maria Forsyth, Fiorenzo G. Omenetto, Douglas R. Macfarlane, and Gordon G. Wallace. A Biodegradable Thin-Film Magnesium Primary Battery Using Silk Fibroin-Ionic Liquid Polymer Electrolyte. *ACS Energy Letters*, 2(4):831–836, apr 2017.
- [37] Xueying Huang, Dan Wang, Zhangyi Yuan, Wensheng Xie, Yixin Wu, Rongfeng Li, Yu Zhao, Deng Luo, Liang Cen, Binbin Chen, Hui Wu, Hangxun Xu, Xing Sheng, Milin Zhang, Lingyun Zhao, and Lan Yin. A Fully Biodegradable Battery for Self-Powered Transient Implants. *Small*, 14(28), jul 2018.

- [38] Vineet Edupuganti and Raj Solanki. Fabrication, characterization, and modeling of a biodegradable battery for transient electronics. *Journal of Power Sources*, 336:447–454, dec 2016.
- [39] Jiaoyang Xia, Zhihao Yuan, and Fengshi Cai. Toward a Biocompatible and Degradable Battery Using a Mg-Zn-Zr Alloy with β -Tricalcium Phosphate Nanocoating as Anode. *Journal of Materials Engineering and Performance*, 27(8):4005–4009, aug 2018.
- [40] Young Jo Kim, Wei Wu, Sang Eun Chun, Jay F Whitacre, and Christopher J Bettinger. Biologically derived melanin electrodes in aqueous sodium-ion energy storage devices. *Proceedings of the National Academy of Sciences of the United States of America*, 110(52):20912–20917, 2013.
- [41] Young Jo Kim, Sang Eun Chun, Jay Whitacre, and Christopher J. Bettinger. Self-deployable current sources fabricated from edible materials. *Journal of Materials Chemistry B*, 1(31):3781–3788, aug 2013.
- [42] Yuanfen Chen, Reihaneh Jamshidi, Kathryn White, Simge Çınar, Emma Gallegos, Nastaran Hashemi, and Reza Montazami. Physical–chemical hybrid transiency: A fully transient li-ion battery based on insoluble active materials. *Journal of Polymer Science, Part B: Polymer Physics*, 54(20):2021–2027, 2016.
- [43] Yang Gao, Maedeh Mohammadifar, and Seokheun Choi. From Microbial Fuel Cells to Biobatteries: Moving toward On-Demand Micropower Generation for Small-Scale Single-Use Applications. *Advanced Materials Technologies*, 4(7):1900079, jul 2019.
- [44] Zhiguang Zhu, Tsz Kin Tam, Fangfang Sun, Chun You, and Y. H. Percival Zhang. A high-energy-density sugar biobattery based on a synthetic enzymatic pathway. *Nature Communications*, 5, jan 2014.
- [45] Maedeh Mohammadifar, Idris Yazgan, Jing Zhang, Victor Kariuki, Omowunmi A. Sadik, and Seokheun Choi. Green Biobatteries: Hybrid Paper–Polymer Microbial Fuel Cells. *Advanced Sustainable Systems*, 2(10), oct 2018.

- [46] Michel Vert, Yoshiharu Doi, Karl Heinz Hellwich, Michael Hess, Philip Hodge, Przemyslaw Kubisa, Marguerite Rinaudo, and François Schué. Terminology for biorelated polymers and applications (IUPAC recommendations 2012). *Pure and Applied Chemistry*, 84(2):377–410, 2012.
- [47] Packaging– requirements for packaging recoverable through composting and biodegradation : test scheme and evaluation criteria for the final acceptance of packaging. page 22.
- [48] ISO 17556:2019 - Plastics — Determination of the ultimate aerobic biodegradability of plastic materials in soil by measuring the oxygen demand in a respirometer or the amount of carbon dioxide evolved.
- [49] ISO 14855-1:2005 - Determination of the ultimate aerobic biodegradability of plastic materials under controlled composting conditions — Method by analysis of evolved carbon dioxide — Part 1: General method.
- [50] Juan P. Esquivel, Perla Alday, Omar A. Ibrahim, Belén Fernández, Erik Kjeang, and Neus Sabaté. A Metal-Free and Biotically Degradable Battery for Portable Single-Use Applications. *Advanced Energy Materials*, 7(18):1700275, sep 2017.
- [51] Myeong Hwan Lee, Jongha Lee, Sung Kyun Jung, Dayoung Kang, Myung Soo Park, Gi Doo Cha, Kyoung Won Cho, Jun Hyuk Song, Sehwan Moon, Young Soo Yun, Seok Joo Kim, Young Woon Lim, Dae Hyeong Kim, and Kisuk Kang. A Biodegradable Secondary Battery and its Biodegradation Mechanism for Eco-Friendly Energy-Storage Systems. *Advanced Materials*, 33(10), mar 2021.
- [52] Kate Raworth. A safe and just space for humanity: can we live within the doughnut? Oxfam Discussion Paper. *State of the World 2003: Progress Towards a Sustainable Society: 20th Edition*, pages 1–240, 2012.
- [53] James Hansen, Pushker Kharecha, Makiko Sato, Valerie Masson-Delmotte, Frank Ackerman, David J. Beerling, Paul J. Hearty, Ove Hoegh-Guldberg, Shi Ling Hsu, Camille Parmesan, Johan Rockstrom, Eelco J. Rohling, Jeffrey Sachs, Pete Smith, Konrad Steffen, Lise Van Susteren, Karina Von Schuckmann, and James C. Zachos. Assessing "dangerous climate change":

- Required reduction of carbon emissions to protect young people, future generations and nature. *PLoS ONE*, 8(12):e81648, dec 2013.
- [54] Fabrizio Ceschin and Idil Gaziulusoy. Evolution of design for sustainability: From product design to design for system innovations and transitions. *Design Studies*, 47:118–163, nov 2016.
- [55] Sebastián P. Bautista, Marcel Weil, Manuel Baumann, and Claudia Tomasini Montenegro. Prospective Life Cycle Assessment of a Model Magnesium Battery. *Energy Technology*, 9(4), apr 2021.
- [56] Maider Iturrondobeitia, Ortzi Akizu-Gardoki, Oier Amondarain, Rikardo Minguez, and Erlantz Lizundia. Environmental Impacts of Aqueous Zinc Ion Batteries Based on Life Cycle Assessment. *Advanced Sustainable Systems*, 6(1):2100308, jan 2022.
- [57] Jason Porzio and Corinne D. Scown. Life-Cycle Assessment Considerations for Batteries and Battery Materials, sep 2021.
- [58] Linda Gaines. To recycle, or not to recycle, that is the question: Insights from life-cycle analysis. *MRS Bulletin*, 37(4):333–338, apr 2012.
- [59] Sustainable Development Knowledge Platform.
- [60] United Nations Statistics División. The Energy Progress Report 2021. *Iea*, pages 158–177, 2021.
- [61] United Nations, Department of Economic, Social Affairs, and Population Division. World Population Prospects 2019 Highlights.
- [62] Alessandro Matese, Francesco Primo Vaccari, Diego Tomasi, Salvatore Filippo Di Gennaro, Jacopo Primicerio, Francesco Sabatini, and Silvia Guidoni. Crossvit: Enhancing canopy monitoring management practices in viticulture. *Sensors (Switzerland)*, 13(6):7652–7667, jun 2013.
- [63] Richard Beckwith, Dan Teibel, and Pat Bowen. Unwired wine: Sensor networks in vineyards. *Proceedings of IEEE Sensors*, 2:561–564, 2004.

- [64] Alexandros Zervopoulos, Athanasios Tsipis, Aikaterini Georgia Alvanou, Konstantinos Bezas, Asterios Papamichail, Spiridon Vergis, Andreana Stylidou, Georgios Tsoumanis, Vasileios Komianos, George Koufoudakis, and Konstantinos Oikonomou. Wireless Sensor Network Synchronization for Precision Agriculture Applications. *Agriculture 2020, Vol. 10, Page 89*, 10(3):89, mar 2020.
- [65] Sai Zou, Fan Yang, Yuliang Tang, Lei Xiao, and Yifong Zhao. Optimized algorithm of sensor node deployment for intelligent agricultural monitoring. 2016.
- [66] Aristotelis C. Tagarakis, Dimitrios Kateris, Remigio Berruto, and Dionysis Bochtis. Low-Cost Wireless Sensing System for Precision Agriculture Applications in Orchards. *Applied Sciences*, 11(13):5858, jun 2021.
- [67] M. A. Parvez Mahmud, Nazmul Huda, Shahjadi Hisan Farjana, and Candace Lang. Comparative Life Cycle Environmental Impact Analysis of Lithium-Ion (Lilo) and Nickel-Metal Hydride (NiMH) Batteries. *Batteries 2019, Vol. 5, Page 22*, 5(1):22, feb 2019.
- [68] Raul Morais, Samuel G Matos, Miguel A Fernandes, António Ant´, António L G Valente, F S P Soares, P J S G Ferreira, and M J C S Reis. doi:10.1016/j.compag.2008.04.005. 2008.
- [69] Yan Xu, Jinhui Li, Quanyin Tan, Anesia Lauren Peters, and Congren Yang. Global status of recycling waste solar panels: A review. *Waste management (New York, N.Y.)*, 75:450–458, may 2018.
- [70] Bouchra Bakhiyi, France Labrèche, and Joseph Zayed. The photovoltaic industry on the path to a sustainable future - Environmental and occupational health issues. *Environment International*, 73:224–234, 2014.
- [71] A O Afolayan and P M B 5382. Accumulation of Heavy Metals from Battery Waste in Topsoil, Surface Water, and Garden Grown Maize at Omilende Area, Olodo, Nigeria. *Global Challenges*, 2(3):1700090, mar 2018.
- [72] Yifei Wang, Shijing Luo, Holly Y.H. Kwok, Wending Pan, Yingguang Zhang, Xiaolong Zhao, and Dennis Y.C. Leung. Microfluidic fuel cells with different types

- of fuels: A prospective review. *Renewable and Sustainable Energy Reviews*, 141:110806, may 2021.
- [73] Erik Kjeang, Ned Djilali, and David Sinton. Microfluidic fuel cells: A review. *Journal of Power Sources*, 186(2):353–369, jan 2009.
- [74] Jin wook Lee and Erik Kjeang. A perspective on microfluidic biofuel cells. *Biomicrofluidics*, 4(4):041301, nov 2010.
- [75] Jaime Hernández Rivera, David Ortega Díaz, Diana María Amaya Cruz, Juvenal Rodríguez-Reséndiz, Juan Manuel Olivares Ramírez, Andrés Dector, Diana Dector, Rosario Galindo, and Hilda Esperanza Esparza Ponce. A Paper-Based Microfluidic Fuel Cell Using Soft Drinks as a Renewable Energy Source. *Energies 2020, Vol. 13, Page 2443*, 13(10):2443, may 2020.
- [76] Omar A. Ibrahim, Marina Navarro-Segarra, Pardis Sadeghi, Neus Sabaté, Juan Pablo Esquivel, and Erik Kjeang. Microfluidics for Electrochemical Energy Conversion. *Chemical Reviews*, apr 2021.
- [77] Denis Desmaële, Thanh Thuy Nguyen-Boisse, Louis Renaud, and Sophie Tingry. Integration of cantilevered porous electrodes into microfluidic co-laminar enzymatic biofuel cells: Toward higher enzyme loadings for enhanced performance. *Microelectronic Engineering*, 165:23–26, nov 2016.
- [78] A. J. Armenta-González, R. Carrera-Cerritos, A. Moreno-Zuria, L. Álvarez-Contreras, J. Ledesma-García, F. M. Cuevas-Muñiz, and L. G. Arriaga. An improved ethanol microfluidic fuel cell based on a PdAg/MWCNT catalyst synthesized by the reverse micelles method. *Fuel*, 167:240–247, mar 2016.
- [79] Keng Guan Lim and G. Tayhas R. Palmore. Microfluidic biofuel cells: The influence of electrode diffusion layer on performance. *Biosensors and Bioelectronics*, 22(6):941–947, jan 2007.
- [80] Denis Desmaële, Louis Renaud, and Sophie Tingry. Gold coated optical fibers as three-dimensional electrodes for microfluidic enzymatic biofuel cells: Toward geometrically enhanced performance. *Biomicrofluidics*, 9(4):1, jul 2015.

- [81] A. Zebda, L. Renaud, M. Cretin, C. Innocent, F. Pichot, R. Ferrigno, and S. Tingry. Electrochemical performance of a glucose/oxygen microfluidic biofuel cell. *Journal of Power Sources*, 193(2):602–606, sep 2009.
- [82] Y. H. Kwok, Y. F. Wang, Alpha C.H. Tsang, and Dennis Y.C. Leung. Graphene-carbon nanotube composite aerogel with Ru@Pt nanoparticle as a porous electrode for direct methanol microfluidic fuel cell. *Applied Energy*, 217:258–265, may 2018.
- [83] A. S. Hollinger, R. J. Maloney, R. S. Jayashree, D. Natarajan, L. J. Markoski, and P. J.A. Kenis. Nanoporous separator and low fuel concentration to minimize crossover in direct methanol laminar flow fuel cells. *Journal of Power Sources*, 195(11):3523–3528, jun 2010.
- [84] Yifei Wang and Dennis Y.C. Leung. A circular stacking strategy for microfluidic fuel cells with volatile methanol fuel. *Applied Energy*, 184:659–669, dec 2016.
- [85] J. Galindo-De-La-Rosa, A. Álvarez, M. P. Gurrola, J. A. Rodríguez-Morales, G. Oza, L. G. Arriaga, and J. Ledesma-García. Alcohol Dehydrogenase Immobilized on TiO₂Nanotubes for Ethanol Microfluidic Fuel Cells. *ACS Sustainable Chemistry and Engineering*, 8(29):10900–10910, jul 2020.
- [86] Denis Desmaële, Louis Renaud, and Sophie Tingry. A wireless sensor powered by a flexible stack of membraneless enzymatic biofuel cells. *Sensors and Actuators B: Chemical*, 220:583–589, dec 2015.
- [87] Elain Fu, Stephen A. Ramsey, Peter Kauffman, Barry Lutz, and Paul Yager. Transport in two-dimensional paper networks. *Microfluidics and nanofluidics*, 10(1):29, jan 2011.
- [88] Warren Batchelor, Daniel Soderberg, Pulp Society, and Paper Fundamental Research. *Advances in pulp and paper research, Oxford 2017 : transactions of the 16th Fundamental Research Symposium held in Oxford: September 2017, in three volumes*. FRC The Pulp & Paper Fundamental Research Society, Bury Lancashire UK, 2017.

- [89] J. P. Esquivel, F. J. Del Campo, J. L. Gómez De La Fuente, S. Rojas, and N. Sabaté. Microfluidic fuel cells on paper: meeting the power needs of next generation lateral flow devices. *Energy & Environmental Science*, 7(5):1744–1749, apr 2014.
- [90] Claudia W. Narvárez Villarrubia, Carolin Lau, Gustavo P.M.K. Ciniciato, Sergio O. Garcia, Scott S. Sibbett, Dimiter N. Petsev, Sofia Babanova, Gautam Gupta, and Plamen Atanassov. Practical electricity generation from a paper based biofuel cell powered by glucose in ubiquitous liquids. *Electrochemistry Communications*, 45:44–47, aug 2014.
- [91] Scott Calabrese Barton, Josh Gallaway, and Plamen Atanassov. Enzymatic biofuel cells for implantable and microscale devices. *Chemical Reviews*, 104(10):4867–4886, oct 2004.
- [92] Matthew Wallenstein, Steven D. Allison, Jessica Ernakovich, J. Megan Steinweg, and Robert Sinsabaugh. Controls on the Temperature Sensitivity of Soil Enzymes: A Key Driver of In Situ Enzyme Activity Rates. pages 245–258, 2010.
- [93] Marina Navarro-Segarra, Perla Patricia Alday, David Garcia, Omar A. Ibrahim, Erik Kjeang, Neus Sabaté, and Juan Pablo Esquivel. An Organic Redox Flow Cell-Inspired Paper-Based Primary Battery. *ChemSusChem*, 13(9):2394–2401, may 2020.
- [94] Sergio Mendez, Erin M. Fenton, Gil R. Gallegos, Dimiter N. Petsev, Scott S. Sibbett, Howard A. Stone, Yi Zhang, and Gabriel P. López. Imbibition in porous membranes of complex shape: quasi-stationary flow in thin rectangular segments. *Langmuir : the ACS journal of surfaces and colloids*, 26(2):1380–1385, jan 2010.
- [95] Zhi Liu, Jie Hu, Yimeng Zhao, Zhiguo Qu, and Feng Xu. Experimental and numerical studies on liquid wicking into filter papers for paper-based diagnostics. *Applied Thermal Engineering*, 88:280–287, sep 2015.
- [96] Carlos Castro, Cindy Rosillo, and Hideaki Tsutsui. Characterizing effects of

- humidity and channel size on imbibition in paper-based microfluidic channels. *Microfluidics and Nanofluidics*, 21(2):1–14, feb 2017.
- [97] Kevin M. Schilling, Anna L. Lepore, Jason A. Kurian, and Andres W. Martinez. Fully enclosed microfluidic paper-based analytical devices. *Analytical chemistry*, 84(3):1579–1585, feb 2012.
- [98] Zhi Liu, Xiaocong He, Jiaxiu Han, Xiuhai Zhang, Fei Li, Ang Li, Zhiguo Qu, and Feng Xu. Liquid wicking behavior in paper-like materials: mathematical models and their emerging biomedical applications. *Microfluidics and Nanofluidics 2018* 22:11, 22(11):1–20, nov 2018.
- [99] Omar A. Ibrahim, Perla Alday, Neus Sabaté, Juan Pablo Esquivel, and Erik Kjeang. Evaluation of Redox Chemistries for Single-Use Biodegradable Capillary Flow Batteries. *Journal of The Electrochemical Society*, 164(12):A2448–A2456, aug 2017.
- [100] Yu Ding and Guihua Yu. A Bio-Inspired, Heavy-Metal-Free, Dual-Electrolyte Liquid Battery towards Sustainable Energy Storage. *Angewandte Chemie International Edition*, 55(15):4772–4776, apr 2016.
- [101] Yu Ding, Changkun Zhang, Leyuan Zhang, Yangen Zhou, and Guihua Yu. Molecular engineering of organic electroactive materials for redox flow batteries. *Chemical Society Reviews*, 47(1):69–103, jan 2018.
- [102] Muhammad Tanveer and Kwang Yong Kim. Flow Configurations of Membraneless Microfluidic Fuel Cells: A Review. *Energies 2021, Vol. 14, Page 3381*, 14(12):3381, jun 2021.
- [103] A. V. Razimov, F. T. Bekmashi, and B. I. Liogon’kii. Thermal polymerization of p-benzoquinone. *Polymer Science U.S.S.R.*, 17(12):3164–3170, 1975.
- [104] Kristina Wedege, Emil Dražević, Denes Konya, and Anders Bentien. Organic Redox Species in Aqueous Flow Batteries: Redox Potentials, Chemical Stability and Solubility. *Scientific Reports 2016 6:1*, 6(1):1–13, dec 2016.
- [105] Bo Yang, Lena Hooper-Burkhardt, Sankarganesh Krishnamoorthy, Advait Murali, G. K. Surya Prakash, and S. R. Narayanan. High-Performance Aqueous

- Organic Flow Battery with Quinone-Based Redox Couples at Both Electrodes. *Journal of The Electrochemical Society*, 163(7):A1442–A1449, may 2016.
- [106] B. H.E. Vanthoor, P. H.B. de Visser, C. Stanghellini, and E. J. van Henten. A methodology for model-based greenhouse design: Part 2, description and validation of a tomato yield model. *Biosystems Engineering*, 110(4):378–395, dec 2011.
- [107] Li Li, Yun He, Qiang Xu, Ting Liu, Shaoyi Bei, Keqing Zheng, Jun Yang, Hongkang Wang, and Michael K.H. Leung. A paper-based self-pumping microfluidic fuel cell stack with a novel vertical structure. *International Journal of Energy Research*, 46(6):8389–8397, may 2022.
- [108] Thomas S. Copenhaver, Krutarth H. Purohit, Kryls Domalaon, Linda Pham, Brianna J. Burgess, Natalie Manorothkul, Vicente Galvan, Samantha Sotez, Frank A. Gomez, and John L. Haan. A microfluidic direct formate fuel cell on paper. *ELECTROPHORESIS*, 36(16):1825–1829, aug 2015.
- [109] Arwa Fraiwan, Sayantika Mukherjee, Steven Sundermier, Hyung Sool Lee, and Seokheun Choi. A paper-based microbial fuel cell: instant battery for disposable diagnostic devices. *Biosensors & Bioelectronics*, 49:410–414, jun 2013.
- [110] Liu Liu Shen, Gui Rong Zhang, Tizian Venter, Markus Biesalski, and Bastian J.M. Etzold. Towards best practices for improving paper-based microfluidic fuel cells. *Electrochimica Acta*, 298:389–399, mar 2019.
- [111] Jing Xu, Bo Wang, Wen hui Zhang, Fu Jian Zhang, Yong dong Deng, Yu Wang, Jian Jie Gao, Yong Sheng Tian, Ri He Peng, and Quan Hong Yao. Biodegradation of p-nitrophenol by engineered strain. *AMB Express*, 11(1):1–8, dec 2021.
- [112] J. Devillers, P. Boule, P. Vasseur, P. Prevot, R. Steiman, F. Seigle-Murandi, J. L. Benoit-Guyod, M. Nendza, C. Grioni, D. Dive, and P. Chambon. Environmental and health risks of hydroquinone. *Ecotoxicology and Environmental Safety*, 19(3):327–354, jun 1990.

- [113] Francisco J. Enguita and Ana Lúcia Leitão. Hydroquinone: Environmental Pollution, Toxicity, and Microbial Answers. *BioMed Research International*, 2013:1–14, 2013.
- [114] J. Pérez, J. Muñoz-Dorado, T. De La Rubia, and J. Martínez. Biodegradation and biological treatments of cellulose, hemicellulose and lignin: an overview. *International microbiology : the official journal of the Spanish Society for Microbiology*, 5(2):53–63, 2002.
- [115] Pierre Béguin and Jean-Paul Aubert. The biological degradation of cellulose. *FEMS microbiology reviews*, 13(1):25–58, jan 1994.
- [116] Raquel Barrena Gómez, Felicitas Vázquez Lima, and Antoni Sánchez Ferrer. The use of respiration indices in the composting process: a review. *Waste management & research : the journal of the International Solid Wastes and Public Cleansing Association, ISWA*, 24(1):37–47, feb 2006.
- [117] Laura Mejias, Dimitrios Komilis, Teresa Gea, and Antoni Sánchez. The effect of airflow rates and aeration mode on the respiration activity of four organic wastes: Implications on the composting process. *Waste Management*, 65:22–28, jul 2017.
- [118] Dimitrios P. Komilis and Ioannis S. Tziouvaras. A statistical analysis to assess the maturity and stability of six composts. *Waste management (New York, N.Y.)*, 29(5):1504–1513, may 2009.
- [119] Yuan Luo, Jie Liang, Guangming Zeng, Ming Chen, Dan Mo, Guoxue Li, and Difang Zhang. Seed germination test for toxicity evaluation of compost: Its roles, problems and prospects. *Waste Management*, 71:109–114, jan 2018.
- [120] Federica Ruggero, Riccardo Gori, and Claudio Lubello. Methodologies to assess biodegradation of bioplastics during aerobic composting and anaerobic digestion: A review. *Waste management & research : the journal of the International Solid Wastes and Public Cleansing Association, ISWA*, 37(10):959–975, oct 2019.
- [121] UNI Ente Italiano di Formazione. UNI 11184:2016.

- [122] Cindy Ballardo, María del Carmen Vargas-García, Antoni Sánchez, Raquel Barrena, and Adriana Artola. Adding value to home compost: Biopesticide properties through *Bacillus thuringiensis* inoculation. *Waste Management*, 106:32–43, apr 2020.
- [123] Dirk Schaefer and Wai M. Cheung. Smart Packaging: Opportunities and Challenges. In *Procedia CIRP*, volume 72, pages 1022–1027. Elsevier, jan 2018.
- [124] Selçuk Yildirim, Bettina Röcker, Marit Kvalvåg Pettersen, Julie Nilsen-Nygaard, Zehra Ayhan, Ramune Rutkaite, Tanja Radusin, Patrycja Suminska, Begonya Marcos, and Véronique Coma. Active Packaging Applications for Food. *Comprehensive Reviews in Food Science and Food Safety*, 17(1):165–199, jan 2018.
- [125] C. M. Costa, R. Gonçalves, and S. Lanceros-Méndez. Recent advances and future challenges in printed batteries. *Energy Storage Materials*, 28:216–234, jun 2020.
- [126] Benoit Clement, Miaoqiang Lyu, Eeshan Sandeep Kulkarni, Tongen Lin, Yuxiang Hu, Vera Lockett, Chris Greig, and Lianzhou Wang. Recent Advances in Printed Thin-Film Batteries. *Engineering*, apr 2022.
- [127] EPRC. Monitoring Report 2020. European Declaration on Paper Recycling 2016-2020. Technical report, 2021.
- [128] Packaging Europe. Paper and cardboard recycling reach record high across Europe, 2019.
- [129] New study suggests cartonboard can be recycled 25 times without loss of integrity | Article | Packaging Europe.
- [130] A. J. Saleh Ahammad, Jae Joon Lee, and Md Aminur Rahman. Electrochemical sensors based on carbon nanotubes. *Sensors*, 9(4):2289–2319, apr 2009.
- [131] Ruquan Ye, Xiao Han, Dmitry V. Kosynkin, Yilun Li, Chenhao Zhang, Bo Jiang, Angel A. Martí, and James M. Tour. Laser-Induced Conversion of Teflon into

- Fluorinated Nanodiamonds or Fluorinated Graphene. *ACS Nano*, 12(2):1083–1088, feb 2018.
- [132] Guiqiang Chen, Yanxia Liu, Fei Liu, and Xiao Zhang. Fabrication of three-dimensional graphene foam with high electrical conductivity and large adsorption capability. *Applied Surface Science*, 311:808–815, aug 2014.
- [133] Yieu Chyan, Ruquan Ye, Yilun Li, Swatantra Pratap Singh, Christopher J. Arnusch, and James M. Tour. Laser-Induced Graphene by Multiple Lasing: Toward Electronics on Cloth, Paper, and Food. *ACS Nano*, 12(3):2176–2183, mar 2018.
- [134] Yadong Xu, Qihui Fei, Margaret Page, Ganggang Zhao, Yun Ling, Dick Chen, and Zheng Yan. Laser-induced graphene for bioelectronics and soft actuators. *Nano Research*, 14(9):3033–3050, apr 2021.
- [135] Yuan Dong, Sean C. Rismiller, and Jian Lin. Molecular dynamic simulation of layered graphene clusters formation from polyimides under extreme conditions. *Carbon*, 104:47–55, aug 2016.
- [136] Jian Lin, Zhiwei Peng, Yuanyue Liu, Francisco Ruiz-Zepeda, Ruquan Ye, Errol L.G. Samuel, Miguel Jose Yacaman, Boris I. Yakobson, and James M. Tour. Laser-induced porous graphene films from commercial polymers. *Nature Communications*, 5(1):1–8, dec 2014.
- [137] Ruquan Ye, Yieu Chyan, Jibo Zhang, Yilun Li, Xiao Han, Carter Kittrell, and James M. Tour. Laser-Induced Graphene Formation on Wood. *Advanced Materials*, 29(37):1702211, oct 2017.
- [138] Sanghee Lee and Sangmin Jeon. Laser-Induced Graphitization of Cellulose Nanofiber Substrates under Ambient Conditions. *ACS Sustainable Chemistry and Engineering*, 7(2):2270–2275, jan 2019.
- [139] Wenli Zhang, Yongjiu Lei, Fangwang Ming, Qiu Jiang, Pedro M.F.J. Costa, and Husam N. Alshareef. Lignin Laser Lithography: A Direct-Write Method for Fabricating 3D Graphene Electrodes for Microsupercapacitors. *Advanced Energy Materials*, 8(27):1–9, 2018.

- [140] Faisal Mahmood, Chi Zhang, Yunchao Xie, David Stalla, Jian Lin, and Caixia Wan. Transforming lignin into porous graphene via direct laser writing for solid-state supercapacitors. *RSC Advances*, 9(39):22713–22720, jul 2019.
- [141] Jesper Edberg, Robert Brooke, Omid Hosseinaei, Andreas Fall, Kosala Wijeratne, and Mats Sandberg. Laser-induced graphitization of a forest-based ink for use in flexible and printed electronics. *npj Flexible Electronics*, 4(1):1–10, dec 2020.
- [142] Zhiwei Peng, Ruquan Ye, Jason A. Mann, Dante Zakhidov, Yilun Li, Preston R. Smalley, Jian Lin, and James M. Tour. Flexible Boron-Doped Laser-Induced Graphene Microsupercapacitors. *ACS Nano*, 9(6):5868–5875, jun 2015.
- [143] Cheng Zhang, Yunchao Xie, Heng Deng, Travis Tumlin, Chi Zhang, Jheng Wun Su, Ping Yu, and Jian Lin. Monolithic and Flexible ZnS/SnO₂ Ultraviolet Photodetectors with Lateral Graphene Electrodes. *Small*, 13(18):1604197–1604198, may 2017.
- [144] Marco R. Bobinger, Francisco J. Romero, Alfonso Salinas-Castillo, Markus Becherer, Paolo Lugli, Diego P. Morales, Noel Rodríguez, and Almudena Rivadeneyra. Flexible and robust laser-induced graphene heaters photothermally scribed on bare polyimide substrates. *Carbon*, 144:116–126, apr 2019.
- [145] Kwan Wee Tan, Byungki Jung, Jörg G. Werner, Elizabeth R. Rhoades, Michael O. Thompson, and Ulrich Wiesner. Transient laser heating induced hierarchical porous structures from block copolymer-directed self-assembly. *Science*, 349(6243):54–58, jul 2015.
- [146] W. Ma, J. Zhu, Z. Wang, W. Song, and G. Cao. Recent advances in preparation and application of laser-induced graphene in energy storage devices. *Materials Today Energy*, 18:100569, dec 2020.
- [147] Athanasios Tiliakos, Alexandra M.I. Trefilov, Eugenia Tanasă, Adriana Balan, and Ioan Stamatina. Laser-induced graphene as the microporous layer in proton exchange membrane fuel cells. *Applied Surface Science*, 504:144096, feb 2020.

- [148] Jingsi Yi, Jiahua Chen, Zheng Yang, Yang Dai, Weimin Li, Jiang Cui, Francesco Ciucci, Ziheng Lu, and Chunlei Yang. Facile Patterning of Laser-Induced Graphene with Tailored Li Nucleation Kinetics for Stable Lithium-Metal Batteries. *Advanced Energy Materials*, 9(38):1901796, oct 2019.
- [149] Muqing Ren, Jibo Zhang, and James M. Tour. Laser-Induced Graphene Hybrid Catalysts for Rechargeable Zn-Air Batteries. *ACS Applied Energy Materials*, 2(2):1460–1468, feb 2019.
- [150] Muqing Ren, Jibo Zhang, Mengmeng Fan, Pulickel M. Ajayan, and James M. Tour. Li-Breathing Air Batteries Catalyzed by MnNiFe/Laser-Induced Graphene Catalysts. *Advanced Materials Interfaces*, 6(19):1901035, oct 2019.
- [151] Leipa Georg Leinfelder GMBH. Manilla-RCK STANDARD-PRODUKT-SPEZIFIKATION, 2011.
- [152] Joan Garcia Reig. Laser Induced Graphene. *Treball de Final de Grau, Universitat Autònoma de Barcelona, Cerdanyola del Vallés*, 2019.
- [153] Yilun Li, Duy Xuan Luong, Jibo Zhang, Yash R. Tarkunde, Carter Kittrell, Franklin Sargunraj, Yongsung Ji, Christopher J. Arnusch, and James M. Tour. Laser-Induced Graphene in Controlled Atmospheres: From Superhydrophilic to Superhydrophobic Surfaces. *Advanced Materials*, 29(27), jul 2017.
- [154] L. J. van der Pauw. A Method of Measuring Specific Resistivity and Hall Effect of Discs of Arbitrary Shape. *Semiconductor Devices: Pioneering Papers*, pages 174–182, mar 1991.
- [155] K. G. Mikheev, R. G. Zonov, T. N. Mogileva, A. E. Fateev, and G. M. Mikheev. Optical anisotropy of laser-induced graphene films. *Optics and Laser Technology*, 141:107143, sep 2021.
- [156] J. E.B. Randles. A cathode ray polarograph. Part II. - The current-voltage curves. *Transactions of the Faraday Society*, 44(0):327–338, jan 1948.
- [157] A. Ševčík. Oscillographic polarography with periodical triangular voltage. *Collection of Czechoslovak Chemical Communications*, 13:349–377, 1948.

- [158] Richard S. Nicholson. Theory and Application of Cyclic Voltammetry for Measurement of Electrode Reaction Kinetics. *Analytical Chemistry*, 37(11):1351–1355, oct 1965.
- [159] Farhad Abasalizadeh, Sevil Vaghefi Moghaddam, Effat Alizadeh, Elahe Akbari, Elmira Kashani, Seyyed Mohammad Bagher Fazljou, Mohammadali Torbati, and Abolfazl Akbarzadeh. Alginate-based hydrogels as drug delivery vehicles in cancer treatment and their applications in wound dressing and 3D bioprinting. *Journal of Biological Engineering*, 14(1):1–22, mar 2020.
- [160] Alexander D. Augst, Hyun Joon Kong, and David J. Mooney. Alginate hydrogels as biomaterials. *Macromolecular Bioscience*, 6(8):623–633, aug 2006.
- [161] Kuen Yong Lee and David J. Mooney. Alginate: properties and biomedical applications. *Prog Polym Sci*, 37(1):106–126, 2012.
- [162] Shaohui Li and Pooi See Lee. Development and applications of transparent conductive nanocellulose paper. *Science and Technology of Advanced Materials*, 18(1):620–633, dec 2017.
- [163] Robert J. Moon, Ashlie Martini, John Nairn, John Simonsen, and Jeff Youngblood. Cellulose nanomaterials review: Structure, properties and nanocomposites. *Chemical Society Reviews*, 40(7):3941–3994, jun 2011.
- [164] Dieter Klemm, Friederike Kramer, Sebastian Moritz, Tom Lindström, Mikael Ankerfors, Derek Gray, and Annie Dorris. Nanocelluloses: A new family of nature-based materials. *Angewandte Chemie - International Edition*, 50(24):5438–5466, jun 2011.
- [165] Erlantz Lizundia and Dipan Kundu. Advances in Natural Biopolymer-Based Electrolytes and Separators for Battery Applications, oct 2021.
- [166] Paloma Villagómez Ornelas. Rural poverty in Mexico: prevalence and challenges. *Expert Meeting*, page 10, 2018.
- [167] CONEVAL. Multidimensional Measurement of poverty in Mexico: an economic wellbeing and social rights approach. 2011.

- [168] Social Progress Imperative. 2020 Social Progress Index. Executive Summary. *2020 Social Progress Index*, pages 1–30, 2020.
- [169] ¿Cómo vamos? México. Índice de progreso social. México 2015-2020. Technical report, 2021.
- [170] México ¿cómo vamos?
- [171] Servicio de Información Agroalimentaria y Pesquera. Producción Agrícola | Servicio de Información Agroalimentaria y Pesquera | Gobierno | gob.mx, 2019.
- [172] Gobierno De Chiapas. Instituto del Café de Chiapas, 2019.
- [173] Rajkumar Rathinavelu and Giorgio Graziosi. Potential alternative use of coffee wastes and by-products. *Coffee Organization*, (942):1–4, 2005.
- [174] Solange I. Mussatto, Ercília M.S. Machado, Silvia Martins, and J. A. Teixeira. Production, Composition, and Application of Coffee and Its Industrial Residues. *Food and Bioprocess Technology*, 4(5):661–672, jul 2011.
- [175] Do Viet Phuong, Le Pham Tan Quoc, Pham Van Tan, and Le Nguyen Doan Duy. Production of bioethanol from Robusta coffee pulp (*Coffea robusta* L.) in Vietnam. *Foods and Raw Materials*, 7(1):10–17, 2019.
- [176] Nikoletta Solomakou, Anastasia Loukri, Panagiota Tsafrakidou, Alexandra Maria Michaelidou, Ioannis Mourtzinis, and Athanasia M. Goula. Recovery of phenolic compounds from spent coffee grounds through optimized extraction processes. *Sustainable Chemistry and Pharmacy*, 25:100592, apr 2022.
- [177] Lina F Ballesteros, José A Teixeira, and Solange I Mussatto. Selection of the Solvent and Extraction Conditions for Maximum Recovery of Antioxidant Phenolic Compounds from Coffee Silverskin. *Food and Bioprocess Technology*, 7(5):1322–1332, 2014.
- [178] P. C. Mayanga-Torres, Daniel Lachos-Perez, C. A. Rezende, J. M. Prado, Z. Ma, G. T. Tompsett, M. T. Timko, and T. Forster-Carneiro. Valorization of coffee industry residues by subcritical water hydrolysis: Recovery of sugars and phenolic compounds. *Journal of Supercritical Fluids*, 120:75–85, feb 2017.

- [179] Lenka Blinová, Maroš Sirotiak, Alica Bartošová, and Maroš Soldán. Review: Utilization of Waste From Coffee Production. *Research Papers Faculty of Materials Science and Technology Slovak University of Technology*, 25(40):91–101, jun 2017.
- [180] M.C. Echeverria and M. Nuti. Valorisation of the Residues of Coffee Agro-industry: Perspectives and Limitations. *The Open Waste Management Journal*, 10(1):13–22, feb 2017.
- [181] Grabiriel Desarnaud. Sustainable Electrification for Asia and Africa. Technical report, 2016.
- [182] SPACE10. Life Without Energy: Needs, Dreams and Aspirations.
- [183] M. N. Chai and M. I.N. Isa. Novel Proton Conducting Solid Bio-polymer Electrolytes Based on Carboxymethyl Cellulose Doped with Oleic Acid and Plasticized with Glycerol. *Scientific Reports*, 6, jun 2016.
- [184] Mehdi Mehrali, Ashish Thakur, Firoz Babu Kadumudi, Malgorzata Karolina Pierchala, Julio Alvin Vacacela Cordova, Mohammad Ali Shahbazi, Mohammad Mehrali, Cristian Pablo Pennisi, Gorka Orive, Akhilesh K. Gaharwar, and Alireza Dolatshahi-Pirouz. Pectin Methacrylate (PEMA) and Gelatin-Based Hydrogels for Cell Delivery: Converting Waste Materials into Biomaterials. *ACS Applied Materials and Interfaces*, 11(13):12283–12297, apr 2019.
- [185] S. Kiruthika, M. Malathi, S. Selvasekarapandian, K. Tamilarasan, and T. Maheshwari. Conducting biopolymer electrolyte based on pectin with magnesium chloride salt for magnesium battery application. *Polymer Bulletin*, 77(12):6299–6317, dec 2020.
- [186] Jin Soo Kang, Seoni Kim, Dong Young Chung, Yoon Jun Son, Kyusik Jo, Xiao Su, Myeong Jae Lee, Hwajoo Joo, T. Alan Hatton, Jeyong Yoon, and Yung Eun Sung. Rapid Inversion of Surface Charges in Heteroatom-Doped Porous Carbon: A Route to Robust Electrochemical Desalination. *Advanced Functional Materials*, 1909387:1–11, 2019.

- [187] L. del Torno-de Román, Marina Navarro, Gareth Hughes, Juan Pablo J.P. Esquivel, R.D. Ross D. Milton, S.D. Shelley D. Minter, Neus Sabaté, Lorena del Torno-de Román, Marina Navarro, Gareth Hughes, Juan Pablo J.P. Esquivel, R.D. Ross D. Milton, S.D. Shelley D. Minter, and Neus Sabaté. Improved performance of a paper-based glucose fuel cell by capillary induced flow. *Electrochimica Acta*, 282, may 2018.
- [188] Allen J. Bard and Larry R. Faulkner. *Electrochemical Methods: Fundamentals and applications, 2nd Edition*. Wiley, dec 2001.
- [189] Joseph Wang. *Analytical Electrochemistry, Third Edition*. 2006.
- [190] Dale A C Brownson and Craig E Banks. *The Handbook of Graphene Electrochemistry | Dale A. C. Brownson | Springer*. 2014.
- [191] Enas M. Ahmed. Hydrogel: Preparation, characterization, and applications: A review. *Journal of Advanced Research*, 6(2):105–121, 2015.

Scientific contributions related with this thesis

JOURNAL ARTICLES

A plant-like battery: a biodegradable power source ecodesigned for precision agriculture

Marina Navarro-Segarra, Carles Tortosa, Carlos Ruiz-Díez, Denis Desmaële, Teresa Gea, Raquel Barrena, Neus Sabaté and Juan Pablo Esquivel

Energy Environ. Sci., 2022, Advance Article

DOI:10.1039/D2EE00597B

This original article gathers the research and results presented in Chapter 3 of this thesis

Microfluidics for Electrochemical Energy Conversion

Omar A. Ibrahim, Marina Navarro-Segarra, Pardis Sadeghi, Neus Sabaté, Juan Pablo Esquivel, and Erik Kjeang

Chemical Reviews 2022, 122 (7), 7236-7266

DOI: 10.1021/acs.chemrev.1c00499

This article is a comprehensive review about microfluidics in conjunction with electrochemical cells, summarizing the best practices in the field over the past years.

An Organic Redox Flow Cell-Inspired Paper-Based Primary Battery

Marina Navarro-Segarra, Perla Patricia Alday, David Garcia, Omar A. Ibrahim, Erik Kjeang, Neus Sabaté and Juan Pablo Esquivel

ChemSusChem 2020, 13, 2394 – 2401

DOI:10.1002/cssc.201903511

This original work laid the foundations for the development of the paper-based battery presented in Chapter 3 of this thesis.

Biopolymer Electrolyte Membranes (BioPEMs) for Sustainable Primary Redox Batteries

Perla Patricia Alday, Sandra Cerqueira Barros, Raquel Alves, José M. S. S. Esperança, Marina Navarro-Segarra, Neus Sabaté, Maria Manuela Silva and Juan Pablo Esquivel

Adv. Sustainable Syst.2020, 4, 1900110

DOI: 10.1002/adsu.201900110

This original contribution laid the foundations for the development of the hydrogel matrices developed within this thesis, in Chapters 4 and 5.

A rationale for the development of sustainable biodegradable batteries

Marina Navarro-Segarra and Juan Pablo Esquivel

Book: Sustainable Energy Storage in the Scope of Circular Economy: Advanced Materials and Device Design

Editor: John Wiley & Sons, Limited, 2022

ISBN: 1119817684, 9781119817680

This book chapter will present the rationale developed in Chapter 2 of this thesis

CONFERENCES

- European Materials Research Society (e-MRS) Fall meeting
Place: Online
Related activity: oral contribution entitle 'A bio-based primary battery with LIG electrodes on cardboard'
Dates: 20-23 of September 2021
This conference work was granted with the 'Graduate Student Award of the European Material Research Society' and the Post Lithium Storage Cluster of Excellence award to early career researchers.
- European Association on Smart Systems Integration (EPoSS Annual Forum)
Place: Online
Related activity: oral contribution entitled 'Biodegradable Batteries for Sustainable Smart Systems'
Dates: 29-30 of September 2020
- 5th Scientific Meeting of PhD Students at UAB Campus (JPhD2020)
Place: Online
Related activity: congress organizer
Dates: 17-18 of September 2020
- Workshop on polymers and batteries
Place: Online
Related activity: attendance
Dates: 1 of October 2020
- Sustainable Energy Storage Days in Madrid (1st/SESDIM)
Place: Madrid, Spain
Related activity: attendance
Dates: 10-11 of October 2019
- XL Meeting of the Electrochemistry Group of Spanish Royal Society of Chemistry (XL GE RSEQ)
Place: Huelva, Spain Related activity: doctoral research plan presentation
Dates: 9-12 of July 2019

Organic Battery Days 2019

Place: Jena, Germany

Related activity: poster contribution entitled 'Eco-friendly cellulose-chitosan hydrogel batteries'

Dates: 3-5 of June 2019

STUDENT WORKS SUPERVISION

- Title: *Sustainable energy storage devices using laser-induced graphene electrodes*
Student: *Joseba M. Ormaetxea Orobengoa*
Type: *Final nanoscience and nanotechnology degree project*
Supervisors: *Marina Navarro-Segarra and Dr. Juan Pablo Esquivel*
Year: *2020/2021*

- Title: *Caracterización y desarrollo de electrodos de carbono*
Student: *Elena Villodre Castellanos*
Type: *Final chemistry degree project*
Supervisors: *Marina Navarro-Segarra and Dr. Irene Merino*
Year: *2020/2021*

- Title: *Development and characterization of chitosan:cellulose based ion-exchange membranes for biodegradable batteries*
Student: *Alejandro Ramo Iurre*
Type: *Final chemistry degree project*
Supervisors: *Marina Navarro-Segarra and Dr. Juan Pablo Esquivel*
Year: *2020/2021*

- Title: *Estudi i caracterització d'una bateria de flux per evaporació*
Student: *Carles Tortosa Valdés*
Type: *Final physics degree project*
Supervisors: *Marina Navarro-Segarra and Dr. Juan Pablo Esquivel*
Year: *2019/2020*

Resumen en español

La digitalización está generando una transformación a nivel global con implicaciones tanto económicas, como sociales y ambientales. A pesar de haber demostrado numerosos beneficios para la sociedad, la digitalización y el consumo de tecnología está generando un inmenso debate sobre cómo asegurar que su impacto sea positivo, sostenible y socialmente justo. A la vez que ocurre esta digitalización masiva, la obsolescencia programada y el modelo de economía basado en la linealidad están generando una cantidad de residuos de aparatos eléctricos y electrónicos (RAEE) sin precedentes. En particular, las baterías, que debido a su idoneidad en muchas áreas se han convertido en las fuentes de energía omnipresentes de hoy en día para alimentar dispositivos electrónicos portátiles, representan un componente crítico dentro del RAEE generado. Para que las baterías portátiles dejen de contribuir a la degradación ambiental y se conviertan en un ejemplo de desarrollo tecnológico sostenible, es crucial cambiar la forma en que se aborda la cadena de valor de las baterías. Esta tesis presenta una nueva metodología para el desarrollo de baterías portátiles sostenibles, mediante la cual se analiza y redefine el ciclo de vida completo bajo los principios del ecodiseño y se aboga por un enfoque 'a medida' de tal manera que la batería acaba integrándose en la cadena de valor de la aplicación que va a alimentar. La metodología, inspirada en el modelo de economía del donut, establece un techo ambiental y un suelo de prestaciones para las baterías portátiles, definiendo de esta manera un espacio seguro para el desarrollo de baterías sostenibles y respetuosas con el medio ambiente. El trabajo se ha organizado en cinco capítulos: un capítulo introductorio, un segundo capítulo en el que se establece la lógica disruptiva para el desarrollo de baterías y luego tres capítulos experimentales, cada uno dedicado a un desarrollo de batería diferente. Cada uno de los tres conceptos disruptivos de baterías primaria presentados ha sido diseñado para un sector y campo de aplicación específico. La primera es una batería de flujo profundamente inspirada en la naturaleza, que imita el transporte de fluidos en las plantas para generar energía eléctrica. Concebida para la agricultura de precisión, la biodegradabilidad se ha demostrado como

escenario alternativo para 3 final de su vida útil. La segunda batería ha sido ecodiseñada para aplicaciones de paquetería inteligente, en este caso, se propone reciclar la batería con el papel y el cartón una vez usada y descargada. Para cumplir con los requisitos de fin de vida, este capítulo gira en torno al desarrollo de los materiales que componen la batería. En particular, el grafeno inducido por láser sobre cartón se evalúa como material de colector de corriente, y un hidrogel basado en polímeros naturales se ha sintetizado como conductor iónico para contener las especies electroactivas. El último capítulo explora la posibilidad de desarrollar baterías de forma local y descentralizada. La conceptualización de la batería se ubica en comunidades cafetaleras de Chiapas, México. En estas regiones hay una falta de infraestructura de reciclaje adecuada para este tipo de dispositivos, por lo que el desarrollo de una batería biodegradable se vuelve especialmente atractivo. La viabilidad del proyecto ha sido evaluada a través de entrevistas y compartiéndolo con la población local. De esta manera, el marco del proyecto se ha creado a partir de las necesidades y aspiraciones de la población local, para concebir una batería sostenible cuyos procesos de fabricación se pueden implementar en dichas comunidades. El objetivo final de la tesis es concienciar de cómo nuestras elecciones y acciones individuales, incluso en la investigación, afectan colectivamente a nuestros recursos naturales. La tesis demuestra que se pueden crear soluciones viables y eficientes colocando la sostenibilidad como prioridad absoluta. En esencia, las baterías presentadas en esta tesis son la evidencia de que es imperativo pero también posible redefinir las prioridades tecnológicas de la sociedad para reducir conscientemente el impacto ambiental de la humanidad.

